



International Agreement Report

Thermal-Hydraulic Post-Test Analysis of OECD LOFT LP-FP-2 Experiment

Prepared by

J. J. Pena/Empresa Nacional del Uranio (ENUSA)

S. Enciso/Central Nuclear Valdecaballeros (C. N. Valdecaballeros)

F. Reventos/Asociacion Nuclear ASCO (ANA)

Consejo de Seguridad Nuclear
Madrid, Spain

Office of Nuclear Regulatory Research
U.S. Nuclear Regulatory Commission
Washington, DC 20555

April 1992

Prepared as part of
The Agreement on Research Participation and Technical Exchange
under the International Thermal-Hydraulic Code Assessment
and Application Program (ICAP)

Published by
U.S. Nuclear Regulatory Commission

NOTICE

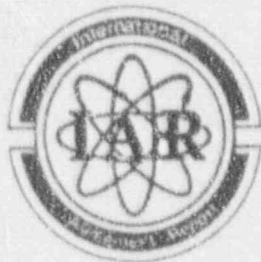
This report was prepared under an international cooperative agreement for the exchange of technical information. Neither the United States Government nor any agency thereof, or any of their employees, makes any warranty, expressed or implied, or assumes any legal liability or responsibility for any third party's use, or the results of such use, of any information, apparatus product or process disclosed in this report, or represents that its use by such third party would not infringe privately owned rights.

Available from

Superintendent of Documents
U S. Government Printing Office
P. O. Box 37082
Washington, D.C. 20013-7082

and

National Technical Information Service
Springfield, VA 22161



NUREG/IA-0049
ICSP-LP-FP-2

International Agreement Report

Thermal-Hydraulic Post-Test Analysis of OECD LOFT LP-FP-2 Experiment

Prepared by
J. J. Pena/Empresa Nacional del Uranio (ENUSA)
S. Enciso/Central Nuclear Valdecaballeros (C. N. Valdecaballeros)
F. Reventos/Asociación Nuclear ASCO (ANA)

Consejo de Seguridad Nuclear
Madrid, Spain

Office of Nuclear Regulatory Research
U.S. Nuclear Regulatory Commission
Washington, DC 20555

April 1992

Prepared as part of
The Agreement on Research Participation and Technical Exchange
under the International Thermal-Hydraulic Code Assessment
and Application Program (ICAP)

Published by
U.S. Nuclear Regulatory Commission

NOTICE

This report documents work performed under the sponsorship of the Consejo De Seguridad Nuclear of Spain. The information in this report has been provided to the USNRC under the terms of an information exchange agreement between the United States and Spain (Technical Exchange and Cooperation Agreement Between the United States Nuclear Regulatory Commission and the Consejo De Seguridad Nuclear of Spain in the field of reactor safety research and development, November 1985). Spain has consented to the publication of this report as a USNRC document in order that it may receive the widest possible circulation among the reactor safety community. Neither the United States Government nor Spain or any agency thereof, or any of their employees, makes any warranty, expressed or implied, or assumes any legal liability of responsibility for any third party's use, or the results of such use, or any information, apparatus, product or process disclosed in this report, or represents that its use by such third party would not infringe privately owned rights.

ABSTRACT

Experiment LP-PP-2 was conducted on July 9, 1985, in the Loss-of-Fluid Test (LOFT) facility located at the Idaho National Engineering Laboratory (INEL). The LP-PP-2 experiment was the final experiment in a series of eight experiments conducted under the support and direction of the objectives of the Organization for Economic Cooperation and Development (OECD). The objectives of the experiment were to obtain information on the release of fission products from fuel rods at temperatures in excess of 2100 K (3320°F), and to observe the transport of these fission products in a vapor/aerosol dominated environment from the primary coolant system (PCS), through a simulated low pressure injection system (LPIS) line, to a blowdown suppression tank (BST). The thermal-hydraulic conditions specified for the experiment were based on a V-sequence accident scenario. The emergency core cooling system (ECCS) injection was delayed until the specified temperature limits on the center bundle thermal shroud were reached, thereby obtaining the desired time-at-temperature condition for fission product release and transport. The reactor was then brought to a safe condition with full ECCS injection. Specially designed fission product measurements were made in the PCS, LPIS, and BST during the transient, with some measurements continuing for several weeks following the experiment. Fission products were detected at all measurement locations; however, the vast majority of the released fission product activity was contained in the PCS liquid following the experiment. In addition, it was observed that large quantities of control rod aerosol material were deposited in the lower sections of the upper plenum (near the top of the core).

This document presents the thermal-hydraulic posttest analysis of the experiment conducted at Spain by using the RELAPS/MOD2 and SCDAP/MOD1 computer codes.

CONTENTS

ABSTRACT.....	1, 1E
EXECUTIVE SUMMARY.....	xv
ACKNOWLEDGMENTS.....	xviii
ABBREVIATIONS, ACRONYMS AND NOTATION.....	xix
PLOT IDENTIFIERS.....	xxi
1. INTRODUCTION.....	1
2. LP-FP-2 EXPERIMENT DESCRIPTION.....	5
2.1 Objectives.....	5
2.2 Systems Description.....	5
2.3 Experiment Description.....	15
3. SUMMARY OF THE THERMAL-HYDRAULIC DATA.....	18
3.1 Slowdown Hydraulics.....	26
3.2 Core Thermal Response.....	29
4. RELAP5/MOD2 SIMULATION OF LP-FP-2 Experiment.....	37
4.1 General Overview of the Methodology used for the Analysis	37
4.2 RELAP5/MOD2 Modalization for Experiment LP-FP-2.....	41
4.3 Simulation of the Core Geometry Changes in the Base RELAP5 /MOD2 Calculation.....	45
5. RESULTS OF THE RELAP5/MOD2 BASE CALCULATION.....	49
5.1 Calculation of the Steady State.....	49
5.2 Base Transient Calculation.....	52

CONTENTS (continued)

	<u>PAGE</u>
6. RELAP5/MOD2 SENSITIVITY ANALYSIS.....	85
6.1 Results of the Sensitivity with Respect to the Blockages.....	85
6.2 General Conclusions of the RELAP5/MOD2 Calculations.....	94
7. SCDAP/MOD1 NODALIZATION FOR LP-FP-2 EXPERIMENT.....	95
7.1 SCDAP Model for Experiment LP-FP-2.....	95
7.2 Nodalization.....	96
7.3 Input Data.....	96
7.3.1 Basic Input Deck.....	96
7.3.2 Modifications.....	100
7.3.3 CFM Inlet Mass Flow for the best estimate SCDAP Analysis.....	102
8. RESULTS OF THE SCDAP/MOD1 CALCULATION.....	106
8.1 SCDAP Results using CFM Inlet Flow directly taken from the RELAP5 Base Calculation.....	106
8.2 SCDAP Results using "Best Estimate" CFM Inlet Flow.....	110
8.3 Conclusions of the SCDAP/MOD1 Calculations.....	133
9. SUMMARY AND CONCLUSIONS.....	134
10. REFERENCES.....	136
APPENDIX A LP-FP-2 EXPERIMENT INSTRUMENTATION.....	A-1
APPENDIX B BRIEF DESCRIPTION OF THE COMPUTER CODES USED FOR THE ANALYSIS.....	B-1
APPENDIX C RELAP5/MOD2 INPUT DATA.....	C-1
APPENDIX D SCDAP/MOD1 INPUT DATA.....	D-1
APPENDIX E COMPUTER RUN STATISTICS.....	E-1

LIST OF FIGURES

	<u>Page</u>
Figure 1.1 Flow chart of computer codes used in the analysis, showing the interdependency between them.....	4
Figure 2.1 Axonometric view of the LOFT primary coolant system.	7
Figure 2.2 Schematic of the LPIS line showing line lengths.....	9
Figure 2.3 LOFT reactor vessel cross section.....	10
Figure 2.4 CFM instrumentation.....	12
Figure 2.5 Schematic diagram of the LOFT system showing the relative positions of FPMS instrumentation	14
Figure 2.6 Preexperiment power history	17
Figure 3.1 Primary system pressure history showing significant events	25
Figure 3.2 Intact loop hot leg density	27
Figure 3.3 Conductivity level probe response above Fuel Assembly 3	28
Figure 3.4 Comparison of cladding temperatures at the 1.14-, 0.38-, and 0.28- m (45-, 15-, and 11-in.) elevations in Fuel Assembly 2 with saturation temperature	31
Figure 3.5 Comparison of cladding temperatures at the 1.07-, 0.69-, and 0.25- m (42-, 27- and 10-in) elevations in Fuel Assembly 5 with saturation temperature	31
Figure 3.6 Comparison of three guide tube temperatures at the 0.69-m (7-in) elevation in Fuel Assembly 5	32

	<u>Page</u>
Figure 3.7 Comparison of two cladding temperatures at the 0.69- m (27- in) elevation in Fuel Assembly 5	34
Figure 3.8 Comparison of four external wall temperatures at the 1.07-, 0.81-, 0.69-, and 0.25- m (42-, 32- 27-, and 10- in) elevations on the south side of the flow shroud	34
Figure 3.9 Comparison of cladding temperatures at the 1.24-, 0.99-, 0.71-, and 0.28- m (49-, 39-, 28-, and 11-in) elevations in Fuel Assembly 2	35
Figure 3.10 Comparison of two cladding temperatures at the 0.69- m (27- in) elevation in Fuel Assembly 5 with saturation temperature	35
Figure 4.1 Flow chart of computer codes used in the analysis, showing the interdependency between them	38
Figure 4.2 RELAP5/MOD2 calculational scheme, showing the interactions between RELAP5 and SCDAP	39
Figure 4.3 RELAP5/MOD2 nodalization diagram	40
Figure 4.4 RELAP5/MOD2 base case calculational scheme, showing the interactions between RELAP5 and SCDAP	47
Figure 5.1 Primary System Pressure (MPa) at the Intact Loop Hot leg location. RELAP5/EXPERIMENT comparison	56
Figure 5.2 Secondary System Pressure (MPa) at the steam dome location. RELAP5/EXPERIMENT comparison	59
Figure 5.3 Steam Generator liquid level (m). RELAP5/EXPERIMENT comparison	60

	<u>Page</u>
Figure 5.4 Fluid Density (Mg/m^3) at the intact loop hot leg. RELAP5/EXPERIMENT comparison	61
Figure 5.5 Fluid Density (Mg/m^3) at the broken loop hot leg. RELAP5/EXPERIMENT comparison	62
Figure 5.6 Pressurizer liquid level (m). RELAP5/EXPERIMENT comparison	64
Figure 5.7 Mass flow (kg/s) at the intact loop hot leg. RELAP5/EXPERIMENT comparison	65
Figure 5.8 Primary coolant system mass inventory calculated by RELAP5/NOBR	66
Figure 5.9 Primary coolant system mass inventory derived from mass increase in the BST	67
Figure 5.10a Intact loop cold leg line break mass flow (kg/s). RELAP5 results	69
Figure 5.10b LPIS line break mass flow (kg/s). RELAP5 result ...	70
Figure 5.11 LPIS line break mass flow (kg/s). RELAP5/EXPERIMENT comparison	71
Figure 5.12 FP-2 core inlet steam mass flow rates (kg/s) (Peripheral and center assemblies). RELAP5 results .	72
Figure 5.13 Reactor vessel liquid level (m) through peripheral and center bundles. RELAP5 results	73
Figure 5.14 Central bundle clad outer temperature at the 0.25- m (10-in) elevation. RELAP5/EXPERIMENT comparison	75

	<u>Page</u>
Figure 5.15 Central bundle clad outer temperature at the 0.69- m (27- in) elevation. RELAP5/EXPERIMENT comparison ...	77
Figure 5.16 Central bundle clad outer temperature at the 1.07- m (42- in) elevation. RELAP5/EXPERIMENT comparison ...	78
Figure 5.17 Peripheral bundle clad outer temperature at the 0.29- m (11- in) elevation. RELAP5/EXPERIMENT comparison	80
Figure 5.18 Peripheral bundle clad outer temperature at the 0.66- m (26- in) elevation. RELAP5/EXPERIMENT comparison	81
Figure 5.19 Peripheral bundle clad outer temperature at the 1.14 m (45- in) elevation. RELAP5/EXPERIMENT comparison	83
Figure 5.20 Outer CFM shroud wall temperature at the 0.69 m (27- in) elevation. RELAP5/EXPERIMENT comparison	84
Figure 6.1 Primary system pressure (MPa) at the intact loop hot leg location. RELAP5 sensitivity study	86
Figure 6.2 Center fuel bundle inlet mass flow rate (kg/s). RELAP5 sensitivity study	89
Figure 6.3 Peripheral bundle inlet steam mass flow rate (kg/s). RELAP5 sensitivity study	90
Figure 6.4 Peripheral bundle clad outer temperature at the 1.14- m (45- in) elevation. RELAP5 sensitivity study	91
Figure 6.5 Center bundle clad outer temperature at the 0.25- m (10- in) elevation. RELAP5 sensitivity study	92

	<u>Page</u>
Figure 6.6	Center bundle clad outer temperature at the 0.69- m (27- in) elevation. RELAP5 sensitivity study 93
Figure 6.7	Center bundle clad outer temperature at the 1.07- m (42.3- in) elevation. RELAP5 sensitivity study 94
Figure 7.1	SCDAP center bundle rod grouping 98
Figure 7.2	SCDAP nodalization diagram for center bundle 99
Figure 7.3	SCDAP shroud nodalization diagram 100
Figure 7.4	Center bundle inlet steam mass flow rate (kg/s). SCDAP/RELAP5 comparison 106
Figure 8.1	Center bundle fuel rod clad outer temperature (K) at 0.25- m (10- in) elevation, calculated by SCDAP using the inlet flow given by the RELAP5 base calculation. SCDAP/RELAP5/EXPERIMENT comparison 108
Figure 8.2	Center bundle fuel rod clad outer temperature (K) at 0.69- m (27- in) elevation, calculated by SCDAP using the inlet flow given by the RELAP5 base calculation. SCDAP/RELAP5/EXPERIMENT comparison 109
Figure 8.3	Center bundle fuel rod clad outer temperature (K) at 1.07- m (42- in) elevation, calculated by SCDAP using the inlet flow given by the RELAP5 base calculation. SCDAP/RELAP5/EXPERIMENT comparison 110
Figure 8.4	Center bundle average fuel rod cladding temperatures (K) at different axial levels calculated by SCDAP/MOD1/V21 112
Figure 8.5	Center bundle axial steam fractions calculated by SCDAP/MOD1/V21 114

	<u>Page</u>
Figure 8.6 Center bundle control rod cladding temperature at different axial levels calculated by SCDAP/MOD1/V21.	115
Figure 8.7 Center bundle hot fuel rod clad temperature at 0.25- m (10- in) elevation. SCDAP/RELAP5/EXPERIEMENT comparison	116
Fi. 8.8 Center bundle hot fuel rod clad temperature at 0.69- m (27- in) elevation. SCDAP/RELAP5/EXPERIEMENT comparison	117
Figure 8.9 Center bundle hot fuel rod clad temperature at 1.07- m (42- in) elevation. SCDAP/RELAP5/EXPERIEMENT comparison	118
Figure 8.10 Center bundle average fuel rod fission product gap inventory (kg) calculated by SCDAP/MOD1/V21	120
Figure 8.11 Center bundle average fuel rod fission product gap release (kg) calculated by SCDAP/MOD1/V21	121
Figure 8.12 Center bundle average fuel rod soluble fission product release (kg) calculated by SCDAP/MOD1/V21...	122
Figure 8.13 Center bundle average fuel rod noncondensable fission product release (kg) calculated by SCDAP/MOD1/V21	123
Figure 8.14 Center bundle total oxidation heat generation (W) calculated by SCDAP/MOD1/V21	125
Figure 8.15 Center bundle total hydrogen generation rate (kg/s) calculated by SCDAP/MOD1/V21	126
Figure 8.16 Total hydrogen generated in the center fuel bundle (kg) calculated by SCDAP/MOD1/V21	127

	<u>Page</u>
Figure 8.17 Center fuel bundle flow area blockages at different axial elevations (%) calculated by SCDAP/MOD1/VE1 ..	130
Figure 8.18 Configuration of the center fuel bundle average fuel rod at the end of the transient (1770 s)	131
Figure A-1 Axonometric representation of the LOFT primary coolant system	A-15
Figure A-2 LOFT piping schematic with instrumentation	A-16
Figure A-3 Simulated LPI break line instrumentation	A-17
Figure A-4 Instrument Locations-Steam Generator	A-18
Figure A-5 Instrument Locations-Pressurizer	A-19
Figure A-6 Instrument Locations-Accumulator Tank	A-20
Figure A-7 Instrument Locations-Suppression Vessel (External) .	A-21
Figure A-8 Instrument Locations-Suppression Vessel (Internal) .	A-22
Figure A-9 LOFT Upper Plenum Instruments (Side View)	A-23
Figure A-10 Instrument Elevations-Reactor Vessel Upper Plenum ..	A-24
Figure A-11 LOFT reactor vessel station numbers	A-25
Figure A-12 Instrument Locations-Liquid Levels and neutron detectors in reactor vessel (Top view)	A-26
Figure A-13 Instrument Locations-Angular position of thermocouples on core fuel assemblies	A-27
Figure A-14 LOFT secondary coolant System Instrumentation	A-28

	<u>Page</u>
Figure A-15 Center Fuel bundle Instrumentation	A-29
Figure E-1 RELAP5 CPU time versus transient time	E-3
Figure E-2 RELAP5 total CPU time versus transient time	E-4

LIST OF TABLES

Table 2.1 LP-FP-2 Fuel Description	13
Table 3.1 Initial conditions for experiment LP-FP-2	19
Table 3.2 Chronology of events for experiment LP-FP-2	22
Table 5.1 Initial Conditions for experiment LP-FP-2 Comparison between calculated and measured values	51
Table 5.2 Chronology of events for experiment LP-FP-2. Comparison between calculated and measured values	53
Table 7.1 SCDAP posttest specific power level	102
Table 7.2 CFM best estimate inlet flow	105
Table 8.1 Chronology of core damage events. Comparison between observations and the SCDAP results	128
Table 8.2 Core damage parameters calculated by SCDAP/MOD1/V21 ...	132
Table A-1 Measurement identifiers and descriptions for LP-FP-2 ..	A-3

EXECUTIVE SUMMARY

Experiment LP-FP-2, conducted on July 9, was the second fission product release and transport experiment conducted in the Loss-of-Fluid Test (LOFT) facility at the Idaho National Engineering Laboratory under the auspices of the Organization for Economic Cooperation and Development (OECD). The principal objectives of the experiment were to determine the fission product release from the fuel during a severe fuel damage scenario and the subsequent transport of these fission products (in a predominantly vapor/aerosol environment) in the primary coolant system.

The thermal-hydraulic boundary conditions for fission product release and transport were generated by a simulated interfacing systems loss-of-coolant accident (LOCA), a hypothetical event labeled the V-sequence. The specific interfacing systems LOCA that was simulated during experiment LP-FP-2 involved a pipe break in the low pressure injection system (LPIS), also called the residual heat removal system (RHRS). The system thermal-hydraulic and core uncover conditions simulated those calculated to occur in a four-loop Pressurized Water Reactor (PWR) from rupture of an RHRS pipe as a result of a V-sequence accident. The transient was initiated by a reactor scram followed by the insertion of the central assembly control rods (designed to provide typical control rod behavior and potential aerosol material during the transient). A break line in the intact loop cold leg (ILCL) was opened to start the depressurization. A second break path, which simulated the LPIS line, was opened in the broken loop hot leg. The intact loop cold leg break was then closed in accordance with the Experiment Operation Specification (EOS) procedures; however, the subsequent system depressurization was slower than calculated and the pressure remained too high for operation of the fission product measurement system (FPMS). Therefore, in accordance with the EOS procedures, the power operated relief valve (PORV) and de ILCL break lines were opened to assist in lowering the system pressure. Before fission product release, both the PORV and the ILCL break lines were closed. Consequently, only the LPIS line was opened during the transient when fission products were released from the core. The core was allowed to uncover and to heatup until a high temperature trip on the outside wall of the center fuel module (CFM) shroud was reached. By that time, the estimated peak fuel temperatures in the CFM exceeded 2100 K (3320°F) for 4.5 min. The emergency core cooling system (ECCS) was then activated to reflood the reactor vessel and recover the plant.

Comparison with the measured data shows that the passive link between RELAP5/MOD2 and SCDAP/MOD1 is an excellent tool to simulate the thermal-hydraulic behaviour of LP-FP-2 experiment. The timing and extent of the core thermal response is closely calculated, with the exception of the lack of steam starvation in the upper parts of the center fuel module. This discrepancy results from a larger than calculated center fuel module steam flow which, in turn, is judged to be caused by a greater than calculated primary system pressure during the severe core damage period of the transient. This lower calculated system pressure is thought to be due to some inconsistency in the LPIS flow: either a code deficiency or an unaccurate LPIS line nodalization.

The LP-FP-2 experiment was successfully accomplished and represents the second fission product experiment performed in LOFT and the last experiment in the LOFT-OECD program. To date, it is the only severe fuel damage experiment performed in an integral facility where fission product release, transport, deposition phenomena, and thermal-hydraulic conditions, were simultaneously measured throughout the primary coolant system (PCS) and simulated LPIS line of a scaled pressurized water reactor (PWR). The data from this experiment have shown to provide a very valuable information for assessing the ability of computer codes for calculating the effects and consequences of similar accident scenarios at large PWRs (LPWRs).

FOREWORD

This report represents one of the assessment/application calculations submitted in fulfilment of the bilateral agreement for cooperation in thermalhydraulic activities between the Consejo de Seguridad Nuclear of Spain (CSN) and the United States Nuclear Regulatory Commission (US-NRC) in the form of Spanish contribution to the International Code Assessment and Applications Program (ICAP) of the US-NRC whose main purpose is the validation of the TRAC and RELAP system codes.

The Consejo de Seguridad Nuclear has promoted a coordinated Spanish Nuclear Industry effort (ICAP-SPAIN) aiming to satisfy the requirements of this agreement and to improve the quality of the technical support groups at the Spanish Utilities, Spanish Research Establishments, Regulatory Staff and Engineering Companies, for safety purposes.

This ICAP-SPAIN national program includes agreements between CSN and each of the following organizations:

- Unidad Eléctrica (UNESA)
- Unión Iberoamericana de Tecnología Eléctrica (UITESA)
- Empresa Nacional del Uranio (ENUSA)
- Centro de Investigaciones Energéticas y Medioambientales (CIEMAT)
- TECNATOM
- LOFT-ESPAÑA

The program is executed by 12 working groups and a generic code review group and is coordinated by the "Comité de Coordinación". This committee has approved the distribution of this document for ICAP purposes.

ACKNOWLEDGMENTS

We would like to gratefully acknowledge the cooperation received from L. J. Siofken for his assistance in the SCDAP calculations; M. Modro for his assistance in the RELAPS/MOD2 model development; and all of the Spanish participants in the OECD LOFT project for their support and their technical review of this report.

Special thanks to J. Puga, the Spanish member of the Program Review Group, for his continuous support to the authors.

ABBREVIATIONS, ACRONYMS, AND NOTATION

BL	Broken loop
BLCL	Broken loop col leg
BLHL	Broken loop hot leg
BST	Blowdown suppression tank
CFM	Center Fuel module
CPU	Central Processor Unit
d	Day(s)
DAVDS	Data acquisition and visual display system
DIRC	Data integrity review committee
EASR	Experiment Analysis Summary report
ECCS	Emergency core cooling system
EOS	Experiment operation specification
ESD	Experiment specification document
°F	Degree fahrenheit
ft	Foot (feet)
FP	Fission Product
FPMS	Fission product measurement system
F3	Fission product Filter 3
g	Gram
h	Hour(s)
HL	Hot leg
HPIS	High pressure injection system
ID	Inside diameter
ILCL	Intact loop cold leg
in.	Inch
INEL	Idaho National Engineering Laboratory
K	Kelvin
kg	Kilogram
kW	Kilowatts
L	Liter
LOCA	Loss-of-coolant accident
LOCE	Loss-of coolant experiment
LOFT	Loss-of-Fluid Test
LP	Lower plenum
LP-FP-2	LOFT Program Fission Product Experiment 2

LP-SB-3	LOFT Program Small Break Experiment 3
LPIS	Low pressure injection system
LPWR	Large pressurized water reactor
m	Meter(s)
min	Minute(s)
Mg	Megagrams
MPa	Megapascal
MW	Megawatts
MWD/TMU	Megawatt days per metric tonne uranium (burnup)
MWR	Metal water reaction
OECD	Organization for Economic Cooperation and Development
OD	Outside diameter
PBF	Power Burst Facility
PCP	Primary coolant pump
PCS	Primary coolant system
PFM	Peripheral fuel module
PIE	Postirradiation examination
PORV	Power operated relief valve
ppm	Parts per million
PRA	Probabilistic risk assessment
psia	Pounds per square inch, absolute
PWR	Pressurized water reactor
QLR	Quick Look Report
QOV	Quick opening blowdown valve
RAS	Remote data acquisition system
RELAP	Reactor excursion and leakage analysis program
RHRS	Residual heat removal system
rpm	Revolutions per min
RV	Reactor vessel
s	Second(s)
SCDAP	Severe Core Damage Analysis Package
SCS	Secondary coolant system
SG	Steam generator
SPND	Self-powered neutron detector
TH	Thermal-Hydraulic
t_0	Time zero (for LP-FP-2 this was Tuesday July 9, 1985 at 14 h 7 min and 44.9 s)
TC	Thermocouple
UP	Upper plenum

PLOT IDENTIFIERS

- I. The RELAP5/MCD2 calculational results can be identified in the plots by the following notation:

Alphabetic code-Numeric code-XXX

The alphabetic code indicates the magnitude of the computed variable, such as

P	for pressure
PHO	for density
TEMFF	for fluid (liquid) temperature
TEMFG	for gas (vapor) temperature
HTTEMP	for Heat structure (wall) temperature
MFLOWJ	for Mass flow at a junction
CNTRLVAR	for Control variable, generally in this report for a liquid level

The numeric code indicates the control volume of the nodalization diagram where the variable is being calculated.

The XXX code is for distinguish between the base or sensitivity RELAP5 calculation

RCR	Reactor Core Renodalization (BASE case)
NRN	No Reactor Core Renodalization (SENSITIVITY case)

- II. The Experimental measurements are identified by a similar to RELAP5 alphanumeric code

Alphabetic code-Alphanumeric code-Numeric code

The alphabetic code stands for the measured magnitude, while the rest of the code (alphanumeric-Numeric) indicates the instrument location.

III. The SCDAP/MOD1 calculational results are easily identified by the following code

Alphabetic code = Numeric code

As usually the alphabetic code stands for the magnitude, i.e.

CADCT	for cladding temperature
THVFRG	for vapor fraction
CGGIVY	for component gap inventory
CGGREL	for component gap release
BGTFPRS	for bundle gap fission product release of solubles
BGTFPRN	for bundle gap fission product release of noncondensable
BGTHO	for bundle total oxidation heat
BGTH	for bundle total hydrogen generation rate
THFLWA	for bundle free flow area

And, again, the numeric code indicates the component location of the computed variable.

THERMAL-HYDRAULIC POSTTEST ANALYSIS OF
OECD LOFT FISSION PRODUCT EXPERIMENT LP-FP-2

1. INTRODUCTION

This report presents the thermal-hydraulic posttest analysis of LP-FP-2 Experiment, made by the Spanish FP-2 calculation group using the RELAP5/MOD2 and SCDAP/MOD1 computer codes.

Experiment LP-FP-2 was the second Fission Product (FP) release and transport test performed at the Loss-of-Fluid Test (LOFT) facility, located on the Idaho National Engineering Laboratory (INEL). This experiment was initiated on July 9, 1985, and represents the eighth and final experiment conducted under the auspices of the Organization for Economic Cooperation and Development (OECD).

Experiment LP-FP-2 provides information on the release, transport, and deposition of fission products and aerosols during a severe core damage event performed in a large scale nuclear reactor facility. The phenomena governing fission product and aerosol release, transport, and deposition are associated with postulated severe pressurized water reactor (PWR) accidents that lead to fuel rod failure, control rod melting, fuel relocation, and the loss of fission products from the UO_2 fuel. For the LP-FP-2 experiment, the fuel rod cladding temperatures in the center fuel module (CFM) exceeded 2100 K (3320°F) for ~4.5 min before test termination temperatures were reached on the exterior wall of the CFM shroud. The 4.5 min fission product release and transport transient simulated the initial portion of a severe damage transient with delayed emergency core cooling system (ECCS) operation, wherein the core damage originated from a V-sequence scenario.

Probabilistic Risk Assessment (PRA) studies¹ have shown that the interfacing systems loss-of-coolant accident (LOCA), a hypothetical event first postulated in the Reactor Safety Study² and labeled the V-sequence, represents a significant contribution to the risk associated with PWR operation. Consequently, this risk dominant accident sequence was selected as the thermal-hydraulic event in which fission product release and transport would be measured in Experiment LP-FP-2. The specific interfacing systems LOCA associated with the V-sequence accident scenario is a pipe break in the low

pressure injection system (LPIS), also referred to as the residual heat removal system (RHRS). This system typically performs two functions on a commercial PWR: (a) it provides emergency coolant injection for core recovery during intermediate and large break LOCAs, and (b) it provides for decay heat removal during normal shutdown. The LPIS represents a potential pathway for release of primary coolant from the reactor vessel (RV). If core cooling were not maintained during such an event and if fuel rods failed, fission product release to the environment could occur if the auxiliary building also failed.

Experiment LP-FP-2 simulated the system thermal-hydraulics and core uncover conditions during fission product release and transport that are expected to occur in a four-loop PWR from rupture of a LPIS pipe as a result of a V-sequence accident. The initial conditions for the experiment represented typical commercial PWR operations. The break size resulted in a depressurization that was bounded by previously conducted LOFT experiments L8-2 and L5-1 on the upper end and by experiments L3-1, L3-5/3-5A, and L3-6/L8-1 on the lower end³.

The thermal-hydraulic posttest calculation of the LOFT System as a whole was performed using the RELAP5/MOD2/36.04⁴ computer code. On the other hand the SCDAP/MOD1/21⁵ computer code was used to calculate the detailed thermo-mechanical core behaviour during the heatup phase of the experiment. Figure 1.1 shows the interdependency between these two codes usually known as the RELAP5-SCDAP passive link.

The RELAP5/MOD2 and SCDAP/MOD1 input decks used for this analysis were based on those used by the INEL to prepare the Best Estimate Prediction Document (BEP)⁶. Several improvements and error corrections on the pretest deck were made: (a) to correct some errors, (b) to match the experimental sequence of events, (c) to improve the primary system depressurization process, and (d) to try to avoid the steam starvation observed in the pretest calculation.

The calculation results have been compared to the measured data to assess the capabilities of RELAP5/MOD2 and SCDAP/MOD1 for simulating the thermal-hydraulic conditions which might occur during a PWR severe accident. Section 2 of this report presents the objectives and a brief description of the LP-FP-2 experiment. Section 3 summarizes the thermal-hydraulic results measured during the transient. Section 4 describes the RELAP5/MOD2 input model used for the

base case calculation. Section 5 discusses the results of the posttest calculation in comparison with the measured data. Section 6 shows a RELAP5 sensitivity study compared to the base case results. Section 7 introduces the SCDAP/MOD1 nodalization model. Section 8 discusses the SCDAP results in comparison with the measured and the RELAP5 data. Conclusions and recommendations derived from this analysis are presented in section 9. A short description of the special configuration of the LOFT plant and its instrumentation for the LP-FP-2 experiment is shown in the Appendix A. Appendix B gives a brief description of the computer codes used in our analysis. Appendix C contains a full listing of the RELAP5/MOD2 input model used for these analyses, while a full listing of the SCDAP input data is given in Appendix D. Appendix E presents some statistics of the computer time consumed during the calculations.

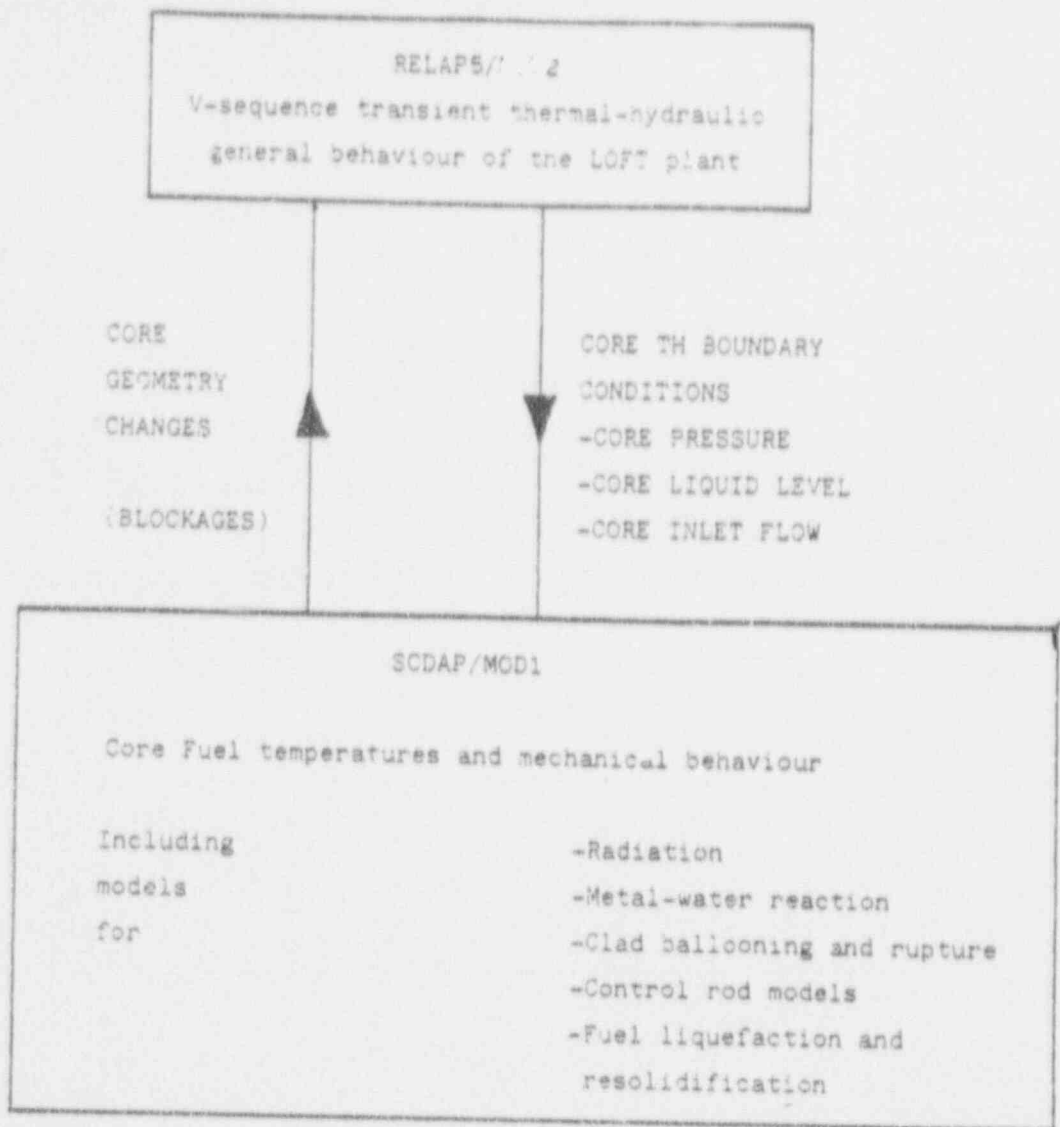


FIGURE 1.1 Flow chart of computer codes used in the analysis, showing the interdependency between them.

(PASSIVE LINK BETWEEN RELAP5/MCD2 AND SCDAP/MOD1)

2. LP-FP-2 EXPERIMENT DESCRIPTION

2.1. Objectives

The governing objective for the LP-FP-2 Experiment was:

To obtain fission product release, transport, and deposition data during the early phases of a risk dominant reactor transient in order to establish a benchmark data base for:

1. Assessing the understanding of the physical phenomena controlling reactor system fission product behavior.
2. Assessing the capability of computer models to predict the reactor system fission product release and transport.

To support this objective, the following two thermal-hydraulic and four fission product objectives were defined:

Thermal-hydraulic Objectives:

1. To provide LPIS interfacing system LOCA thermal-hydraulic conditions from the initiation of the LPIS pipe break through the early phases of severe core damage.
2. To provide transient fuel rod temperatures in the center fuel assembly up to the rapid metal-water reaction temperature of 2100 K (3320°) with aerosol generation from the (Ag/In/Cd) control rods.

Fission Product Objectives:

1. To determine the fraction of the volatile fission products (Cs, I, Te, Xe, Kr) and aerosols released to and from the upper plenum region.

3. To determine the fraction of volatile fission products and aerosols transported out of the primary coolant system.
3. To determine the retention of volatile fission products on representative primary coolant system surfaces in the plenum and piping.
4. To determine the general mass balance of volatile fission products in the fuel, primary coolant system, and blowdown tank.

In order to meet the former objectives the LOFT plant was specially modified as is summarized in the next section.

2.2. Key features of the LOFT facility including changes for the LP-FP-2 experiment.

The LOFT PWR is an 1/50 size model of a commercial 4-loop PWR that has been used to study phenomena associated with loss of coolant, subsequent ECC injection, and finally fission product transport with aerosols at the initial stages of core damage.

The experimental assembly includes five major subsystems that have been instrumented in such a way that system variables can be measured and recorded during a LOCA simulation. The subsystems include the reactor vessel, the intact loop, the broken loop, the blowdown suppression tank (BST), and the ECC systems. Complete information on the LOFT system is provided in Reference 7 and a discussion of the LOFT scaling philosophy and specific modifications for LP-FP-2 experiment is provided in Reference 8.

The following is a brief description of the LOFT facility as it was built for the LP-FP-2 experiment.

The arrangement of the major LOFT components is shown in Figure 2.1. The intact loop simulated three loops of a commercial four-loop PWR and contains a

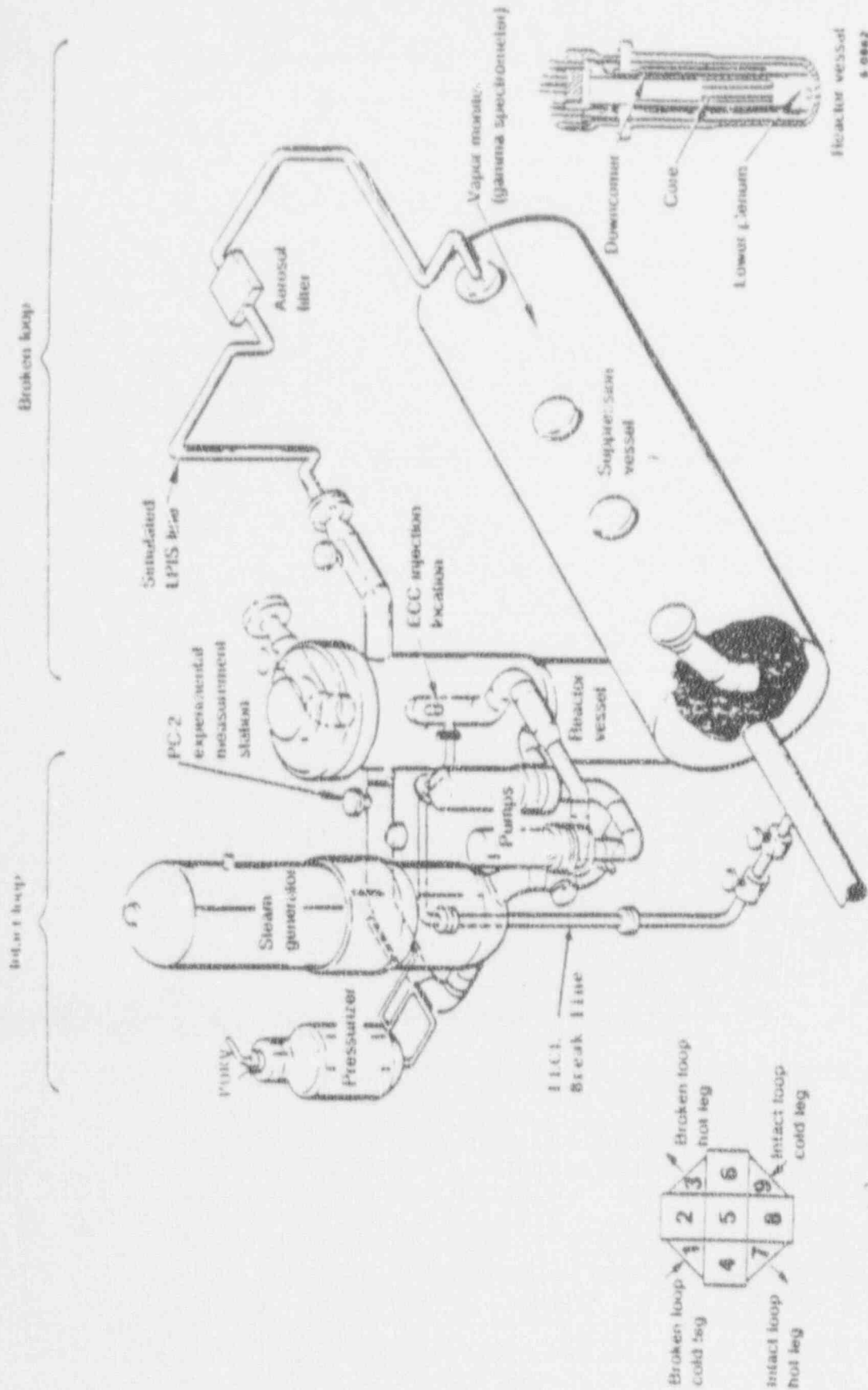


Figure 2.1 Asymmetric view of the LOFI primary coolant system.

steam generator, two primary coolant pumps in parallel, a pressurizer, a Venturi flowmeter, and connecting piping. A spool piece was connected to the intact loop cold leg downstream of the pump discharge. This provided the initial break path during the blowdown. The piping of this break path is 1-1/4 in nominal Sch 160 pipe having an inner diameter of 1.16 in. The full flow area was used to vent PCS coolant. This line was closed prior to fission product release so the fission product transport would be solely in the simulated LPIS line.

The broken loop consists of a hot leg and a cold leg. For this experiment, the broken loop cold leg was flanged off and the broken loop hot leg pump and steam generator simulators were removed. The simulated LPIS line was connected to the end of the broken loop hot leg and provided the path for fission product transport from the primary system to the BST. The simulated LPIS line is illustrated in Figure 2.2. The pipe size selected for the LOFT LPIS pipe simulation line was 1-1/4 in. nominal Schedule 160, having an inner diameter of 0.0295 m (1.16in.). The entire LPIS line was designed with a total length of 21.34 m (70 ft) and the distance between the isolation valves CV-P138-100 and CV-P138-191 was 15.67 m (51.4 ft).

The LOFT reactor vessel, shown schematically in Figure 2.3, has an annular downcomer, a lower plenum, lower core support plates, a nuclear core, and an upper plenum. The downcomer is connected to the cold legs of the intact and broken loops, and the upper plenum, to the hot legs. The core consists of 1196 enriched uranium fuel rods arranged in five square and four triangular (corner) fuel assemblies (see figure 2.1). The fuel rods were designed to commercial PWR specifications except that they are only 1.68 m (5.5 ft) long and several fuel rods have special instrumentation.

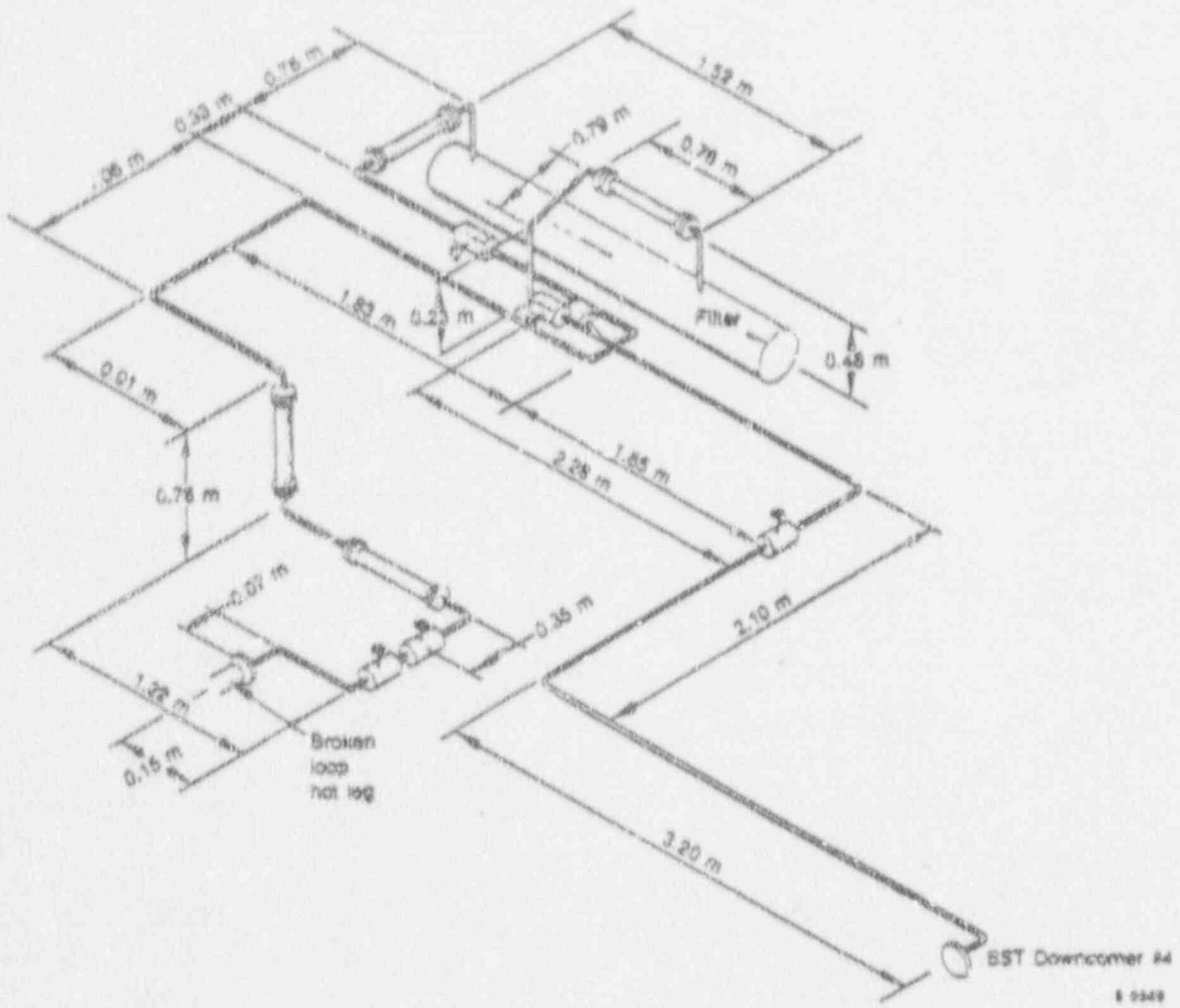
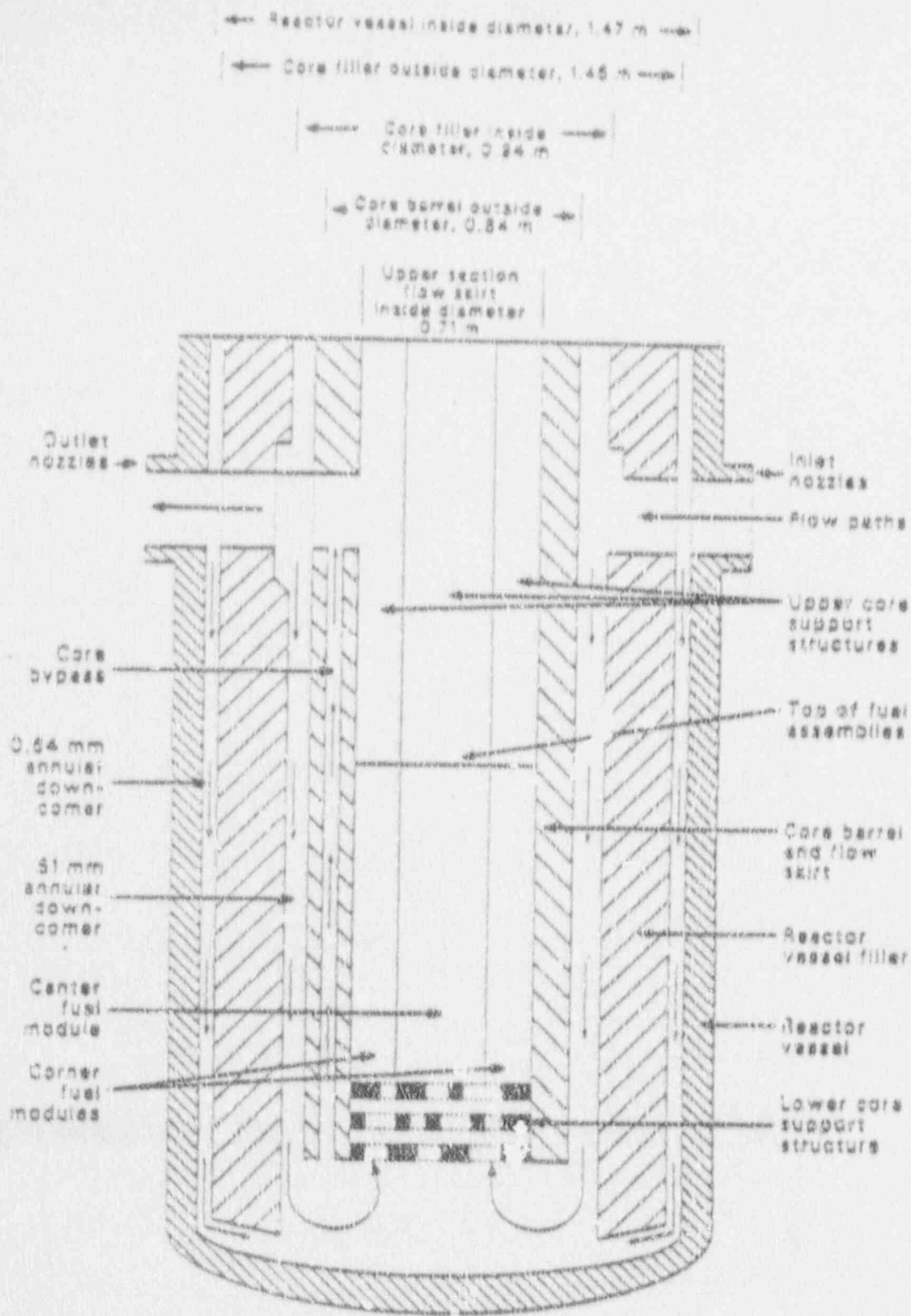


Figure 2.4. Schematic of the LPIS line showing line lengths.



L183-KM189-07

Figure 1.0 LOFT reactor vessel cross section

The requirements imposed on the LP-FP-2 Experiment, from the standpoint of facility decontamination and recovery, were:

1. Experiment LP-FP-2 must be conducted with peripheral assembly fuel rod cladding temperatures limited to 1533 K (2300° F).
2. The structural integrity of the center fuel assembly must be maintained to facilitate removal from the reactor vessel.

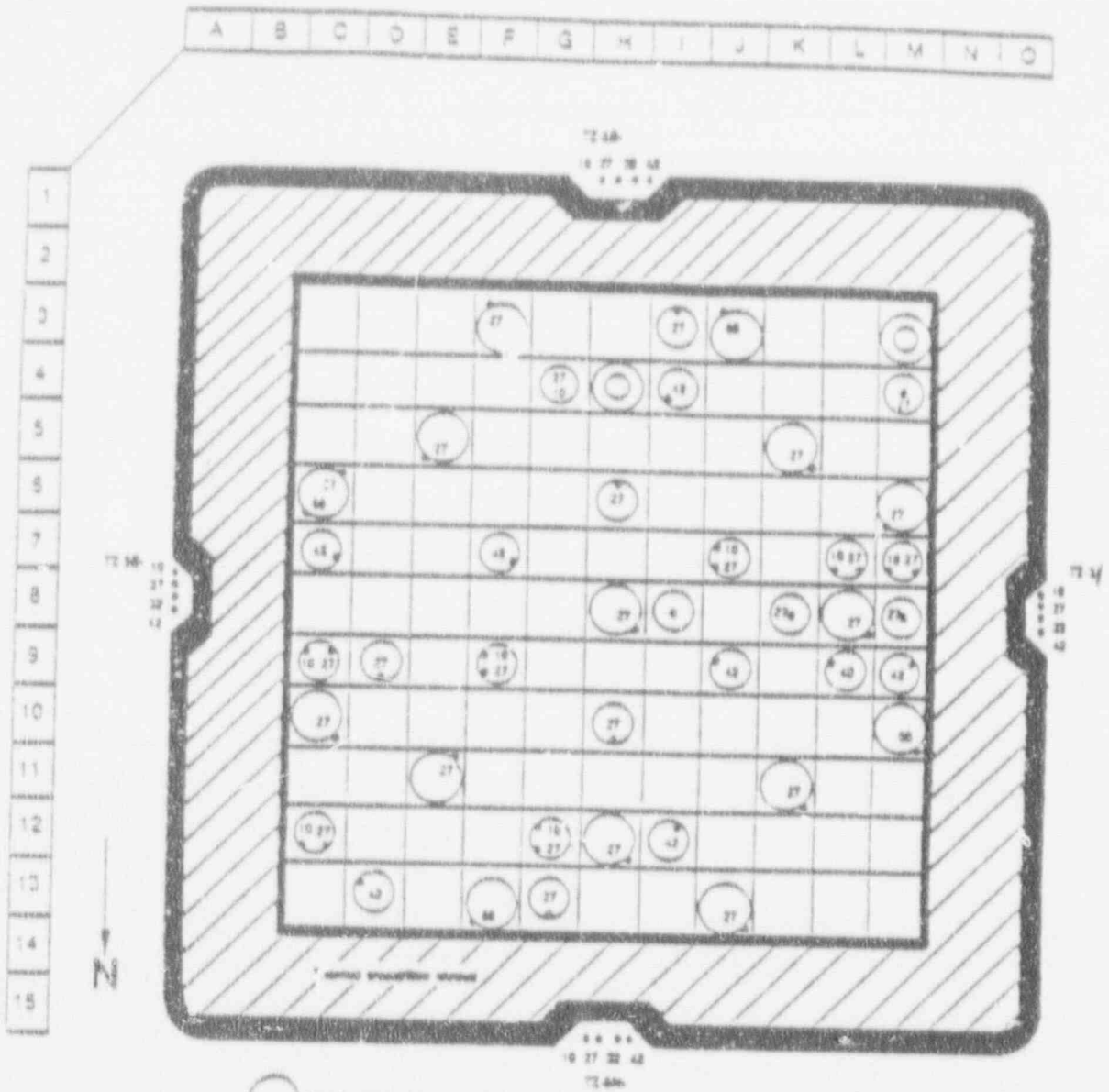
To meet the above facility requirements, a center fuel module was specially designed and fabricated for the experiment (see figure 2.4). The fuel module consisted of 11 control rods, 100 prepressurized (2.41 MPa, 350 psi) fuel rods enriched to 9.744-wt% U^{235} , and 10 instrumented guide tubes. The CFM was separated from the peripheral fuel assemblies by a 0.025-m (1-in.) thick, zircaloy cladding, zirconium-oxide insulated thermal shroud. The center fuel assembly was designed to enable the 9.744-wt% enriched fuel rods, or simply referred to as the test rods, to heatup above 2100 K (3320°F), while maintaining the peripheral fuel rods below 1390 K (2044°F) for a sufficient period of time to allow for fission product release and transport.




Table 2.1 gives a more detailed description of the fuel used for the LP-FP-2 experiment.

The two LOFT ECC systems are capable of simulating the emergency injection of a commercial PWR. Each of them consists, of an accumulator, a high-pressure and a low-pressure injection systems. There were no programmatic considerations inherent in ECC operation; therefore, the ECC injection was not scaled to represent commercial PWR operations during Experiment LP-FP-2.

The LOFT steam generator, located in the intact loop, is a vertical U-tube design steam generator. Operation of the secondary coolant system during Experiment LP-FP-2 approximated that of a commercial PWR.

A complete Fission Product Measurement System (FPMS) was designed and fabricated for the detection, identification and collection of radioactive



-  Instrumented guide tube
 -  Instrumented fuel pin
 -  Neutron flux scan tube (tip)
- Note: Thermocouple at location 27-42 failed prior to bundle installation

5 0983

Figure 2.4 CPM Instrumentation.

TABLE 2.1. LP-7P-2 FUEL DESCRIPTION

Fuel Rod Parameters

Active Length	1.67 m
Cladding OD	10.7 mm
Cladding Thickness	0.62 mm
Cladding material	Zr-4
Gap thickness	0.305 mm

Fuel Bundle Parameters

Number of Fuel Rods, Outer Square Bundles	204
Number of Fuel Rods, Corner Bundles	70
Number of Fuel Rods, Center Bundle	100
Total number of Fuel Rods	1196
Rod Array, Square and Center	15 x 15
Rod Array, Corner	12 x 12, triangular
Rod Pitch, in.	0.563

Fuel Parameters

	<u>CFM</u>	<u>Peripheral</u>
Total UO ₂ per pin	1.137 kg	1.134 kg
Fuel Density	93%	93%
Enrichment	9.744 wt%	4.05 wt%

Control Rod Parameters

Total control rods in core	80
CFM control rods for aerosol source	10
Cladding material	304 SS
Cladding thickness	0.51 mm
Poison Material	80Ag-15In-5Cd
Poison Rods per Cluster	20

CFM Thermal Shield

Cladding material	Zr-4
Outer Cladding thickness, mm	3.175
Inner Cladding thickness, mm	0.62
Insulation material	ZrO ₂
Insulation density	
lower section (0-0.30m)	2160-2480 kg/m ³
second section (0.30-0.91m)	2000-2160
third section (0.91-1.42m)	2160-2480
top section (1.42-1.76m)	2480-2720
Total shield thickness, mm	29.2
Total shield height, m	1.76

isotopes in the LOFT PCS, LPIS, and SST. This system, illustrated in Figure 2.5, consisted of three basic subsystems: (a) four gamma spectrometer systems and one gross gamma detector, (b) a deposition sampling system, and (c) filter sampling systems. Each of these subsystems is fully described in reference 9. Because the object of our analysis are only the thermal-hydraulic conditions during the LP-FP-2 transient we do not get into further details of the FPMS.

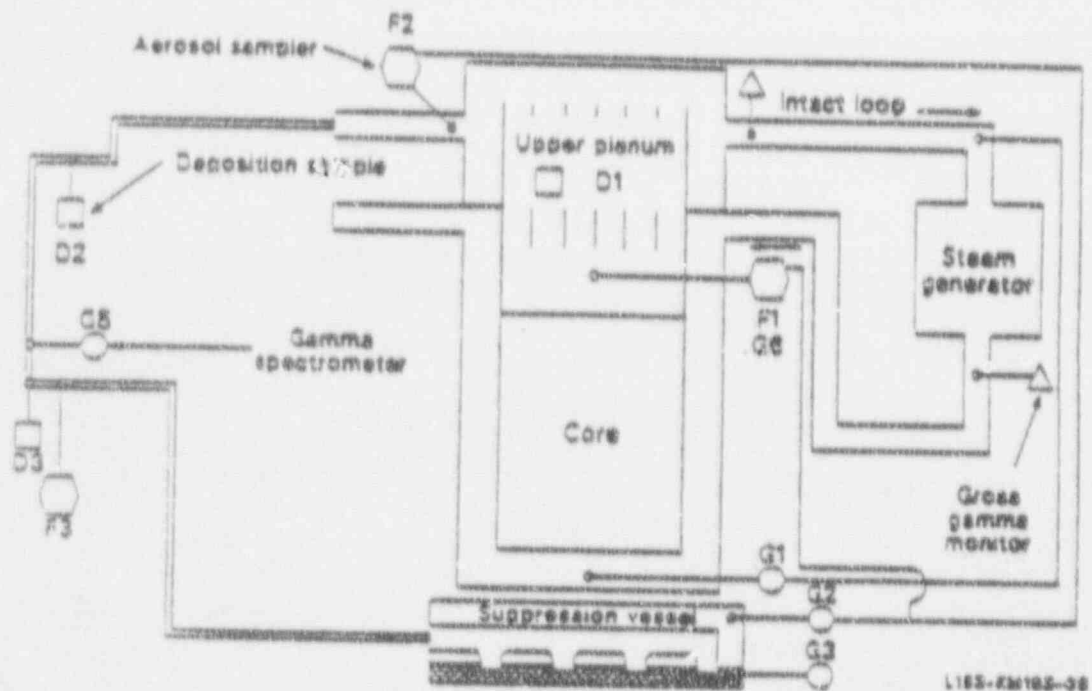


Figure 2.5 Schematic diagram of the LOFT system showing the relative positions of FPMS instrumentation.

Additional details of the LOFT system and the instrumentation can be found in Appendix A and in reference 9.

2.3. Experiment Description

Experiment LP-FP-2 consisted of four distinct phases: (a) fuel preconditioning, (b) pretransient, (c) transient and (d) posttransient. The four phases were contiguous; however, each phase had a specifically defined beginning and ending. The fuel preconditioning and posttransient phases of the experiment consisted of relatively long periods of time as compared with the much shorter pretransient and transient phases.

The purpose of the fuel preconditioning phase, in conjunction with the pretransient phase, was to subject the CFM fuel rods to a minimum burnup of 325 MWD/MTU. This was achieved by operating the LOFT reactor at a thermal power of 32 MW for 84 h, shutting down for 75 h, and then operating at 26.5 MW for a period of 80 h. The burnup that the CFM received during this initial preirradiation period is calculated to be 346 MWD/MTU.

The pretransient phase consisted of a reactor shutdown interval of about 96 h, followed by a power operation interval. The purpose of the final irradiation period was to finish the planned burnup on the CFM and to establish the initial conditions for the experiment. Figure 2.6 shows the preexperiment power history for the LP-FP-2 experiment. The initial condition requirements included a core decay heat of between 675 kW and 695 kW at 200 s following

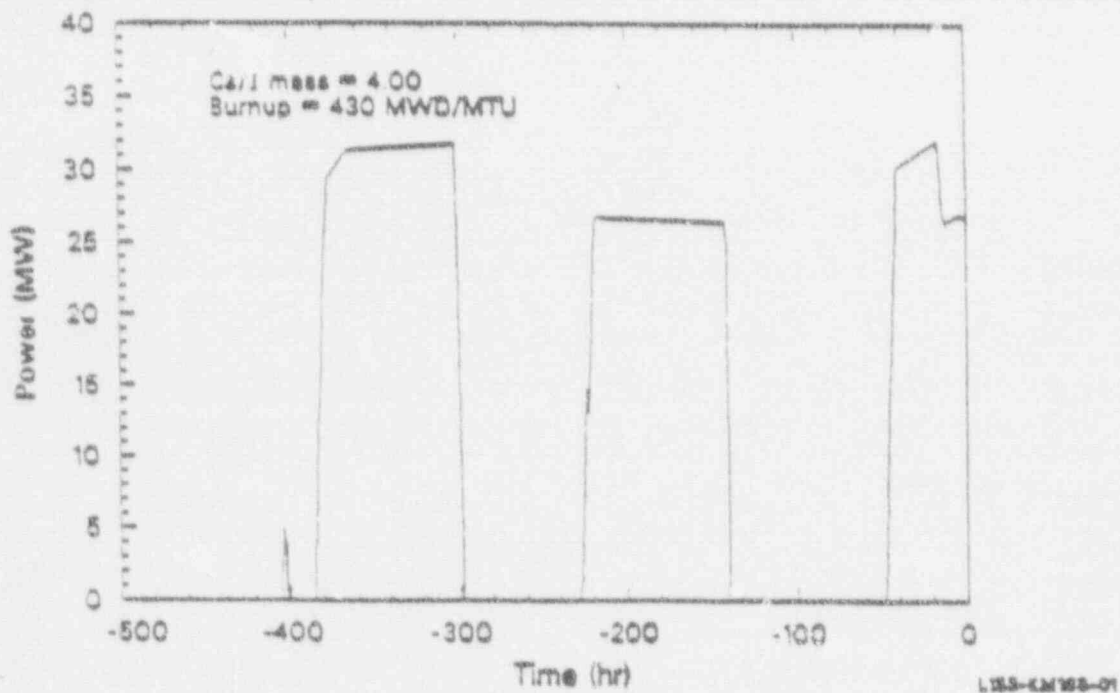


Figure 2.6. Preexperiment power history

reactor scram, and also the establishment of typical pressure, temperature, and flow conditions that would simulate a commercial PWR. This phase of the experiment immediately followed the termination of the preconditioning phase and ended with the initiation of the transient phase at t_0 (reactor scram). The pretransient included the operation of the LOFT reactor at an average thermal power of 31 MW for 26 h, followed by 15 additional hours of irradiation at approximately 26.5 MW. The estimated burnup on the CFM following this irradiation was 84 MWD/MTU. Consequently, the total burnup on the CFM prior to test initiations was 400 MWD/MTU. The ORIGEN2 calculated core decay heat at 200 s was 684.1 kW, well within the planned limits³.

The actual burnup on the CFM was much higher than originally planned. This occurred because the LP-FP-2 Experiment was initially planned to be run on July 3 with a CFM burnup of 346 MWD/MTU; however, the CFM control rods would not fall during this first attempt and the experiment had to be aborted. It was later discovered that high flow conditions in the core caused this condition and tripping the primary coolant pumps (PCPs) early into the transient would allow the CFM control rods to fall. The LP-FP-2 Experiment was successfully run 6 days later on July 9. A serendipitous result of the extended down time and extra irradiation was the achievement of a higher Cs to I ratio than originally predicted (e.g., 4.0 vs. 2.9).

The LP-FP-2 transient was initiated by a reactor scram at 14:07:44.9 on July 9, 1985 (defining t_0), followed by the insertion of the CFM control rods 2.4 s later. The main purpose of the CFM control rods was to provide Ag/In/Cd material for aerosol generation and deposition sites for fission products during the high temperature portion of the experiment, as would be present in a PWR during a V-sequence accident. The break line in the intact loop cold leg (ILCL) was opened at 32.9 s to begin depressurization of the PCS. At 221.6 s the other break line, which simulated the LPIS, was opened in the broken loop hot leg (BLHL). The ILCL break was closed after 735.5 s in accordance with the experiment operational specifications³. However, the subsequent system depressurization was much slower than expected and the pressure remained too high for operation of the fission product measurement system (FPMS).

In order to reduce the system pressure below 200 psi (1.38 MPa), the ILCL break was reopened at 877.6 s, and the PORV from the pressurizer was opened at 882 Sec. With the PORV, ILCL, and LPIS lines open, the PCS pressure fell below

the 1.38 MPa (200 psig) design limit for operation of the FPMS at 1013 s. The ILCL break was then closed at 1021.5 s, and the PORV was closed at 1162 s. The core was allowed to uncover and to heatup, resulting in the failure of the control rods and fuel rods in the CFM. Fission products were first detected at about 1200 s in the F1 and F2 sample lines. The experiment was continued until about 1766 s when a high temperature trip on the exterior wall of the CFM shroud was reached. By that time, the CFM had reached an estimated maximum temperature in excess of 2400 K (3860°F) and had been above 2100 K (3320°F) for at least 4.5 min. The emergency core cooling system (ECCS) was then activated at 1782.6 s and the core was quenched by 1795 s.

The final, or posttransient phase of the experiment consisted of a time interval of 44 days during which the redistribution of fission products in the gas and liquid volumes in the blowdown suppression tank and the leaching of fission products from the damaged fuel rods in the CFM were measured. This phase began at the closure of the simulated LPIS line, which terminated the lowdown and initiated the reflood of the reactor vessel, and ended 44 days later.

3. SUMMARY OF THE THERMAL/HYDRAULIC DATA

This section summarizes the thermal/hydraulic (TH) measured data of the system prior to and during fission product release and transport and has been taken from the QLR². Included are the hydraulic response during the blowdown, the fluid and metal temperatures during fission product release and transport, and the fuel rod cladding response during the blowdown and heatup phases. Reference 9 gives a full description of the TH results.

Table 3.1. lists the specified and measured system conditions immediately prior to the LP-FP-2 transient. Except for the liquid level in the BST, all initial conditions were within the limits specified in the Experiment Specification Document (ESD)². Since no attempt had been made to use the BST to simulate a containment vessel, this single out-of-specification value did not affect the outcome of the experiment.

The significant events for Experiment LP-FP-2 are chronologically listed in Table 3.2. The intact loop pressure history is shown in Figure 3.1 along with the identification of important events.

The LP-FP-2 transient was initiated by scrambling the reactor with the peripheral control rods, which defined t_0 . The primary coolant pumps (PCPs) were then turned off at about 10 s (or t_0+10 s; note that all experiment times are referenced relative to t_0). After the PCS flow had decreased to 190 kg/s (1.5×10^5 lbm/h) at 22 s, the center fuel assembly control rods were unlocked from the D1 device and allowed to fall into the CFM. At 24 s the control rods were fully inserted in the core. The ILCL break was then opened at 33 s, and the LPS line was opened at 222 s. The core started heating up when the liquid level decreased in the peripheral bundles at 662 s. The CFM began heating up at 689 s. The ILCL break was closed at 736 s; however, it was reopened at 878 s to accelerate the PCS depressurization rate.

Table 3.1 Initial conditions for experiment LP-FP-2

Parameter	Specified ^a Value	Measured Value
Primary Coolant System		
Core delta T (K)	--	11.7 ± 1.0
(°F)	--	21.1 ± 2.5
Primary system pressure (hot leg) (MPa)	14.95 ± 0.1	14.98 ± 0.1
(psia)	2168 ± 15.0	2173 ± 15
Hot leg temperature (K)	571 ± 1.1	571.6 ± 0.8
(°F)	569 ± 2	569.2 ± 1.4
Cold leg temperature (K)	--	559.9 ± 1.1
(°F)	--	548.2 ± 2
Loop mass flow (kg/s)	479 ± 19	475 ± 2.5
(lbm/h × 10 ⁶)	3.8 ± 0.15	3.77 ± 0.02
Boron concentration (ppm)	--	499 ± 15
Primary coolant pump injection (both pumps) (L/s)	0.127 ± 0.016	0.128 ± 0.003
(gpm)	2.0 ± 0.25	1.98 ± 0.02
Reactor Vessel		
Power level (MW)	26.5 ± 0.5	26.8 ± 1.4
Decay heat (200 s) (kW)	685 ± 10	684.8
Maximum linear heat generation rate (kW/m)	40 ^c	42.6 ± 3.6
(kW/ft)	12 ^c	12.97 ± 1.1
Control rod position (above full-in position) (m)	1.37 ± 0.01	1.38 ± 0.01
(in.)	54.0 ± 2.0	54.3 ± 2.0
Steam Generator		
Secondary system pressure (MPa)	--	6.38 ± 0.08
(psia)	--	925 ± 12
Water level ^d (m)	--	0.17 ± 0.06
(in.)	--	6.7 ± 2.4

Table 3.1. (continued)

Parameter	Specified ^a Value	Measured Value
Pressurizer		
Liquid volume (m ³)	--	0.57 ± 0.03
(ft ³)	--	20.13 ± 1.06
Steam volume (m ³)	--	0.37 ± 0.03
(ft ³)	--	13.07 ± 1.06
Water temperature (K)	--	616.9 ± 2.1
(°F)	--	650.8 ± 3.8
Pressure (MPa)	--	15.1 ± 0.1
(psia)	--	2150 ± 14.5
Liquid level (m)	1.12 ± 0.1	1.06 ± 0.06
(in.)	44 ± 4	44.4 ± 2.4
Suppression Tank		
Liquid level (m)	1.19 + 0.051	1.18 ± 0.06
(in.)	- 0.0	
	47.0 + 2	46.5 ± 2.4
	- 0.0	
Gas volume (m ³)	--	59.11 ± 2.02
(ft ³)	--	2087 ± 71
Water temperature (K)	<311	295.6 ± 0.5
(°F)	<100	72 ± 1
Pressure (gas space) (kPa)	100 ± 20	95 ± 3
(psia)	14.7 ± 3	13.8 ± 0.4
Boron concentration (ppm)	--	3710 ± 15

Table 3.1. (continued)

Parameter	Specified ^a Value	Measured Value
Emergency Core Cooling System		
Borated water storage tank Temperature (K)	303 ± 3	301.3 ± 3
	85 ± 5	82 ± 5
Accumulator A liquid level (m)	<2.17	1.81 ± 0.02
	<86	71.3 ± 0.8
Accumulator A pressure (MPa)	>4.21	5.1 ± 0.06
	>611	740 ± 9
Accumulator A liquid temperature (K)	303 ± 3	303.1 ± 0.7
	85 ± 5	86 ± 1.3
Accumulator B liquid level (m)	<2.16	1.81 ± 0.02
	<86	71 ± 0.8
Accumulator B pressure (MPa)	>4.21	4.95 ± 0.06
	>611	718 ± 9
Accumulator B liquid temperature (K)	303 ± 3	305.6 ± 0.7
	85 ± 5	90.4 ± 1.3

a. If no value is listed, none was specified.

b. Steam generator liquid level referenced to 2.95 m (116 in.) above the top of the tube sheet.

c. Approximately equal to this value.

Table 3.2. Chronology of events for experiment LP-PP-2

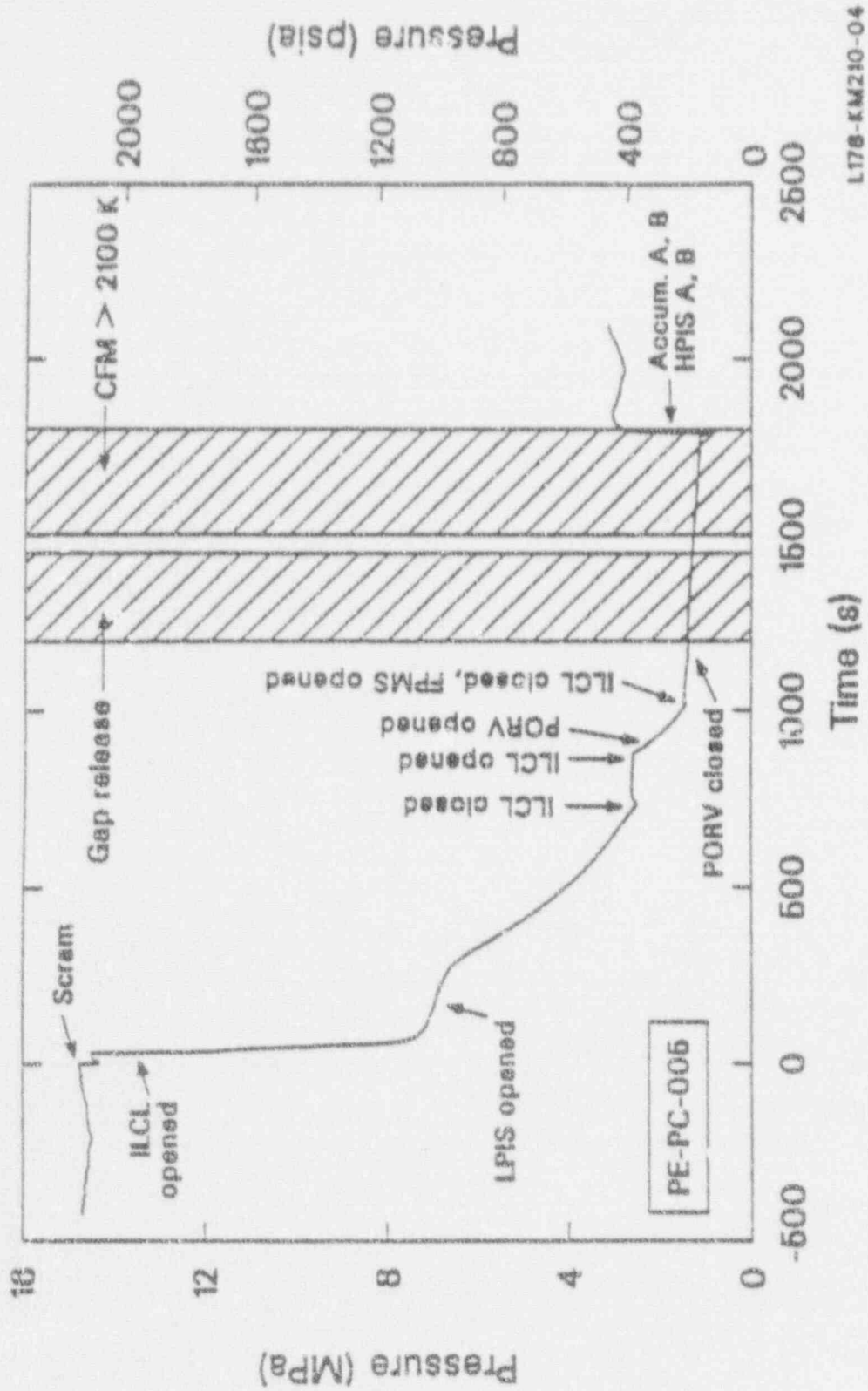
Event	Time After Experiment Initiation (s)
Scram	0.0
Control rods fully inserted	2.4 ± 0.1
PCP coastdown initiated	9.7 ± 0.1
CFM control rods fully inserted	23.4 ± 0.5
ILCL break initiated	32.9 ± 0.1
PCP coastdown complete ^a	25.1 ± 0.1
End of subcooled blowdown ^b	53 ± 1
Secondary relief valve cycle	56 ± 1
Pressurizer empty	60 ± 5
LPIS line break initiated	221.6 ± 0.1
Secondary pressure exceeded primary system pressure	260 ± 10
Earliest coolant thermocouple deviation from saturation (voidage at that location)	
Upper plenum	300 ± 10
Hot leg pipe	390 ± 10
Downcomer	730 ± 10
Lower plenum	800 ± 20
Fuel rod cladding heatup started in PFM	662 ± 2
Fuel rod cladding heatup started in CFM	689 ± 2
ILCL break closed	735.5 ± 0.1
ILCL break reopened	877.6 ± 0.1
PORV opened	882.0 ± 0.1
F3 filter on line	950.8 ± 0.1
LPIS bypass closed	951.9 ± 0.1
FPMS lines opened	1013.1 ± 0.1

Table 3.2. (continued)

Event	Time After Experiment Initiation (s)
ILCL closed	1021.5 ± 0.1
PORV closed	1162.0 ± 0.1
First indication of (gap) fission products at F1	1200 ± 20
First indication of (gap) fission products at F2	1200 ± 20
First indication of (gap) fission products at F3	1249 ± 60
Peripheral fuel cladding reached 1460 K (2172°F)	-- ^c
Maximum upper plenum coolant temperature reached ^d	1495 ± 5
First indication of (fuel) FPs at F1, F2, and F3	1500 ± 10
Cladding temperatures reach 2100 K (3320°F)	1504 ± 1
Shroud temperature reached trip setpoint	
1st thermocouple	1743 ± 1
2nd thermocouple	1766 ± 1
Maximum cladding temperature reached	-- ^e
LPIS line break closed	1777.6 ± 0.1
FPMS lines closed	1778.1 ± 0.1
Maximum upper plenum metal temperature reached ^d	1780 ± 5
Deposition coupons isolated	1780.6 ± 0.1
ECCS initiated	1782.6 ± 0.1
Accumulator flow stopped	1795 ± 2
Maximum LPIS line coolant temperature reached	1800 ± 5
Core quenched	1795 ± 5 ^f
Cooldown initiated	-- ^f
Steam generator feed-and-bleed started	2600 ± 10
PORV opened	3350 ± 10
PORV closed	3380 ± 10
PORV opened	3680 ± 10
PORV closed	3690 ± 10
Experiment terminated	-- ^g

Table 3.2. (continued)

- a. The pumps were allowed to coastdown under the influence of the motor generator flywheel until the pump speed reached 750 rpm. At that time, the flywheel was disconnected from the motor generator and the pumps quickly stopped adding energy to the fluid. The time at which the flywheel was disconnected is defined as the time the PCP coastdown was complete.
- b. End of subcooled blowdown is defined as the time when the first measured fluid temperature outside of the pressurizer reaches saturation conditions.
- c. None of the cladding thermocouples in the peripheral fuel bundle measured validated temperatures above the setpoint. The two that gave readings above this setpoint failed before reaching the setpoint.
- d. These temperatures represent the maximum measured temperatures before reflood at these locations. The thermocouple output during reflood could not be interpreted.
- e. Because of the large number of cladding thermocouples in the central fuel module that failed at high temperatures during the transient, it is not possible to determine the precise maximum temperature or the time at which it occurred. The time is estimated to be between 1782 and 1795 s. The maximum temperature exceeded 2400 K (3860°F) based on extrapolations from valid temperature readings before thermocouple failure.
- f. The peripheral fuel modules were quenched by 1793 s. Most of the central fuel module cladding thermocouples were quenched by 1795 s. Some isolated thermocouples indicated persistent high (superheated) temperatures a few minutes later. Interpretation of the temperature data is complicated by the large number of thermocouples in the center fuel module that failed during or just before reflood.
- g. Because of the high background in the area surrounding the G1, G2, and G3 spectrometers, data were collected for several weeks after termination of the thermal transient.



L178-KM210-04

Figure 3.1. Primary system pressure history showing significant events.

In addition to reopening the ILCL break, the PORV was opened at 882 s. After the system pressure dropped below 200 psi (1.38 MPa), the ILCL and PORV lines were closed at 1022 and 1162 s, respectively. Fission product activity was first detected in the F1 and F2 lines at about 1200 s. The hottest measured cladding temperatures reached 2100 K (3320°F) by 1504 s. The transient continued until the outer shroud wall temperature limitation of 1517 K (2272°F) was reached at 1766 s. Subsequently, the FPMS lines were isolated at 1777 s and ECCS injection was initiated at 1783 s. The core was quenched at 1795 s (although a few isolated thermocouples indicated temperatures in excess of saturation for several minutes thereafter), and the plant was maintained in a quiescent state for 14 days while fission product measurements were taken using the on-line measurements systems. Also, batch samples were taken from the BST and PCS for several days: BST liquid samples (21 d), BST vapor samples (28 d), and PCS liquid samples (44 d). During the early part of the cooldown or posttransient phase, the PORV was cycled twice (see Table 3.2) to prevent the PCS from overpressurizing, and a feed-and-bleed operation on the steam generator was initiated.

3.1. Blowdown Hydraulics

This section discusses the reactor vessel liquid level, PCS mass inventory, center fuel module mass flow rate, and PCS reflood.

The experiment hydraulics resulted in a gradual PCS level decrease and, ultimately, in a slow core boil-off. The loops began to void at approximately 50 s (intact loop hot leg) as shown in Figure 3.2, which compares the individual average chordal densities measured by the gamma densitometer in this leg. The level decreased until the loops were completely voided by 470 s (bases on dryout of thermocouples in the upper plenum). The upper plenum was voided by approximately 600 s and the level continued to drop, entering the top of the core by 700 s. The entire core was voided by approximately 1355 s as indicated by the level probe in the 3rd. fuel module. The data from this probe are shown in Figure 3.3. As discussed below, the completion of voiding as indicated by the level probe occurred more than 300 s after all cladding thermocouples in the core indicated heatup.

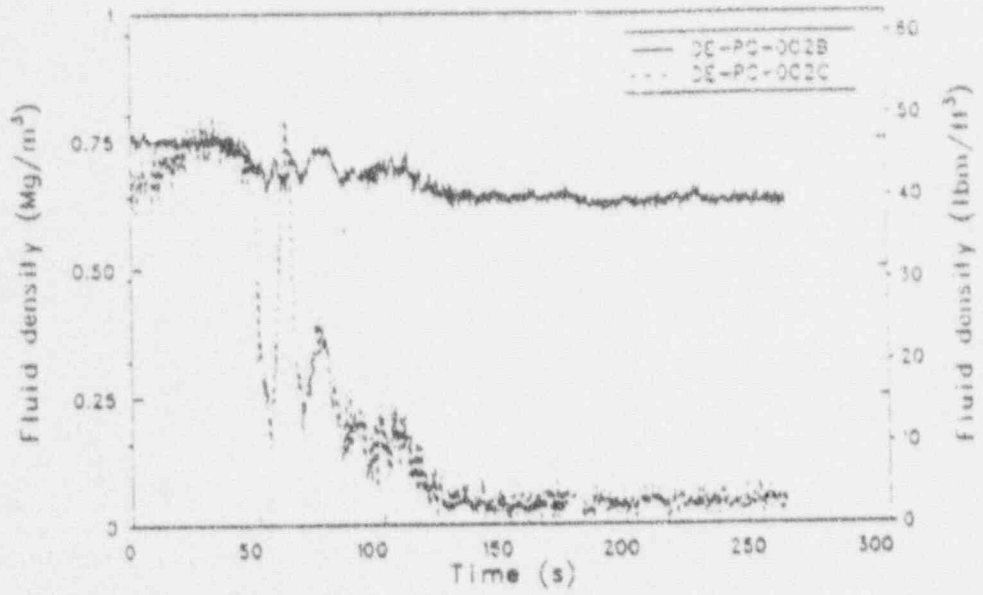
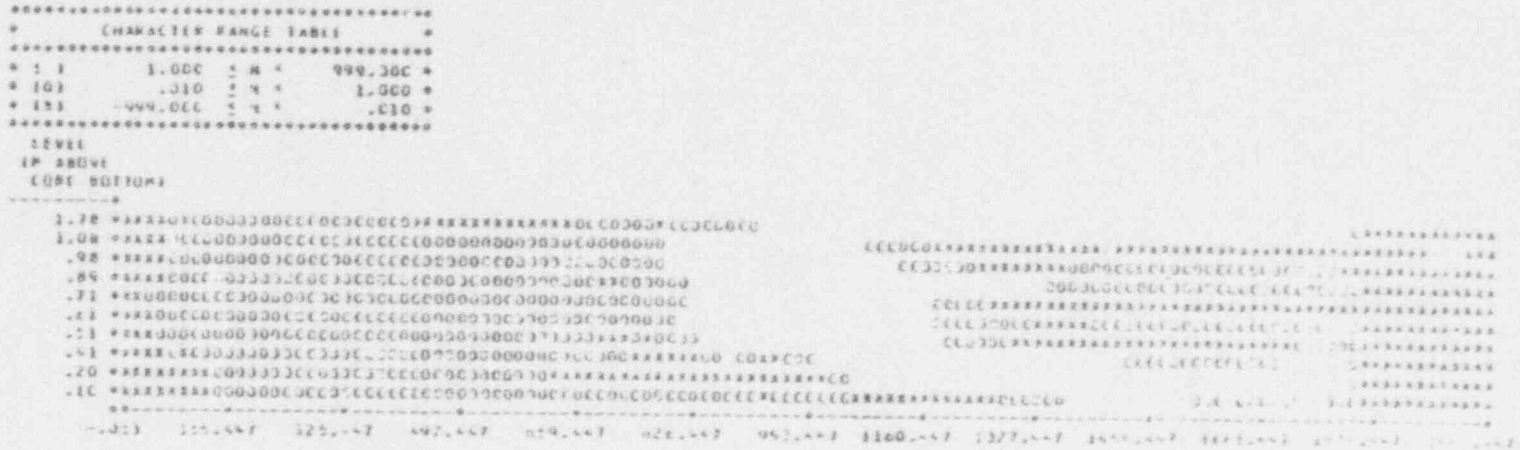


Figure 3.2. Intact loop hot leg density

CONDUCTIVITY PROBE RESPONSE ABOVE FUEL ASSEMBLY 3.



10
00

Figure 3.3. Conductivity level probe response above Fuel Assembly 3.

The PCS mass inventory declined to a minimum of approximately 500 kg (based on the blowdown suppression tank level increase) by 1300 s. At that time, the center fuel module mass flow had decreased to approximately 0.04 kg/s (this mass flow rate was calculated from the measured cladding temperature response; the details of the calculation can be found in Reference 9) and the flow out the LPIS line, to approximately 0.3 kg/s. This mass flow, though very small, was sufficient to sustain a rapid metal-water reaction in much of the central fuel module as the temperatures increased above 1700 K (2600°F). The center fuel module mass flow resulted in an average of 0.4 gm/s/fuel rod (0.04 kg/s per 100 fuel rods). Data from the Power Burst Facility indicate that flows as little as 0.1 g/s/fuel rod are sufficient to sustain the metal-water reaction without steam starvation¹².

When the shroud temperatures reached the experiment termination setpoint of 1517 K (2272°F), the FPMS and LPIS lines were closed and reflood of the plant was initiated using both ECC systems. Rapid injection of approximately 1000 kg (2200 lbm) of water from the accumulators resulted in a PCS repressurization from 1.2 to approximately 3 Mpa (174 to 435 psia). This caused the accumulator flow to momentarily cease. Additional cycles of accumulator flow and PCS repressurization were required before all of the damaged core could be quenched; the ECCS was fully capable of accomplishing this and the plant was in a safe shutdown condition within a few hundred seconds of ECCS injection initiation. The peripheral fuel rods quenched rapidly, in a manner similar to previous LOFT core uncover experiments. Most of the center fuel module also quenched rapidly, though more slowly than in previous experiments. A small fraction of the center fuel module, however, took much longer to quench, indicating the disruption of the fuel rod geometry in part of this module.

3.2 Core Thermal Response

This section summarizes the fuel rod cladding temperature response, including the initiation of dryout at various core locations, the effect of control rod melting on the thermal response, the occurrence and propagation of a rapid metal-water reaction, and the quench of the core during reflood.

The temperature excursion began in the upper part of the peripheral fuel modules at 662 s and moved downwards as the coolant boiled away. The propagation of the core heatup was generally top-to-bottom in the peripheral

module, with the dryout reaching elevations of 1.14, 0.38, and 0.28 m (45.1-, and 11 in.) above the core bottom at 662, 730 and 930 s, respectively. This is illustrated in figure 3.4, which compares cladding and saturation temperatures at these elevations in the 2nd fuel module. The quench at the 10-in. elevation associated with the opening of the PORV is also seen. Figure 3.5 is a similar figure for the central fuel module, with temperatures shown from the 1.07-, 0.69-, and 0.25-m (42-, 27-, and 10-in.) elevations. The dryout started a little later in this module, with the corresponding times being 689, 740 and 938 s, respectively.

At approximately 1050 K (1430°F), the guide tube temperatures responded to a phenomena that is thought to be connected with melting of the absorber material (Ag-In-Cd) at the 0.69-m (27-in.) elevation. The temperatures on guide tubes 5J13 and 5K08 both show a definitive decrease in the heatup rate (from 1.2 K/s down to 0.7 K/s) which is interpreted as resulting from the melting of the control rod material in these guide tubes. The argument is that the latent heat of melting absorbed some of the decay heat, causing a decrease in the heatup rate. This is consistent with the observation that the heatup rate of guide tube 5H08, which does not contain a control rod, was not similarly affected. Figure 3.6 compares these three temperatures. The latent heat associated with the melting of the control rods could account for a temperature shift of up to 280 K (504°F). The difference between this value and the 50 K (90°F) measured shift could be explained by the metal-water reaction, which was occurring at that time.

At about 1550 s, several control rod guide tube thermocouples at the 27-inch elevation showed a small discontinuity that is thought to be associated with the failure of the rod (see, for example, Figure 3.5). This occurred at approximately 1200 K (1700°F). Once again, the effect is absent from thermocouple TE-5H08-027, which is in an empty guide tube.

The first recorded and qualified rapid temperature rise associated with the rapid reaction between zircaloy and water occurred at about 1430 s and 1400 K on a guide tube at the 0.69-m (27-in.) elevation. This temperature is shown in Figure 3.7. A cladding thermocouple at the same elevation (see Figure 3.7) reacted earlier, but was judged to have failed after 1310 s, prior to the rapid temperature increase. Note that, due to the limited number of measured cladding temperature locations, the precise location of the initiation of metal water reaction on any given fuel rod or guide tube is not likely to

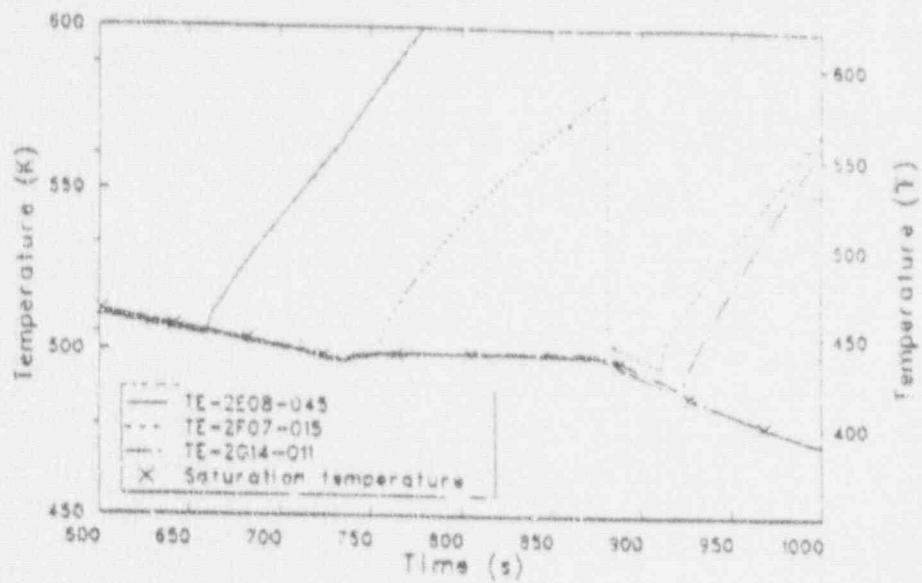


Figure 3.4 Comparison of cladding temperatures at the 1.14-, 0.38-, and 0.28-m (45-, 15-, and 11-in.) elevations in Fuel Assembly 2 with saturation temperature.

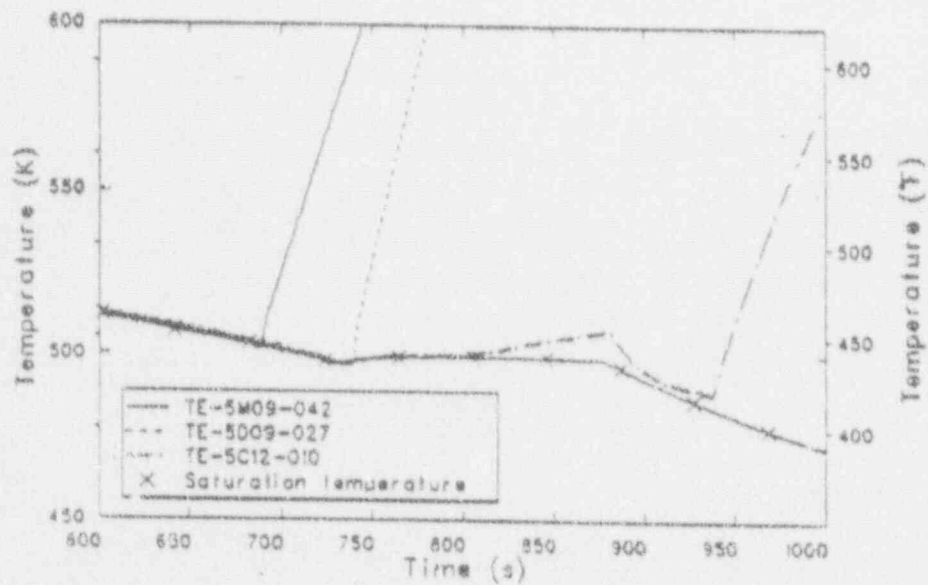


Figure 3.5 Comparison of cladding temperatures at the 1.07-, 0.69-, and 0.25-m (42-, 27-, and 10-in.) elevations in Fuel Assembly 5 with saturation temperature.

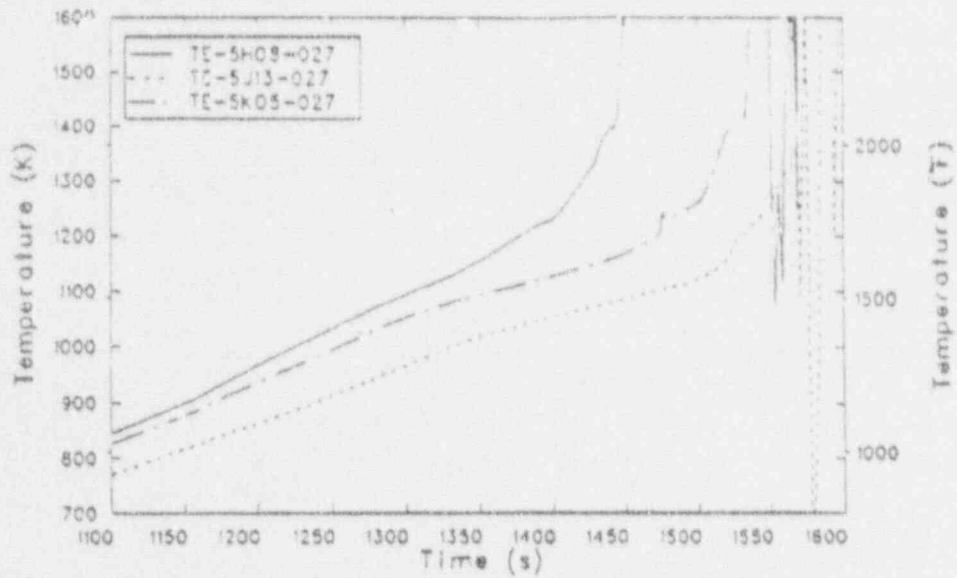


Figure 3.6 Comparison of three guide tube temperatures at the 0.69-m (27-in.) elevation in Fuel Assembly 5.

coincide with the location of a thermocouple. Thus, the temperature rises are probably associated with precursory heating as the metal-water reaction propagates away from the initiation point. Care must be taken in determining the temperature at which the metal water reaction initiates, since the precursory heating can occur at a much lower temperature. It can be concluded from examination of the recorded temperatures that the oxidation of zircaloy by steam becomes rapid at temperatures in excess of 1400 K (2060°F).

The temperatures in the center fuel module reached the target temperature of 2100 K (3320°F) due to the rapid reaction between the zircaloy and the steam, and remained above this temperature for four-and-a-half minutes. The maximum temperature reached is difficult to determine because of the failure of the thermocouples at the high temperatures experienced, but it was certainly in excess of 2400 K (3860°F).

During the transient, the temperatures on the outside of the shroud increased steadily from 740 to about 1700 s. This is illustrated in Figure 3.8, which compares the temperatures on the south side of the shroud. At approximately 1700 s, the heatup rate increases. At about the same time, the thermocouples near the outside of the shroud also start to heat up more rapidly. Figure 3.9 illustrates this by comparing the temperatures at various elevations in the 2nd fuel module, just adjacent to the shroud south wall. By the time the reflood turns the temperatures around (1785 s), all of these temperatures exceed the shroud temperatures at the same elevation. The cause of this rapid heatup is not presently known, but it may be an effect caused by the thermocouple leads passing through a hot area as they exit from the top of the core (shunting) rather than by a true local effect.

The cooling of the core took much longer than any previously measured quench in LOFT. This was in part due to the much higher temperatures that existed prior to quench (2400 K - 3860°F - for this experiment compared with the previous maximum of 1261 K - 1810°F - measured during Experiment LP- 1¹³). More important, however, is the geometry of the core during reflood. Relocation of the core undoubtedly resulted in masses of core material much thicker than normal. These masses would require much more time to cool than the ones corresponding to a

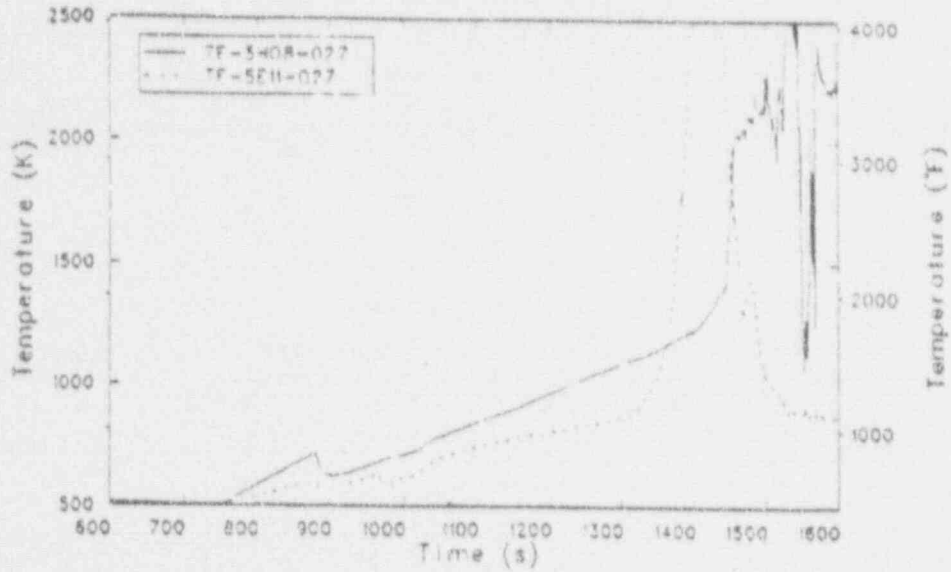


Figure 3.7 Comparison of two cladding temperatures at the 0.69-m (27-in.) elevation in Fuel Assembly 5.

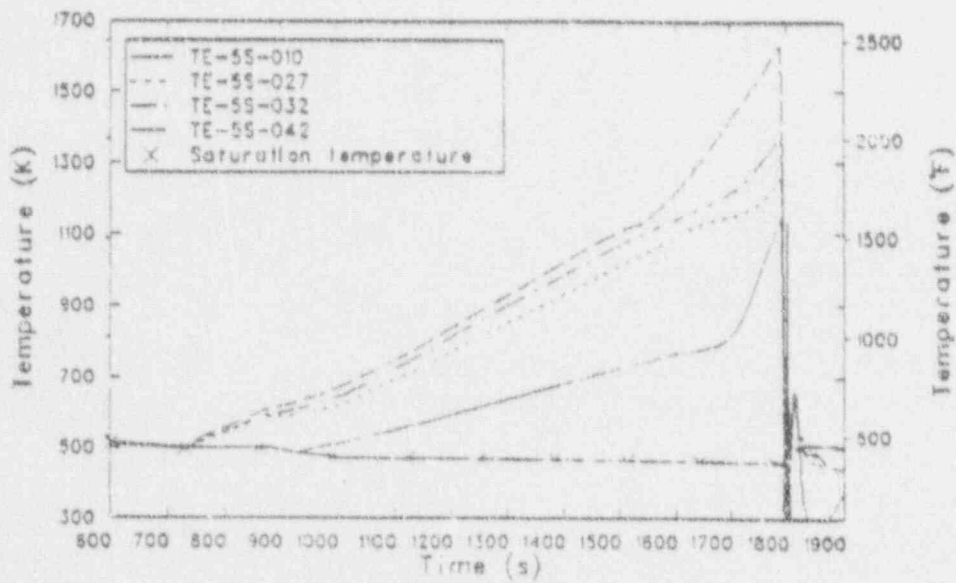


Figure 3.8 Comparison of four external wall temperatures at the 1.07-, 0.81-, 0.69-, and 0.25-m (42-, 32-, 27-, and 10-in.) elevations on the south side of the flow shroud.

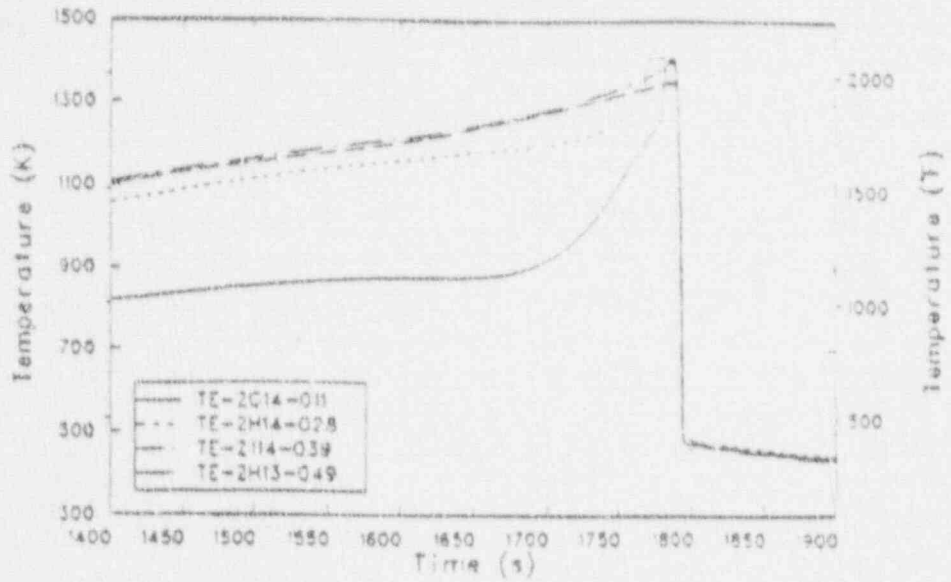


Figure 3.9 Comparison of cladding temperatures at the 1.24-, 0.99-, 0.71-, and 0.28-m (49-, 39-, 28-, and 11-in.) elevations in Fuel Assembly 2.

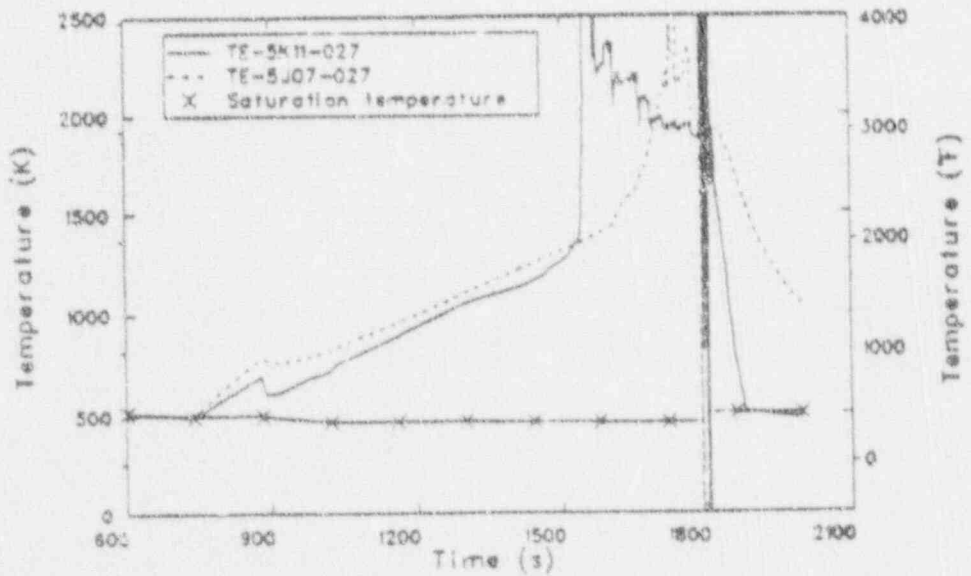


Figure 3.10 Comparison of two cladding temperatures at the 0.69-m (27-in.) elevation in Fuel Assembly 5 with saturation temperature.

regular fuel rod geometry. This is postulated to be the cause of the slow cooldown manifested by thermocouple TE-5007-C27 (failed), shown in Figure 3.10. (Even though this thermocouple failed, it is believed that the failure mode is a junction relocation and that the thermocouple is indicating a temperature at some location in the center fuel module). That thermocouple was slowly cooling towards saturation until 2010 s, when the junction apparently broke. Thus, even though the core had been essentially quenched for more than 200 s, the temperature was only slowly decreasing, indicating the insulating effect of a large mass of material surrounding the thermocouple.

4. RELAP5/MOD2 SIMULATION OF LP-FP-2 EXPERIMENT

4.1. General overview of the methodology used for the analysis

It is well known that RELAP5/MOD2 has not been designed to analyze severe accidents. In fact, to handle this limitation the Idaho National Engineering Laboratory (INEL) is developing a special severe core damage computer package called RELAP5/SCDAP¹⁰. The RELAP5/SCDAP computer code is the integration of three well known stand-alone codes: RELAP5/MOD2⁴, SCDAP/MOD1⁵ and TRAPMELT-2¹¹. The integrated code is being designed to perform best estimate analysis of the behaviour of a LWR under severe accident conditions.

However the actual version of the integrated code only runs in a CRAY machine. Because of the unavailability of any CRAY machine at Spain (by the time the group began the calculations) we were forced to use the same methodology decided for the Best Estimate Prediction (BEP)⁶ of the experiment, i.e.: passive coupling between the RELAP5/MOD2 and the SCDAP/MOD1 computer codes.

The fundamental idea of this methodology consists in simulating the general thermal-hydraulic behavior of the LOFT system using the RELAP5/MOD2 code; while the detailed core behavior is simulated using the SCDAP/MOD1 code.

A brief summary of the highlights of these two codes is presented in Appendix B. The interdependency between both codes is schematically shown in figure 4.1.

According to this passive coupling methodology, prior to the main driver RELAP5/MOD2 calculation, a first SCDAP run is required in order to estimate the core geometry changes (blockages) following the fuel damage. This first SCDAP calculation is, in turn, driven by a preliminary RELAP5/MOD2 run to provide the necessary boundary conditions for SCDAP (see figure 4.1.) Once the first SCDAP run is completed we have estimations for the amount of blockage due to the fuel cladding ballooning and rupture, the control rod material relocation due to the melting of the zircaloy at some corresponding temperatures. Now we can go further on doing the main RELAP5/MOD2 calculation making some core reinitializations at the previously determined corresponding temperatures (see figure 4.2.)

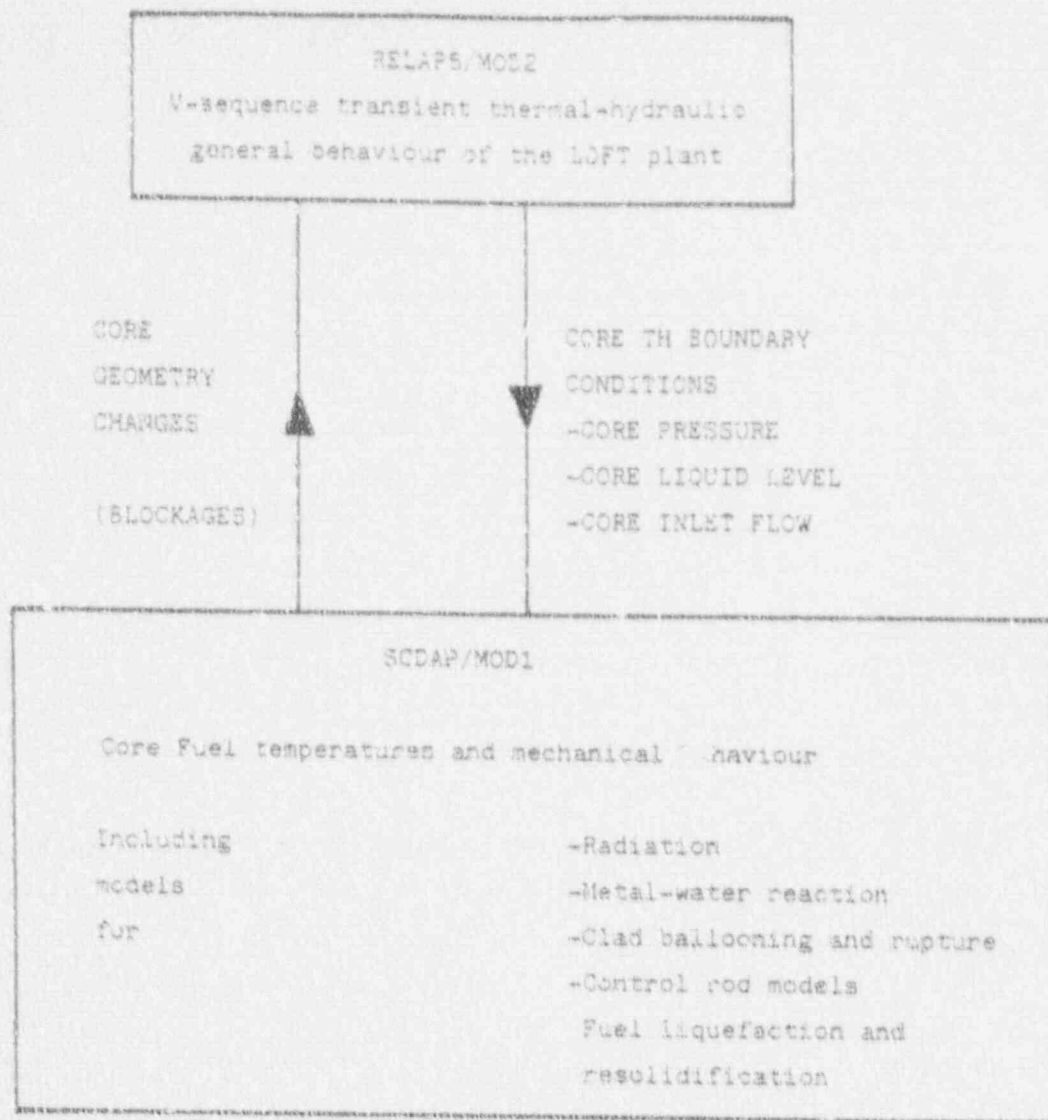


FIGURE 4.1 Flow chart of computer codes used in the analysis, showing the interdependency between them.

(PASSIVE LINK BETWEEN RELAPS/MOD2 AND SCDAP/MOD1)

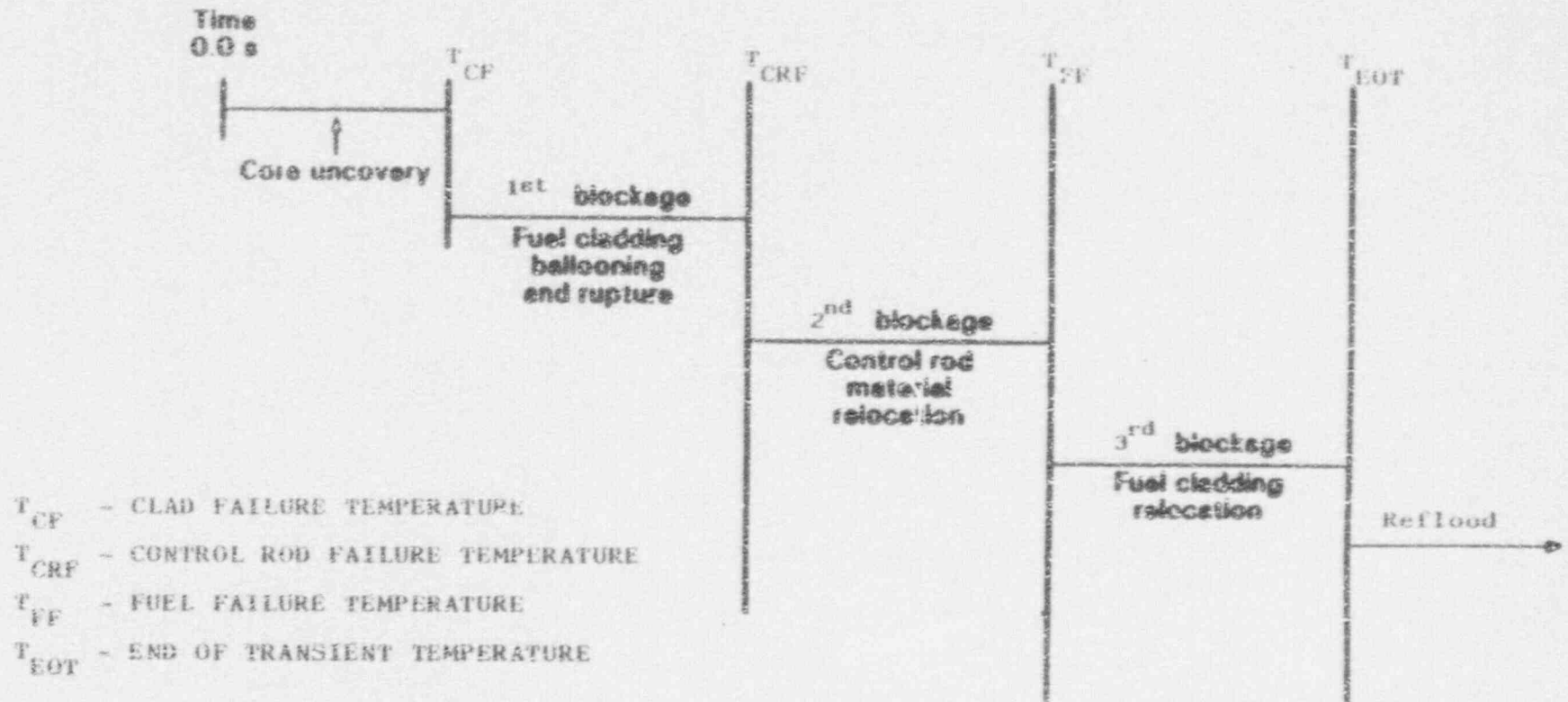


Figure 4.2 RELAP5/MOD2 calculational scheme, showing the interactions between RELAP5 and SCDAP.

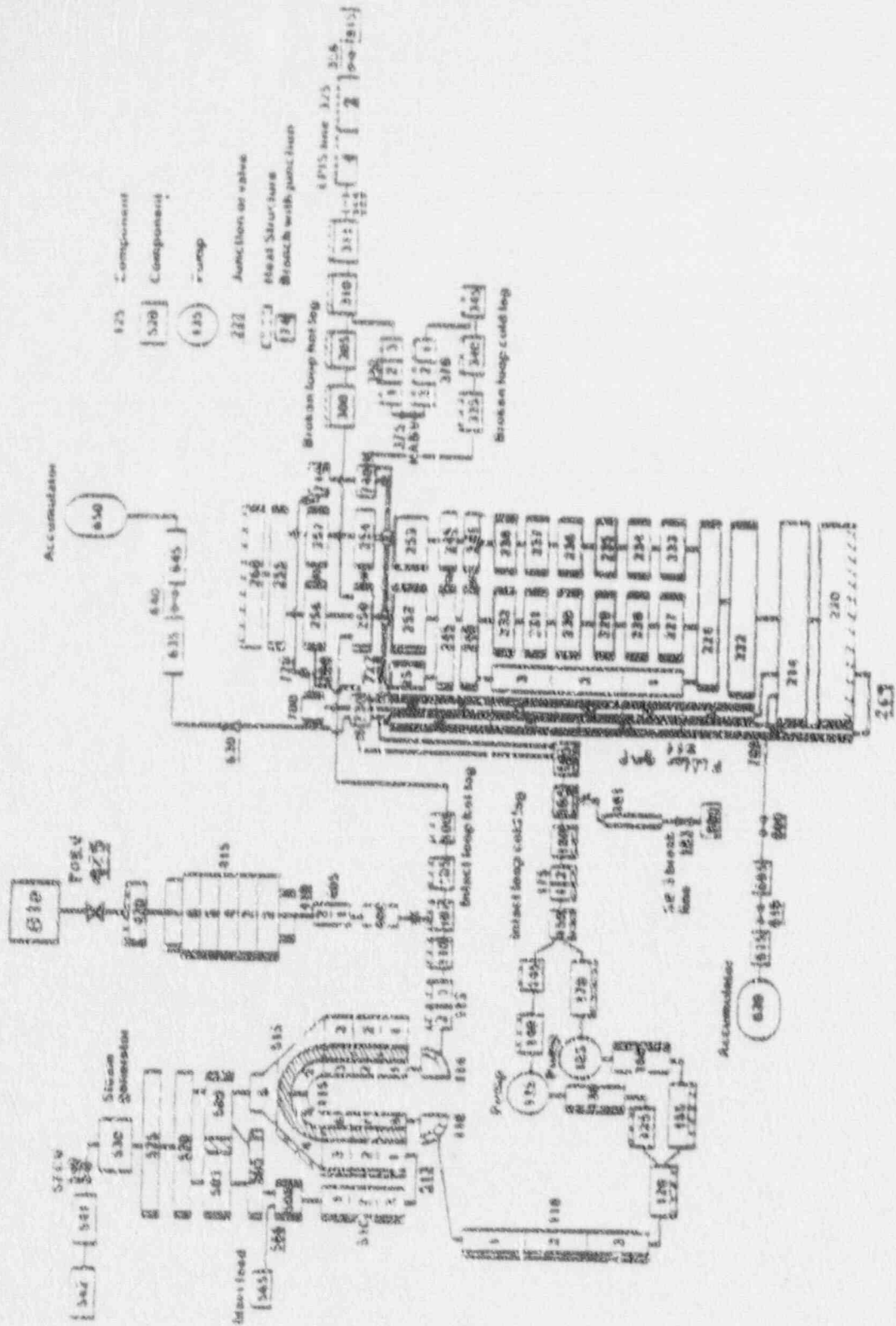


Figure 4.3 NILEAP/NSM's mobilization diagram

To end up this iterative process, the main RELAP5/MOD2 calculation, employing the indicated blockages between the indicated temperature intervals, provides the thermal-hydraulic information required for the SCDAP code to calculate the detailed core thermal response.

4.2. RELAP5/MOD2 Nodalization for Experiment LP-FP-2

The nodalization used for the base case calculation was based on the RELAP5/MOD2 input deck that was used for the planning and prediction of the experiment at the INEL⁶, and also in several input decks used for the posttest analysis of the LP-SB-3^{14, 15}.

Basically the nodalization used in RELAP5/MOD2 for this calculation is a standard LOFT nodalization, with changes which were necessary to represent the particular system configuration for Experiment LP-FP-2.

Figure 4.3. shows the nodalization diagram for this calculation.

The nodalization model differs from the standard RELAP5 model in the following aspects (see Reference 6):

1. The broken loop hot leg pump and steam generator simulator and the quick-opening blowdown valve were replaced by a pipe simulating the LPIS break line with two valves attached at both ends.
2. The quick-opening valve on the broken loop cold leg and its connection piping to the cold leg were deleted. The broken loop cold leg is a dead end volume.
3. The reactor vessel was extensively remodeled to represent the special core configuration and to better simulate the flow splitting and mixing. Special emphases were given to peak cladding temperature behavior in the center and peripheral fuel bundles, and also to the thermal response of the guide tubes, control rods and thermal shroud surrounding the center bundle assembly.

4. The cross flow model was applied to the junctions connecting the cold legs to the vessel and to the junction connecting the pressurizer to the intact loop hot leg.
5. The emergency core coolant system (ECCS) and its two injection locations for the LP-FP-2 experiment (one into the lower plenum and the other into the downcomer) were modeled, in order to simulate the reflood.
6. The blowdown piping was attached to the ILCL leg with a nodalization similar to that used in the BEP calculation⁶, but using the cross-flow model for simulating the tee connection of the break line to the ILCL¹⁵.
7. RELAP5/MOD2 code does not include a metal-water reaction model. However, when the fuel rod cladding temperature rises above 1273 K (1832°F) metal-water reaction becomes the principal heat source. Therefore, a metal-water reaction model was included using the RELAP5 control system⁶. Heat generation was calculated using the Cathcart-Powell¹⁶ model for cladding temperature in the range 1273 to 1853 K (1832 to 2876°F) and the Urbanic¹⁶ model for cladding temperatures above 1853 K (2876°F). A steam limitation model was included to account for the steam availability for the reaction. The main limitation of the model is that the center bundle flow should always be positive. The metal-water reaction was also calculated on the cladding of the guide tubes and the inner surface of the thermal shroud. These models were included in the input deck and can be seen in Appendix C.
8. Detailed upper plenum nodalization was designed to better simulate the flow mixing⁶. The detailed upper plenum model specifically considers the mixing in the upper end box represented by Volumes 240 and 241 with a cross flow junction between these volumes. The mixing between the flows coming from the center bundles below the 5.69 m (224 in.) elevation, with reference to the bottom of the reactor vessel, is also modeled by the cross flow junction between Volumes 245 and 246. No mixing is allowed between Volumes

252 and 153 due to the geometry of the upper plenum between the 5.69 m (1224 in.) elevation and the nozzle level.

9. A split downcomer upper annulus was used, with the cross flow connections^{6,14}.

10. The core is divided into two channels, each containing six axial fluid cells of equal length. The channels are hydraulically isolated. The thermal shroud, which is represented by a heat structure, is the thermal link between the two core channels. The leak path between the downcomer annulus and the upper plenum is modeled by a cross flow junction connecting Volumen 730 (downcomer annulus) and 256 (upper portion of the nozzle area above the peripheral bundles)^{6,14}.

11. The eight hot rods in the center bundle and remaining 9.72% enriched fuel rods are represented by two heat structures. The 10 guide tubes and 11 control rods are separately represented by two heat structures. The fuel rods in the peripheral bundles are represented by two heat structures. One structure represents the four rows of rod groups surrounding the thermal shroud outer surface. The remaining fuel rods are represented by the second heat structure. The guide tubes with and without the control rods are not simulated. This will result in a slightly increased temperature excursion in the peripheral bundle (Reference 6).

The former characteristics of the input model were common to the BEP deck⁶. However several updates were made in order to improve the calculation results.

Basic changes made to the best estimate prediction deck were:

1. Renodalization of ILCL break piping; use of cross flow volume in cold leg for tee modelling (vol 184)¹⁵; and the volume 182 has been deleted, using a new length of 11.3 m for the break line volume number 181.

2. Renodalization of the LPIS break line (Reference 17). New break isolation valve area (valve 355, $A = 2.8521E-4 \text{ m}^2$). When bypass line is active the length of volume 325 is 16.02 m; when the FPMS is aligned 950.3 sec; the LPIS line was renodalized to include the new length of 21.53 m. Additional losses from valves and bends were taken into account: when bypass line is used the added loss coefficient was 43.59; for the slowdown through the FPMS the loss coefficient was 47.29. Discharge coefficients for the subcooled and saturated flows were 0.93 and 0.82 respectively¹⁸.
3. To perform these calculations with ILCL break, LPIS line and PORV opened as in the experiment. The final closure time of the ILCL break and PORV was simulated when the primary system pressure dropped below 1.38 MPa, following the experiment specifications⁸.
4. Simplification of the lower plenum nodalization, in order to avoid core flow oscillations during the transient.
5. Downcomer annulus is modeled as a single volume stack, similar to LP-SB-3^{14,15}.
6. Filler gap was separately modeled^{14,15}.
7. New steam generation (SG) Break nodalization: Components 549 and 550 of the BEP deck were deleted. The SG leak was simulated keeping a minimum area of the Steam Isolation Valve (MSIV) of 0.2 % (Valve 540).

Other minor changes were applied:

- a) To correct some errors in several control variables.
- b) To finely tune the experimental sequence of events

b) To finely tune the experimental sequence of events

c) To match the initial reactor vessel pressure drop and, in turn, the initial pump speeds (removing several additional loss coefficients in the upper plenum).

The final version of the input model contains a total of 134 control volumes and 147 junctions. A full input data listing is supplied in Appendix C.

4.3. Simulation of the core geometry changes in the base RELAP5/MOD2 calculation.

Because of the special configuration of the LOFT core for the LP-PP-2 Experiment the damage was reduced to the center fuel module (CFM) (See Reference 8 and 9 and also section 2.2. of this report). Therefore, following the general methodology described in section 4.1., prior to the main RELAP5 calculation, a SCDAP calculation was performed for the center bundle to estimate the amount of blockage due to the fuel cladding ballooning and rupture, the control rod material relocation after the control rod failure, and the fuel cladding relocation due to the melting of zircaloy.

A preliminary posttest analysis¹⁹ using RELAP5/MOD2 provided the TH boundary conditions (CFM pressure, CFM inlet flow, CFM liquid level) to run SCDAP.

SCDAP calculated²⁰ approximately a 53% blockage as a result of fuel cladding ballooning and rupture at the hot plane, an additional 5% blockage at the first elevation due to control rod material relocation, and at the corresponding temperatures of approximately 1200, 1700 °K, respectively.

No blockage due to fuel liquefaction was calculated by the code, because the maximum calculated clad temperature was only 2500 °K. Up to this temperature the outer ZrO_2 layer did not fail, thus avoiding the melted zircaloy relocation.

However these results were not considered as best estimate by the group. By

reviewing the SCDAP data, the group decided that the 53% blockage at 1200 K is a reasonable value for the main RELAPS/MOD2 calculation.

The control rod failure temperature of 1700 °K estimated by SCDAP was considered too high especially looking at the LP-FP-2 Data Report⁹. As it is explained in that document, the most probable temperature at which the control rods failed in the LP-FP-2 Experiment was 1250 °K. Therefore the group decided to assume the failure of the control rods when they reached 1250 °K. Meantime, and, although the 5% blockage calculated by SCDAP was considered too low, the group determined to employ such a value, in order to increase the CFM inlet mass flow during the rapid metal-water reaction phase of the transient. The reason for this was the steam starvation conditions calculated in the preliminary posttest analysis¹⁰ where the blockages were 50% - 67% - 80%. This reduced the extension of the metal-water reaction such that SCDAP could not predict the fuel cladding relocation observed in the experiment⁹.

Then, the 80% blockage due to fuel cladding relocation (see Reference 6), although not calculated by SCDAP, was considered still applicable to the main RELAPS/MOD2 simulation, at the corresponding temperature of 2245 °K (melting temperature of the α -Zr(O)).

Therefore a 53%-5%-80% blockage case was run as a base case for the thermal-hydraulic analysis. As discussed previously, Figure 4.4, presents the calculational scheme and shows the interactions between the RELAPS, and SCDAP results.

The analysis assumed the fuel cladding ballooning and rupture-induced blockage at the fourth elevation until 1250 K (1790°F) were reached on the control rods. An additional 5% blockage was applied to the second elevation until 2245 K (3580°F) were reached on the fuel rod due to control rod material relocation. During the final stage of the calculations, an 80% blockage due to fuel liquefaction was applied to the first elevation. The blockages at the fourth and second elevations were removed when the first elevation blockage occurred because of the material relocations at these elevations.

The RELAPS/MOD2 code, employing the indicated blockages between the indicated temperature intervals, provided the thermal-hydraulic information required for the SCDAP code for the detailed core thermal response calculations, which will

CENTER BUNDLE

TIME	1200 K	1250 K	2245 K	1460 K
0.0 s	FUEL CLAD	CONTROL ROD	FUEL CLAD	PERIPHERAL
CORE UNCOVERY				
	53% BLOCKAGE			
	FUEL CLADDING			
	BALLOONING			
	AND RUPTURE AT	5% BLOCKAGE		
	4 TH ELEVATION			
		CONTROL ROD		
		MATERIAL		
		RELOCATION AT	80% BLOCKAGE	
		2 ND ELEVATION		
			FUEL CLADDING	
			RELOCATION AT	REFLOOD
			1 ST ELEVATION	

FIGURE 4.4 RELAP5/MOD2 BASE CASE CALCULATIONAL SCHEME,
SHOWING THE INTERACTIONS BETWEEN RELAP5 AND SCDAP

be described in section 7.

The 53-67-80% blockage case was also analyzed to determine the sensitivity of the RELAPS -calculated LOFT system thermal-hydraulic behavior to blockage. The results of the 53-67-80 blockage case will not be shown in the next section because the differences with the base case were negligible (A similar trend was observed during the BEP calculations)⁶.

5. RESULTS OF THE RELAPS/MOD2 BASE CALCULATION

This section presents the thermal-hydraulic results of Experiment LP-PP-2 base posttest calculation. Prior to perform the posttest calculation, a steady state calculation was executed to obtain the initial conditions measured during the experiment. Following the steady state calculation, the transient calculation was started with the trip setpoints taken from the experiment sequence of events. The following subsections discuss the steady state and transient calculations.

5.1. Calculation of the Steady State

Using the steady state controller package added to the SEP input deck⁶, the simulated LOFT system was brought to the required initial conditions. The steady state calculation was performed with the transient option. The calculation was continued until the observed variations of the calculated values of these parameters from their desired values were acceptable. The key parameters controlled using the control variables were the primary system pressure, pressurizer level, cold leg temperature, primary system mass flow rate and steam generator secondary level. The behaviors of the secondary side feed and steam flows, pump speed and head, pressurizer heater power, pressurizer spray valve and steam generator main steam valve positions, and primary side charge or let down flows were the other parameters checked for the steady state.

The system pressure was controlled by the pressurizer spray which injected cold leg fluid to the pressurizer to reduce the pressure if the pressure was calculated to be greater than the measured value. The second controller on the system pressure was the pressurizer heaters. These heaters, although in reality were located close to the bottom of the pressurizer, were placed at the mixture level in the RELAPS model to increase the boiling. The pressurizer level was controlled by two controllers. One controller which charged fluid at the cold leg temperature to the cold leg if the pressurizer level was lower than the setpoint. The second controller dumped the system fluid to a time dependent volume if the pressurizer liquid level was higher than the setpoint. The final values of the primary pressure and pressurizer level were calculated to be almost the same as their measured values. The final valve positions controlling the pressurizer spray, primary system charge or let down

flows were zero. The final pressurizer heater power was zero. The pressurizer surge line flow was negligible at the end of the steady state calculation.

The primary loop flow was adjusted by using a proportional/integral controller based on loop flow error to control pump speed. The steady state intact loop flow was calculated to be the same as the experimental value. The pump speed and head were in agreement with the measured initial values. The broken loop flow (from the vessel to the cold leg and via the reflood assist valve to the hot leg and back to the vessel) was small and based on the leak flow through the reflood assists by-pass valve. The total by-pass leak flow based on the flow loss coefficients used in the input deck was calculated to be 6.9% of the total loop flow. This value compares well with the generally accepted 7% of the loop flow.

The cold leg temperature was controlled by the main steam valve position with a proportional/integral control system. Based on the steam flow rate and heat transfer to the secondary side, the code calculated the secondary system pressure. Another control logic was used to adjust the feed flow to control the steam generator required level. This controller was also coupled to the main steam flow. The steam generator level, main steam and feed water flows were calculated to be the same as measured. Although the steam and feed water flow rates were correctly calculated, the steam generator secondary side pressure was the only parameter being calculated offset by 0.19 Mpa from the measured equivalent.

After about 200 s of calculation the steady state was considered acceptably stable. Tables 5.1 compares the calculated and measured steady state values. Most of the values are in good agreement with the measured initial conditions.

Despite of the trials done to increase the steam generator secondary pressure, (decreasing the hydraulic diameter) no success was reached. The complex geometry and atypical internal structure of the steam generator with rather simple nodalization are the possible causes of the problem.

Table 5.1. Initial conditions for experiment LP-FP-2
 Comparison between calculated and measured
values

<u>Parameter</u>	<u>Calculated</u> <u>Value</u>	<u>Measured</u> <u>Value</u>
<u>Primary Coolant System</u>		
Core delta T (K)	10.54	11.7 ± 1.4
Primary system pressure (hot leg) (MPa)	14.98	14.98 ± 0.1
Hot leg temperature (K)	570.37	571.6 ± 0.8
Cold leg temperature (K)	559.83	559.9 ± 1.1
Loop mass flow (kg/s)	475.04	475.0 ± 2.5
Primary coolant pump speeds (both pumps) (rpm)	3240.1 3273.7	3200.0 3200.0
Pump differential pressure (KPa)	450.0	475.0
<u>Reactor Vessel</u>		
Power level (MW)	26.8	26.8 ± 1.4
Pressure drop (KPa)	190.0	195.0 ± 5.6
<u>Steam Generator</u>		
Secondary system pressure (MPa)	6.19	6.38 ± 0.08
Water level (m)	3.12	3.12 ± 0.06
Pressure drop (primary side) (KPa)	237.1	230.0
<u>Pressurizer</u>		
Water temperature (K)	613.5	616.9 ± 2.1
Pressure (MPa)	14.95	15.1 ± 0.1
Liquid level (m)	1.06	1.06 ± 0.06

5.2. Base Transient Calculation

This section presents a comparison of the postexperiment calculation using RELAP5/MOD2/36.04 and the measured thermal-hydraulic data.

Once the steady-state results were considered acceptable, the steady state controllers associated with the pressurizer heaters, pressurizer spray, primary system mass charger and letdown, pump speed, and various valve position were removed. The trips for various actions were defined based on the measured data.

The transient calculation was started from time zero and using the last restart record in the steady state restart-plot file. The complete transient was calculated in five major intervals, as it is depicted in figure 4.4. The whole transient calculation was carried out in 1860 se

A summary of the calculated significant events for Experiment LP-FP-2 are chronologically listed in Table 5.2. in comparison with the measured values. The agreement can be considered as remarkable.

Figure 5.1 shows a comparison of the calculated and measured primary system pressures. Both curves show a slight drop in pressure following scram and a subsequent rapid decrease down to saturation pressure following break initiation. The end of subcooled blowdown happened at 62 s, compared with the 53 s indicated from measurements. A slightly lower pressure was reached in the calculation due to the slightly lower initial fluid temperature (see Table 5.1). The pressure response agreed well with the observed data for the period until initiation of the LPIS line break at 221.6 s.

Table 5.2. Chronology of events for Experiment LP-FP-2. Comparison
between calculated and measured values.

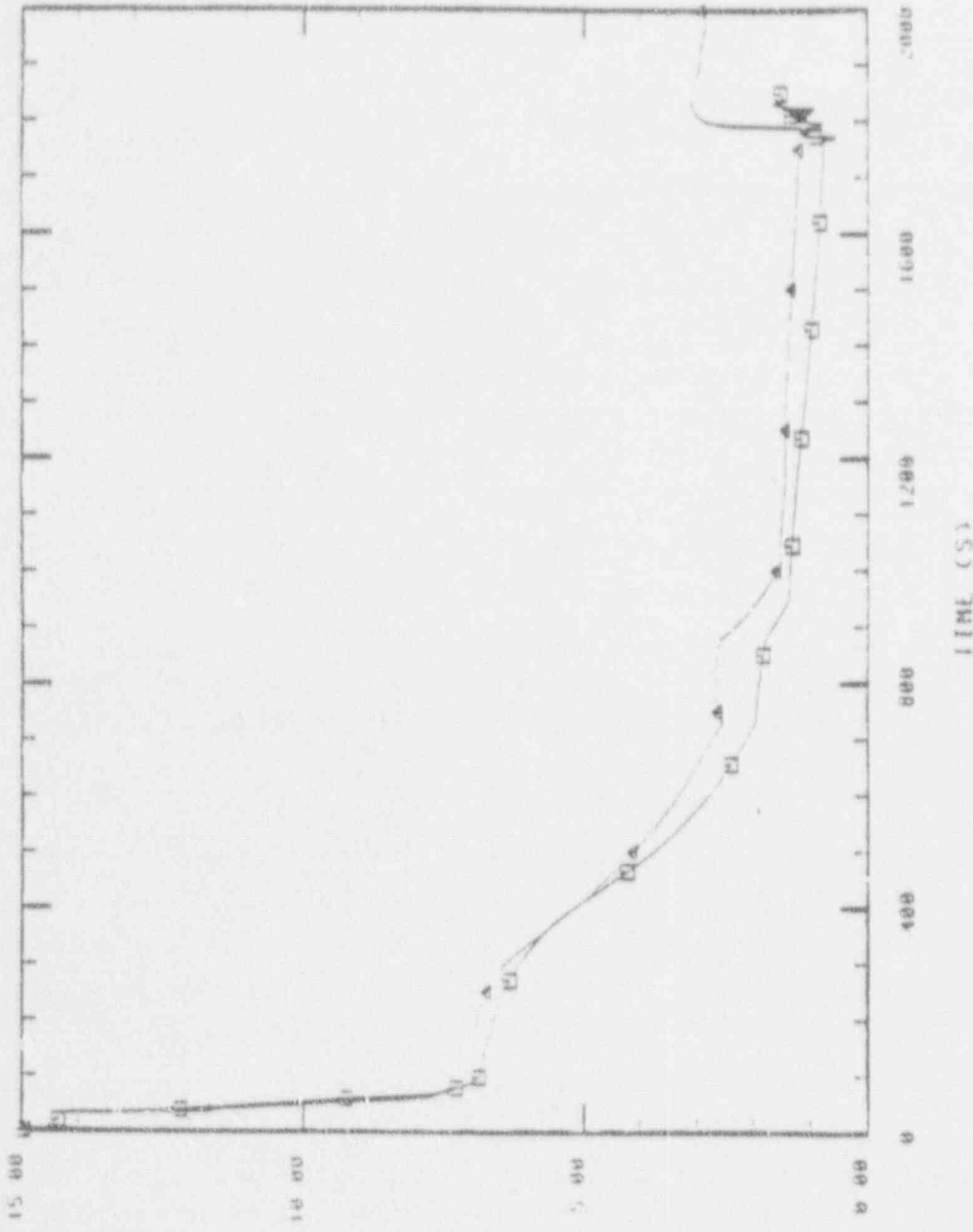
Event	RELAP5/MOD2	Time After Experiment	
	Calculated	Initiation	
	Time (s)	Time (s)	
Scram	0.0	0.0	
PCP coastdown initiated	9.7	9.7	± 0.1
ILCL break initiated	32.9	32.9	± 0.1
PCP coastdown complete ^a	28.5	25.1	± 0.1
End of subcooled blowdown ^b	62.0	53.0	± 1.0
Secondary relief valve cycle	70.0	56.0	± 1.0
Pressurizer empty	60.0	60.0	± 5.0
LPIS line break initiated	221.6	221.6	± 0.1
Secondary pressure exceeded primary system pressure	230.0	260.0	± 10.0
Earliest coolant thermocouple deviation from saturation (voidage at that location)			
Upper plenum	415.0	300.0	± 10.0
Hot leg pipe	390.0	390.0	± 10.0
Downcomer	741.0	730.0	± 10.0
Lower plenum	970.0	800.0	± 20.0
Fuel rod cladding heatup started in PFM	666.0	662.0	± 2.0
Fuel rod cladding heatup started in CFM	711.0	689.0	± 2.0
ILCL break closed	735.5	735.5	± 0.1
ILCL break reopened	877.6	877.6	± 0.1
PORV opened	882.0	882.0	± 0.1
F3 filter on line	950.0	950.8	± 0.1

Table 5.2. (continued)

Event	RELAPS/MOD2 Calculated (Time (s))	Time After Experiment Initiation (s)
ILCL closed	950.0 ^c	1021.5 ± 0.1
PORV closed	950.0 ^d	1182.0 ± 0.1
First indication of (gap) fission products at F1 (clad rupture at about 1200 °K)	1178.1	1200.0 ± 20.0
Control Rod Failure (1250 °K)	1428.0	1500.0
Peripheral fuel cladding reached 1460 K (2172°F)	1769.3 ^d	--d
Maximum upper plenum coolant temperature reached ^e	1767.0	1495.0 ± 5.0
First indication of (fuel) FPs at F1, F2, and F3 (Fuel Failure at about 2245 °K)	1539.8	1500.0 ± 10.0
Cladding temperatures reach 2100 K (3320°K)	1490.0	1504.0 ± 1.0
Shroud temperature reached trip setpoint		
1st thermocouple	-	1743.0 ± 1.0
2nd thermocouple	-	1766.0 ± 1.0
Maximum cladding temperature reached	1769.0	--f
LPIS line break closed	1778.5	1777.6 ± 0.1
Maximum upper plenum metal temperature reached ^e	1770.0	1780.0 ± 5.0
ECCS initiated	1769.3	1782.6 ± 0.1
Accumulator flow stopped	1825.0	1795.0 ± 1
Maximum LPIS line coolant temperature reached	1777.5	1800.0 ± 5.0
Core quenched	1805.0	1795.0 ± 5.0 ^g

Table 5.2 (continued)

- a. The pumps were allowed to coastdown under the influence of the motor generator flywheel until the pump speed reached 750 rpm. At that time, the flywheel was disconnected from the motor generator and the pumps quickly stopped adding energy to the fluid. The time at which the flywheel was disconnected is defined as the time the PCP coastdown was complete.
- b. End of subcooled blowdown is defined as the time when the first measured fluid temperature outside of the pressurizer reaches saturation conditions.
- c. The ILCL Break and the PORV were closed when the calculated primary system pressure dropped below 1.38 MPa.
- d. None of the cladding thermocouples in the peripheral fuel bundle measured validated temperatures above the setpoint. The two that gave readings above this setpoint failed before reaching the setpoint. However the calculated cladding temperatures reached this ECCS trip setpoint before that the shroud setpoint.
- e. These temperatures represent the maximum measured temperatures before reflood at these locations. The thermocouple output during reflood could not be interpreted.
- f. Because of the large number of cladding thermocouples in the central fuel module that failed at high temperatures during the transient, it is not possible to determine the precise maximum temperature or time at which it occurred. The time is estimated to be between 1780 and 1795 s. The maximum temperature exceeded 2400 K (3860°F) based on extrapolations from valid temperature readings before thermocouple failure.
- g. The peripheral fuel modules were quenched by 1793 s. Most of the central fuel module cladding thermocouples were quenched by 1795 s. Some isolated thermocouples indicated persistent high (superheated) temperatures a few minutes later. Interpretation of the temperature data is complicated by the large number of thermocouples in the center fuel module that failed during or just before reflood.



PRIMARY SYSTEM PRESSURE (MPA)
AT THE II HOT LEG LOCATION
RELAPS/EXPERIMENT COMPARISON (SPAIN)

Figure 5.2.

1
2
3
4
5
6
7
8
9
10

In contrast with the good agreement for the period prior to LPIS line break initiation (221.6 s), the subsequent depressurization rate was initially underestimated until 350 sec, and overestimated from 425 s up to the closure of the ILCL break at 735.6 s. This anomalous behaviour is not well understood. It was postulated in the QLR³ that the complicated network of bends in the LPIS line resulted in a higher flow resistance under single phase conditions and also inhibited the draining of liquid from the line under two phase conditions. There is an indication from measurements of the fluid temperature that the LPIS line was not completely drained until after about 1200 s. The latter effect differs from the calculation in which the LPIS line was completely void after about 425 s. The venting of steam, calculated by the code, would not readily take place with liquid remaining in the line. The higher system pressure observed affects all the comparisons of system hydraulics and core thermal response beyond 425 s.

The LPIS line and break characteristics had previously been considered to be a major source of uncertainty.⁶ An attempt was made in the BEP document to estimate the effect of the uncertainty by performing a sensitivity calculation with the break flow areas reduced by 30%. This provided a slightly better agreement, but still overpredicted the depressurization rate.

In fact, our group found one error in the BEP input deck. This was a wrong area in the component 355 which simulated the LPIS isolation valves. The true area is a 42% lower than the LPIS line full flow area (6.818 E-4 m^2) - See reference 17 for more details. This update along with new length and loss coefficients in the LPIS pipe component 325 (also wrong in the BEP deck) have been taken into consideration in our analysis, as it was discussed in section 4.3 of this report. It is obvious that the present posttest analysis improves largely the BEP results. But it is still unable to give a full satisfactory representation of the LPIS line flow characteristics.

It is not clear enough if it is still a nodalization problem or a code deficiency (errors in the critical flow model).

The present analysis could be improved using two different discharge coefficients for the two-phase and single phase flow periods of the LPIS discharge process (0.82 has been employed for this calculation all through the transient - see section 4.2-). However this does not seem to be very consistent with previous experiences using RELAP5/MOD2.

After the initial closure of the ILCL break at 735.6 sec, the calculated depressurization rates agreed well with the data. The only exception is that the closure times of the ILCL break and the PORV (Pressure lower than 1.38 MPa) were calculated very soon (see table 5.2) due to the lower than measured calculated pressure.

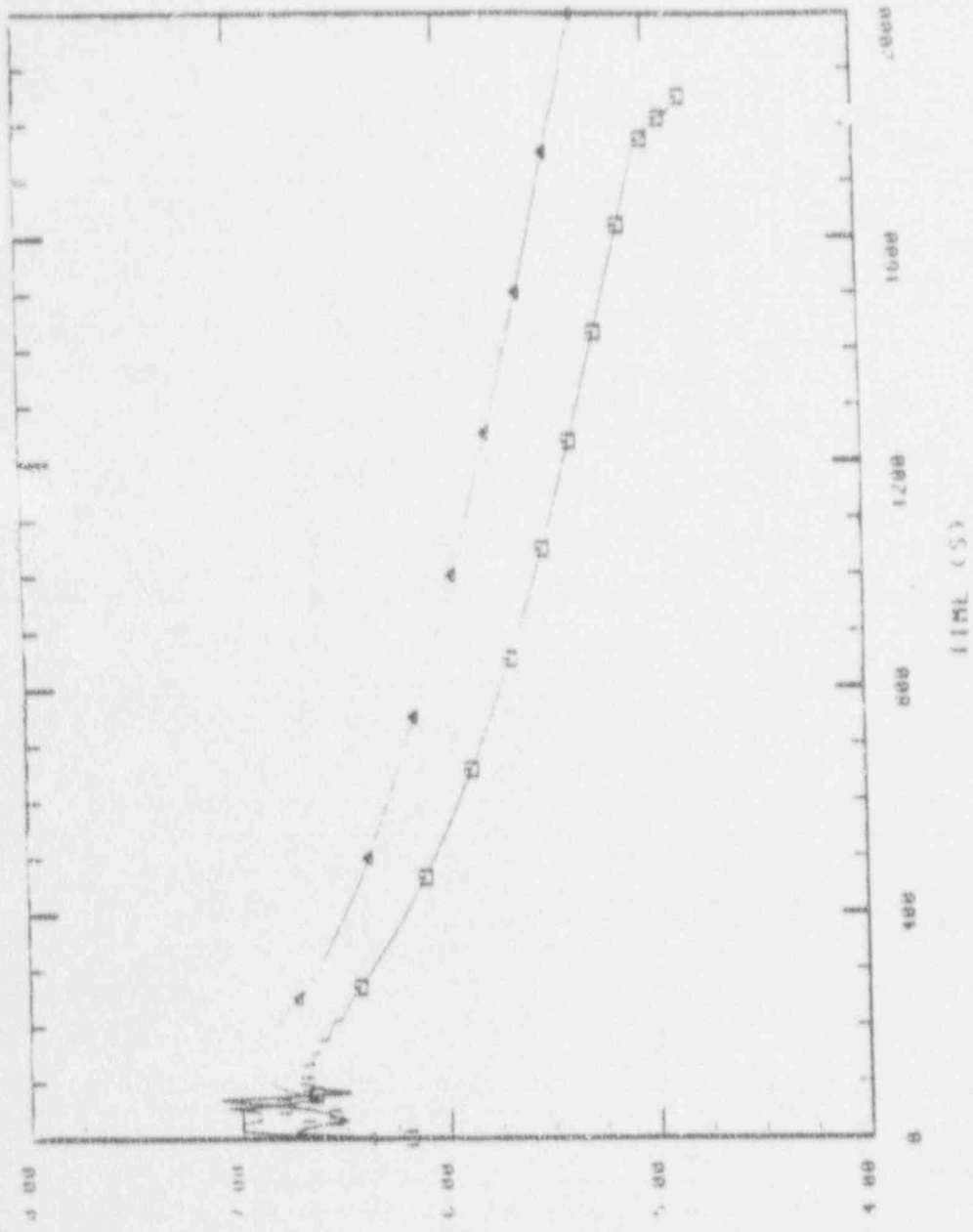
The measured and calculated secondary system pressures are shown in Figure 5.2. The measured steam generator secondary pressure, after termination of feedwater and steam flows, increased to the main steam valve cycling setpoint of 7.11 MPa (1031 psia) at 56 s compared with the 70 s predicted. The differences in pressure increase and time of valve cycling are possibly due to slightly different initial conditions and to the SG leak model. The secondary system continued to act as a heat sink until the primary pressure had dropped below the secondary pressure. This was predicted at 230 s compared with the observed time of 250 s.

The rate of depressurization is slightly overestimated due to the differences in the primary system pressure and possibly to some unaccuracy of the steam generator simple leak modelling, used for the analysis.

Figure 5.3. shows a comparison of the calculated and measured collapsed liquid level in the steam generator. The discrepancies can be associated to the leak modelling, but they are considered to be unrelevant for the calculation.

Figures 5.4 and 5.5 show the average fluid densities measured by the gamma densitometers in the broken and intact loop hot legs compared to the values calculated by RELAPS/MOD2. The gamma densitometer sources were prematurely isolated. These density data are available only for the first 250 s of the transient. These data show that the voiding started at about 50 s in the intact loop hot leg and at 85 s in the broken loop hot leg what is in good agreement with the RELAPS/MOD2 results. While the level decrease in the loops could not be directly monitored later than 250 s, it is clear from thermocouple data on the upper plenum that the loop was void by 470 s⁹. As shown in Figures 5.4 and 5.5 RELAPS/MOD2 calculated that the intact loop and broken loop hot legs were voided at 390 s and 415 s respectively.

The pressurizer emptied at about 60 s, time which was well determined by RELAPS/MOD2 as it is shown in Figure 5.6.

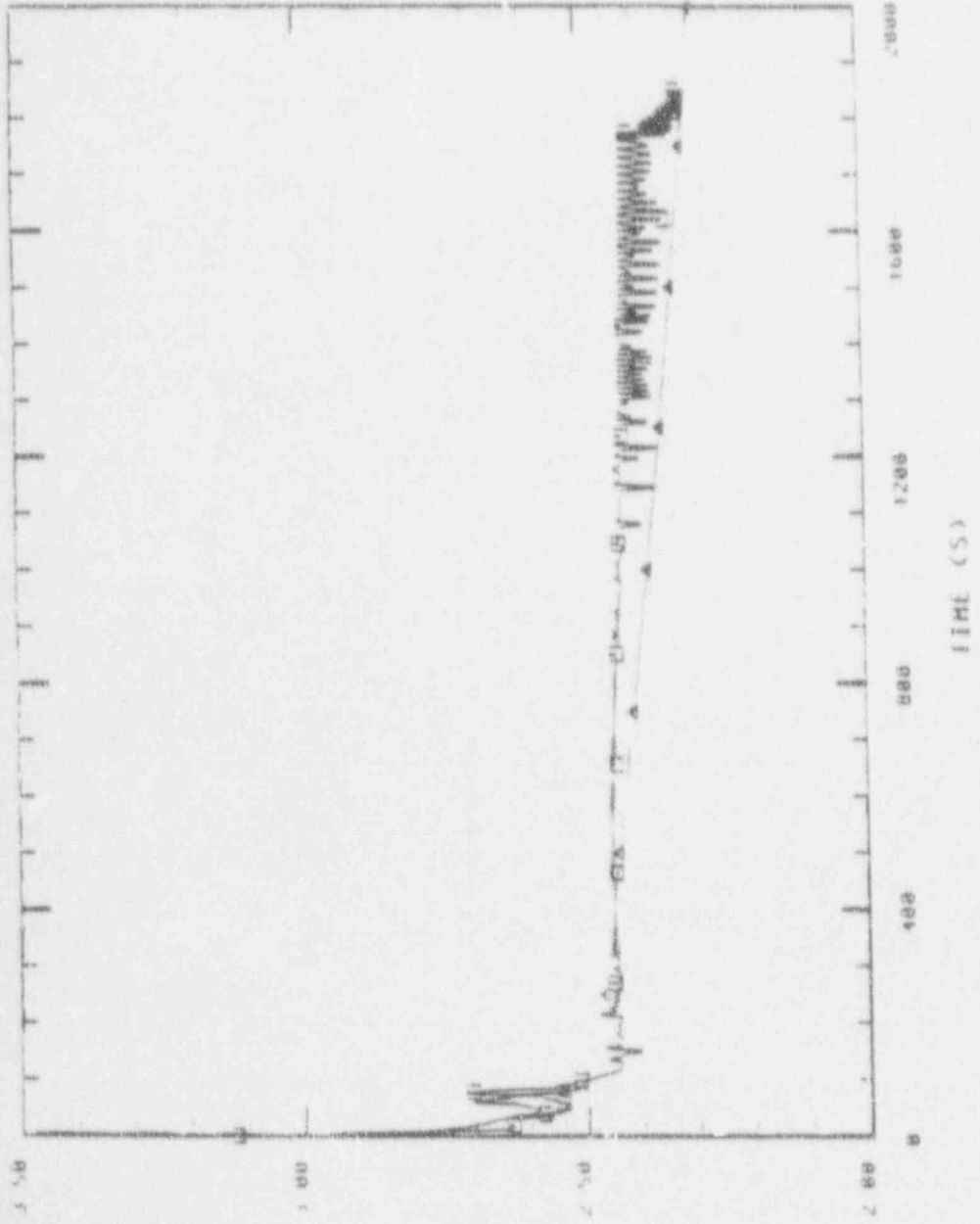


SECONDARY SYSTEM PRESSURE (MPa)
AT THE STEAM DOME LOCATION
RELAP5/EXPERIMENT COMPARISON (SPAIN)

Figure 5.2.

7.00 6.00 5.00 4.80

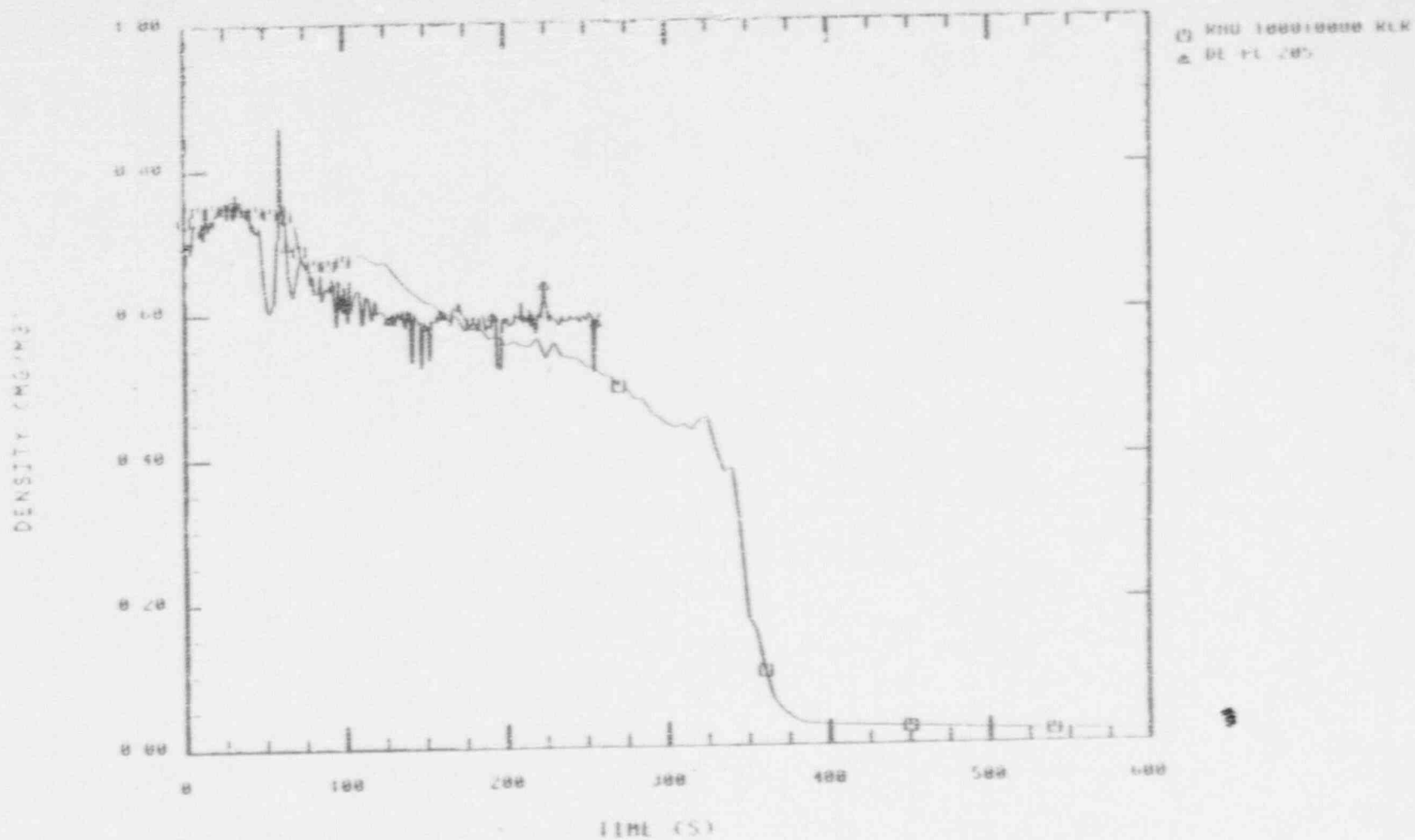
UNIKLWAR I KLR
A 11 P004 000A



STEAM GENERATOR LIQUID
LEVEL (M)
RELAP5/EXPERIMENT COMPARISON (SPAIN)

Figure 5.3.

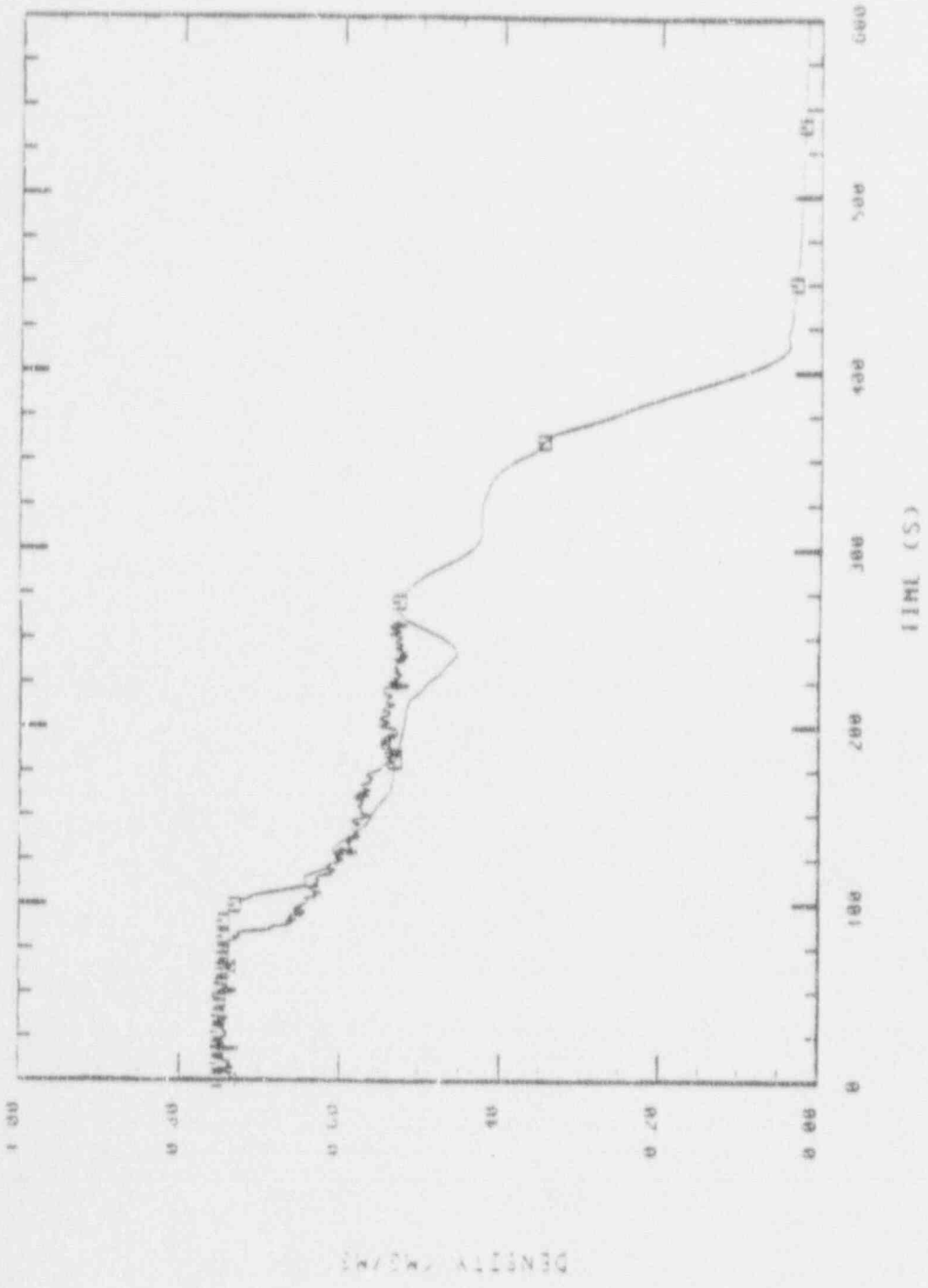
LEVEL (M)



FLUID DENSITY (MG/M3) AT THE
 INTACT LOOP HOT LEG
 RELAPS/EXPERIMENT COMPARISON (SPAIN)

Figure 5.4.

□ RELAP5
△ EXP. DATA



FLUID DENSITY (MG/M3) AT THE
BROKEN LOOP HOT LLG
RELAP5/EXPERIMENT COMPARISON (SPAIN)

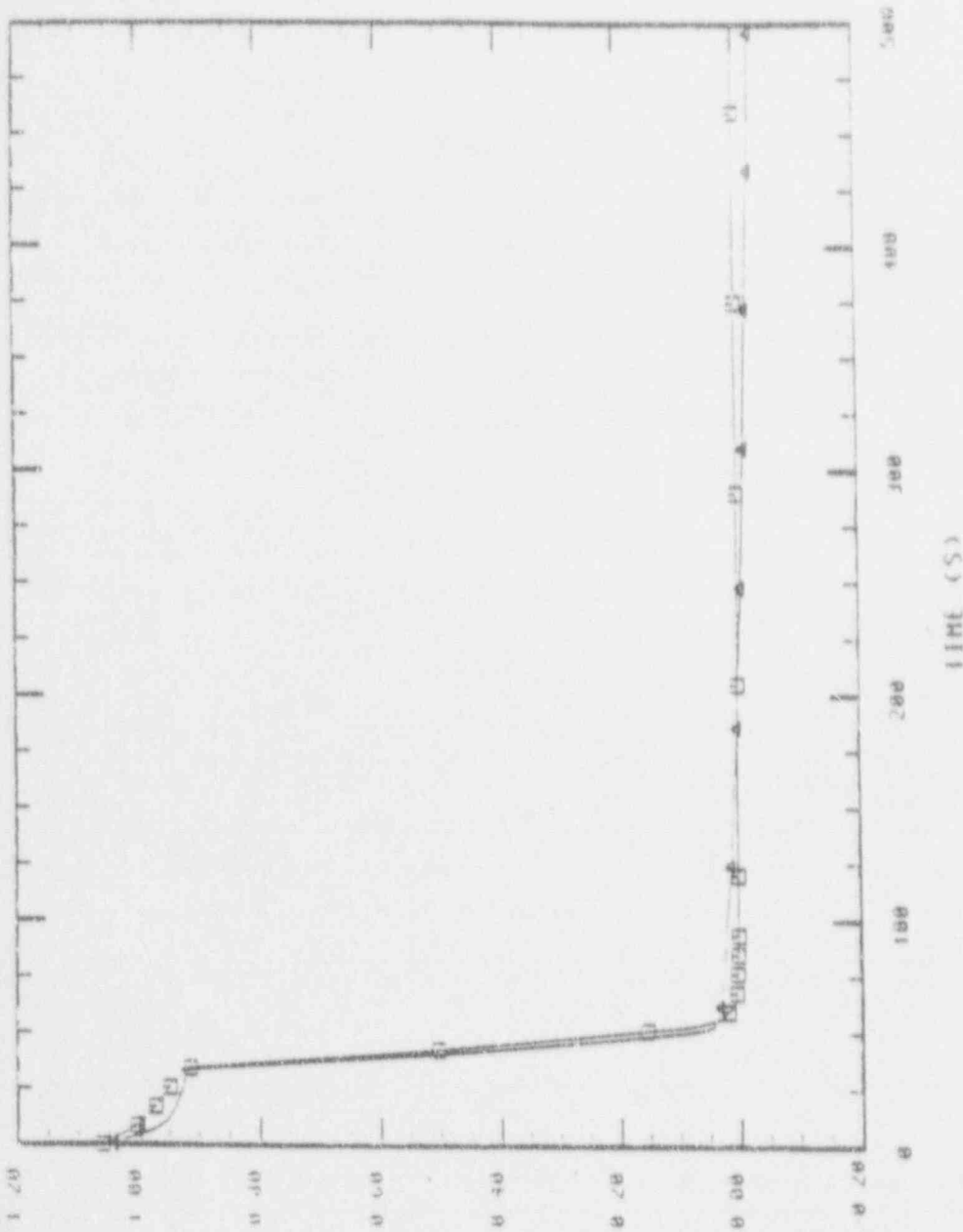
Figure 5.5.

Figure 5.7 shows the measured and calculated intact loop hot leg flow for the first 500 s. Measured data were lost after opening of the LPIS line break. An excellent agreement was obtained for this initial phase of the transient. Mass flowrates in the intact loop hot leg show that loop flow ceased when the pressurizer emptied, at about 60 s.

Figure 5.8 shows the calculated Primary Coolant System Mass Inventory. The transmittal magnetic tape containing the experimental data did not contain any mass inventory results. However, lately, the PCS mass inventory has been derived from the mass increase in the BST⁹. These data have not been qualified during the transient. Thus, the derived PCS mass inventory is useful for trend information, though not for absolute magnitudes during the transient. The trends are reasonable, and a single point check of the mass inventory can be made since the levels were qualified both for initial conditions and for the time after isolation of the PCS. The derived mass inventory is shown in Figure 5.9 and indicates that the inventory decreased from an initial value of 4700 kg (10360 lbm) to a minimum of just over 500 kg (1100 lbm) at 1300 s. This single points can be compared to the computed values of 4362 kg at the beginning and 668.6 kg at 1769.

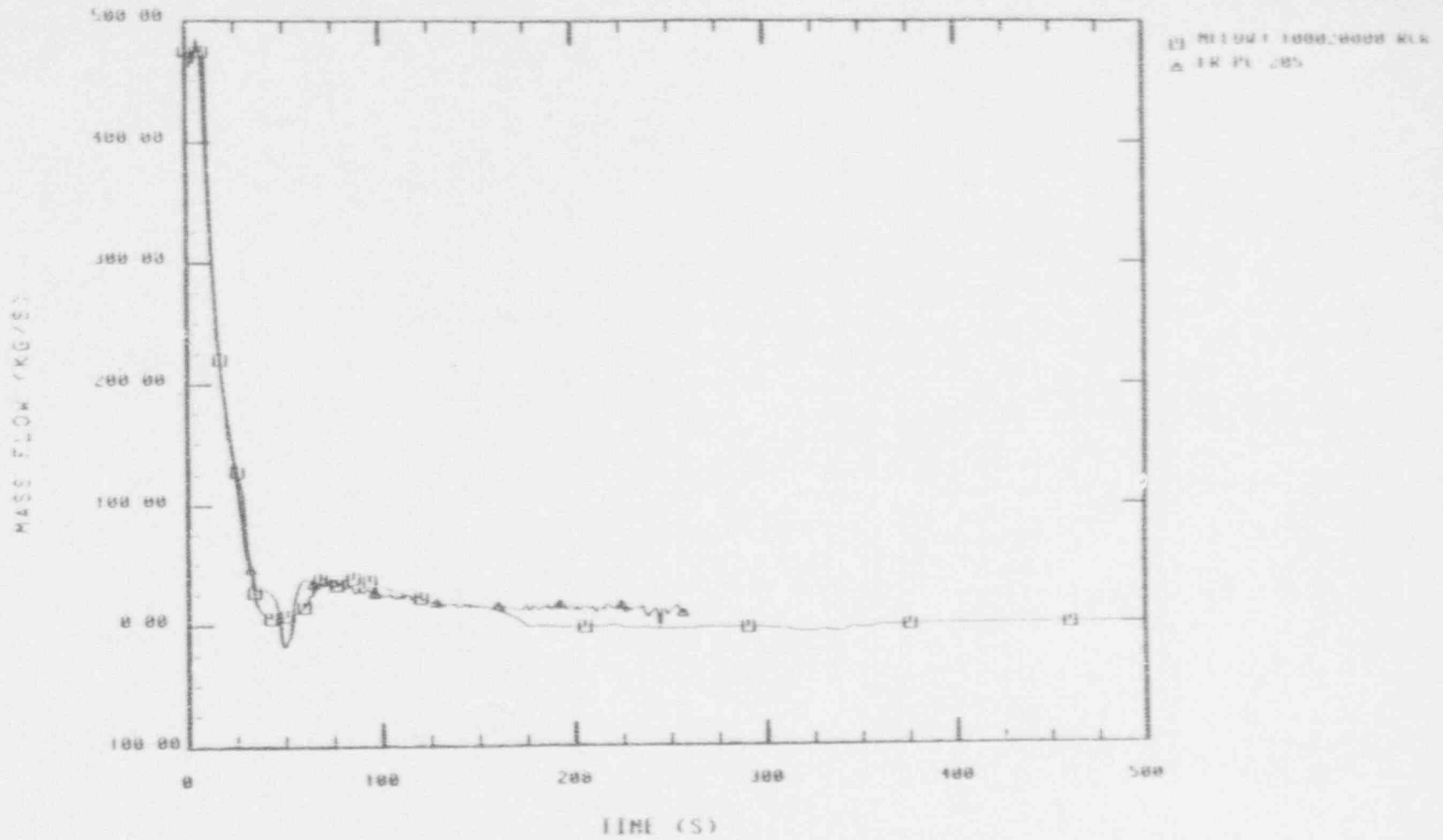
By comparing Figures 5.8 and 5.9 we can see that the PCS mass inventory decreased rates are well computed by RELAP5. For the first 300 s RELAP5 determines a rate of 8.6 kg/s versus the 8 kg/s observed experimentally. From 300 s to 1000 s RELAP5 calculates 2.2 kg/s versus a measured value of 3 kg/s. And finally between 1000 s and 1300 s the values are 0.2 kg/s versus 1 kg/s respectively. This last larger difference can be attributed to the earlier than measured closure time of the ILCL break and the PORV (Table 5.2).

The calculated break mass flow rates are presented in Figures 5.10.a and 5.10.b. The fact that the actual primary system pressure (Fig 5.1) was higher during the heat up and core damage phase -from 1200 to 1760 s- means that there was a greater driving head to sustain the LPIS break flow. The measured pressure data were in the range 1.2 to 1.45 MPa, compared with the RELAP5/MOD2 values of 0.76 to 1.2 MPa for the same time period. The LPIS line flow calculated and some measured single points are compared in Figure 5.11 for the critical time period, for which the flow of single phase vapor was both determined by the code and indicated by measurements. During the time of fission product release and transport, the steam flowrate was approximately 0.2 kg/s.



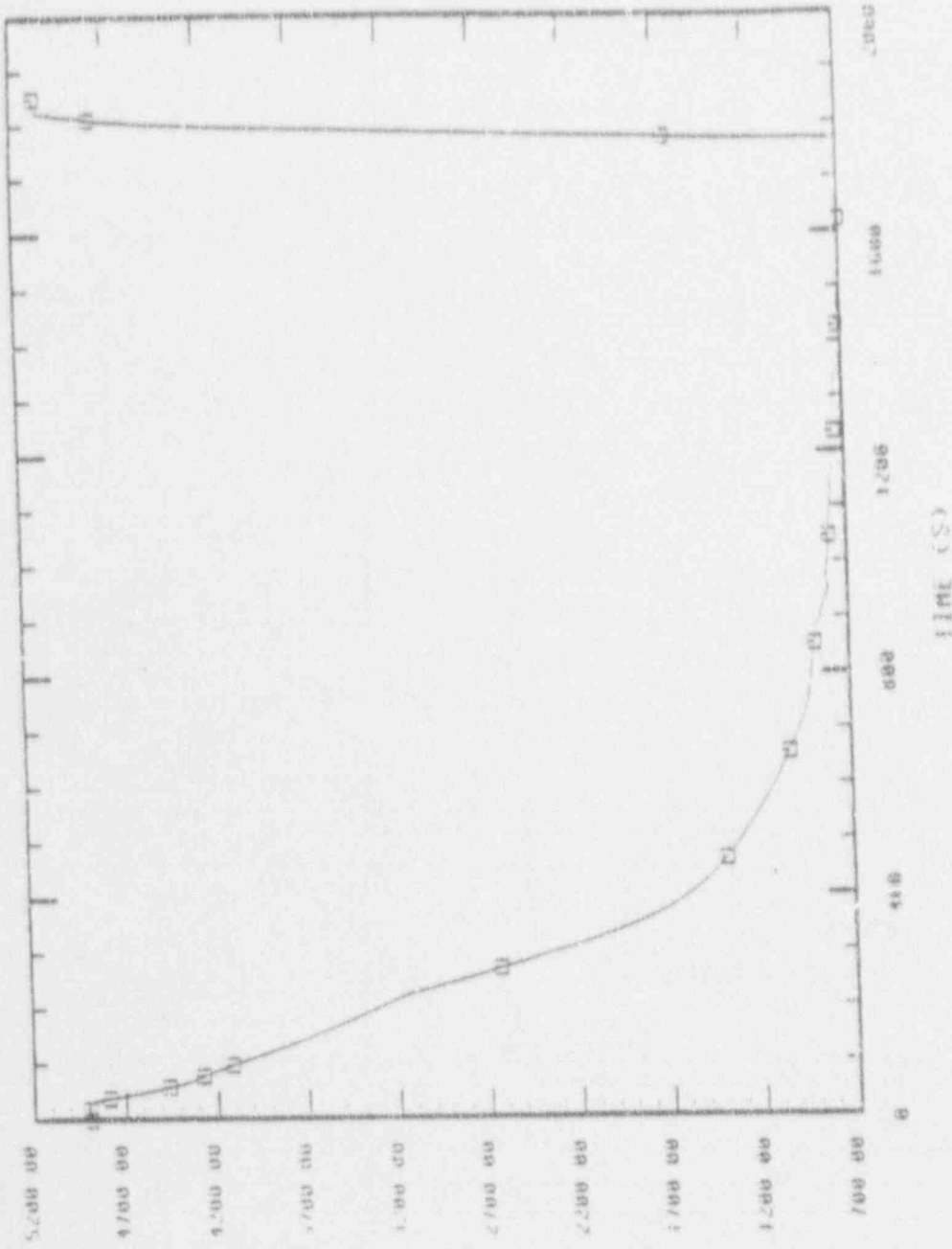
PRESSURIZER LIQUID LEVEL (H)
RELAP5/EXPERIMENT COMPARISON (5PAIN)

Figure 5.6.



MASS FLOW (KG/S) AT THE
 INTACT LOOP HOT LEG
 RELAP5/EXPERIMENT COMPARISON (SPAIN)

Figure 5.7.



PRIMARY COOLANT SYSTEM MASS (KG)
RELAPS RESULTS (SPAIN)

Figure 5.8.

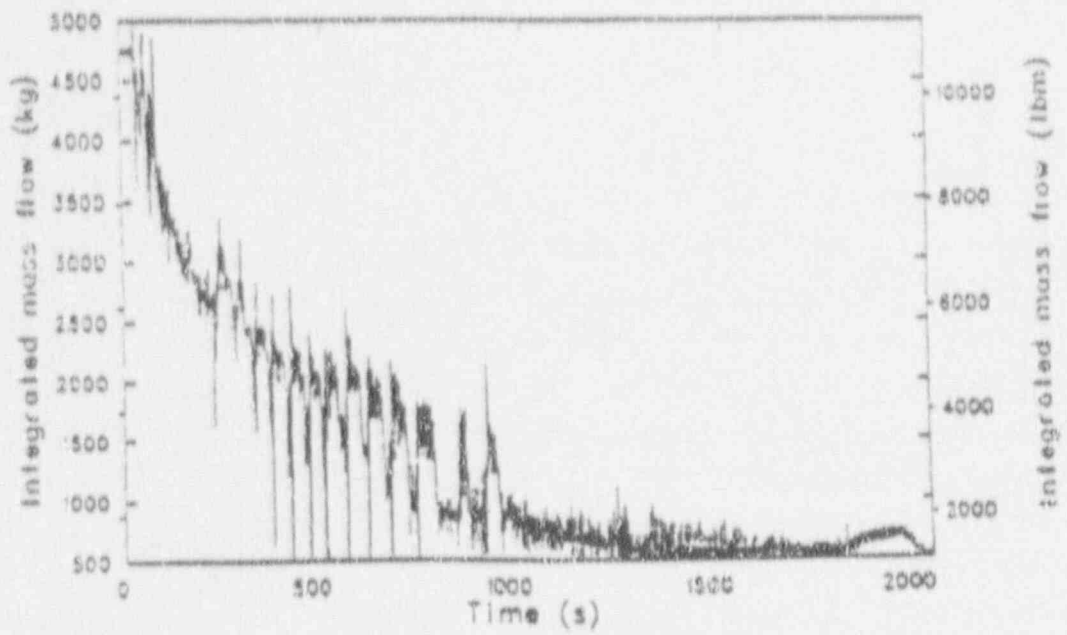


Figure 5.9 Primary coolant system mass inventory.

The experimental mass flow rate is slightly greater than the calculated one, what is consistent with the higher primary system pressure. However the differences with the calculated values (7 to 15% in flow) are much smaller than those found in the planning of the LP-FP-2 experiment (see Appendix F of Reference 3).

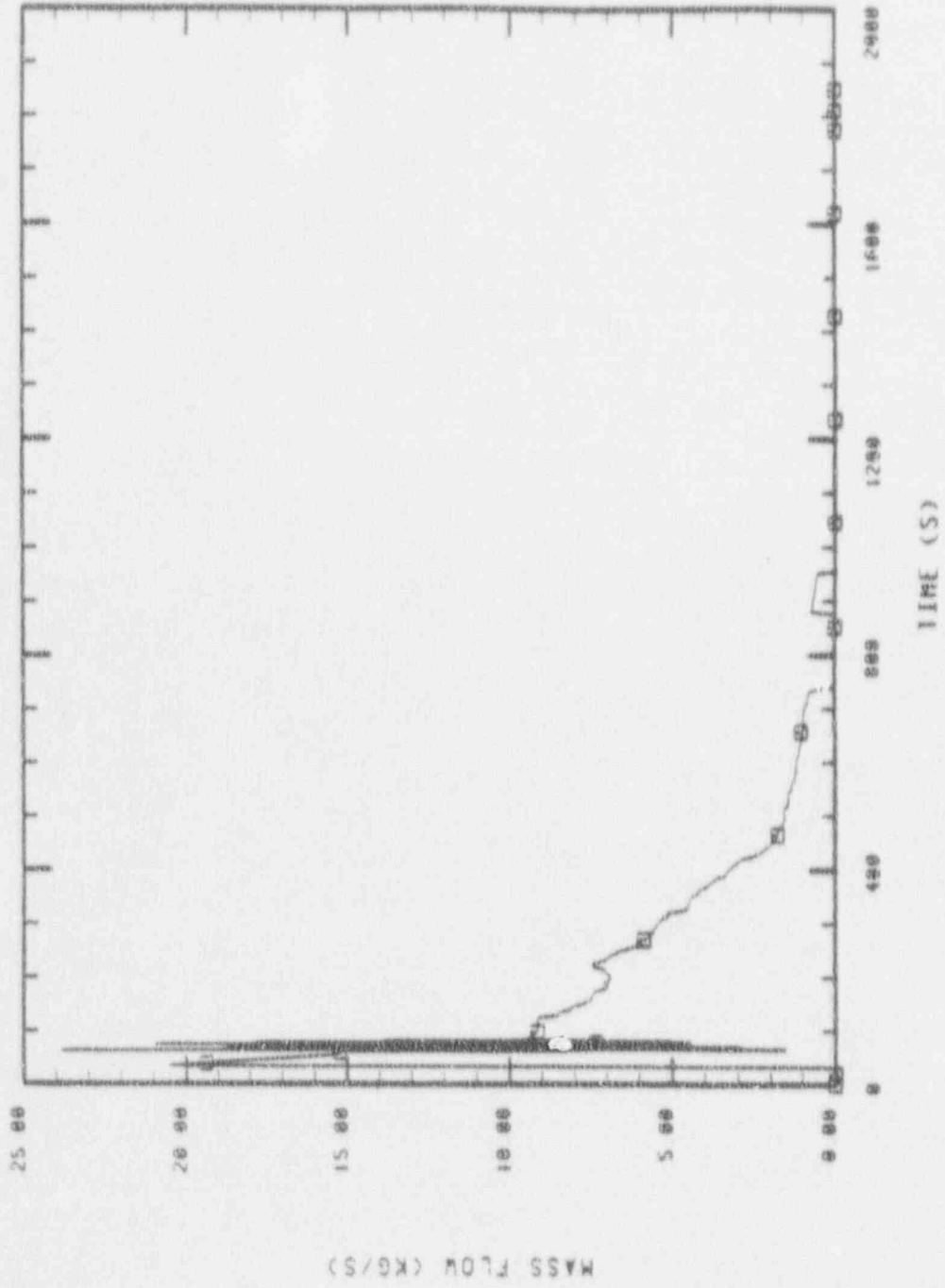
In any case these differences in the break flow have an impact in the core flow. Although there was no direct measurement of the core mass flow, the experimental steam flow rate in the center fuel module was obtained in Reference 9 from an analysis of the core thermal measured data. The resulting total mass flow rate for the center fuel module was 0.04 kg/s (0.09 lbm/s) or 0.4 g/s (9×10^{-4} lbm/s) per fuel rod, which is 3 times the value calculated prior to the experiment³. The mass flow rate was sufficient to allow the metal-water reaction to proceed without steam starvation, as it was observed in the experiment.

This value can be compared to the core flows calculated by RELAP5/MOD2 which are shown in Figure 5.12. The calculated CFM inlet flow during the damage phase (1200 to 1750 s) is a factor 5 to 25 lower than the experimentally derived value. This will be the cause of the calculated steam starvation conditions that will be shown later on this section. This enormous difference in the CFM inlet flow calculation can not be explained in terms of the differences in the LPIS line flow.

As will be explained in section 5.3, the lower than measured CFM inlet flow can be related to either errors in the calculation of the core flow redistribution due to blockages or to phenomena which have not been considered in the calculations (i.e. steam generation due to the slumping of some molten material into the lower plenum), or both.

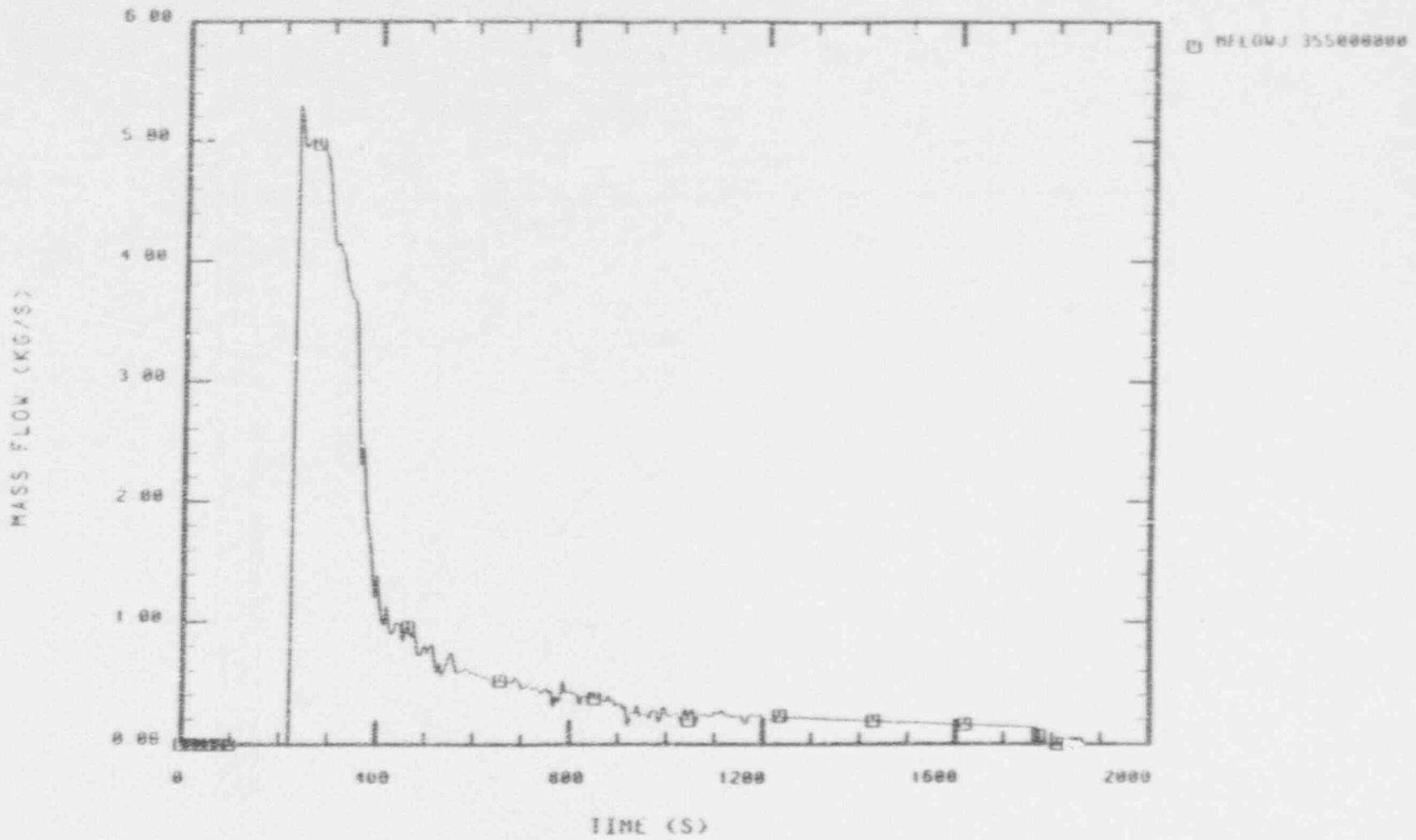
Figure 5.13 shows the calculated collapsed liquid level in the reactor vessel. Two curves are shown in this picture. One is the liquid level calculated through the average channel in the core -see the nodalization diagram in Figure 4.3- and the other is the one calculated through the CFM. No significant differences were found between both calculations.

The progression of core uncovering in the center and peripheral fuel assemblies is fairly rapid until the cold leg break was closed at 735 s; thereafter the



ILCL LINE BREAK MASS FLOW (KG/S)
RELAPS RESULTS (SPAIN)

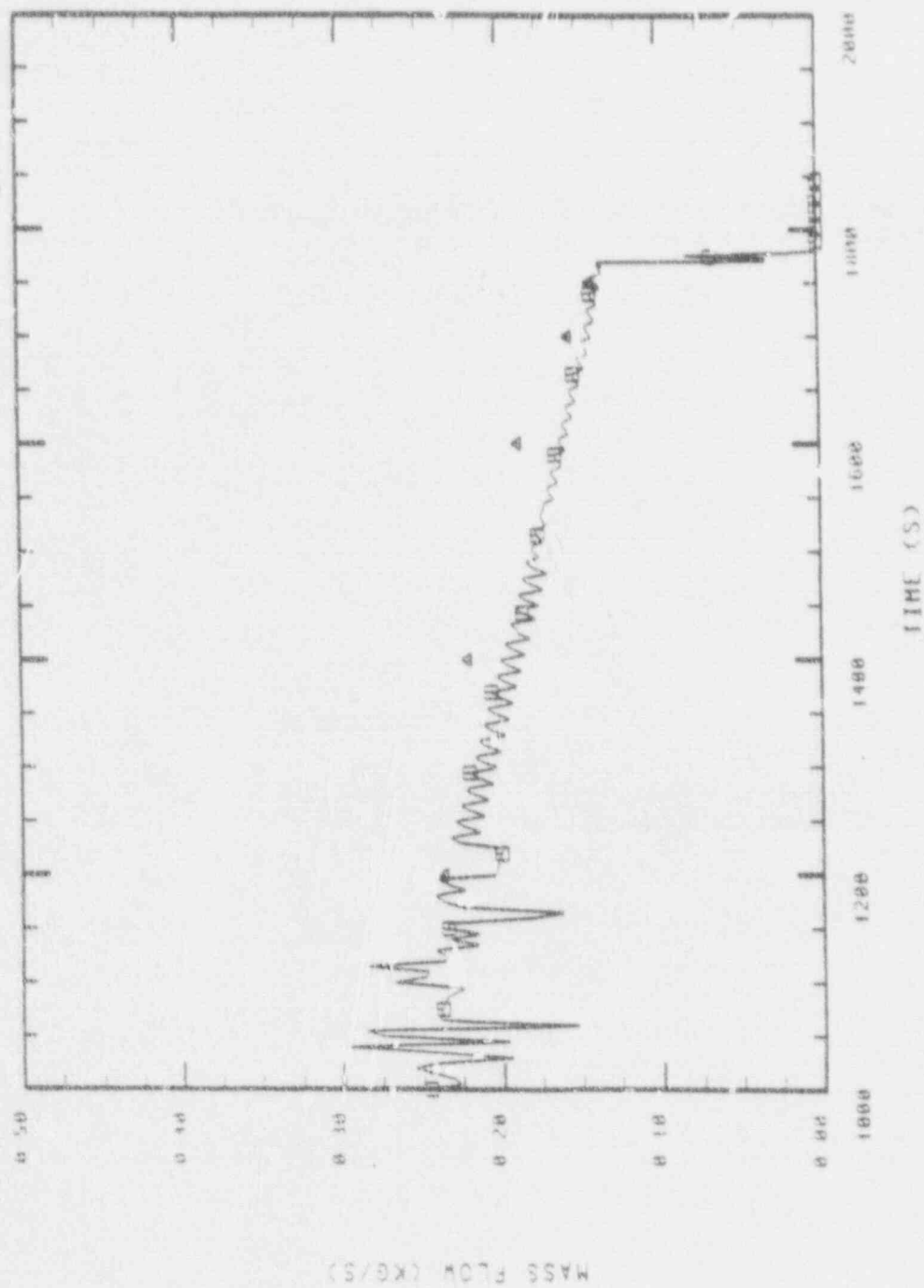
Figure 5.10.a



LPIS LINE BREAK MASS FLOW (KG/S)
RELAP5 RESULTS (SPAIN)

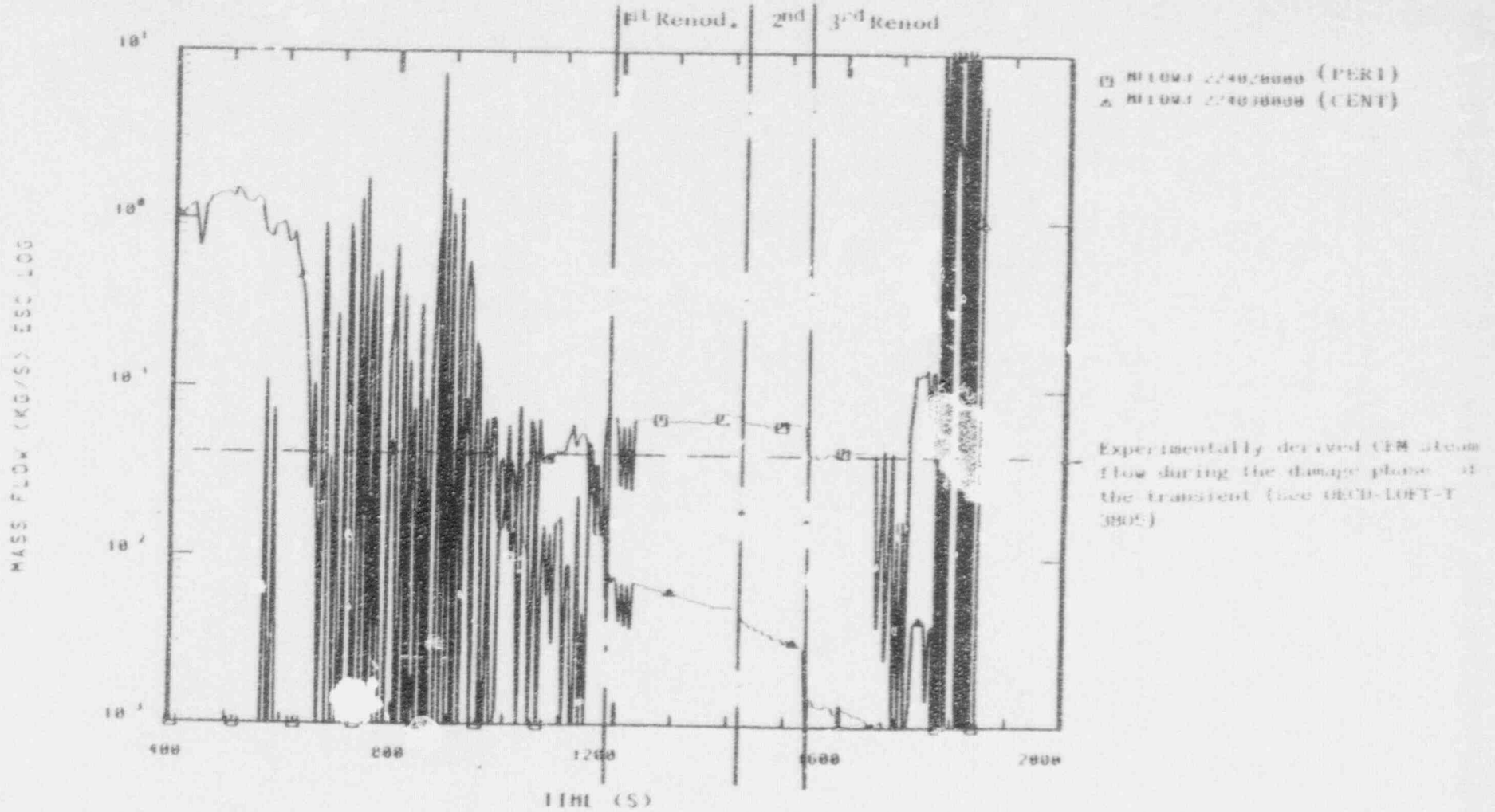
Figure 5.10.e

MFLOWJ 35500000-KCR
DATA



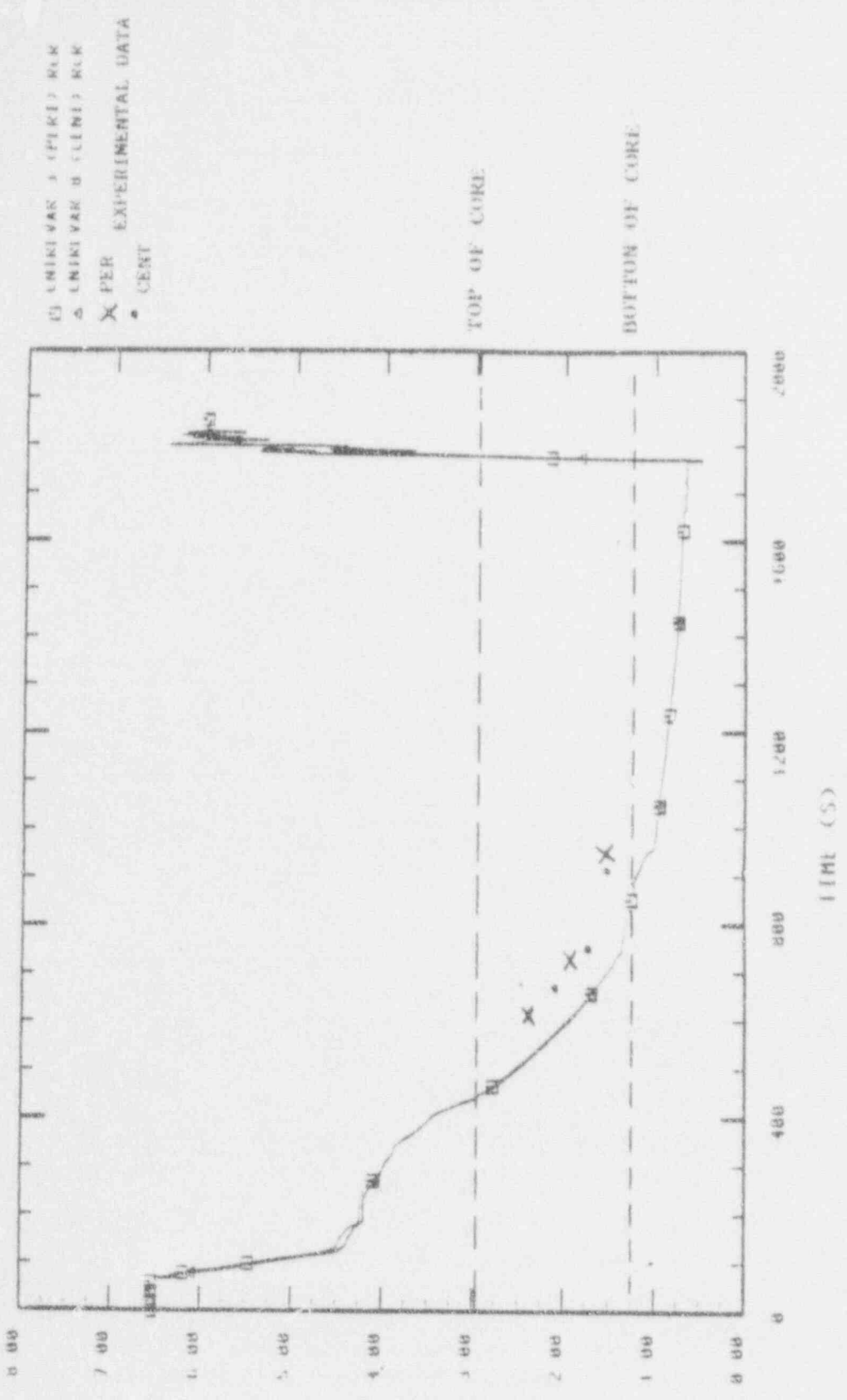
LPIS LINE BREAK MASS FLOW (KG/S)
RELAPS/EXPERIMENT COMPARISON (SPAIN)

Figure 5.11.



TP2 CORE INLET STEAM MASS FLOW RATES (KG/S) (PERIPHERAL/CENTER) RLLAP5/MOD2 (TP2 SPANISH GROUP)

Figure 5.12.



REACTOR VESSEL LIQUID LEVEL (M)
 THRU PERIPHERAL & CENTRAL BUNDLES
 RELAP5 RESULTS (SPAIN)

Figure 5.13.

(X) 07A01

uncovery progresses very slowly. It is hypothesized that closure of the cold leg break, in terminating the system depressurization, caused a sharp reduction in the rate of vapor generation and thereby brought about a total or partial collapse of the froth level in the vessel. Following the reopening of the ILCL the liquid level decreased again rapidly but after the final ILCL break closure the system pressure then remained almost constant so that the continuation of core uncovery until the end of transient was solely dependent on heat input from the fuel and metalwork.

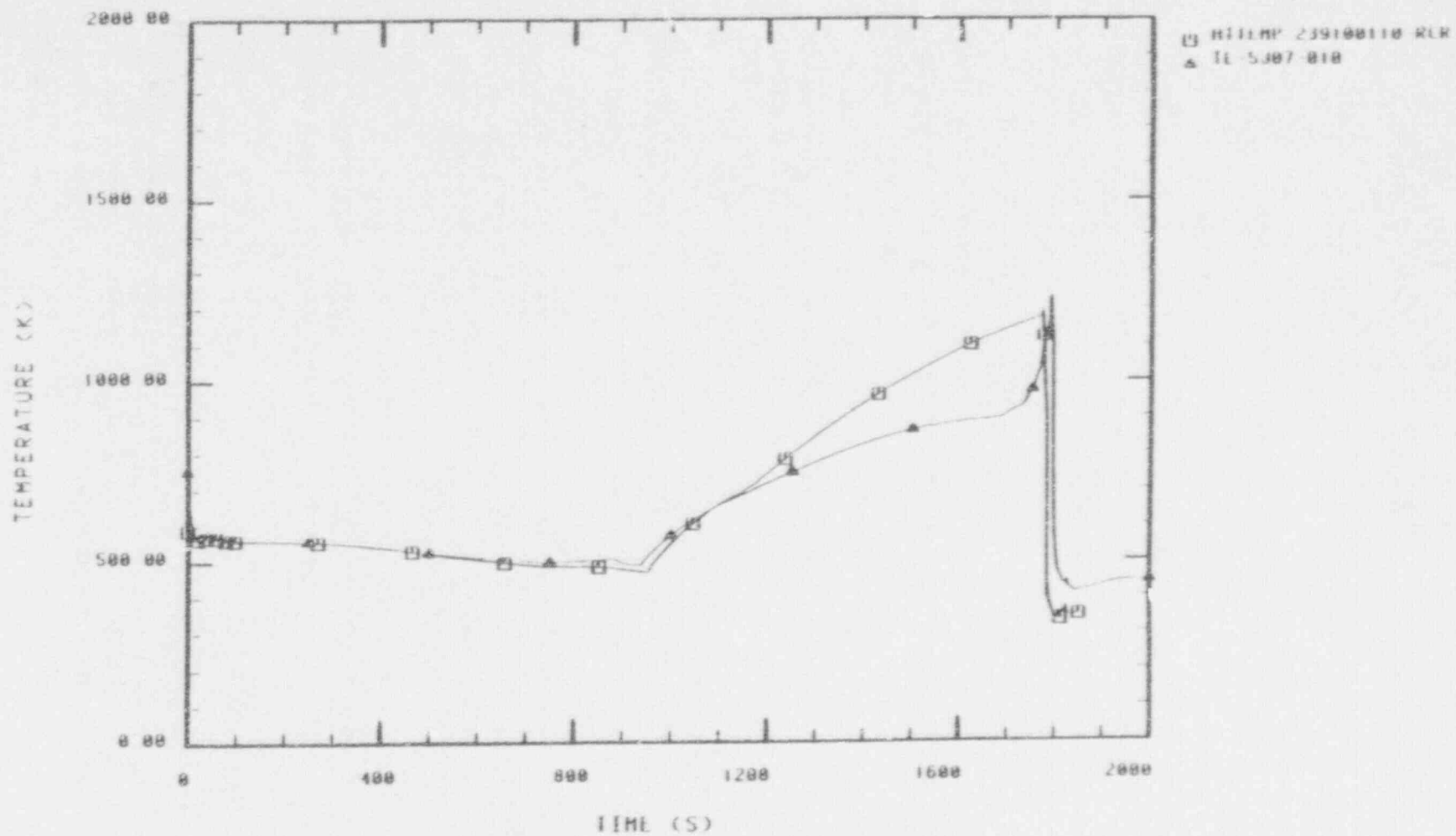
Several points representing the experimental progression of core uncovery as indicated by the observed initiation of heatup are also shown. The differences are not considered to be very important as long as the Departure from Nucleate Boiling (DNB) times at different axial levels are very accurately determined as will be shown below.

Comparison of Core Thermal Response

First of all it should be emphasized the known limitations in the capability of RELAP5/MCD2 to model the core thermal response during a severe accident. Keeping in mind this fact, the core temperature excursion calculated by RELAP5 should be considered only as an approximation to the reality.

Figure 5.14 presents the measured cladding temperatures at the 0.25 m (10 inch) elevation in the center fuel assembly with the calculation at the nearest modeled location. The DNB time and the initial heat up rate are in close agreement with the measured data. However after the first CFM blockage simulated in RELAP5 due to clad ballooning (1176s) -see Table 5.2- the rise rate was overpredicted until the end of the transient. The average temperature rise rate until 1700 s was calculated to be about 0.8 K/s, higher than the 0.5 K/s observed in the experiment.

The underprediction of mass flow of steam through the CFM is believed to have resulted in an underprediction of heat transfer coefficient. The observed increase in the temperature rise rate at 1700 s occurred at a too low temperature of about 900 K (1652K), to be the result of rapid metal-water reaction at this location and was not calculated. The observed behaviour may



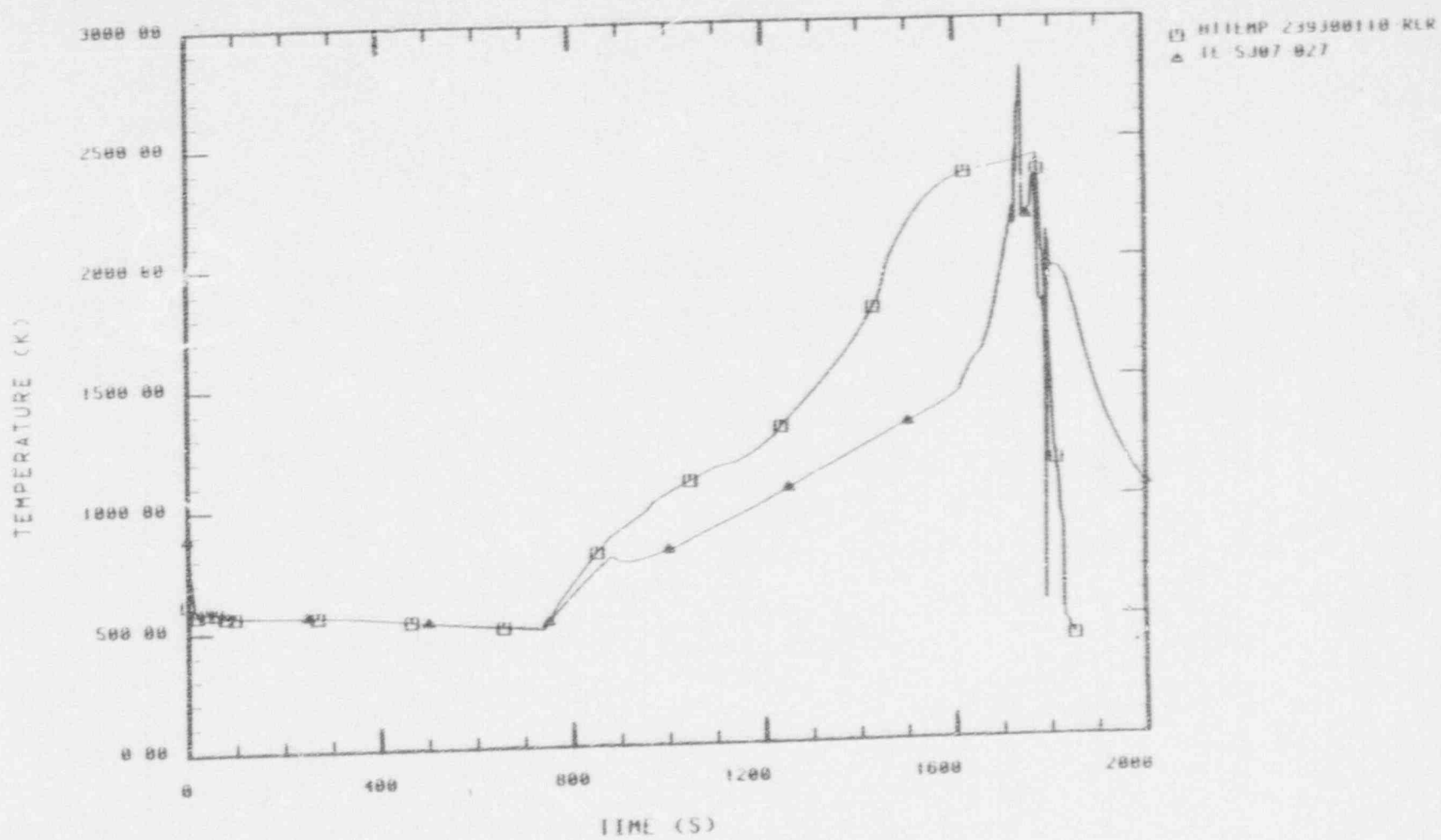
CENTRAL BUNDLE CLAD OUTER
TEMPERATURE, AXIAL LEVEL #1 (K)
RELAPS/EXPERIMENT COMPARISON (SPAIN)

Figure 5.14.

be the result of the thermal radiation due to the temperature of the material at higher elevations or to material relocation (most probable). Neither thermal radiation in the axial direction nor the direct effect of material relocation on local temperature is modeled by RELAP5.

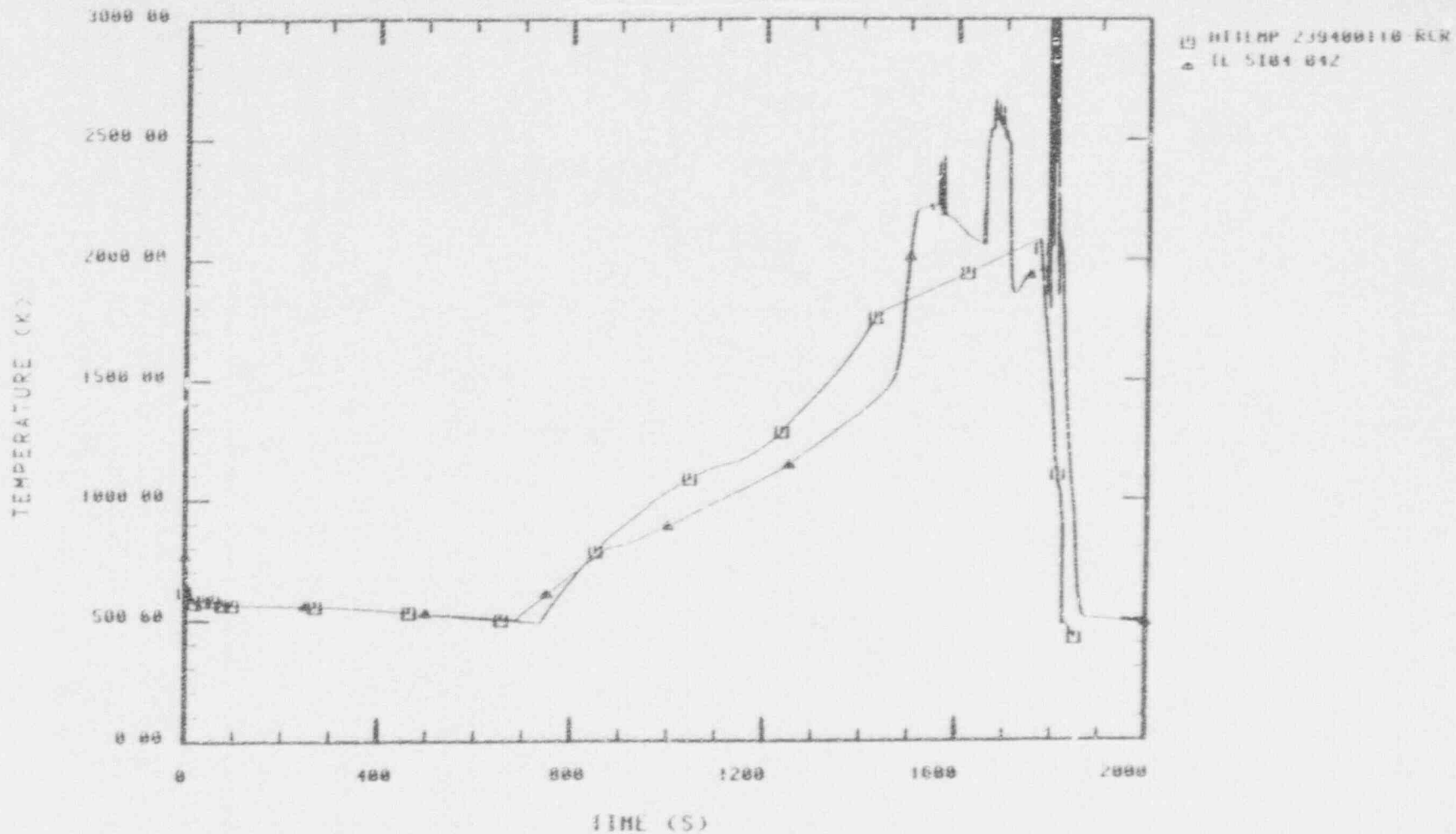
Figure 5.15 compares the fuel rod cladding temperature measured at the 0.69 m (27 inch) elevation in the center assembly with the corresponding RELAP5 results. Good agreement with the initial heat-up rate of 2.2 K/s (4.0 F/s) was obtained in the calculation during the period prior to PORV operation and reopening of the cold leg break. The observed temperature rise rate then decreased, apparently due, to flashing of liquid in the lower plenum induced by the depressurization. However this effect is not so strong in the calculation because of the lower than measured depressurization rate during this period. This causes a higher than measured temperature prior to the initiation of the Metal-Water reaction (MWR). As a consequence, the initiation of the MWR dominated temperature excursion begins much earlier in the calculation (1225 s) than in the data (1590 s). What is more surprising is that the observed oxidation of zircaloy by steam becomes important at temperatures in excess of 1400 K (2560 °F)⁹, in contrast with the 1273 °K considered in the Cathcart-Powell model. We have not found any satisfactory explanation to this fact. Following M-W reaction onset as predicted by RELAP5, the rise rate was then overestimated until about 1550 s, when the code calculates a too low CFM steam flow, which is not enough to maintain the exothermic reaction. Even though this steam starvation situation, the maximum calculated clad temperature of 2430°K is very close to the maximum validated experimental data. The calculated cooldown due to the ECCS injection is much faster than the observed one at this elevation.

Figure 5.16 compares the measured fuel rod cladding temperature at the 1.07 m (42 inch) elevation in the center assembly with the nearest corresponding calculated temperatures (0.84- to 1.12-m (33- to 44-inches) elevation). The average rate of temperature rise was observed to be about 1.3 K/s (2.3 F/s) until 1450 s (after which the temperature increased very rapidly due to the metal-water reaction). Up to this point in time the temperature increase calculation was not too different from the data. As before, the initially higher than measured temperatures can be associated with the underprediction of the CFM steam flow. The observed temperature rise rate increased rapidly after 1450 s, when the cladding temperature was about 1500 K (2240°F), to about 22 K/s (40°F/s). Only a small increase in the temperature rise rate was



CENTRAL BUNDLE CLAD OUTER
 TEMPERATURE, AXIAL LEVEL #3 (K)
 RELAP5/EXPERIMENT (SPAIN)

Figure 5.15.



CENTRAL BUNDLE CLAD OUTER
 TEMPERATURE, AXIAL LEVEL 14 (K)
 RELAP5/EXPERIMENT COMPARISON (SPAIN)

Figure 5.16.

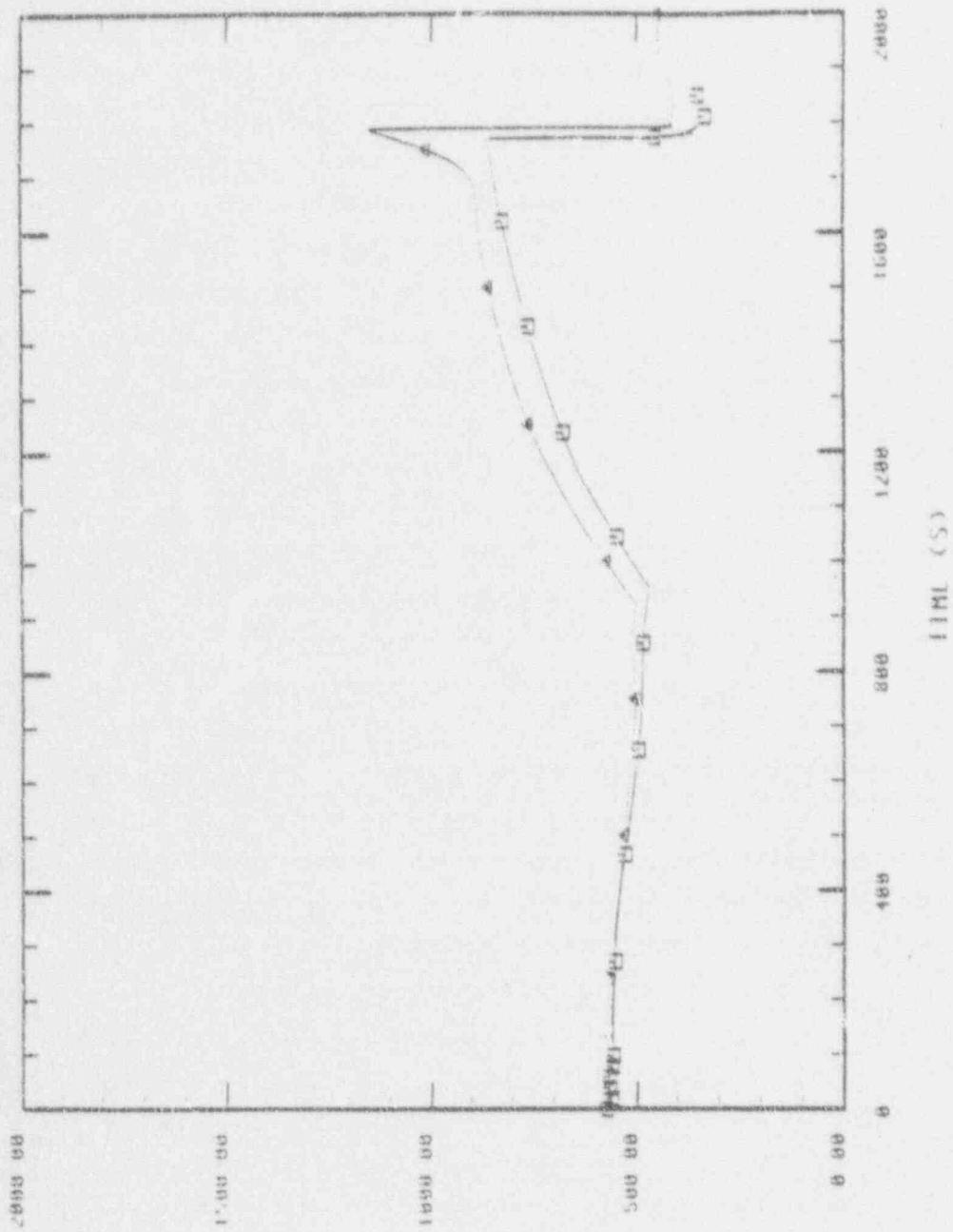
calculated because the comparatively low mass flow rate in the center assembly, about 0.0035 Kg/s, resulted in steam limitation at this elevation. It should be noticed that the maximum cladding temperatures measured (2400 K) were located at this elevation, whereas the maximum predicted temperatures occurred at the 0.56- to 0.84-m (22- to 33-inch) elevation.

In contrast with the previous picture, the quenching of the clad due to the reflood is accurately simulated.

Figures 5.17 to 5.19 compare the code results with the measured cladding temperatures in the peripheral fuel assemblies at different elevations.

Figure 5.17 shows an excellent agreement between the calculated and measured peripheral clad temperatures at the 10- in elevation until about 1700 s. At 1700 s, the thermocouples near the outside of the shroud, particularly at lower elevations, began an extraordinary temperature excursion. The cause of the rapid peripheral temperature rise is somewhat uncertain. The exothermic reaction between zircaloy and water is not considered a possibility because the initiation temperatures were too low; nor is radiation from the shroud wall likely because the wall temperature is lesser than that reached by the fuel rod thermocouples at this elevation. It is judged that the rapid temperature rise was caused by shunting of the thermocouple leads, where they passed through an area of high temperature⁹ (near the top of the core). Therefore the differences with the calculated results are meaningless.

The maximum cladding temperatures measured in the peripheral fuel assemblies occurred at the 0.66 m (26 inch) elevation on fuel rods adjacent to the insulating shroud. Figure 5.18 shows the temperature history recorded by thermocouple TE-4H15-026 together with the corresponding temperatures predicted by RELAP5/MOD2. The agreement is excellent until the opening of the PORV (882 s). Due to the lower than measured primary system pressure, the cooling induced by the opening of the PORV (flow increase) is less effective in the calculations than in the measurements. Taking also into account the earlier closure of the PORV, the calculated temperatures of the peripheral modules are greater than the observed ones until about 1600 s. Then the same sudden temperature excursion took place. As explained in Figure 5.18, no credit was taken of this excursion. The calculated maximum peripheral cladding temperatures (1460 K) occurs at 4th elevation in contrast with the experimental observations. This can be easily justified in terms of the strange



PERIPHERAL BUNDLE CLAD OUTER
 TEMPERATURE AXIAL LEVEL 11 (K)
 RELAPS/EXPERIMENT COMPARISON (SPAIN)

Figure 5.17.

(X) 11 00 17 00 00 00 00

03 HITEMP 237300110 RUK
▲ 1c 4015 026

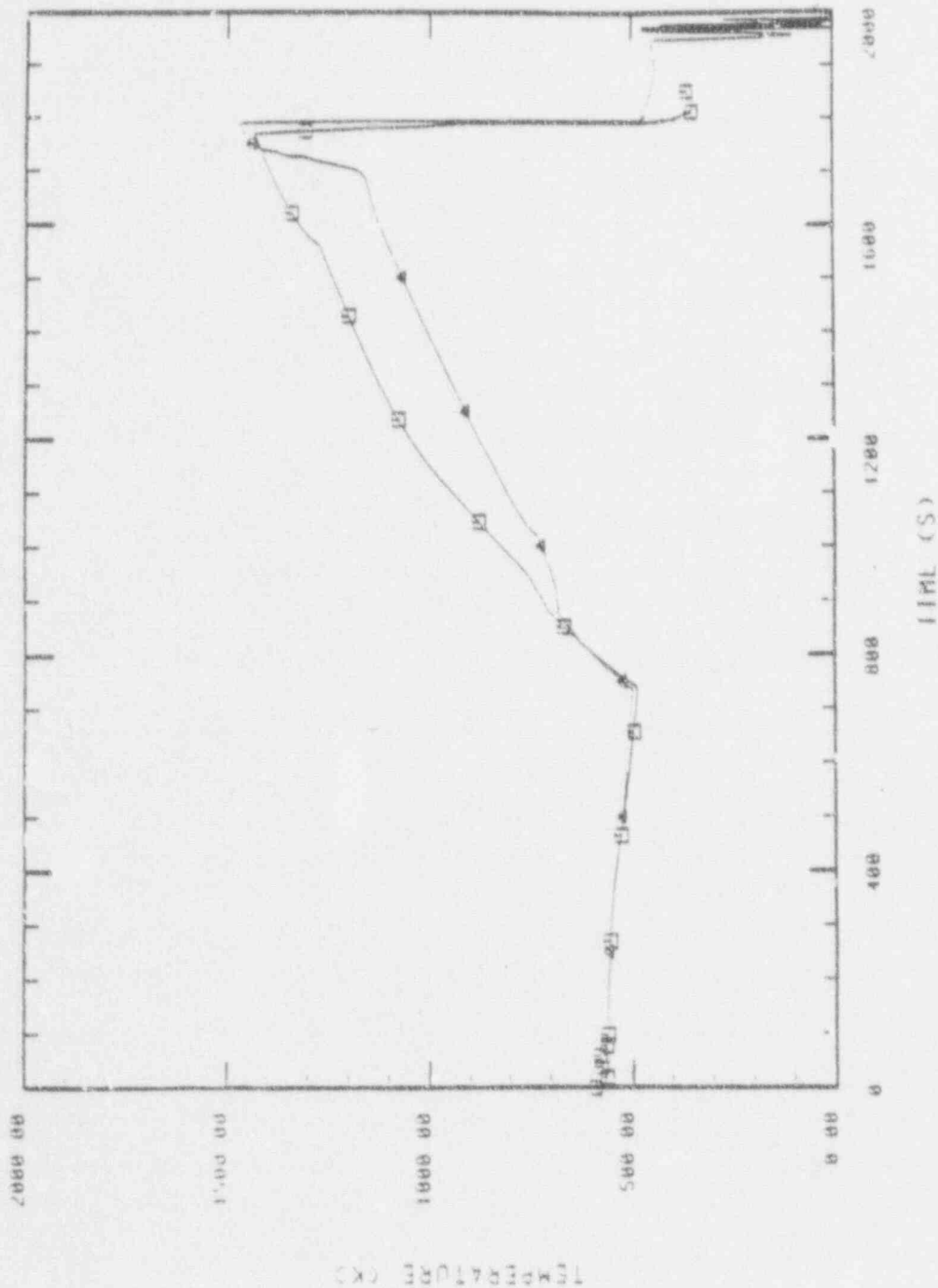


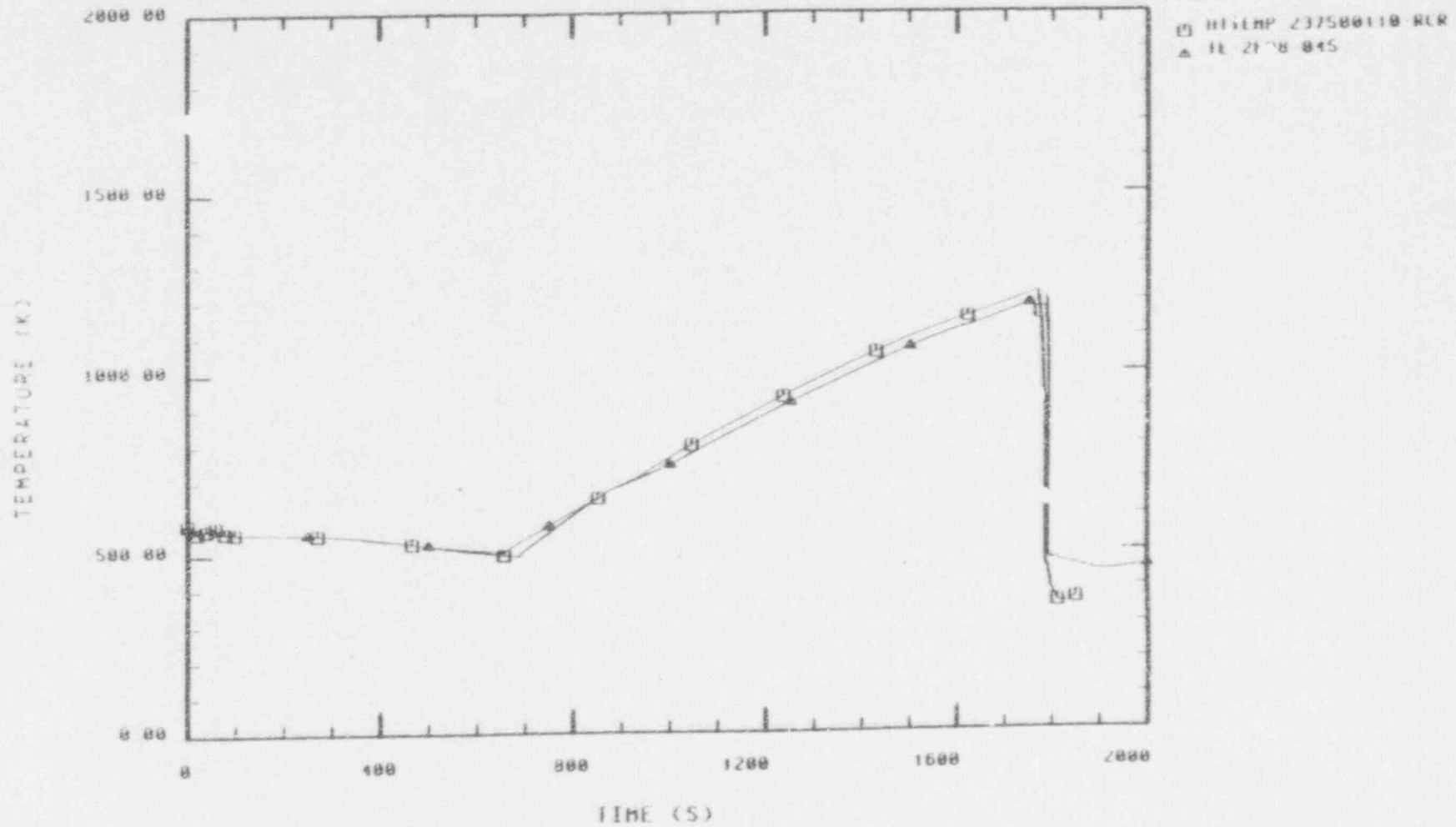
Figure 5.18.

recorded temperature excursion at lower elevations.

Figure 5.19 shows a comparison of the recorded peripheral fuel assembly temperatures at 45 in elevation with the corresponding RELAP5 results. The agreement between data and computational results is remarkable.

The temperature measured on the outer wall of the shroud at the location close to 1E-2H15-026 and the temperature calculated by RELAP5 are shown in Figure 5.20. The programmatic experiment termination criterion was reached on the shroud outer wall (temperature above 1517 °K). However the calculation using RELAP5/MOD2 underpredicted the shroud temperature measured at this location and also those measured at the 0.81 m (32 inch), and 1.07 m (42 inch) elevations due to the lack of a model for thermal radiation, an important mechanism controlling the temperature rise of unheated structures. For this reason the ECCS trip criterion chosen for the RELAP5/MOD2 simulation was only the maximum peripheral clad temperature (1460 K), neglecting the shroud criterion.

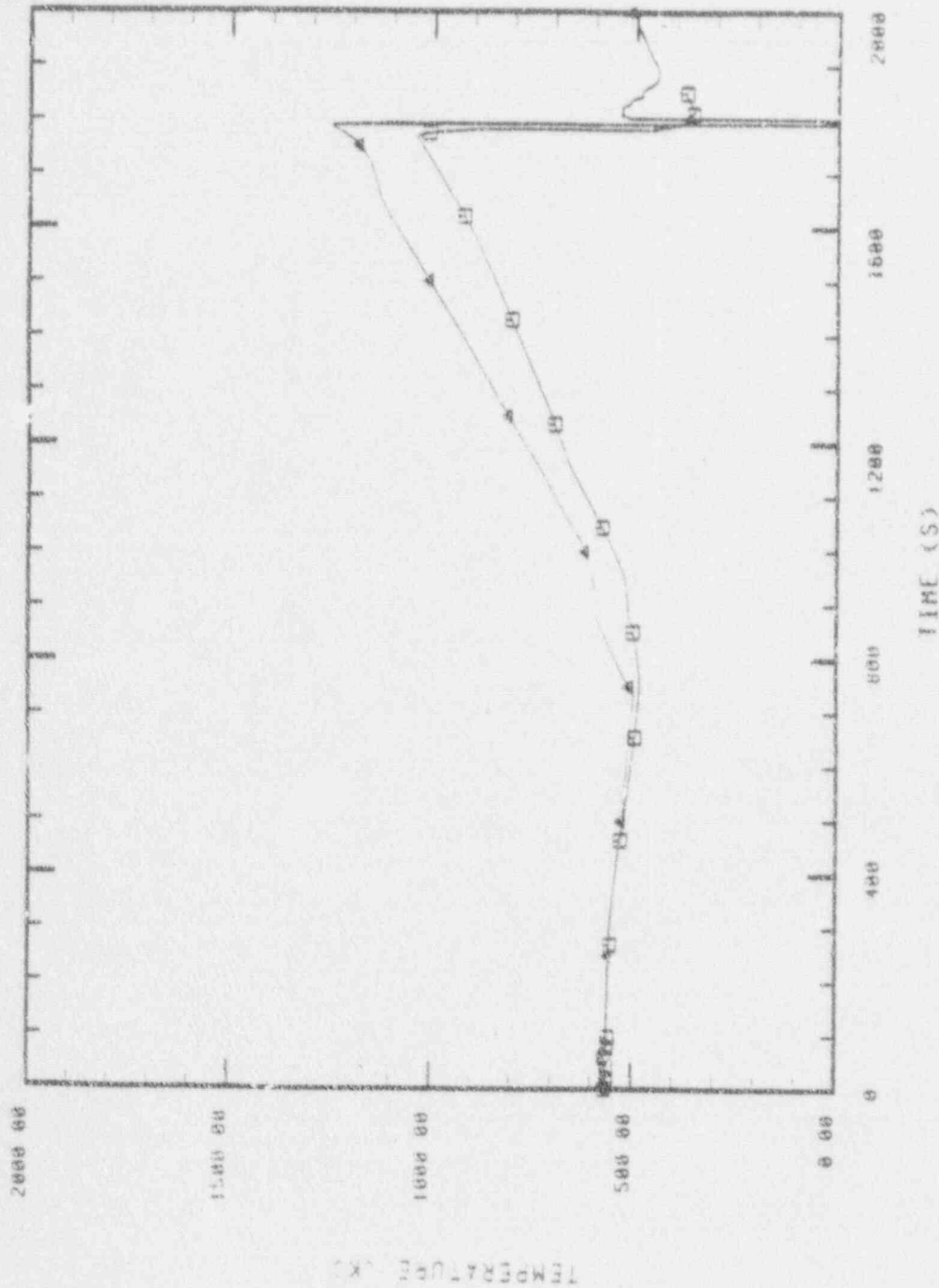
In any case, the relationship between the center and peripheral fuel rod temperatures and the shroud ones was in good agreement with the data. As a result, the time above 2100 K (3321°F) in the center bundle was calculated to be about 279 s -Table 5.2- in very close agreement with the 270 s measured in the plant.



PERIPHERAL BUNDLE CLAD OUTER
 TEMPERATURE, AXIAL LEVEL #5 (K)
 RELAPS/EXPERIMENT COMPARISON (SPAIN)

Figure 5.10

□ HTXMP 10000301-RUR
 ▲ TE-55-027



OUTER CFM SHROUD WALL
 TEMPERATURE, AXIAL LEVEL #3 (K)
 RELAPS/EXPERIMENT COMPARISON (SPAIN)

Figure 5.20

5.3. Conclusions of the Base Case Transient Calculation

- Even though RELAP5/MOD2 has been used beyond its own design capabilities, the calculations reproduced, in general, reasonably well the experimental data.
- The major problem observed in system hydraulic calculations is the lower than measured primary system pressure after LPIS line break opening.
- It is believed that the LPIS line flow characteristics completely affect the pressure evolution.
- The calculated and measured core uncover processes are in very close agreement (DNB time at different elevations is fairly accurately computed).
- The global core thermal response during Experiment LP-rP-2 was, in general, reasonably well calculated by RELAP5/MOD2, keeping in mind the limited capability of the code to model the processes that take place at high temperatures. (neither radiation nor location models)
- Measured and calculated core heat-up rates prior to the onset of the rapid oxidation are in overall agreement. The differences are explained considering the lower core mass flow induced by the lower than measured primary system pressure.
- After a rapid oxidation begins, the calculation significantly underestimates the rate of heatup in the upper part of the CFM due to the steam starvation calculated by the code.
- Uncertainties in the degree of CFM blockage, core flow redistribution caused by blockage, and amount of steam flow generated by the slumping of molten core materials into the lower plenum are thought to be the most probable causes for the steam limitation observed in the calculations.

6. RELAP5/MOD2 SENSITIVITY ANALYSIS

As discussed in previous sections of this report, the amount of CFM blockage during the transient is one of the major uncertainties in the RELAP5/MOD2 calculation.

The different than observed CFM heat-up behavior is clearly due to the very low CFM mass flow calculated by RELAP5. This, in turn, is strongly influenced by the amount of CFM blockage. Until more experimental evidence of the degree of blockage can be known from PIE's²¹, it is very difficult to estimate the real blockages of the CFM. In the same way, considering the sensitivity studies conducted at the INEL for the SEP document³, and based on our own experience in performing several RELAP5 posttest runs, the RELAP5/MOD2 does not seem to be very sensitive to variations in the degree of blockage. Also, the large number of runs required to obtain a reasonable value of the amount of blockage for every different physical phenomena, drove us to choose the simplest option, i.e.: To run a NON-CFM-BLOCKAGE RELAP5 calculation.

The idea behind this NON BLOCKAGE sensitivity analysis was to get the same global thermal-hydraulic calculated results, but with different core mass flow distribution, and so different clad temperature excursions.

A non-blockage calculation would a priori increase the CFM inlet mass flow, providing more steam available to react with the Zr such that the cladding temperatures would reach higher values than previously calculated.

The results of this sensitivity analysis with respect to the blockages are presented below.

6.1 Results of the Sensitivity with Respect to the Blockages.

In the following paragraphs, the results of this RELAP5/MOD2 sensitivity study with respect to blockages are presented. In the figures, the notation is as follows:

RCR stands for the RELAP5 calculated results taking into account the core renodalizations induced by the blockages.

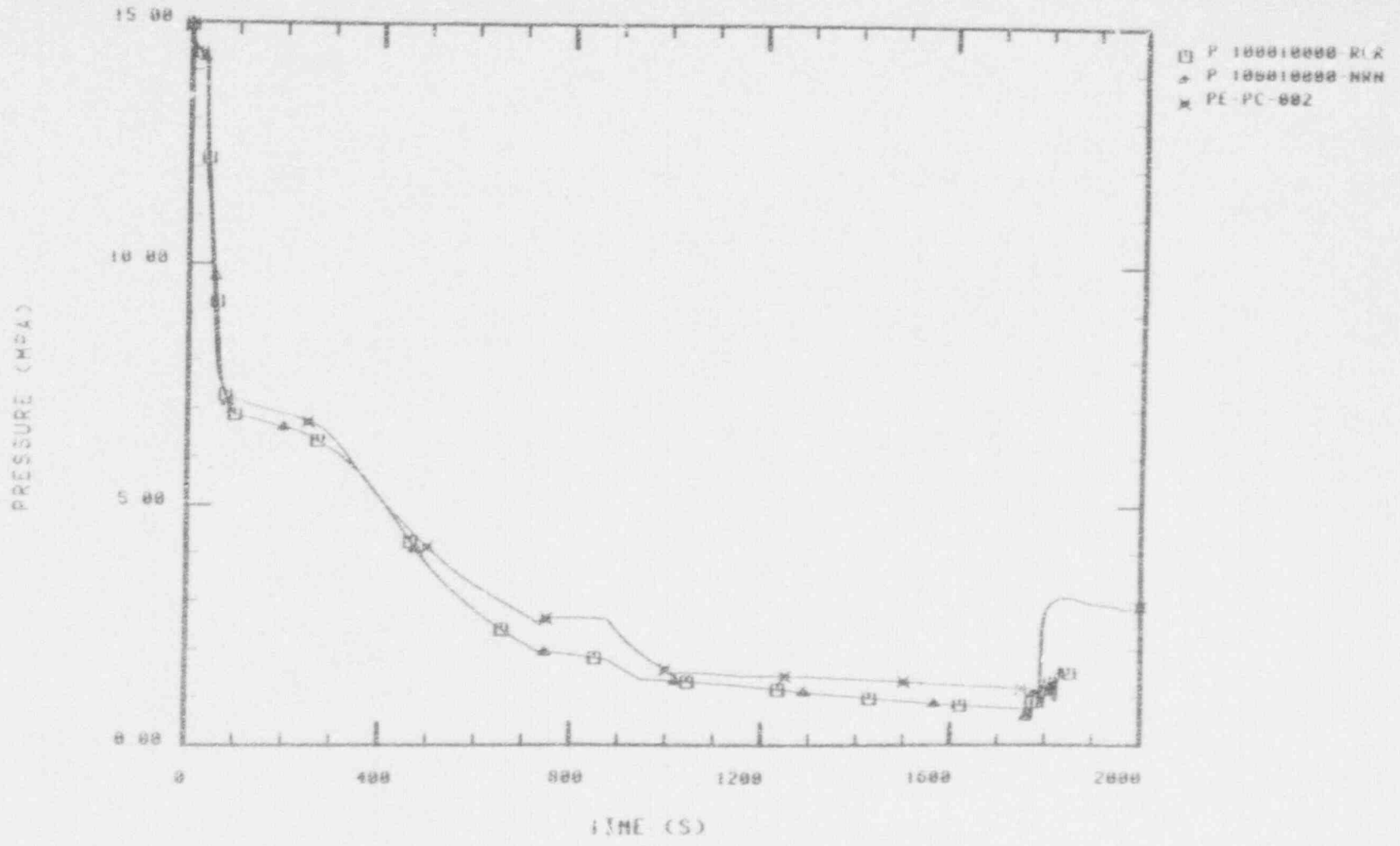
NRN stands for the RELAP5 calculated results neglecting the core geometry changes.

As expected, the general LOFT system behaviour, best represented by the primary system pressure, was not affected by the non-blockage simulated conditions (see Figure 6.1). The same was true for other important thermal-hydraulic parameters as secondary system pressure, loop densities, break flows and core liquid level.

The major impact of this NON-BLOCKAGE CASE is the mass flow distribution within the core. Figures 6.2 and 6.3 show a comparison of core flows between the RELAP5/MOD2 base case and the sensitivity analysis results. Figure 6.2 shows a comparison of both calculated CFM inlet flows. The CFM mass flow calculated by RELAP5/MOD2 without blockages is about the double than the calculated for the base case during the period 1200 s to 1550 s, and a factor 6 for the latest phase of the transient (1550 s to 1750 s). As a consequence, the flow through the peripheral channel calculated for the NO BLOCKAGES case is lower than that of the base case.

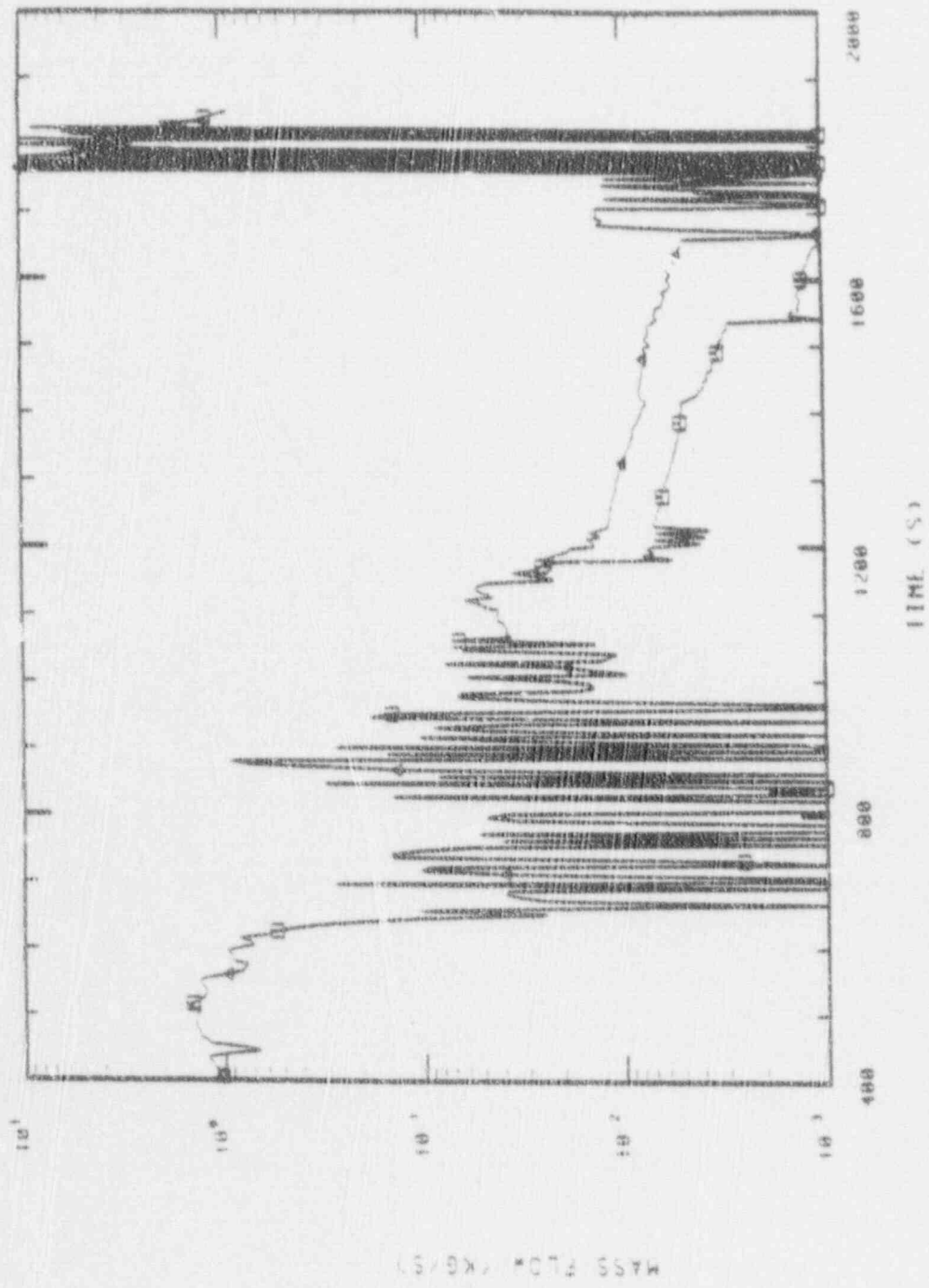
These differences in the mass flow through the peripheral channels are not large enough to substantially modify the heatup process in those assemblies (see figure 6.4). However, the new higher CFM inlet flow dramatically affects the temperature excursion in this assembly, which is basically controlled by the metal-water reaction.

Figures 6.5 to 6.7 present a comparison of both calculated CFM clad temperatures results with the measured values. The reduced pressure drop in the CFM (No-blockages) allows enough vapor flow through it to sustain the metal-water reaction, obtaining clad temperatures even higher than the measured ones. Not only the maximum temperatures, but also the heatup rates are in closer agreement with the experimental data than those previously calculated.



PRIMARY SYSTEM PRESSURE (MPa)
AT THE IL HOT LEG LOCATION
RELAPS SENSITIVITY STUDY (SPAIN)
Figure 6.1

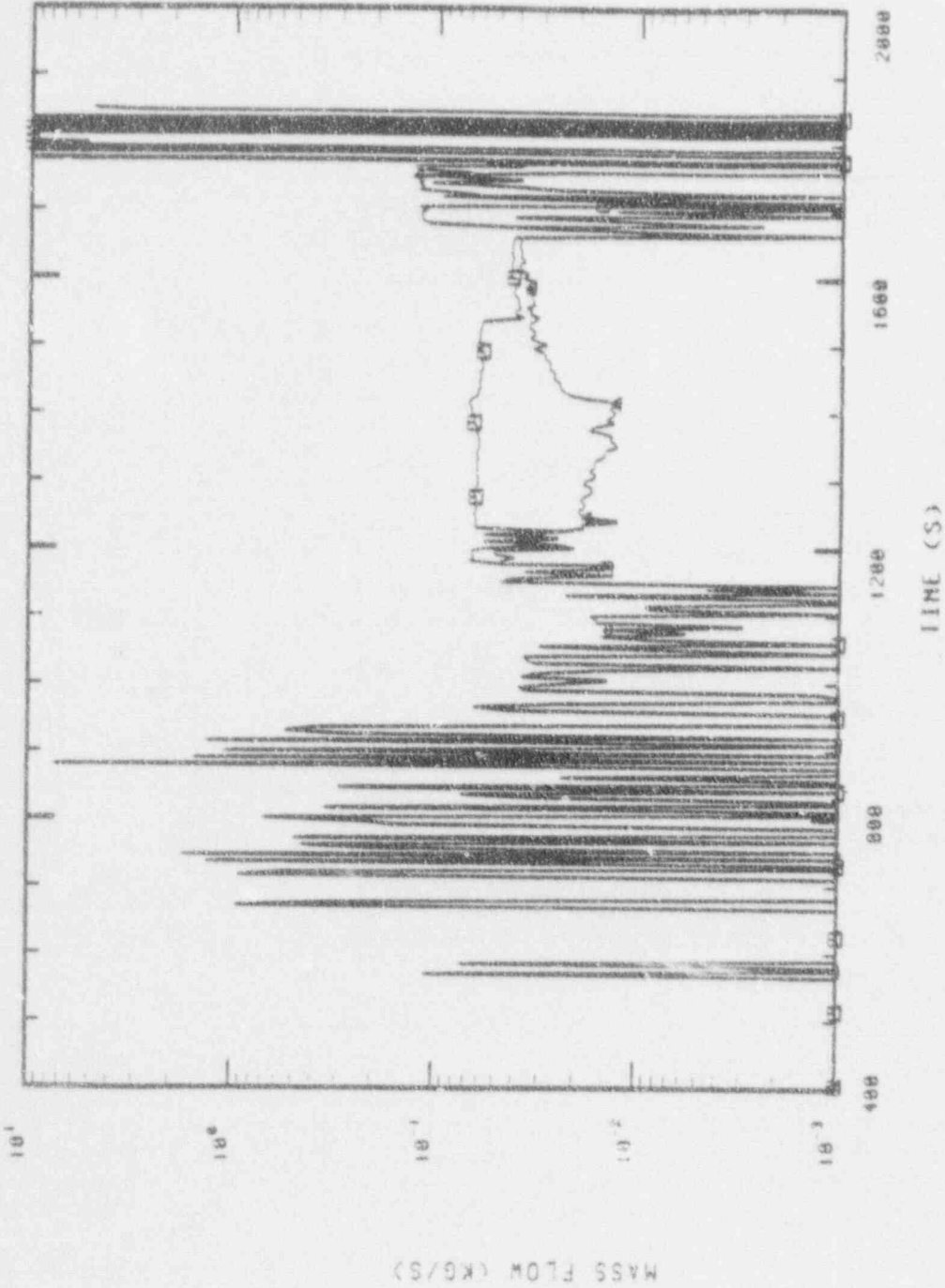
□ M1041 224818888 K1R
 △ M1041 224818888 M1R



CENTER FUEL BUNDLE INLET MASS
 FLOW RATE (KG/S)
 RELAP5 SENSITIVITY STUDY

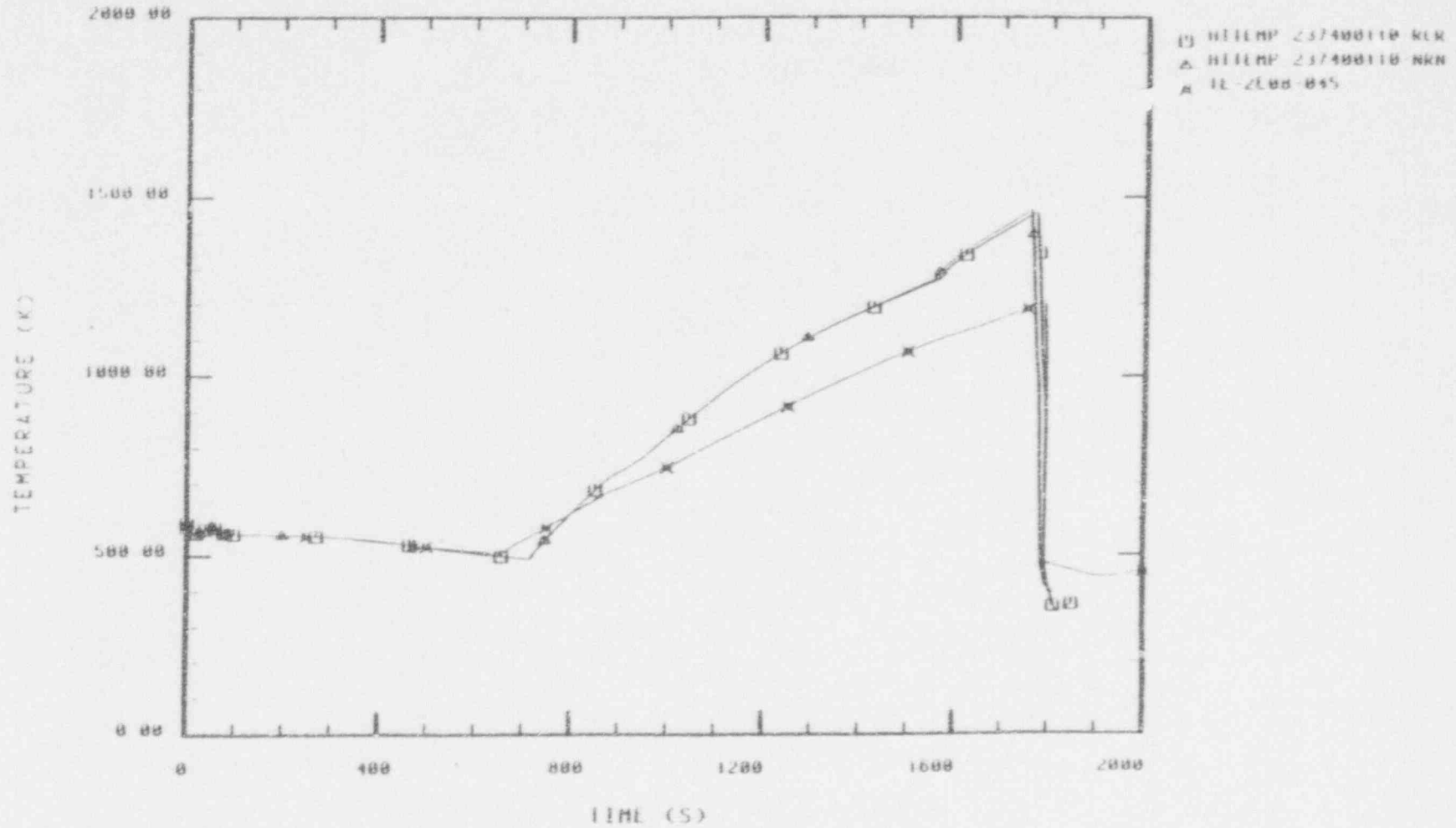
Figure 6.2

01 M1100J 224020000 RCR
A. M1100J 224020000 RCR



PERIPHERAL BUNDLE INLET STEAM
MASS FLOW RATE (KG/S)
01 ELAP5/MOD2 (FP2 SPANISH GROUP)

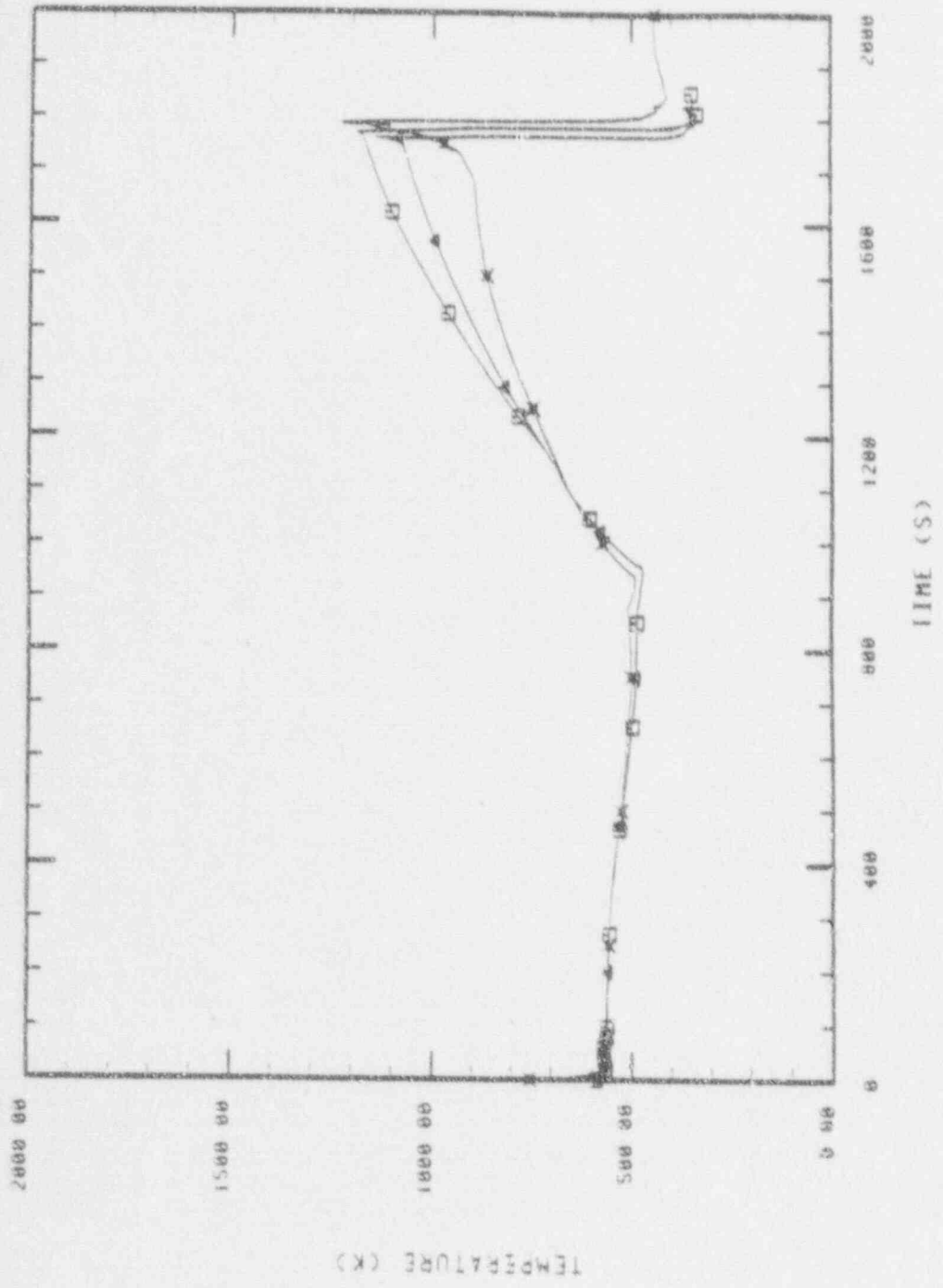
Figure 6.3



PERIPHERAL BUNDLE CLAD OUTER
TEMPERATURE, AXIAL LEVEL #4 (K)
RELAPS SENSITIVITY STUDY (SPAIN)

Figure 6.4

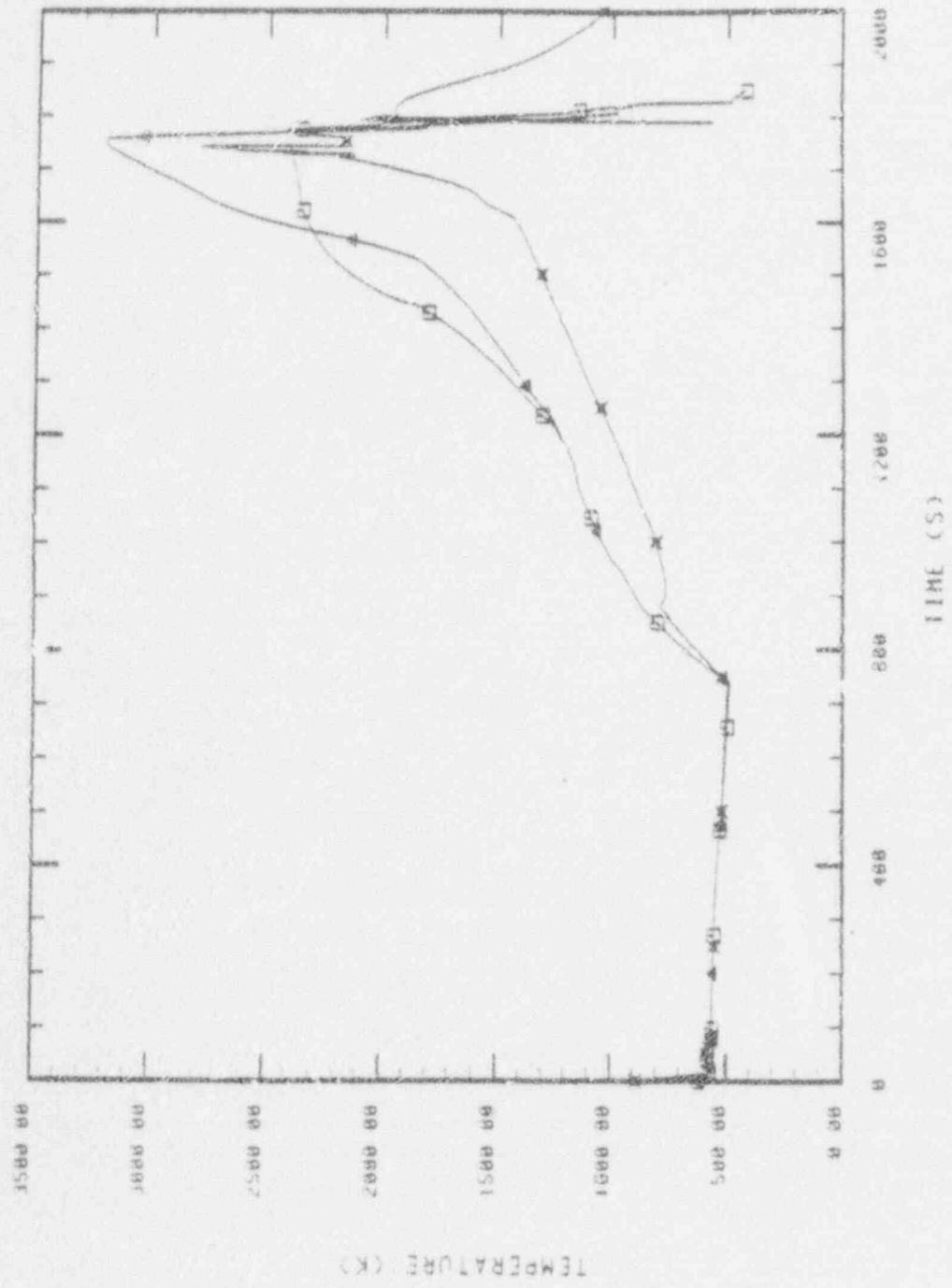
□ HELLIP 239100110 RLR
 △ HELLIP 239100110 NRR
 × LL 5007-010



CENTER BUNDLE CLAD OUTER
 TEMPERATURE, AXIAL LEVEL #1 (K)
 RELAPS SENSITIVITY STUDY (SRAIN)

Figure 6.5

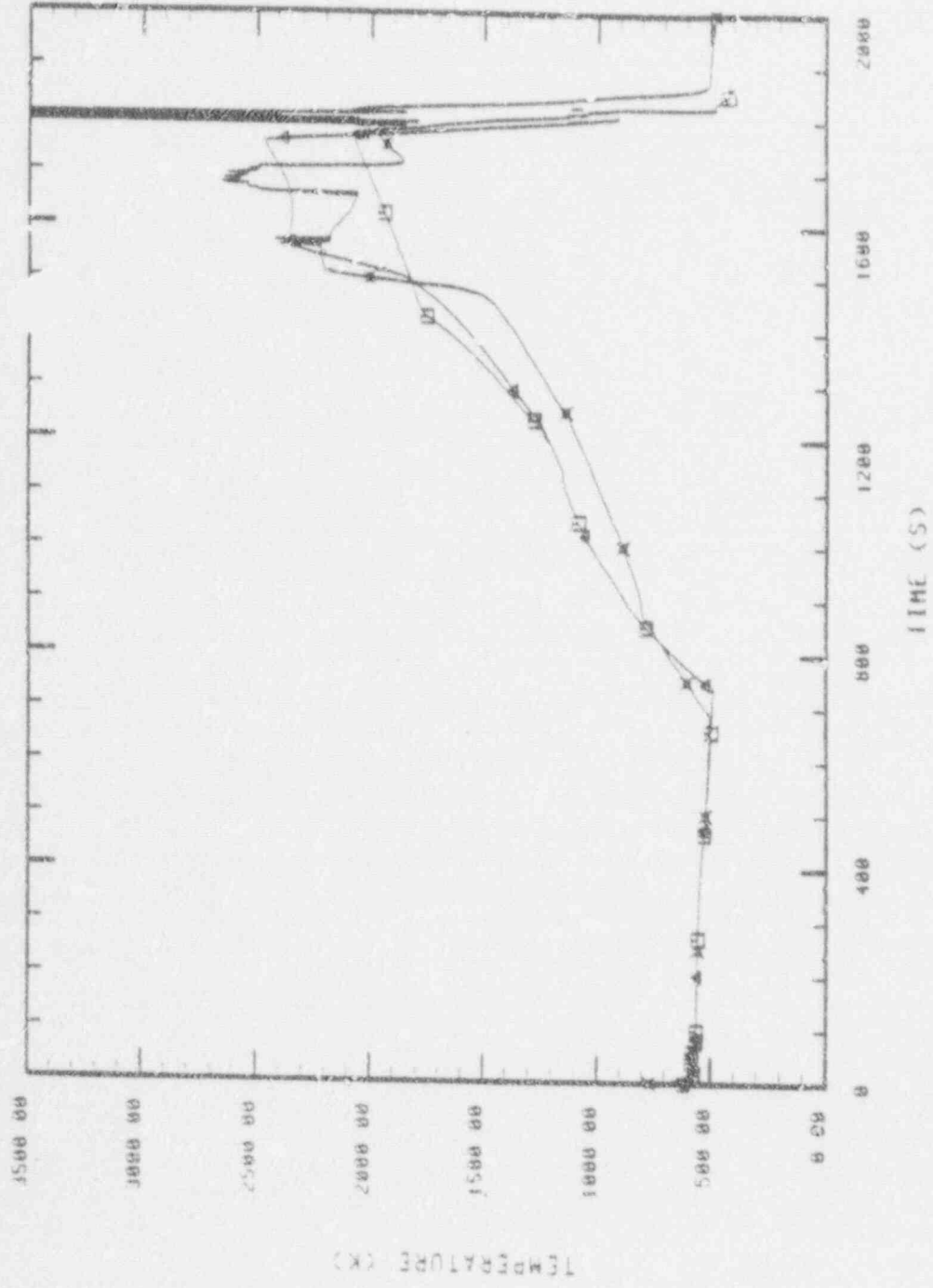
(□) N11MP 2.39J00110 R1R
 (△) N11MP 2.39J00110 MRK
 (x) N11 5.307-027



CENTER BUNDLE CLAD OUTER
 TEMPERATURE, AXIAL LEVEL R3 (K)
 RELAP5 SENSITIVITY STUDY (SPAIN)

Figure 6.6

05 H11MP 239400110 XLR
 A H11MP 239400110 NNM
 X H11MP 239400110



CENTER BUNDLE CLAD OUTER
 TEMPERATURE, AXIAL LEVEL #4 (K)
 RELAP5 SENSITIVITY STUDY (SPAIN)

Figure 6.7

Therefore it has been shown that a RELAP5/MOD2 calculation neglecting the center fuel assembly geometric changes can reproduce reasonably well the experimental thermal response of the LP-FP-2 core.

It can be then concluded that the core flow redistribution following blockages is one of the most important uncertainties associated with the RELAP5/MOD2 simulation.

6.2 General Conclusions of the RELAP5/MOD2 Calculation

- RELAP5/MOD2 has shown to be a more than expected powerful tool to reproduce reasonably well the LP-FP-2 experimental results.
- The uncertainties associated with the LPIS line nodalization have been considerably reduced in the present analysis.
- Core flow redistribution after blockage is probably the most important phenomenon for the experiment LP-FP-2 simulation.
- It is difficult to establish the possible RELAP5/MOD2 deficiencies in predicting the flow redistribution until the actual blockages are known from postirradiation examinations (PIE)²¹
- However, it has been shown that the LP-FP-2 core thermal response can be approximated using RELAP5/MOD2 by doing some sensitivity analysis with respect to the CFM blockages.
- Of course, an integral RELAP5/SCDAP simulation should reduce the calculational uncertainties (better estimation of the amount of blockage and timing).
- The steam generated by the slumping of hot core material into the lower plenum water should be taken into account in the calculation. This might be only possible in the integrated code simulations.

7. SCDAP/MOD1 NODALIZATION FOR LP-FP-2 EXPERIMENT

7.1. SCDAP model for Experiment LP-FP-2

Following the initiation of the LP-FP-2 core uncover, the damage phase of the transient began to take place.

In order to simulate the core damage propagation, we need to use a tool suitable for analyzing the thermal, mechanical and chemical behaviour of the core during this period of the transient.

The relevant phenomena to be considered are the following:

- Geometric changes due to fuel clad ballooning and relocation of molten material.
- Cladding oxidation.
- Heat transfer at high temperatures (rod-to-rod radiation)

To simulate these phenomena we have used the SCADP/MOD1/V21 code⁵ in its stand-alone version.

As discussed in Section 4 of this report, RELAP5/MOD2 is to compute the general thermal-hydraulic behaviour of the plant and the boundary conditions required by SCDAP. Meantime, SCDAP is to calculate the core fuel temperatures and mechanical behaviour including blockages and the new flow areas required by RELAP5/MOD2. After a short number of interdependent calculations the final results can be considered as a "best estimate" analysis. In fact, boundary conditions are not very sensitive to small variations of the blockages. So this passive link between both codes becomes useful and enough accurate for our purposes.

SCDAP was used to simulate only the response of the centre bundle. The peripheral bundles do not reach temperatures high enough to appreciate any significant change with respect to the RELAP5/MOD2 calculation. This procedure saved computer time, while keeping the required precision.

7.2. Nodalization

For the SCDAP calculations, the input model for the center bundle is defined as shown in Figures 7.1 and 7.2. The model has two fuel rod components with radial peaking factors of 0.93 and 1.022 with respect to the center bundle average power, and 1 control rod, 1 guide tube, and 1 shroud components. All components are divided into six axial nodes, each 0.2794 m (11 in.) long, as shown in Figure 7.2. Every fuel rod was divided into six radial (annular) nodes: four for the fuel pellets, one for the gap, and one for the zircaloy cladding.

The guide tube with the control rod is divided into five fixed radial nodes for the material layers which includes the poison, stainless steel cladding, gap, and zircaloy guide tube. The thermal shroud is divided into 20 radial nodes as shown in Figure 7.3. The argon gas gaps in both sides of the insulator are modeled. An adiabatic boundary is assumed to be on the outside of the thermal shroud.

7.3. Input Data

7.3.1. Basic input deck.

The basic input deck is very similar to that used in the "Best Estimate Prediction for LOFT Project Fission Product Experiment LP-FP-2" (Ref. 6), apart from several modifications that were made in order to update the input to the actual conditions of the experiment.

The following parameters were updated for this posttest analysis:

- Power level
- Burn-up
- Decay power
- Initial temperatures
- TH Boundary conditions
- Other minor modifications.

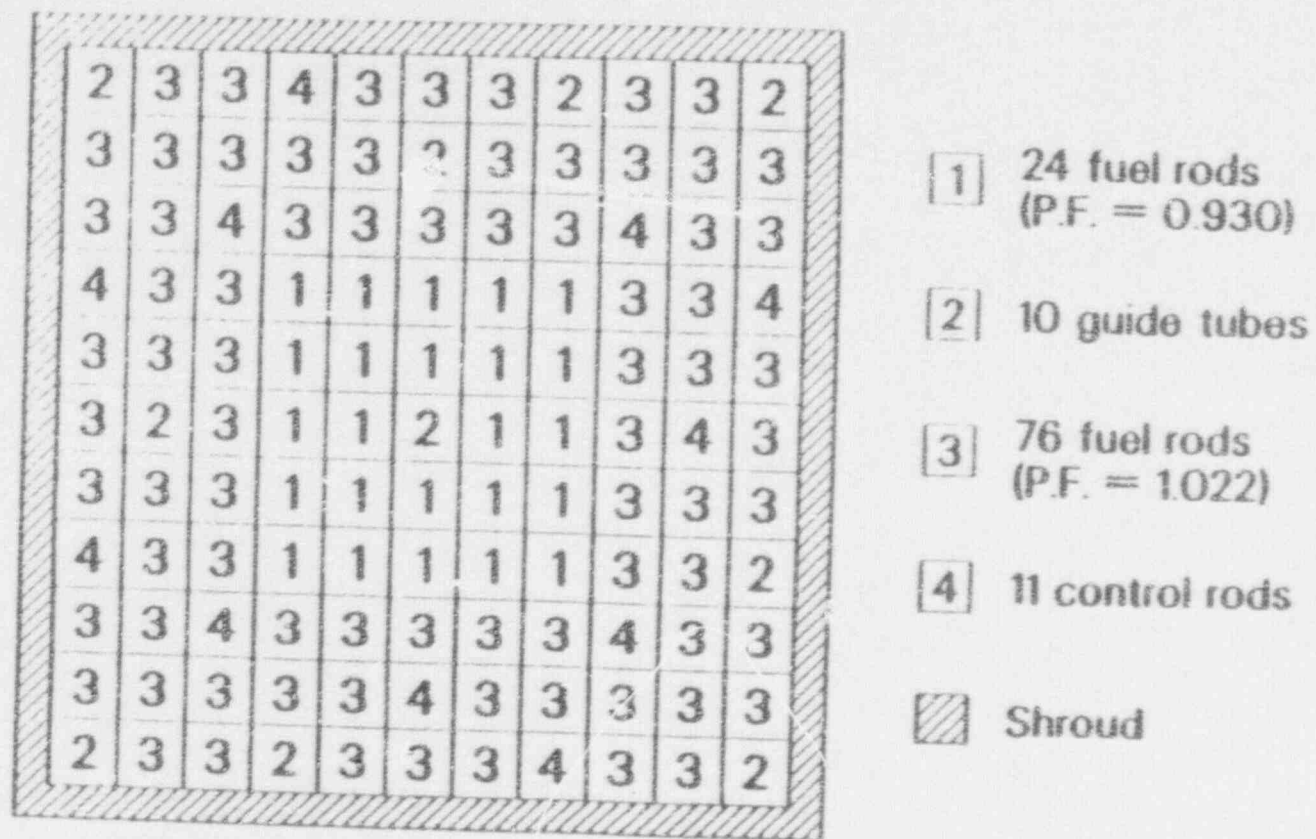
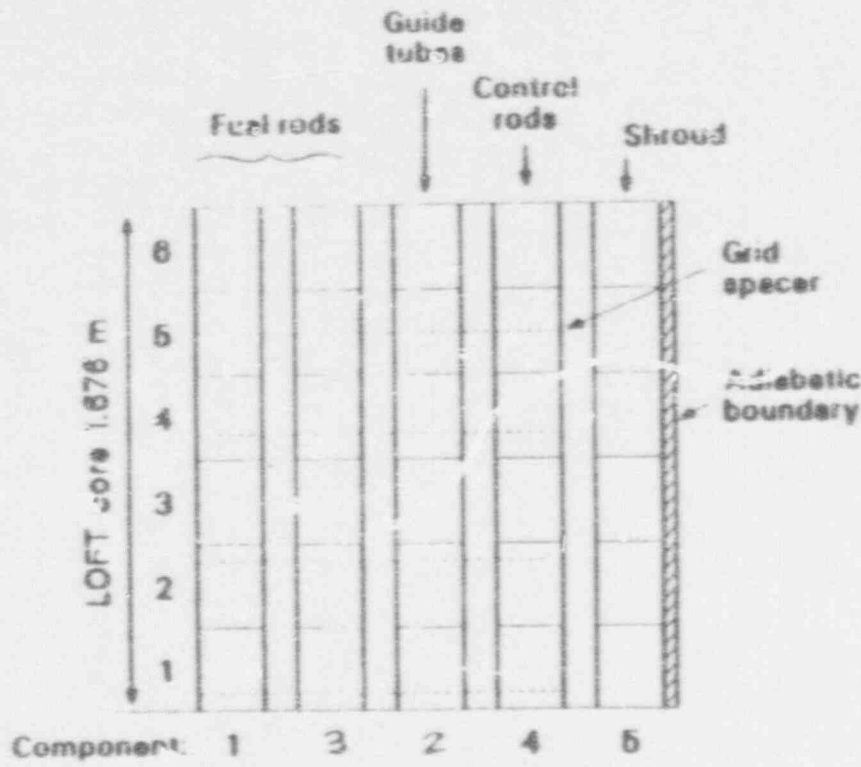


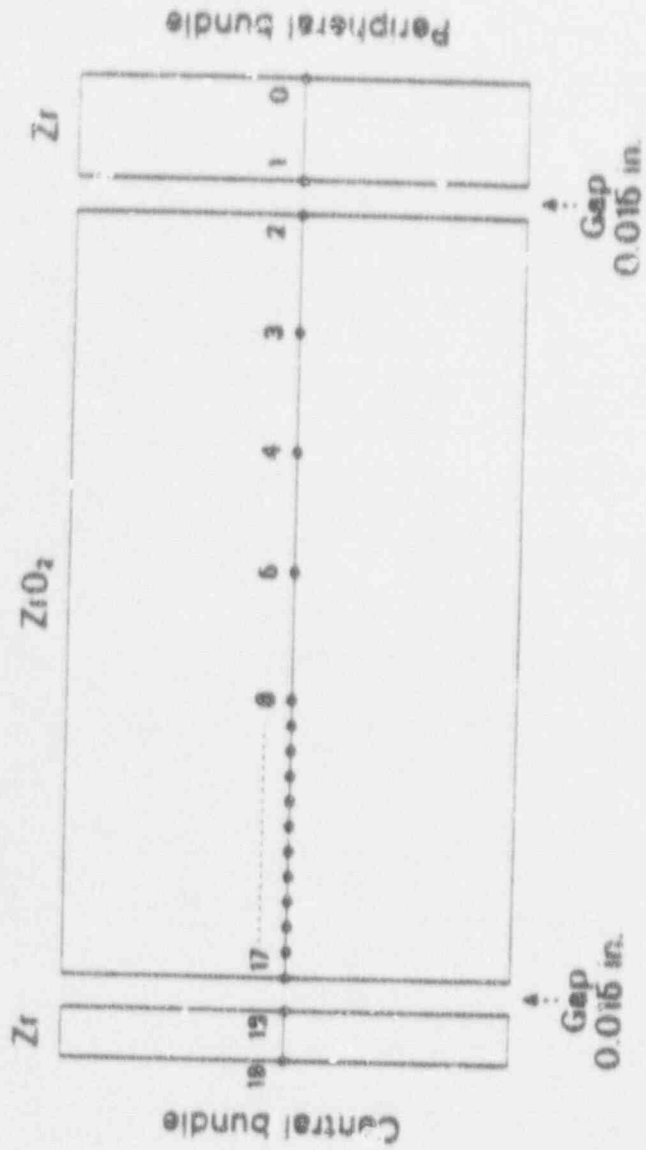
Figure 7.1. SCDAP center bundle rod grouping



LOI-KM118-07

Figure 7-2. SUDAP nodalization diagram for center bundle

20 radial nodes



101-KM16-08

Figure 7.3. SCDAP shroud nodalization diagram.

7.3.2. Modifications

An updated specific power level was calculated taking into account that the power of the core during the pretransient phase was 26.8 MW (Ref. 3) and a power fraction of 17.43% generated by the centre bundle (See Appendix F of Ref. 9). The results of this calculation were $4.37436E8$ W/m³ and $3.98073E8$ W/m³ for the hot (PF=1.022) and average (PF= 0.93) fuel rods respectively.

The actual centre fuel bundle burn-up was 429.4 MWD/MTU (Ref. 3). Instead of the detailed core power history, given in Figure 2.6 a constant power of 26.8 MW was assumed during 9.17 days to obtain the same CFM burnup, to simplify the SCDAP input.

The posttest decay power has been calculated from the relative posttest decay power received from INEL ²² corrected by the actual specific power (see table 7.1). As seen on table 7.1, 420 s is the starting time for the SCDAP analysis, because RELAP5/MOD2 calculated the core uncovering beginning at about that time.

Initial CFM rod temperatures, pressure, and liquid level (collapsed liquid level) values all throughout the transient were taken from the RELAP5/MOD2 base calculation.

The inlet mass flow to the centre bundle is the most important parameter for the SCDAP analysis. Its large influence on the heat-up and steam starvation was the reason to perform several sensitivity studies. The input and the results of these studies will be discussed in section 7.4.

The outer ZrO_2 layer failure temperature specified in the input deck was 2960 K (melting temperature of the ZrO_2).

Other minor update was the addition of the input card 80.1 required by SCDAP/MOD1 version 20 and successives which was not previously required by former code versions.

Table 7.1. SCADP posttest specific power level

TRANSIENT TIME (s)	SCDAP TIME (s)	POWER FRACTION INEL	HOT ROD (w/m ³)	COLD ROD (w/m ³)
0	-	1.0	4.3744E8	3.9807E8
420	0	-	9.5415E6	8.6828E6
600	180	.020035	8.7641E6	7.9753E6
700	280	.019260	8.4251E6	7.6668E6
800	380	.018581	8.1281E6	7.3965E6
900	480	.017977	7.8639E6	7.1561E6
1000	580	.017434	7.6263E6	6.9400E6
1100	680	.016939	7.4098E6	6.7429E6
1200	780	.016486	7.2116E6	6.5626E6
1300	880	.016068	7.0288E6	6.3962E6
1400	980	.015681	6.8595E6	6.2421E6
1400	1080	.015320	6.7016E6	6.0984E6
1600	1180	.014982	6.5577E6	5.9639E6
1800	1380	.014368	6.2851E6	5.7195E6
1900	1480	-	-	-
2000	1580	.013822	6.0463E6	5.5021E6
2400	1880	-	-	-
2500	2080	.012688	5.5502E6	5.0507E6
3000	2580	.011794	5.1592E6	4.6940E6

7.3.3. CFM Inlet Mass flow used for the SCDAP Analysis

The transient phenomenology calculated by SCDAP during the damage phase of the LP-FP-2 experiment is very sensitive to the CFM inlet mass flow.

As shown in Figure 5.12, the RELAP5 base calculation gave a CFM inlet mass flow ranging from 0.007 kg/s to 0.001 kg/s during the most significant time period of the transient, (1200 s to 1770 s). These small flow values seem to be too low, because steam starvation took place too soon, limiting the calculated clad temperature excursion at upper core elevations (See Figure 5.16).

As will be shown in section 8.1, SCDAP, using the CPM inlet flow determined by RELAP/MOD2 in the base case calculation, gave even lower clad temperatures than those predicted by RELAP5.

From the experimental clad temperatures it is obvious, that the metal-water reaction proceeded in the experiment without steam starvation. This means that the actual CFM mass flow was higher than predicted by the RELAP5 base case analysis.

Although there was no direct measurement of the core mass flow, a mean value of 0.04 kg/s for the CFM was obtained in Reference 9, based upon the experimental core thermal response. A SCDAP run was performed using the same input, except that the minimum CFM inlet mass flow was fixed at 0.04 kg/s.

The major result of this sensitivity analysis, not presented in this report, was the fact that, if the minimum CFM inlet flow was 0.04 kg/s, the flow would be high enough to cool the fuel, precluding cladding temperatures higher than 1200 K.

Therefore, the actual CFM flow should be between 0.001 kg/s and 0.04 kg/s. Several sensitivity studies were conducted using different minimum fixed values for the CFM inlet flow, covering the formerly mentioned range. Cladding temperatures and total hydrogen production were the experimental measured

parameters used to check the goodness of the calculations. This pseudo-empirical procedure drove us to obtain a minimum CFM inlet steam flow rate of about 0.01 kg/s.

A SCDAP calculation with a constant flow of 0.01 kg/s since about 1200 s to the reflooding calculated time of 1769.3 s, gave a good approximation of the clad temperatures and the hydrogen production. This single value agrees well with the experimental data available from the Power Burst Facility (PBF)²³. Data from PBF indicate that flows as little as 0.1 g/s/fuel rod are sufficient to sustain the metal-water reaction without steam starvation^{3,23}. Considering that the LP-PP-2 center bundle contains 100 rods, we get a minimum CFM inlet flow of 0.01 kg/s to sustain the metal water reaction (MWR) reaction, the same one that we obtained in our SCDAP sensitivity study.

In order to somehow take into account the blockages associated to the CFM damage process, this 0.01 kg/s flow was reduced in the final best estimate posttest analysis by the same factor and timing the SCDAP computed CFM flow area was blockaged.

Table 7.2 presents the effective flow area factors calculated by SCDAP for the whole transient using 0.01 kg/s as the minimum CFM inlet flow. These factors were applied to the flow calculated by RELAP5/MOD2 right before the fuel clad rupture (1176 s) to get a best estimation of the actual flow entering the CFM.

Figure 7.4 shows the CFM inlet flow (THINFLW) given as a boundary condition to SCDAP for the final best estimate posttest analysis along with both the RELAP5/MOD2 base (RCR) and the sensitivity (NRN) calculated results, for comparison.

A full listing of the SCDAP input deck is provided in Appendix D of this report. Using this deck, SCDAP predicts a more realistic estimation of cladding temperatures, cladding oxidation and hydrogen production, as will be presented in section 8.2 of this report.

Table 7.2 CFM best Estimate Inlet Flow

<u>Time</u>	<u>CFM Flow Area</u>	<u>CFM Inlet Flow</u>
0 s to 1176 s ^a	100%	As calculated by RELAP5 (base case)
1176 s to 1545 s ^b	47%	0.01 kg/s
1545 s to 1660 s ^c	42%	0.009 kg/s
1660 s to 1769.3 s	31%	0.0066 kg/s
1769.3 s to EOT	31%	As calculated by RELAP5 (base case)

a. Cladding Rupture time as predicted by RELAP5 (1200K)

b. Control rod failure time as predicted by ECDAP using a minimum CFM inlet flow of 0.01 Kg/s

c. Fuel failure time as predicted by SCDAP using a minimum CFM inlet flow of 0.01 kg/s

d. ECCS injection time as predicted by RELAP5.

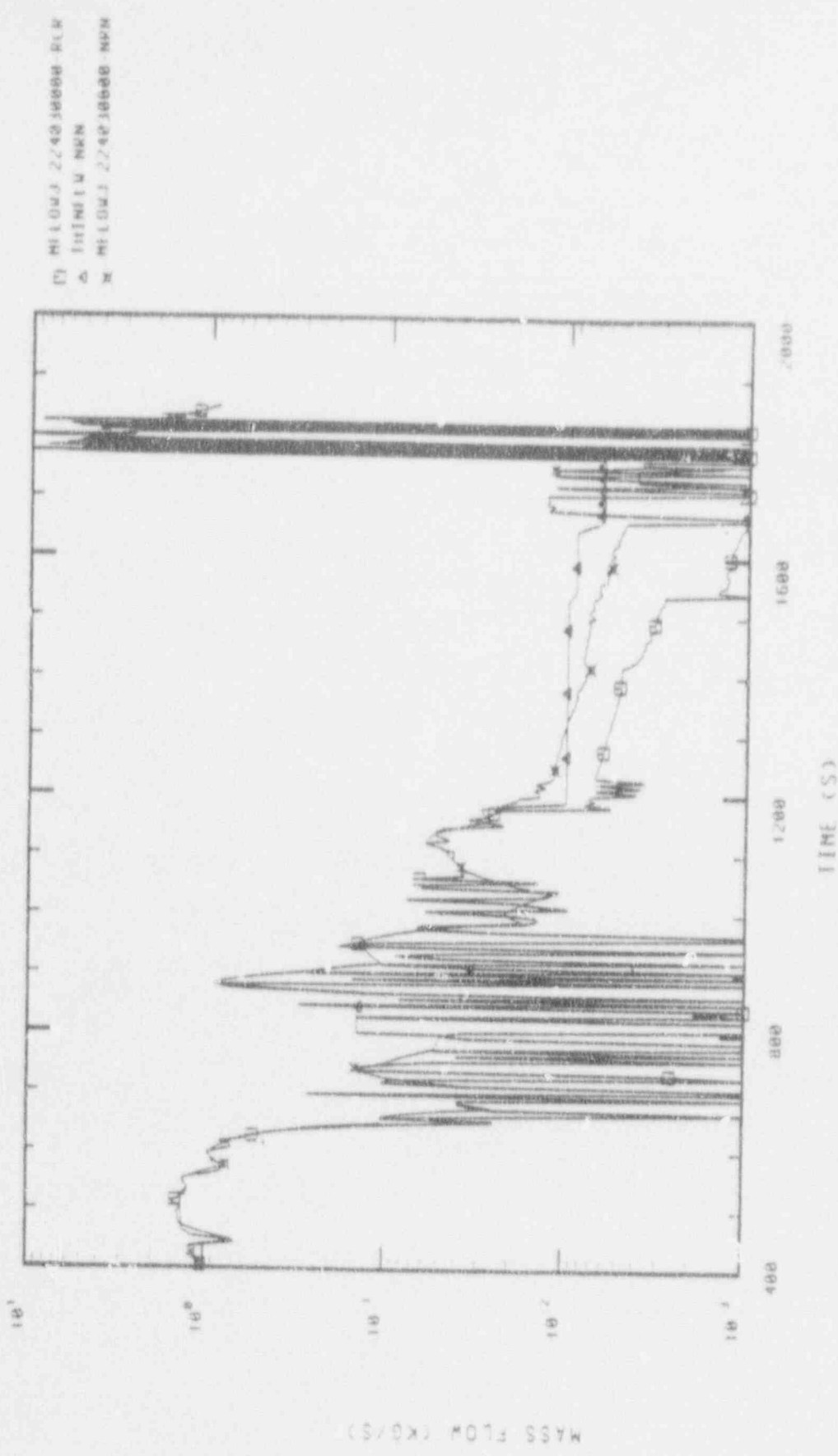


Figure 7.4. CENTER BUNDLE INLET STEAM MASS FLOW RATE (KG/S) SCDAP/RELAP5 (FP2 SPANISH GROUP)

8. RESULTS OF THE SCDAP/MOD2 CALCULATION

The SCDAP code calculated the detailed representation of the central bundle heatup, and included effects due to cladding oxidation, hydrogen generation, and the geometry changes caused by clad ballooning and material relocation.

Two main analyses have been performed to take into account the influence of inlet flow entering the CFM.

The results of both calculations are described in the following subsections.

8.1 SCDAP Results using CFM Inlet Flow directly taken from the RELAP5 Base Calculation.

Using the same flow values obtained by RELAP5 in the base calculation, the Central Fuel Module Inlet Flow was unable to provide enough steam to sustain the initiated metal/water reaction. Because of that, the excursion of temperatures did not take place in such an extension and so, the experiment was hardly simulated. Figure 8.1 to 8.3 show the clad temperatures calculated by SCDAP in comparison with the measured data and the RELAP5/MOD2 base calculated results. It is interesting to point out the earlier DNB time calculated by SCDAP. This can be due to the fact that the collapsed liquid level given to SCDAP as a boundary condition is smaller than the real mixture level, which accounts for the voiding effect. Also it should be remarked that under the LP-FP-2 conditions, the RELAP5/MOD2 heat transfer package does not predict DNB until the void fraction is greater than 0.999.

Besides these discrepancies the heatup rates calculated by SCDAP are in very close agreement with the experimental data until the onset of the MWR.

The blockages calculated in this way were only due to ballooning and control rod material relocation. The temperatures were not high enough to melt the Zr and to produce the fuel liquefaction.

03 HI TEMP 23198110 RCLW
 A CADDET 6 1 1
 M TE 5J07 010

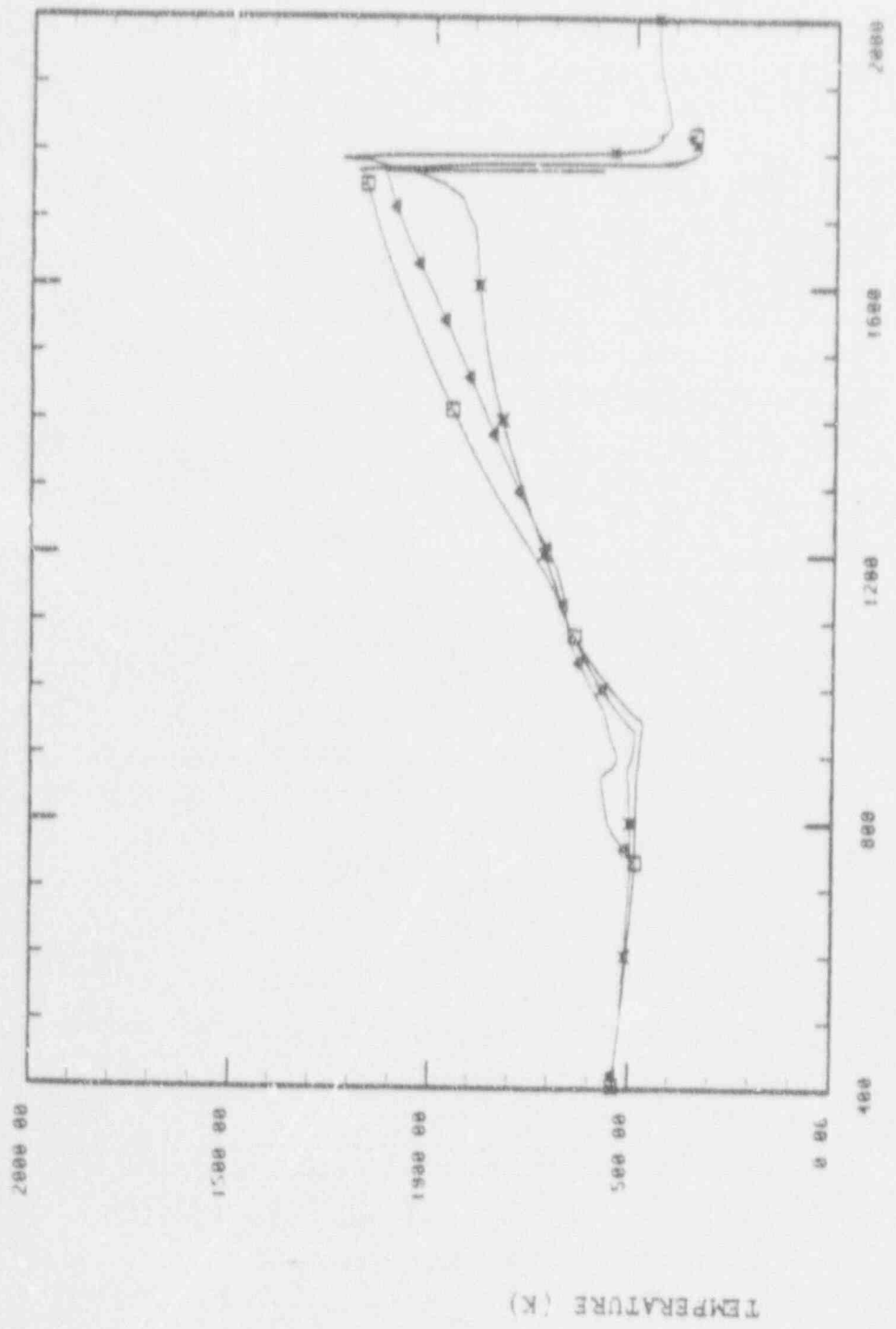


Figure 8.1 C. BUNDLE: FUEL ROD CLAD OUTER TEMPERATURE (K)
 AT LEVEL 1, USING INLET FLOW AS GIVEN BY
 RELAP5/MOD2 BASE CALCULATION
 SCDAP/RELAP5/EXPERIMENT COMPARISON

□ MITEM 239J00110 RCR
 ▲ CPDCL 6 3 7
 ✕ 1E-5J07 027

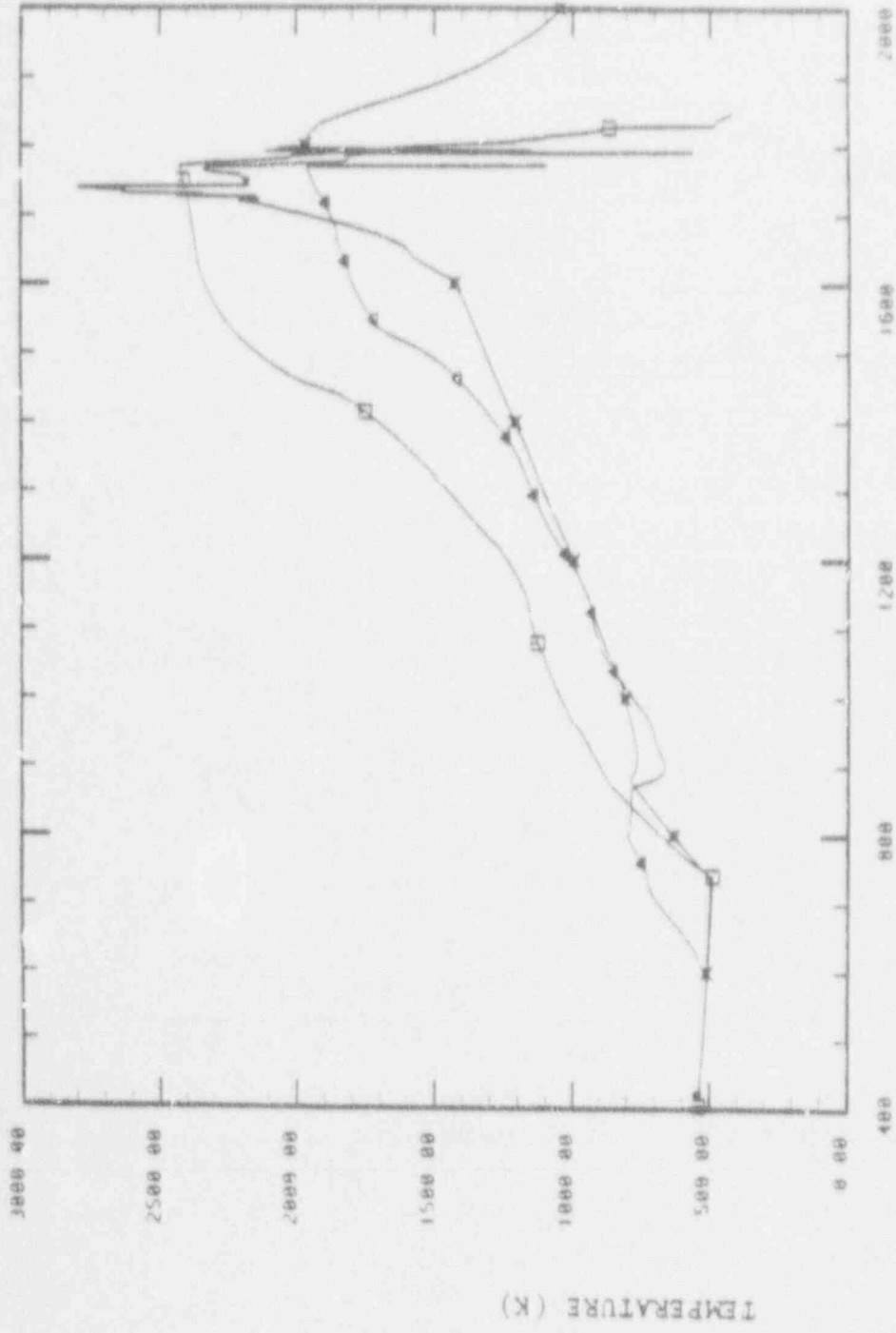


Figure 8.2 C. BUNDLE: FUEL ROD CLAD OUTER TEMPERATURE (K) AT LEVEL 3, USING INLET FLOW AS GIVEN BY RELAP5/MOD2 BASE CALCULATION SCDAP/RELAP5/EXPERIMENT COMPARISON

03 HITEMP 239400110 RCR
 A CADCI 6 4 1
 K TE-5184 042

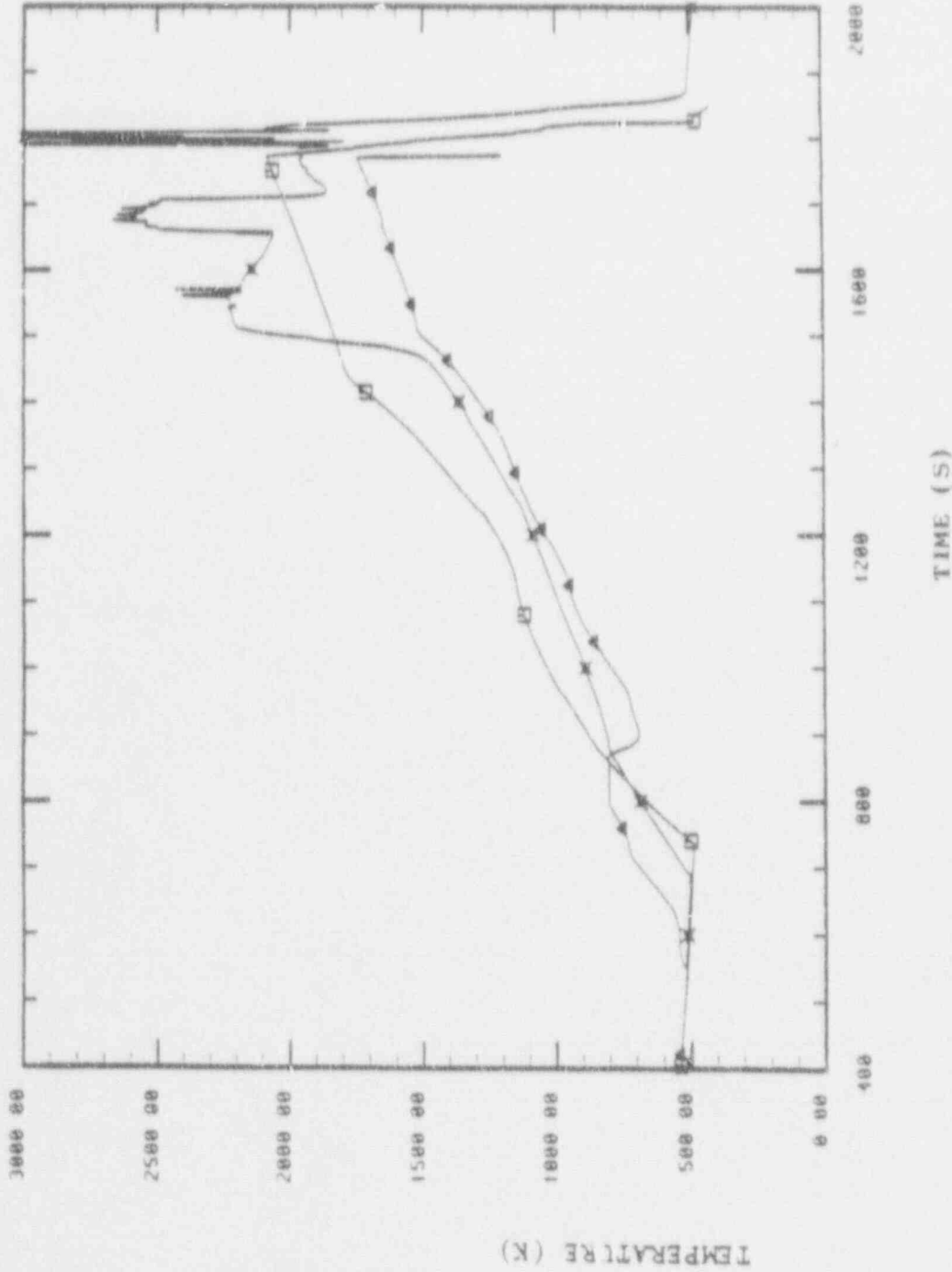


Figure 8.3
 C. BUNDLE: FUEL ROD CLAD OUTER TEMPERATURE (K)
 AT LEVEL 4, USING INLET FLOW AS GIVEN BY
 RELAP5/MOD2 BASE CALCULATION
 SCDAP/RELAP5/EXPERIMENT COMPARISON

This steam starvation led us to analyze several parametric studies to conclude that an inlet flow of 0.01 Kg/s should be enough, as it has been explained before in section 7.4.

8.2 SCDAP Results using "Best Estimate" CFM Inlet Flow

This section presents the results of the best estimate posttest analysis of the LP-FP-2 experiment using the SCDAP code.

The base deck for this case is given in Appendix D and has been discussed previously in section 7. The only difference with the case formerly presented in section 8.1 is the different CFM inlet mass flow, which has been extensively discussed in section 7.3.3.

8.2.1 Cladding Temperatures

Before comparing the SCDAP results with the experimental data it can be worthwhile to follow the whole CFM damage process looking at the calculated clad temperatures in the average rod at different axial locations (Figure 8.4).

The CFM uncovering started at about 450 s when the water level dropped below the top of the core and was completed at about 890 s when the liquid level went down the bottom of the core (see figure 5.13).

Figure 8.4 shows the maximum temperature histories of the fuel cladding surface at different axial elevations. After initiation of the dryout the clad temperatures started to increase due to the lower cooling capability of the steam. The heatup is temporarily stopped due to the increased steam flow created by the reopening of the ILCL break (877.6 s) and the opening of the PORV (882 s). Thereafter the temperature excursion proceeded normally driven by the fuel decay heat. Axial node 4th. reached the clad rupture temperature of 1200 K slightly earlier than the peak power node (level 3). This was so because of the smaller heat flux at the 4th. level, in turn, due to the smaller temperature jump between the clad surface and the steam at this elevation compared to the 3rd. level (peak power

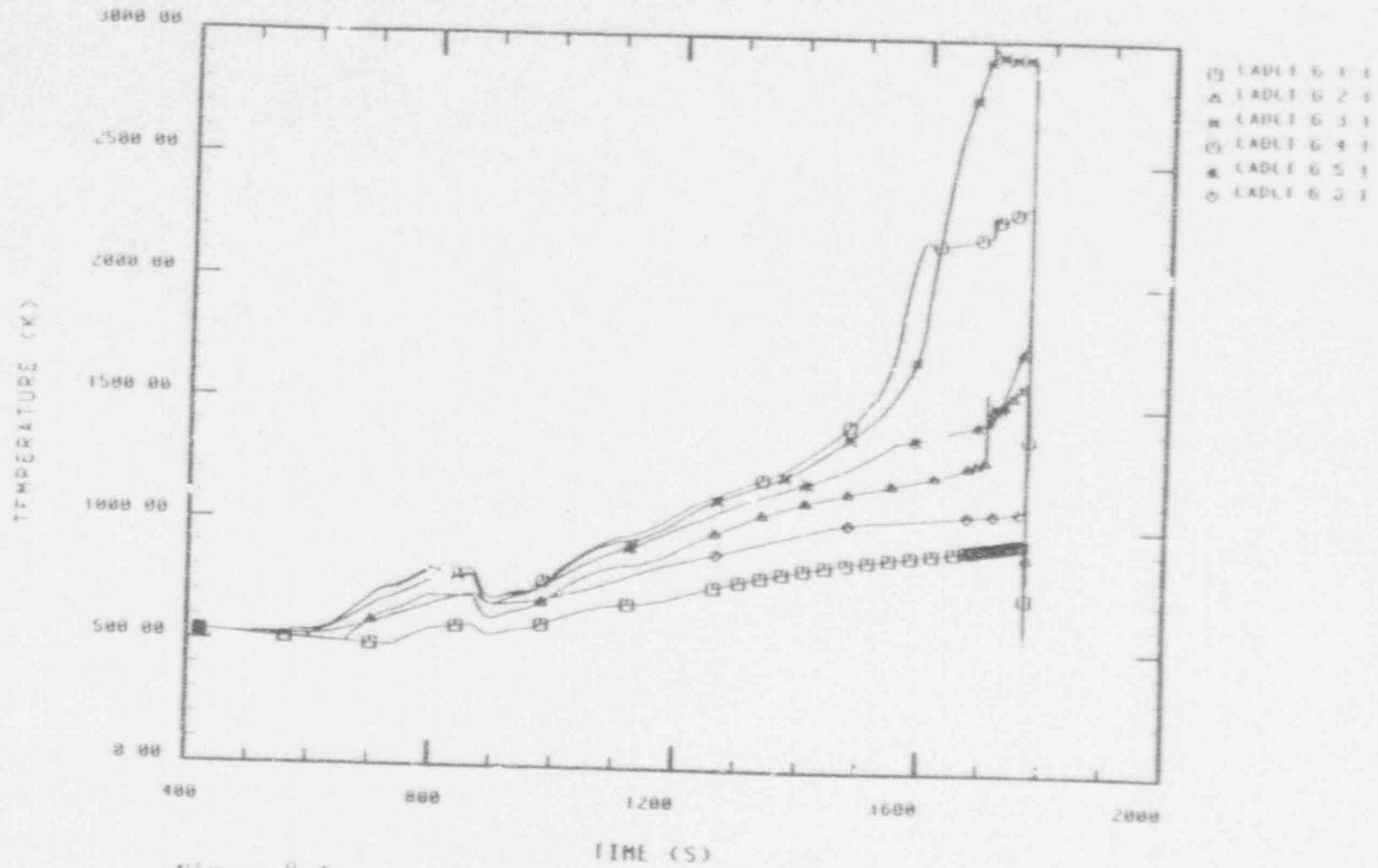


Figure 8.4

CENTER BUNDLE AVG FUEL ROD
CLADDING TEMPERATURES (K)
SCDAP/M1/V21 (EP2 SPANISH GROUP)

node), and also because of the earlier dryout observed at this node.

Above a temperature close to 1200 K the heat generation due to the metal-water reaction became the most important energy source within the CFM, producing a rapid temperature excursion at axial levels 3 and 4. Following the onset of the rapid temperature excursion, the steam that flowed through the CFM began to be consumed by the M-W reaction, decreasing the steam fraction in the bundle, being replaced by hydrogen (see Figure 8.5). At about 1500 s the SCDAP code predicted the total steam starvation at core elevations above the peak power node, reducing the heatup rates to the decay heat level, while there was enough steam available to sustain the reaction at lower elevations. This brought the peak power node to become also the peak temperature node at the end of the transient, reaching a maximum temperature of 2960 K versus the 2800 K calculated for the 4th. axial node.

After reaching 2960 K, the outer ZrO_2 layer failed (as specified in the input deck -see section 7.3-) allowing the molten Zircaloy above the breach node to fall downwards to lower core elevations. The molten Zircaloy relocated at the first and second axial elevations, where it was resolidified. At the 2nd axial node the temperatures were in excess of 1200 K allowing for a rapid temperature excursion due to the M-W reaction.

Similar trends were calculated for the CFM control rods, as shown in Figure 8.6. In this figure it is interesting to note the plateau of the control rod temperatures at 1050 K, melting point of the Ag/In/Cd control material. During certain time, the control rod temperatures remains at 1050 K because the heat generated is being consumed for melting the control alloy.

Figures 8.7 to 8.9 show the comparison for two axial levels (3th. and 4th.) among the different calculated cladding temperatures with those experimentally measured, where the symbols stand for:

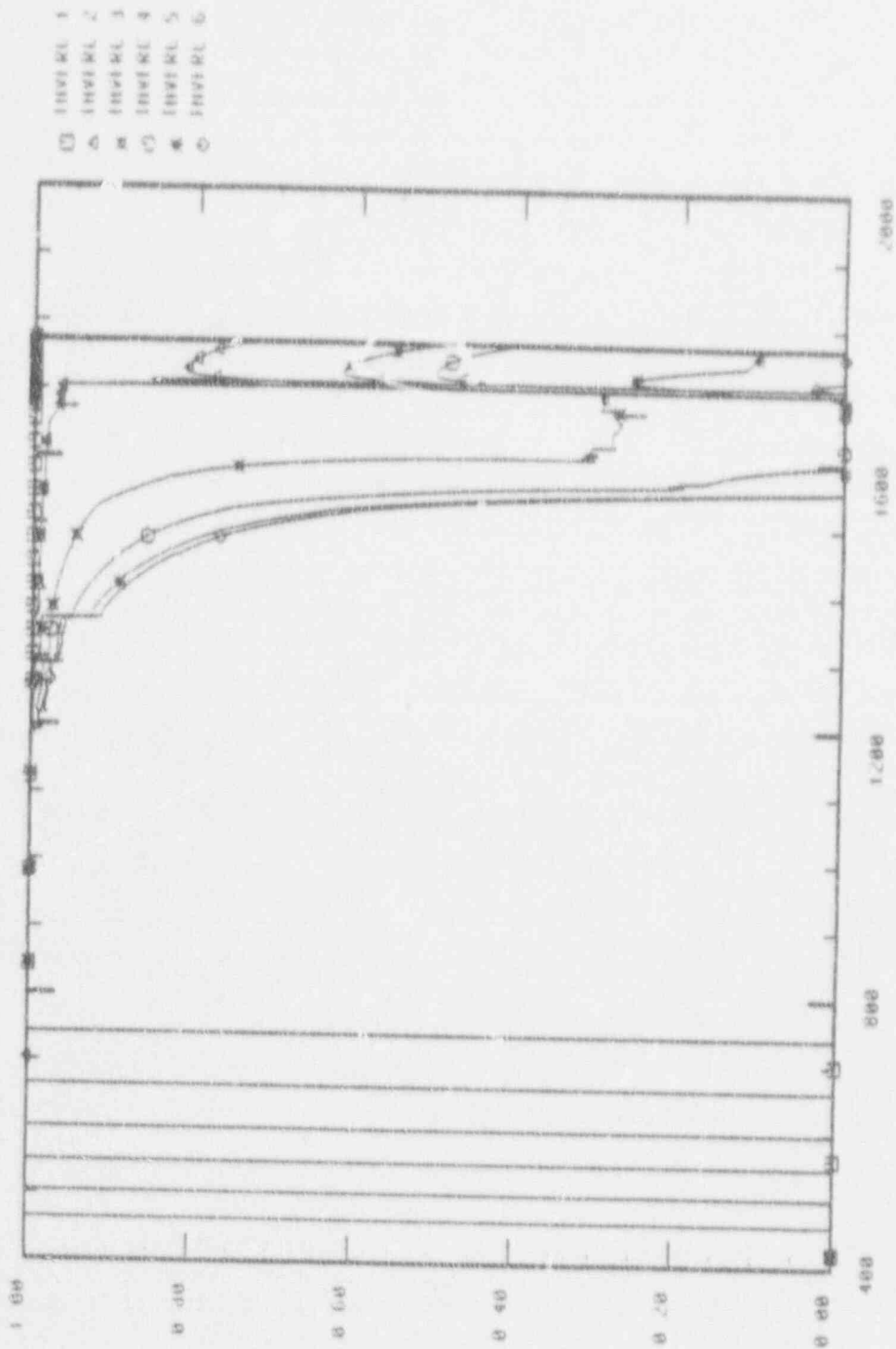


Figure 8.5
 CENTER BUNDLE AXIAL STEAM
 FRACTIONS
 SCDAP/M1/V21 (FP2 SPANISH GROUP)

STEAK FRACTION

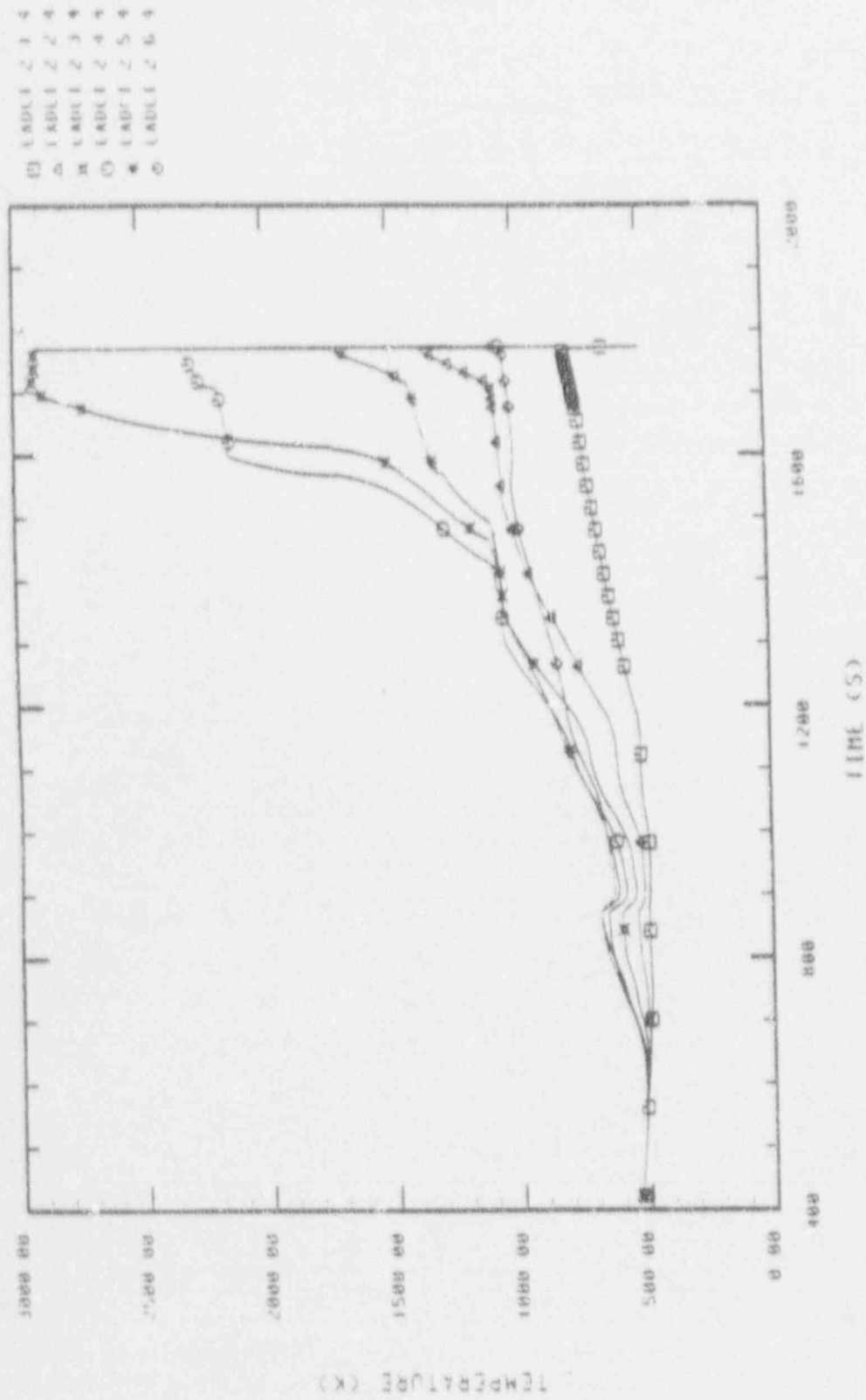


Figure 8.6
 CENTER BUNDLE CONTROL ROD
 CLADDING TEMPERATURES (K)
 SCCAP/M1/V21 (FP2 SPANISH GROUP)

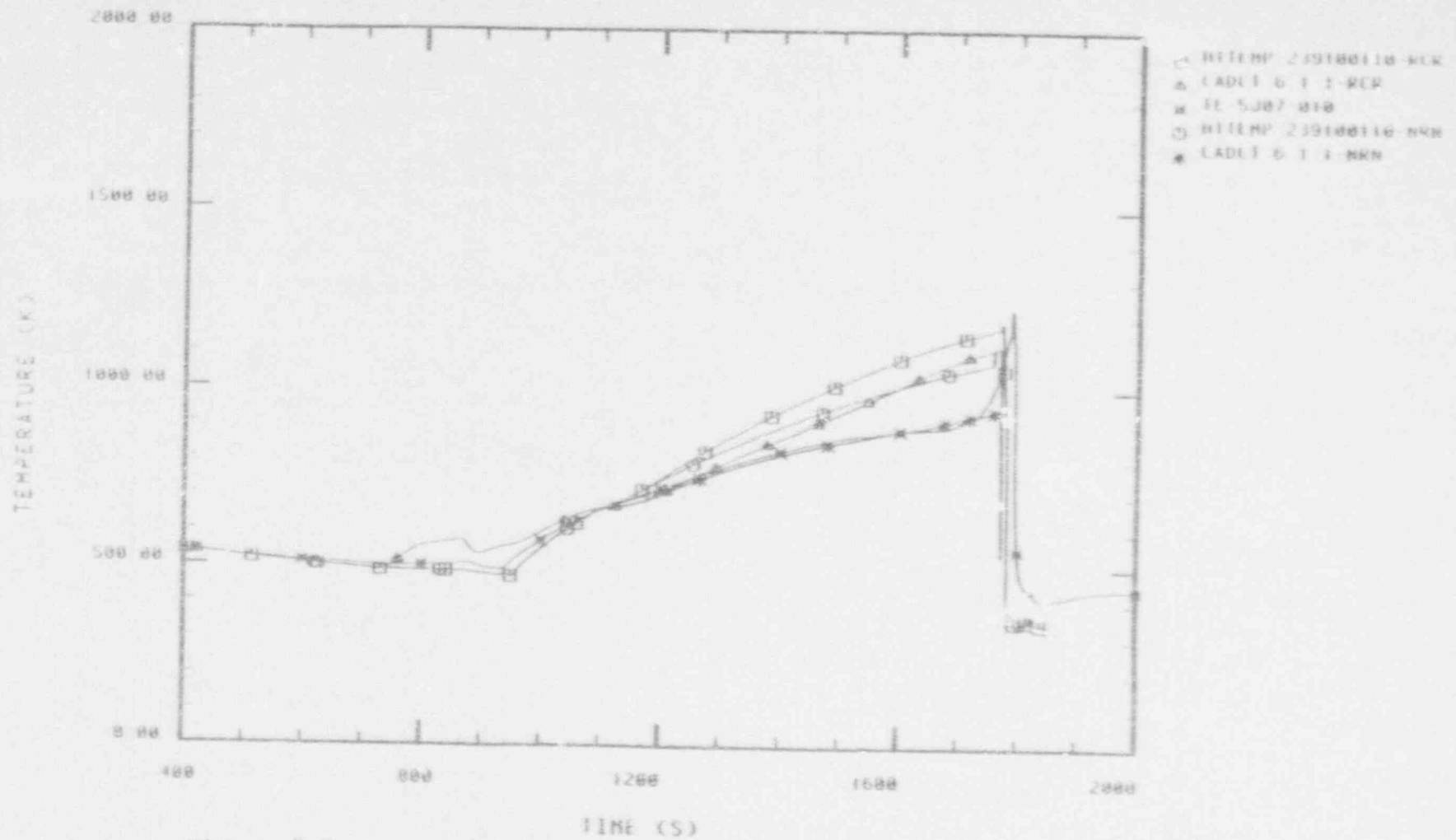


Figure 8.7

CENTER BUNDLE HOT FUEL ROD CLAD
 TEMPERATURE AT AXIAL LEVEL #1 (K)
 SCDAP/RELAPS/EXPERIMENT COMPARISON

□ HTLMP 23930011R NRK
 △ CADLI 6 3 1 NLR
 × TE 5307-027
 ○ HTLMP 23930011R NRN
 * CADLI 6 3 1 NRN

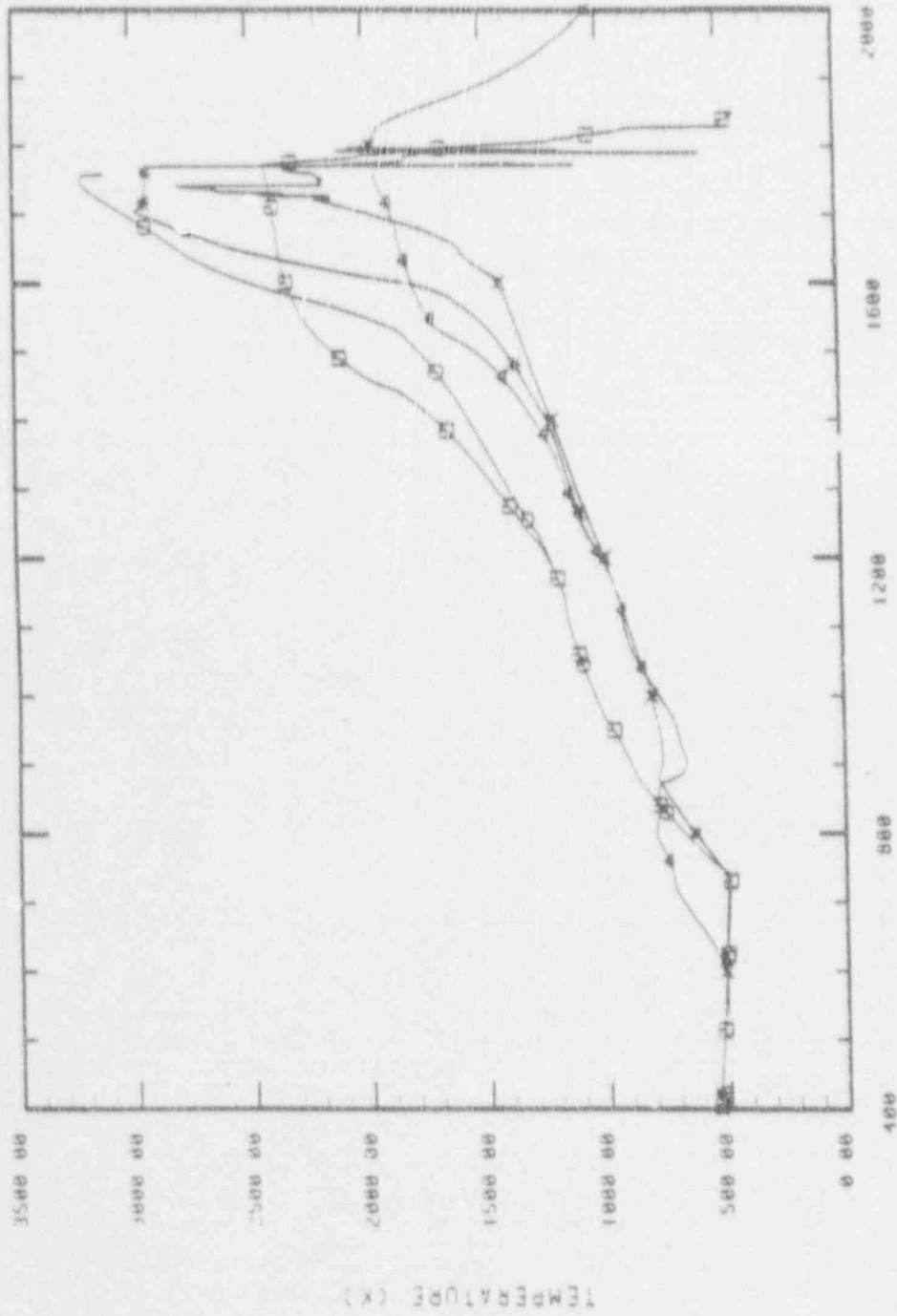
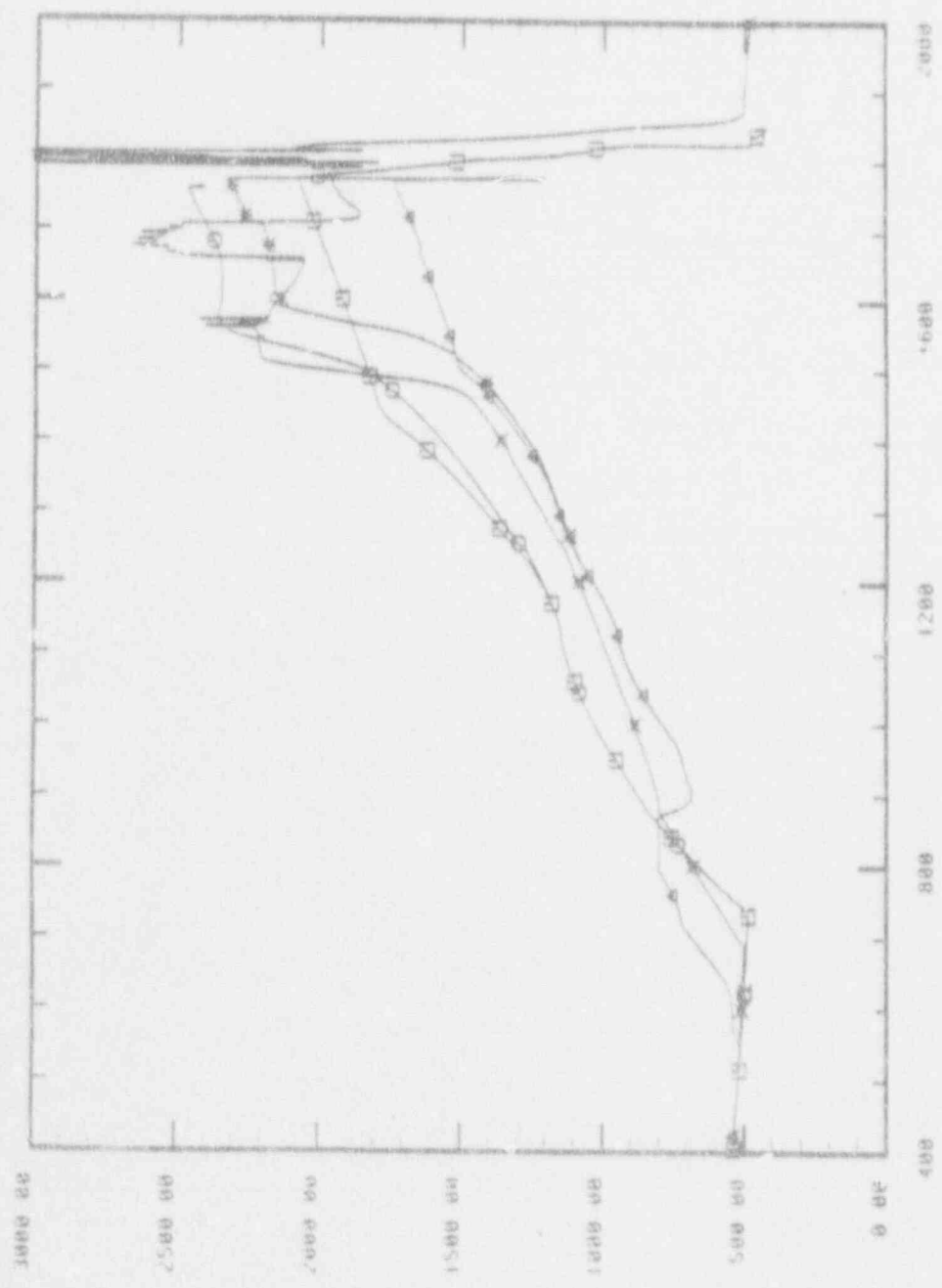


Figure 8.8
 CENTER BUNDLE HOT FUEL ROD CLAD
 TEMPERATURE AT AXIAL LEVEL #3 (K)
 SCDAP/RELAP5/EXPERIMENT COMPARISON



(U) HTTEMP / 23400110 KLN
 (A) CAD1 6 4 1 RES
 (K) TR 5303 042
 (O) HTTEMP / 23400110 KLN
 (X) CAD1 6 4 1 NKN

Figure 8.9
 CENTER BUNDLE H01 FUEL ROD CLAD
 TEMPERATURE AT AXIAL LEVEL #4 (K)
 SCDAP/RELAP5/EXPERIMENT COMPARISON

TE: Experimentally measured temperature
HTTEMP-RCR: Temperature given by RELAP taking into account
blockages.
HTTEMP-NRN: Temperature given by RELAP without renodalization.
CADCT-RCR: SCDAP temperature with inlet flow from RELAP5 base
case.
CADCT-NRN: SCDAP temperature with best estimate inlet flow.

These figures indicate a very good prediction of cladding temperatures by SCDAP using the best estimated inlet flow, very close to that given by RELAP5 without taking into account the blockages.

The shapes follow the experimentally measured temperatures with heatup rates prior to the metal/water reaction in agreement with the data.

There is a slight delay in reaching 2100 K, remaining above this temperature during 186 s versus the 262 s measured. The observed lack of continuity between the two levels (the calculated 3th elevation temperature excursion is anterior to the measured one, and the 4th posterior), could be due to the fact of having divided the fuel rod length in only a few levels.

On the other hand, using the inlet flow given by RELAP5, SCDAP gave very low cladding temperatures because of the steam starvation (see section 8.1).

Figure 8.10 shows the centre bundle average rod fission product gap inventory. At 1358 s, rupture cladding time, the noble gases Xe and Kr were instantly released, while the Cs and I remained longer due to the diffusional release process.

Figure 8.11 indicates the central bundle average rod fission product gap release

Figure 8.12 and 8.13 show the central bundle fission product release of soluble and noncondensable elements respectively.

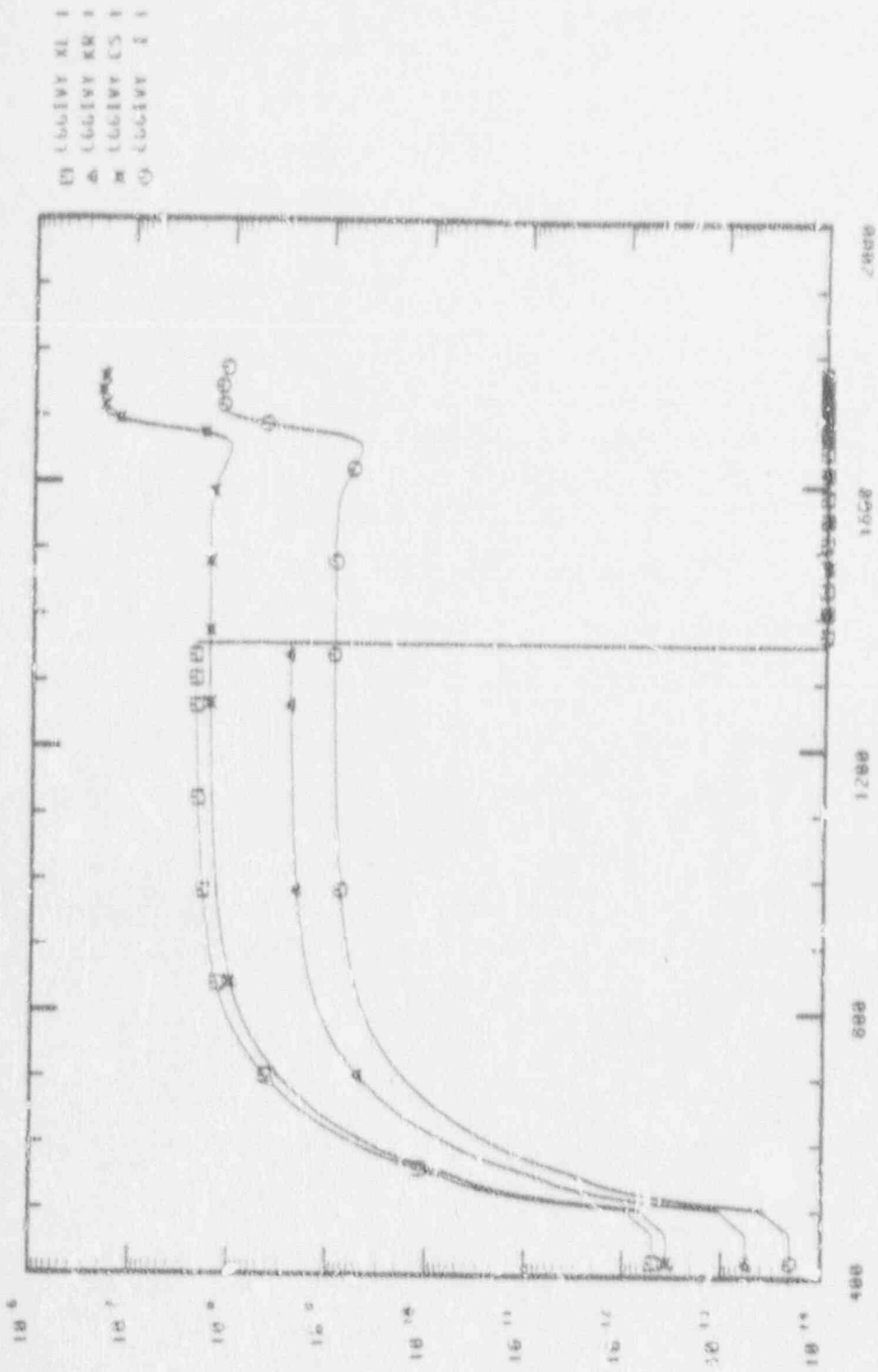


Figure 8.10
 CENT-R BUNDLE AVG ROD FISSION
 PRODUCT GAP INVENTORY (KG)
 SCDAP/M1/V21 (FP2 SPANISH GROUP)

(02) 154K

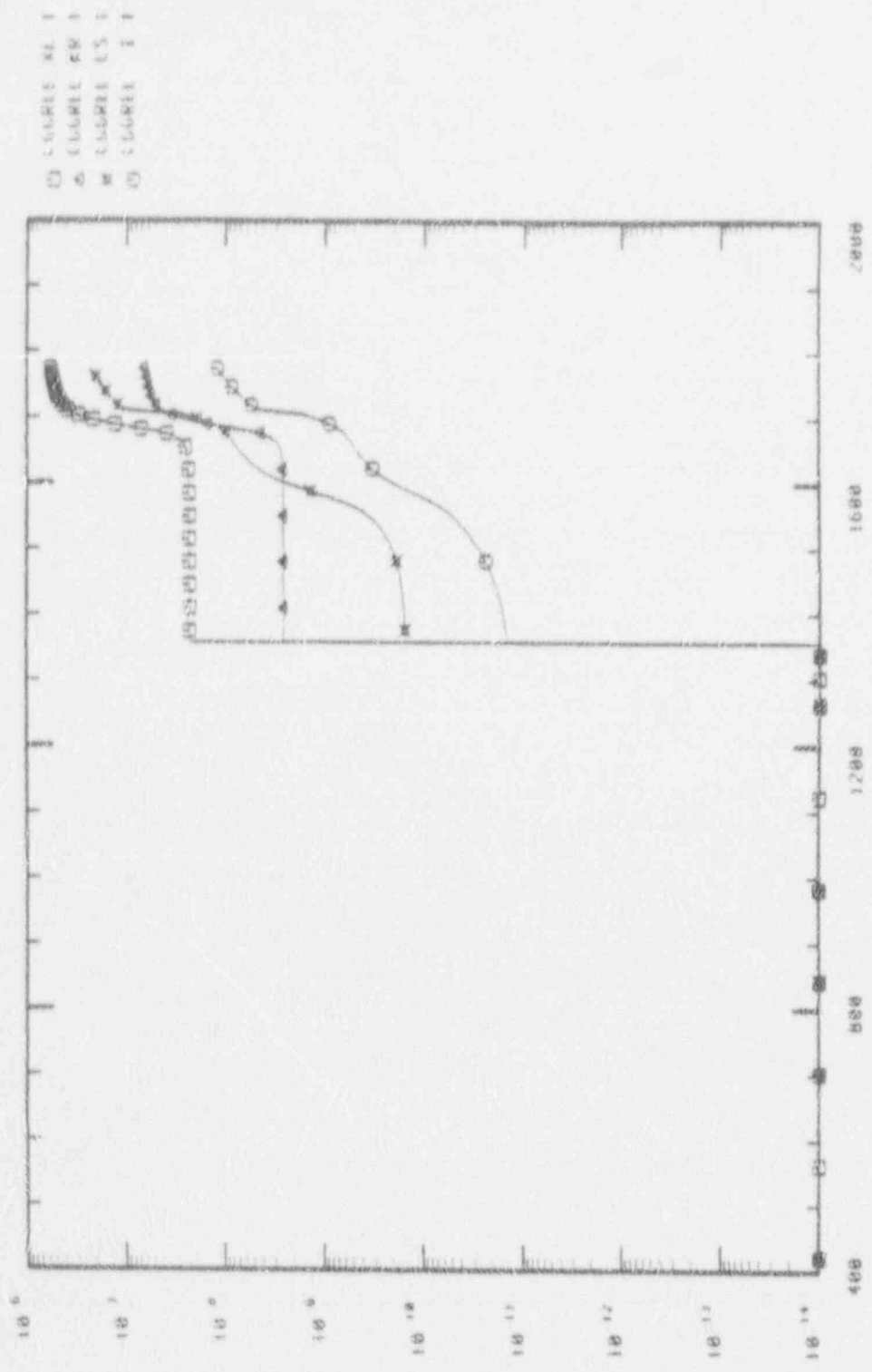


Figure 8.11
 CENTER BUNDLE AVG ROD FISSION
 PRODUCT GAP RELEASE (KG)
 SCDAP/M1/V21 (FP2 SPANISH GROUP)

(X) 4614

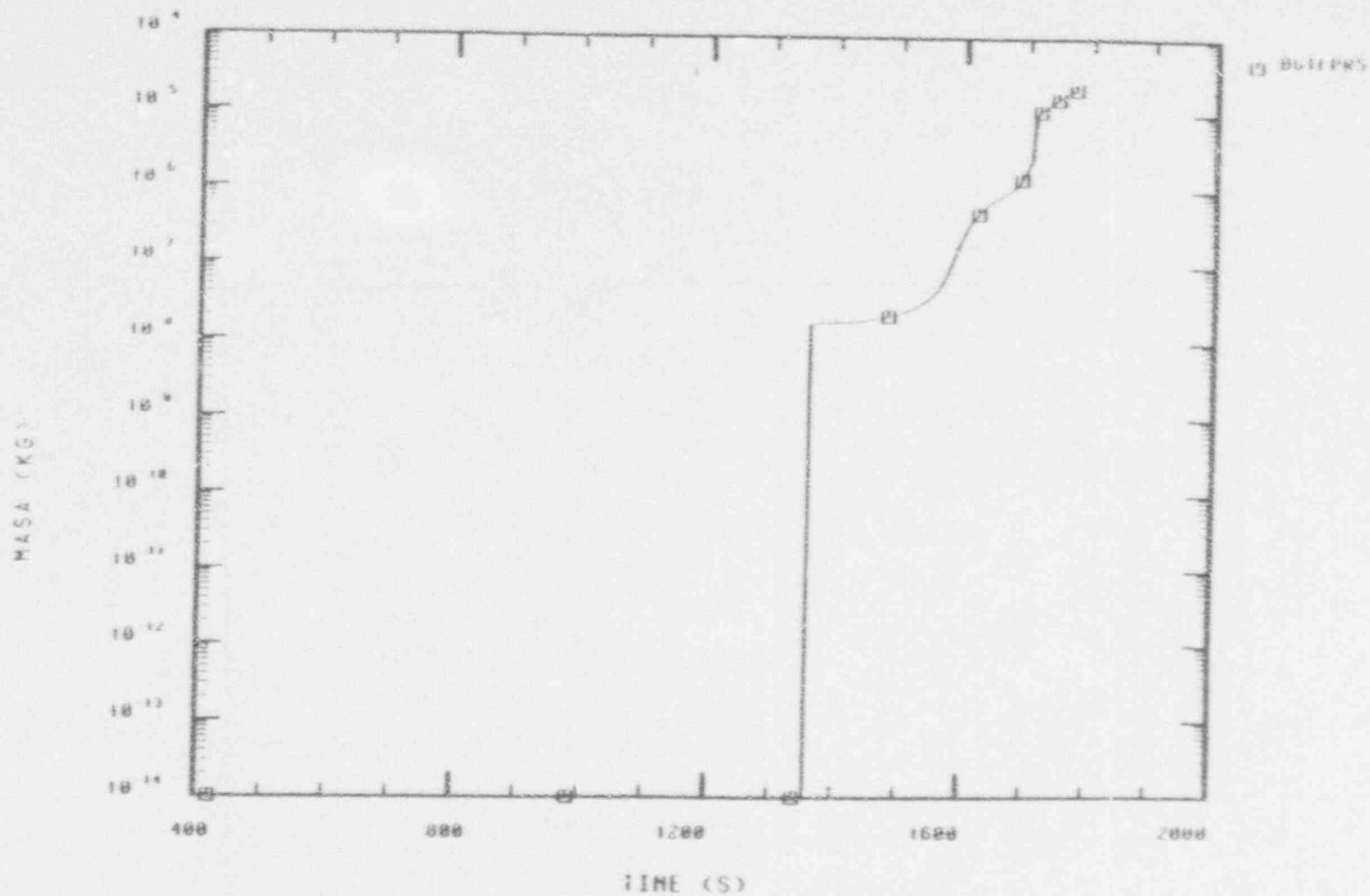


Figure 8.12

CENTER BUNDLE SOLUBLE FISSION
 PRODUCT RELEASE RATE KG
 SCDAP/R1/V21 (FP2 SPANISH GROUP)

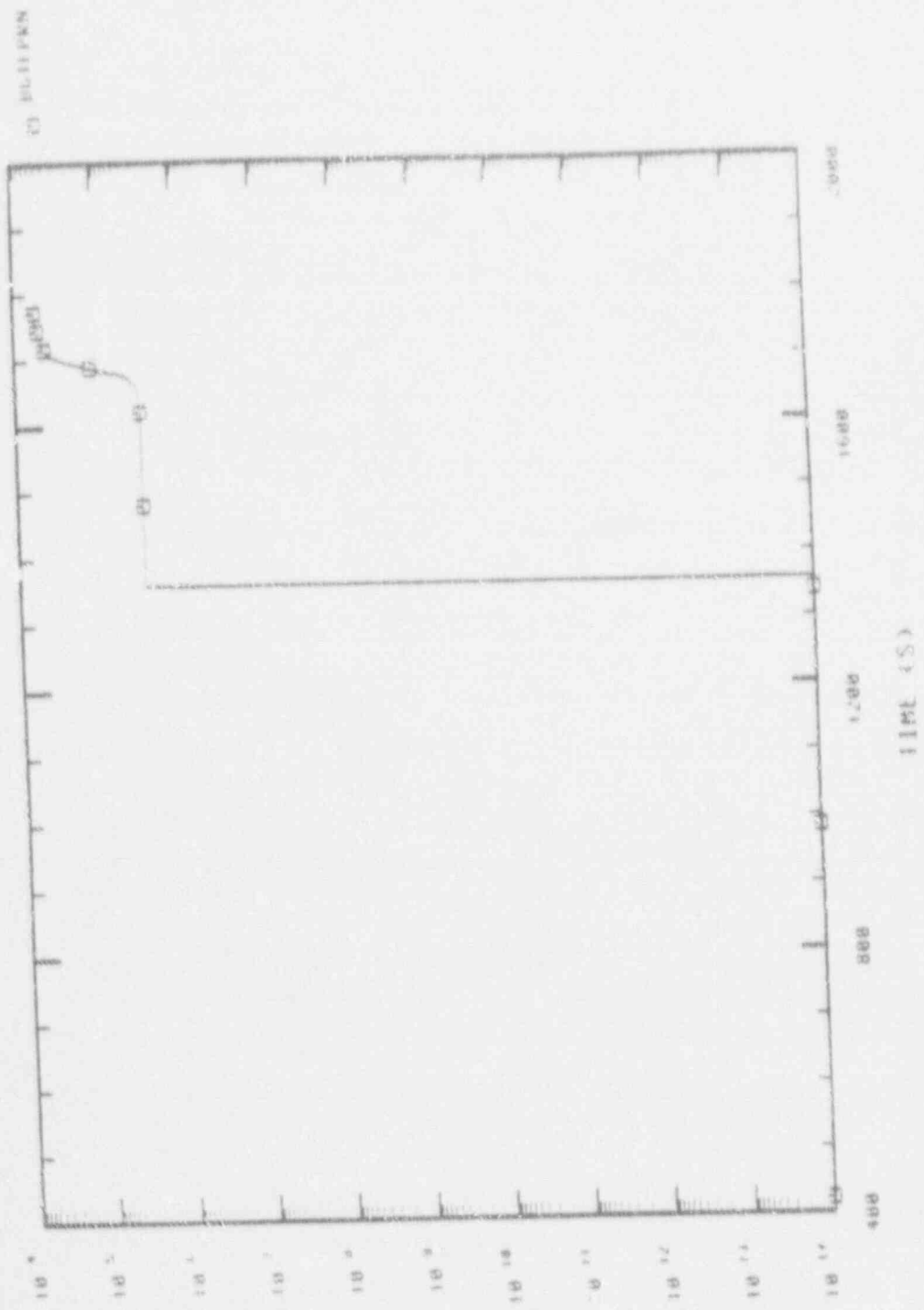


Figure 8.13
 CENTER BUNDLE NONCONDENSIBLE EMISSION
 PRODUCT RELEASE RATE KG
 SCDAP/M1/V21 (CF2 SPANISH GROUP)

(X) 454H

8.2.2 Cladding Oxidation and Hydrogen Generation

The heat generated by the metal/water reaction all throughout the transient shown in figure 8.14 where is relevant the quick excursion in place.

Figure 8.15 shows the central bundle total hydrogen generation rates, and figure 8.16 indicates the total hydrogen generation in the central bundle during the transient.

The calculated total amount of hydrogen generated in the experiment is 300 g. versus 236 g. measured experimentally (see Appendix 2 of Reference 9). Since there are approximately 38 Kg of Zirconium present in the CFM, this amount of H₂ corresponds to an average cladding oxidation of 17.86% versus the 14% derived from the experimentally H₂ measured in the BST.

The maximum oxide thickness was 36% of the cladding at the third elevation at the end of the experiment. The oxidation of the upper half of the bundle was lower due to the partial steam starvation at these locations (only 17% and 7% of cladding oxidation at the fourth and fifth axial nodes).

8.2.3 Center Bundle Damage Propagation and Geometry Changes

The major events that occurred in the CFM during the core damage period are summarized in Table 8.1 in comparison with the results obtained with the SCDAP analysis.

Following the core dryout, fuel rods started ballooning after reaching about 1000 K (1100 s), producing the clad rupture at a temperature of 1204 K (1355 s) at the 4th level. Pressure of the inner gas inside the fuel rods at the rupture time was calculated to be about 7 Mpa. Flow area blockages at six axial elevations of the CFM are shown in Figure 8.17. The clad ballooning process began at 4th level, being followed by levels 3, 5 and 2 successively. This situation is typical of a "sausage type" ballooning. The maximum blockage due to clad bal-

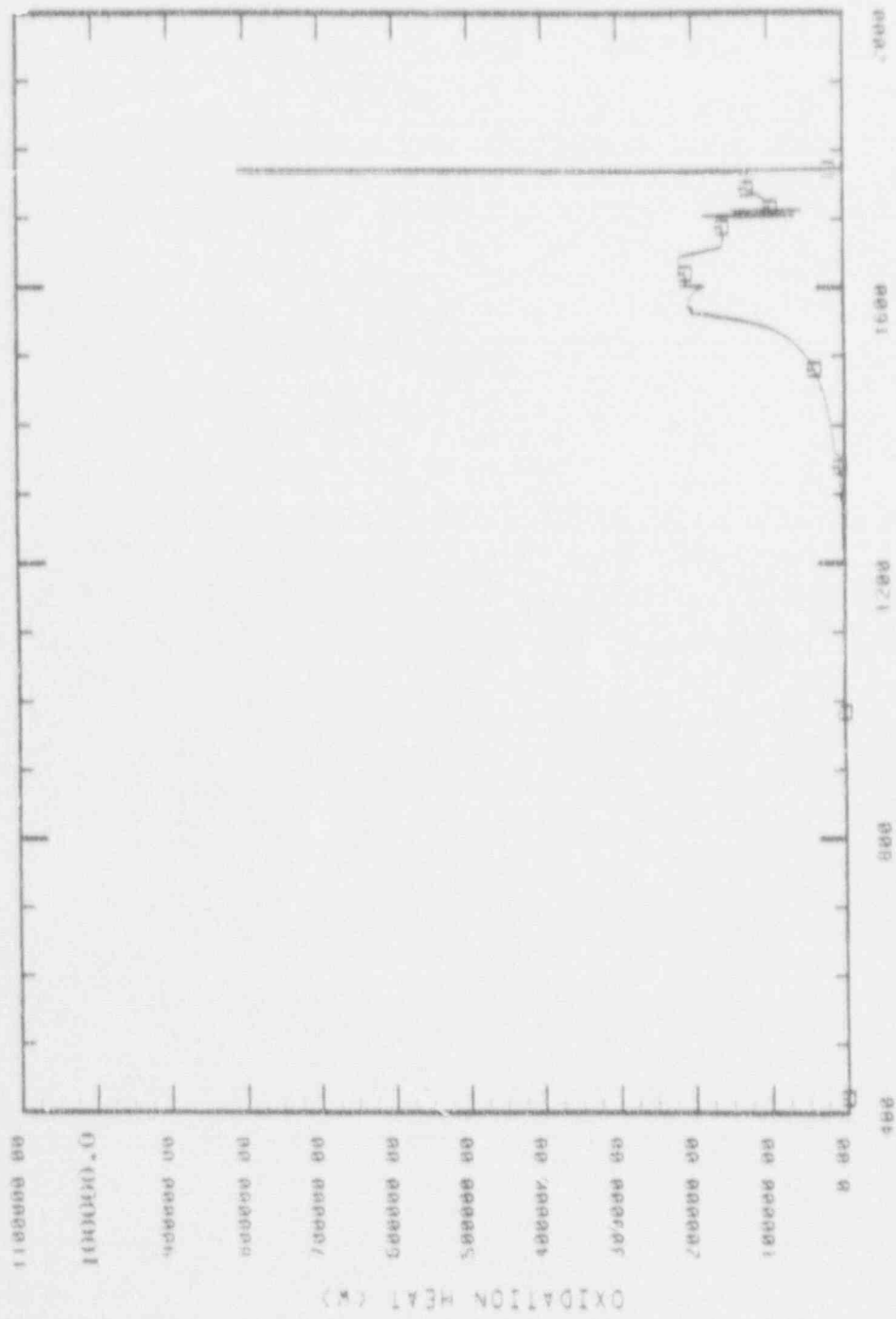


Figure 8.14
CENTER BUNDLE TOTAL OXIDATION
HEAT GENERATION (KW)
SUDAP/M1/Y21 (CFP2 SPANISH GROUP)

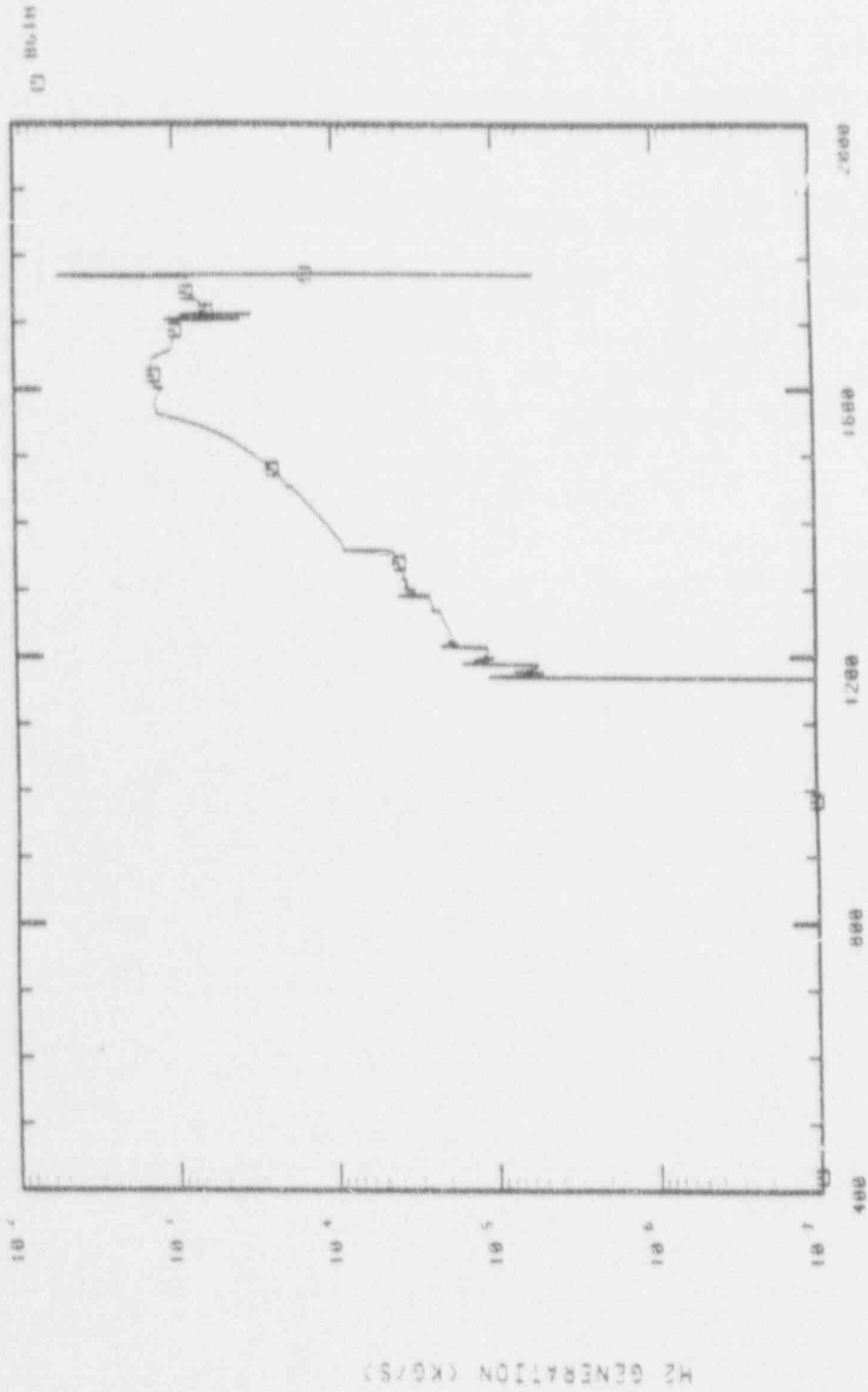


Figure 8.15
 CENTER BUNDLE TOTAL HYDROGEN
 GENERATION RATES (KG/S)
 SCDAP/M1/V21 (FP2 SPANISH GROUP)

03 701(36.10)

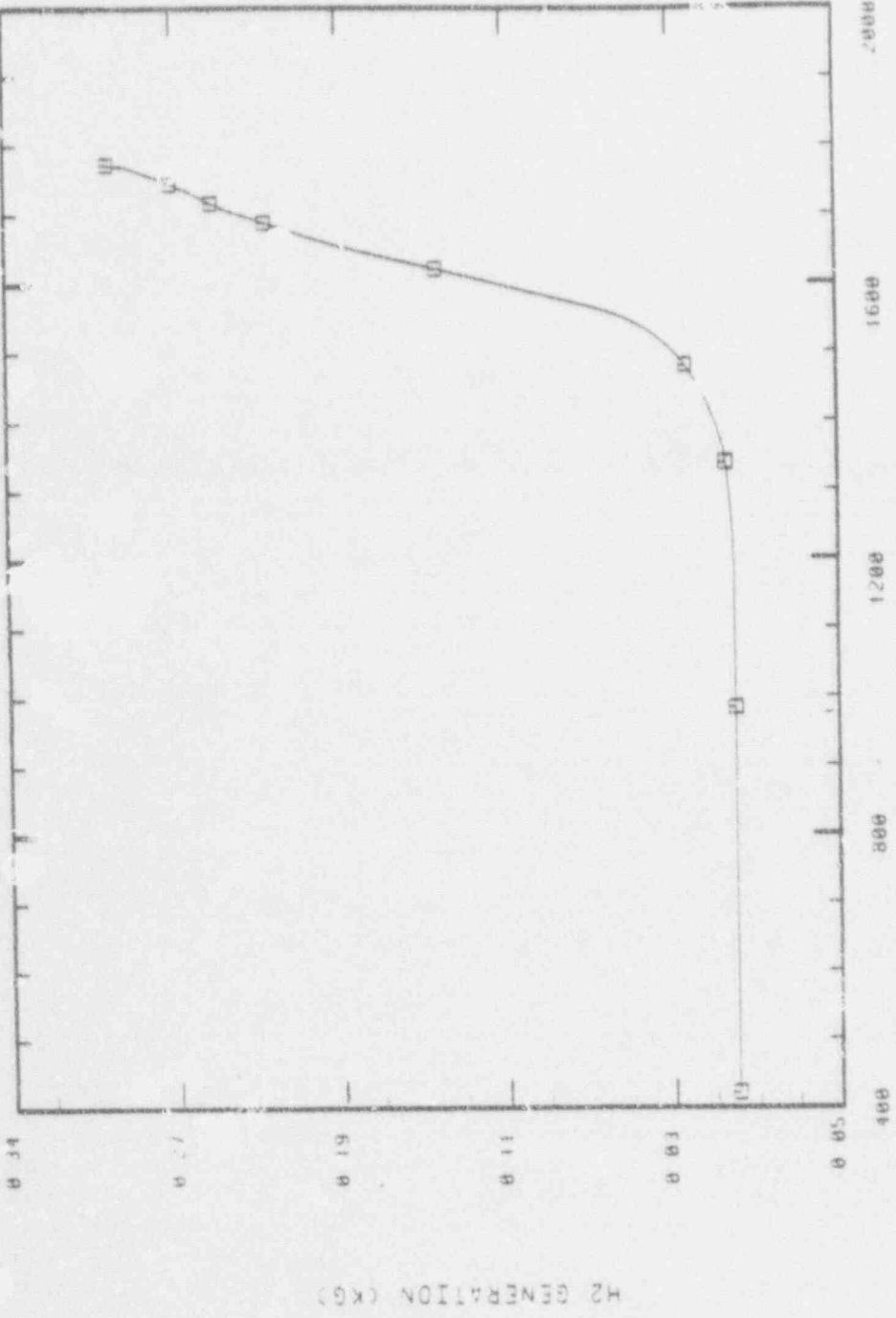


Figure 8.16
TOTAL HYDROGEN GENERATION
IN THE CENTER BUNDLE (KG)
SCLAP/H1/V21 (FP2 SPANISH GROUP)

H2 GENERATION (KG)

TABLE B.1 CHRONOLOGY OF CORE DAMAGE EVENTS

	EXPER. TIME (S)	SCDAP TIME (S)
TIME OF INITIAL FISSION PRODUCT GAP RELEASE	1200	1358
AS-DRIVE MELT AT 0.69M	1300 (LEVEL 3)	1479 (LEVELS 3 AND 4)
METAL-WATER REACTION (LEVEL 3)	1430	1360, 1400
MAXIMUM MEASURED TEMPERATURES REACH 2100°K	1504	1580
MWR SPREADS ACROSS 1.07M ELEVATION (LEVEL 4)	1480 to 1530	1500 to 1600
MWR SPREADS ACROSS 0.69M ELEVATION (LEVEL 3)	1450 to 1595	1500 to 1700
CONTROL ROB C. DRIVING RUPTURE	1500	1570
RELOCATION OF MOLTEN MATERIAL	1520 to 1680	1570 to 1705
PARTIAL BLOCKAGE (CONTROL MATERIAL RELOCATION)	1550	1570
SECOND PARTIAL BLOCKAGE (MOLTEN Zr RELOCATION)	1640	1705
END OF TRANSIENT (THE REFLOOD STARTS)	1782.6	1776

looning is about 53% of the initial flow area.

The control rod material of levels 3, 4 and 5 were completely melted at about 1520 s (see figure 8.8). At about 1570 s the stainless steel clad of the control rods melted, dissolving the Zircaloy guide tube by the formation of an SS-Zr eutectic at about 1800 K. This eutectic formation produced a breach at the 4th. level of the control rod guide tube, allowing the previously molten control alloy to flow downwards the guide tubes. Part of the molten alloy solidified at the first axial elevations, causing a 5% blockage, and the rest of the molten control material dripped below the bottom of the CFM.

Finally, at about 1700 s the Zircaloy clad of fuel and control rods failed after reaching 2960 K, fixed at the input as the ZrO_2 failure temperature. Axial levels 3 and 4 breached, allowing the molten Zircaloy flowing downwards the CFM, causing a new blockage at levels 2 and 1, as shown in Figure 8.17 (see also table 8.1).

Table 8.2 summarizes the geometry changes experienced by the CFM, as calculated by SCDAP.

The CFM average fuel rod configuration at the end of the transient is presented in Figure 8.18. This figure clearly shows the clad deformation due to the "sausage type" ballooning calculated by the code, oxide thickness, and the amount of Zircaloy liquefied and relocated at each elevation span.

It is surprising to observe that the code did not compute any fuel relocation within the rods, although the maximum hoop strain and the fuel void fraction are much larger than the setpoints values which should activate the Axial Fuel Relocation Model (see section 4.9 of Reference 5). By reviewing the FRELOC subroutine, we found that the coded void fraction criteria is 100% instead of the code manual value of 30%, making impossible any axial fuel relocation in the calculations.

Even more surprising is the fact that the UO_2 fuel was not

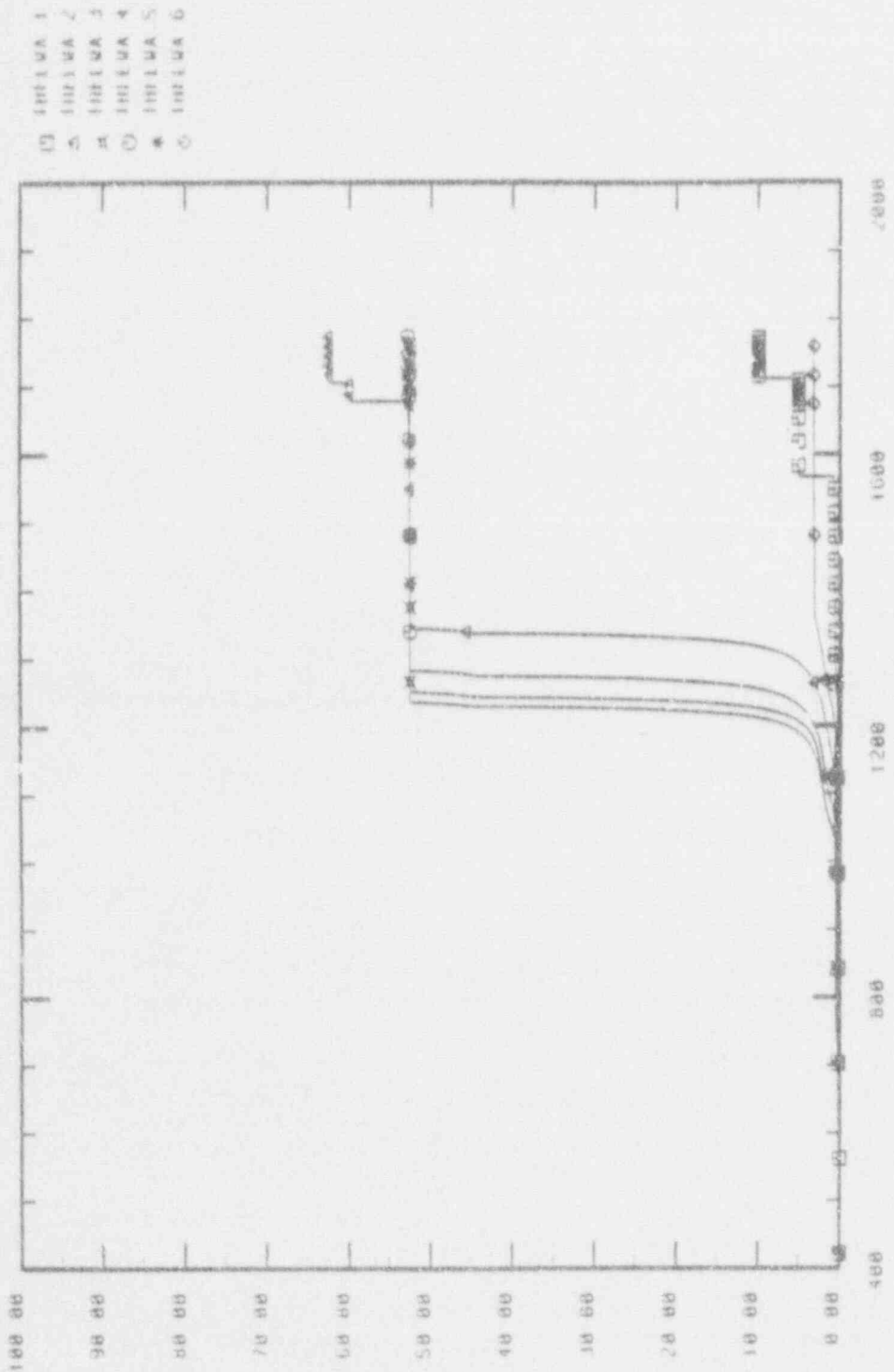
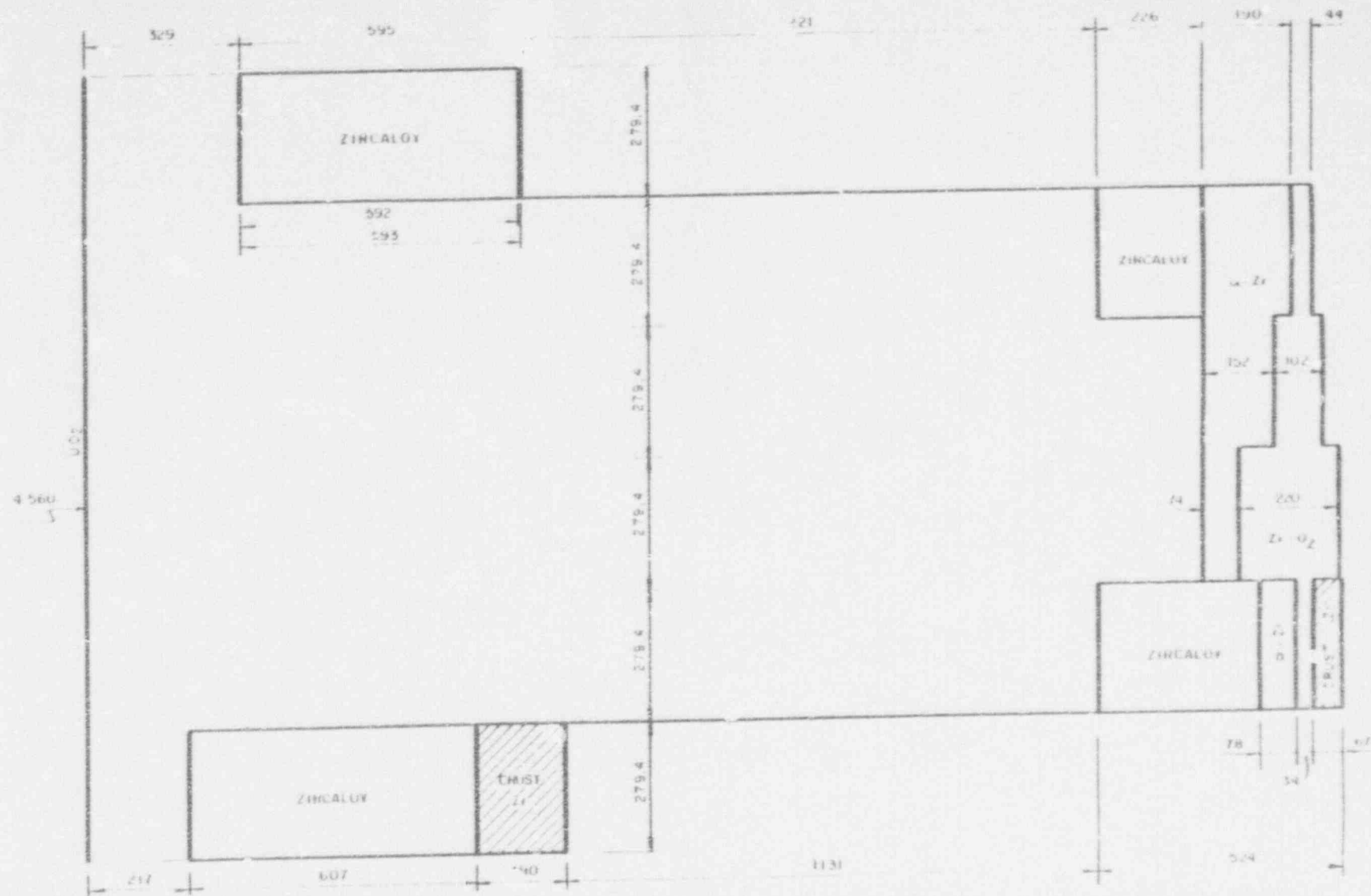


Figure 8.17
 CENTER BUNDLE FLOW AREA
 BLOCKAGES AT DIFF AXIAL LEVELS (%)
 SCDAP/M1/V21 (FP2 SPANISH GROUP)

BLOCKAGE (%)



CONFIGURATION OF FUEL RODS AT 1770S

Figure 8.18

TABLE 8.2 CORE DAMAGE PARAMETERS

1.	CLAD SWELLING AMOUNT	33.45%
	CLAD SWELLING TIME	1238 S. AT 1100°K
	CLAD SWELLING LOCATION	0.98M (LEVELS 4,3,5,2)
2.	CLAD RUPTURE TIME	1358 S. AT 1204°K
	CLAD RUPTURE LOCATION	0.98M (LEVEL 4)
3.	MASS OF CONTROL MATERIAL MELTED	10.1365 K (LEVELS 4,5,3,2)
	LOCATION OF CONTROL MATERIAL MELTED	5.9609 K IN LOWER PLENUM
		1.6412 K AT 0.1397M (LEVEL 1)
		2.5344 K AT 0.4191M (LEVEL 2, INSIDE)
4.	BLOCKAGE DUE TO SLUMPING	
	4.1. CONTROL RODS:	
		AT 1570 S. THE ABSORBENT MATERIAL BLOCKAGES A 5% AT 0.1397M (LEVEL 1)
		AT 1680 S. THE GUIDE TUBE BLOCKAGES A 7.5% AT 0.4191M (LEVEL 2)
	4.2. FUEL RODS:	
		AT 1705 S. THE CLADDING BLOCKAGES
		A 5% AT 0.1397M (LEVEL 1), AND
		A 2.5% AT 0.4191M (LEVEL 2)
	4.3. FINAL TOTAL BLOCKAGE DUE TO SLUMPING:	
		10% IN AXIAL LEVELS 1 AND 2

TABLE 8.2 (Con:)

5. CFM OXIDATION PARAMETERS

300 GRS

TOTAL HYDROGEN PRODUCTION

17.9%

CFM AVERAGE OXIDATION

AVERAGE OXIDE THICKNESS (%)
AT DIFFERENT AXIAL LOCATIONS

3RD LEVEL (0.56m TO 0.84m)

36%

4TH LEVEL (0.84m TO 1.12m)

17%

5TH LEVEL (1.12m TO 1.40m)

7%

calculated to be liquefied at any axial locations, even though the temperatures were well above the eutectic melting temperature of α -Zr (0) and UO_2 (2245 K). This fact was more surprising because the SCDAP/MOD1/V16 used in the pretest simulation⁶ predicted liquefaction of the UO_2 at the hottest two axial elevations.

By reviewing again the coding of version 21, we found that one update from V20 to V21 precluded the fuel dissolution if ballooning and double-side oxidation were considered.

Therefore, taking into account the actual coding of SCDAP/MOD1/V21, the final configuration calculated to occur sound reasonable. However, our group, after reviewing the recently available neutrographies of the LP-FP-2 CFM²⁴ consider important to update the code to simulate the axial fuel relocation and fuel dissolution phenomena.

8.3 Conclusions of the SCDAP/MOD1 Calculations

This section summarizes the major conclusions of our LP-FP-2 post-test analysis using SCDAP1/MOD1/V21.

The conclusions are the following:

1. The core thermal response during the experiment LP-FP-2 was, in general, fairly accurately calculated by SCDAP/MOD1/V21.
2. The heat up rates prior to the M-W reaction initiation are in close agreement with the data.
3. The very late clad rupture time calculated by the code, raises up doubts about if the "sausage type" ballooning calculated by the code is the most reliable model for the LP-FP-2 experiment.
4. The heat up rates after the beginning of the M-W reaction are slightly different from the measured values.
5. The calculated total hydrogen generation is a little bit higher

than the experimental data.

6. The slumping of control rod material to the lower plenum has not been observed experimentally, indicating some possible deficiencies in the resolidification model used in SCDAP/MOD1.

7. The blockages calculated by the code are considered too low. Two reasons can be identified for that:

- Deficiencies in the resolidification model that allows too much control rod material to flow out of the bundle.

- Inadequacy of the elimination of the fuel dissolution model by the eutectic formation with the molten Zircaloy in code version 21.

8. The maximum calculated clad temperature (2960 K) is considered to be too high, in comparison with the experimental data. Probably, diminishing the input temperature at which the ZrO_2 is considered to fail, the maximum temperature calculated by the code could be more realistic.

9. Several updates can be made to the code (Models for the axial fuel relocation, fuel dissolution, clad deformation, and resolidification) that could significantly improve the results.

9. SUMMARY AND CONCLUSIONS

LOFT experiment LP-FP-2 successfully simulated the slowdown thermal-hydraulics, core uncover, and early phases of core damage resulting from a simulated rupture in the LPIS piping of a PWR, the so-called V-sequence accident scenario. The LP-FP-2 results are unique and provide integral data at actual thermal-hydraulic conditions, for radioactive fission product release, transport, and deposition in an appropriate chemical environment.

In general, the TH calculations closely simulated both the general and specific experimental results.

The core boiled, dry, and heated up to temperatures in excess of 2400 K (3830°F) due initially to decay heat and ultimately to a rapid metal-water reaction. The center fuel module control rods melted, as did a substantial fraction of the adjacent fuel rods. Much of the center fuel module between the 0.69-m and 1.07-m (27- and 42-in.) elevations was calculated to relocate to the bottom of the fuel module. The thermal shroud was able to adequately shield the peripheral fuel rods during this time, and fuel rod failure was neither observed nor calculated in the peripheral modules.

The principal discrepancies between data and calculations can be related to the uncertainties in the calculated flow throughout the breaks, and the consequent uncertainties in the calculated core flow.

Despite the differences noted above, the calculational technique used for this thermal-hydraulic posttest analysis (RELAP5/MOD2-SCDAP/MOD1 passive coupling) has proved to be very suitable for the simulation of the thermal-hydraulic conditions present during a V-sequence accident, such as the one simulated by the LP-FP-2 experiment.

10. REFERENCES

1. P.R.Davis, et al., "The Risk Significance of Transient Accidents from PRA Studies", ANS Topical Meeting on Anticipated and Abnormal Transients in Light Water Reactors, Jackson, WY, September 1983.
2. Reactor Safety Study--An Assessment of Accident Risks in U.S. Commercial Nuclear Power Plants, WASH-1400, USNRC, October 1975.
3. J. P. Adams, et al., "Quick Look Report on OECD LOFT Experiment LP-FP-2", OECD LOFT-T-3804, September 1985.
4. V. H. Ransom et al., "RELAP5/MOD2 Code Manual", NUREG/CR-4312 and EGG-2396, August 85.
5. G. A. Berna et al., "SCDAP/MOD1/VO: A computer code for the Analysis of LWR Vessel Behavior During Severe Accident Transients", IS-SAAM-84-002, June 84.
6. S. Guntay, et al., "Best Estimate Prediction for OECD LOFT Project Fission Product Experiment LP-FP-2", OECD LOFT-T-3803, June 1985.
7. D. L. Reeder, "LOFT System and Test Description (5.5-ft Nuclear Core 1 LOCES)", NUREG/CR-0247 TREE-1208, July 1978.
8. V. T. Berta, "OECD LOFT Project Experiment Specification Document Fission Product Experiment LP-FP-2", OECD LOFT-T-3802, Rev. 1, May 1985.
9. M. L. Carboneau et al., "OECD LOFT Fission Product Experiment LP-FP-2 Data Report", OECD-LOFT-T-3805, May 1987.
10. G. A. Berna et al., "RELAP5/SCDAP/MOD0 code manual", FIN No. A6360, September 85.
11. H. Jordan et al., "TRAP-MELT2 User's Manual", NUREG/CR-4205, BMI-2124, May 1985.
12. D. J. Osetek et al., "Fission Product Behavior during the First Two

- PBF Severe Fuel Damage Tests", ANS Topical Meeting on Fission Product Behavior and Source Term Research, Snowbird, Utah, July 15-19 1984.
13. J. P. Adams et al, "Quick-Look Report on OECD LOFT Experiment LP-LB-1", OECD LOFT-T-3504, February 1984.
 14. S. Guntay, "RELAP5/MOD2 Assessment: OECD-LOFT Small Break Experiment LP-SB-3", Gemeinschaftsbericht Nr. 13, April 1986.
 15. C. Harwood and G. Brown, "RELAP5/MOD2 Calculation of OECD LOFT Test LP-SB-03", GD/PE-N/505, March 1986.
 16. D. L. Hagrman, et al, "MATPRO-Version 11 (Revision 2), A Handbook of Materials Properties for use in the Analysis of Light water Reactor Fuel Rod Behavior", NUREG/CR-0497, TREE-1280, Rev. 2, August 1981.
 17. "Hydrodynamic Analysis of the LOFT LPIS Line Subjected to the Conditions of the LP-FP-2 Experiment", OECD-LOFT-I-13-5161.
 18. "Assessment of RELAP5/MOD2 Against Critical Flow Data from MARVIKEN Test JIT-11 and CFT-21", NUREG-IA-0007.
 19. J.J. Peña et. al, "Preliminary Posttest Analysis of OECD LOFT Experiment LP-FP-2", F2-86-003, presented at the 12 OECD-LOFT PRG Meeting in Madrid (Spain), November 1986.
 20. J.J. Peña, S. Enciso, F. Reventós, "ANALISIS TERMOHIDRAULICO DEL EXPERIMENTO LP-FP-2: Parte 1: CALCULOS CON RELAP5/MOD2., Parte 2: CALCULOS CON SCDAP, F2-87-002, presentado en la reunión de revisión del Proyecto LOFT-ESPAÑA en Junio 1987.
 21. S. M. Jensen, "Postirradiation Examination Plan for the LP-FP-2 Center Fuel Module ", OECD-LOFT-I-8701, October 1986.
 22. Letter from G. D. McPherson to J. Puga, "LOFT Reactor Decay Heat Calculations" and "Decay Heat Tables for OECD-LOFT Experiments", December 5, 1985.

23. D. J. Osetek et al, "Fission Product Behavior during the first two PBF Severe Fuel Damage Tests", ANS Topical Meeting on Fission Product Behavior and Source Term Research, Snowbird, Utah, July 15-19, 1984.
24. Letter from G.D. McPherson to all OECD LOFT Extended Analysis Program Review Group Members, "LP-FP-2 Sectioning Requirements and Recommendations", October 13, 1987.

APPENDIX A

LP-FP-2 EXPERIMENT INSTRUMENTATION

APPENDIX A

LP-FP-2 EXPERIMENT INSTRUMENTATION

This Appendix A includes the measurement identification and description of the short term qualified data recorded for the transient phase of the LP-FP-2 experiment (-421 to 2096 s).

Also, a list of figures indicating the location of the most important tracers is provided in this appendix.

For more details see references A-1 and A-2.

TABLE A-1. MEASUREMENT IDENTIFIERS AND DESCRIPTIONS FOR LP-FP-2.
(TAKEN FROM THE SHORT TERM DIRC REPORT)

Measurement Identification	Measurement Description
AH2E-T55-001	H2 CONCENTRATION IN CONTAINMENT VESSEL
AH2E-T55-002	H2 CONCENTRATION IN CONTAINMENT VESSEL
AH2E-T55-003	H2 CONCENTRATION IN CONTAINMENT VESSEL
CR-SUP-A	ROD POSITION-ROD 5
CR-SUP-B	ROD POSITION-ROD 5
CVP165-D115	PURGE GAS ORIFICE BYPASS VALVE
CVP165-D13A	NITROGEN INLET VALVE
CVP165-D14A	PRESSURE RELIEF VALVE TO BST
CVP165-F112	DILUTION GAS INLET VALVE
CVP165-F113	DILUTION GAS (ORIFICE 1) VALVE
CVP165-F114	DILUTION GAS (ORIFICE 2) VALVE
CVP165-F120	ANNULUS GAS INLET VALVE
CVP165-F128	ANNULUS GAS OUTLET VALVE
CVP165-F134A	ISO VALVE F1 LINE
CVP165-F134B	ISO VALVE F1 LINE
CVP165-F166	PRESSURE RELIEF VALVE TO BST
CVP165-F148	OUTLET VALVE
CVP165-F234A	ISO VALVE F2 LINE
CVP165-F234B	ISO VALVE F2 LINE
CVP165-F236	PRESSURE RELIEF VALVE TO BST
CVP165-F248	OUTLET VALVE
CV-P004-008	VALVE POSITION FEEDWATER FLOW CONTROL
CV-P004-010	VALVE POSITION SCS STEAM FLOW CONTROL
CV-P004-090	MAIN STEAM BYPASS VALVE
CV-P004-091	MAIN FEED BYPASS VALVE
CV-P138-070A	VALVE POSITION BLOWDOWN SYSTEM RABV CH
CV-P138-071A	VALVE POSITION BLOWDOWN SYSTEM RABV C.
DE-BL-001A	CHORDAL DENSITY-BROKEN LOOP CL
DE-BL-001B	CHORDAL DENSITY-BROKEN LOOP CL
DE-BL-001C	CHORDAL DENSITY-BROKEN LOOP CL
DE-BL-002A	CHORDAL DENSITY-BROKEN LOOP HL
DE-BL-002B	CHORDAL DENSITY-BROKEN LOOP HL
DE-BL-002C	CHORDAL DENSITY-BROKEN LOOP HL
DE-BL-105	AVERAGE DENSITY-BROKEN LOOP CL
DE-BL-205	AVERAGE DENSITY-BROKEN LOOP HL

TABLE A-1 (continued)

Measurement Identification	Measurement Description
DE-PC-001A	CHORDAL DENSITY-INTACT LOOP CL
DE-PC-001B	CHORDAL DENSITY-INTACT LOOP CL
DE-PC-001C	CHORDAL DENSITY-INTACT LOOP CL
DE-PC-002A	CHORDAL DENSITY-INTACT LOOP HL
DE-PC-002B	CHORDAL DENSITY-INTACT LOOP HL
DE-PC-002C	CHORDAL DENSITY-INTACT LOOP HL
DE-PC-105	AVERAGE DENSITY - INTACT LOOP CL
DE-PC-205	AVERAGE DENSITY - INTACT LOOP HL
FEP165-F1-22	FLOW RATE F1 HEATING GAS LINE
FE-PC-002A	VELOCITY-INTACT LOOP HOT LEG BOTTOM
FE-PC-002B	VELOCITY-INTACT LOOP HOT LEG MIDDLE
FE-PC-002C	VELOCITY-INTACT LOOP HOT LEG TOP
FE-1ST-001	VELOCITY DOWNCOMER STALK 1
FE-1ST-002	VELOCITY DOWNCOMER STALK 1 LOWER
FR-PC-201	MASS FLOW RATE - HL TURB*DENS
FR-PC-205	MASS FLOW RATE - HL DD*DENS
FR-PC-206	MASS FLOW RATE - HL TURB*DD
FTP165-F122	ANNULUS GAS FLOW RT ORFICE DELTA P
FT-P004-012	FLOWRATE-STEAM FLOW CONDENSER IN
FT-P004-72-2	FLOWRATE-SCS FEEDWATER
FT-P128-085	FLOWRATE-HPIS PUMP B DISCHARGE
FT-P128-104	FLOWRATE-HPIS PUMP A DISCHARGE
FT-P139-27-1	FLOWRATE-INTACT LOOP COOLANT
FT-P139-27-2	FLOWRATE-INTACT LOOP COOLANT
FT-P139-27-3	FLOWRATE-INTACT LOOP COOLANT
LEPOT-9139-007	QUID LEVEL - PRESSURIZER CH.B
LE-ECC-01A	ACCUMULATOR A LIQUID LEVEL
LE-1F10	COOLANT LEVEL-FUEL ASSY 1 LOC F10
LE-1ST-001&2	COOLANT LEVEL-INSTR STALK 1 LP & D
LE-3F10	COOLANT LEVEL-FUEL ASSY 3 LOC F10
LE-3UP-001	COOLANT LEVEL-UPPER PLENUM
LIT-P120-013	LIQUID LEVEL A - BWST
LIT-P120-014	LIQUID LEVEL B - BWST
LIT-P120-089	LIQUID LEVEL - ACCUMULATOR B
LT-P004-008A	STEAM GENERATOR LEVEL NARROW RANGE

TABLE A-1 (continued)

Measurement Identification	Measurement Description
LT-P004-003B	LIQUID LEVEL-SCS SECONDARY WIDE RANGE
LT-P004-042	CONDENSATE RECEIVER LEVEL
LT-P004-08AA	STEAM GENERATOR LEVEL NARROW RANGE
LT-P004-08BB	STEAM GEN LEVEL WIDE RANGE
LT-P138-033	LIQUID LEVEL-BST A
LT-P138-058	LIQUID LEVEL-BST B
ME-PC-002A	MOMENTUM FLUX-INTACT LOOP HL BOTTOM
ME-PC-002B	MOMENTUM FLUX-INTACT LOOP HL MIDDLE
ME-PC-002C	MOMENTUM FLUX-INTACT LOOP HL TOP
ME-PC-002	AVE MOMENTUM FLUX-INTACT LOOP HL
ME-1ST-001	MOMENTUM FLUX-INSTR STALK 1 DC
NE-2H08-26	NEUTRON DETECTOR IN CORE FA#2
NE-4H08-26	NEUTRON DETECTOR IN CORE FA#4
NE-6H08-26	NEUTRON DETECTOR IN CORE FA#6
PDE-BLH-001	DIFF PRESS LPIS BRK LN VENTURI HIGH
PDE-BLH-002	DIFF PRESS LPIS BRK LN VENTURI LOW
PDE-BLH-003	DIFF PRESS LPIS BRK LN VENTURI HIGH
PDE-BLH-004	DIFF PRESS LPIS BRK LN VENTURI LOW
PDE-BLH-005	DIFF PRESS LPIS BRK LN ACROSS FILTER
PDT-P139-006	DIFF PRES ACROSS PRESSURIZER CHANGE
PDT-P139-007	DIFF PRES ACROSS PRESSURIZER CHANGE
PDT-P139-030	DELTA P - REACTOR VESSEL
PDT-P139-30A	DELTA P-PRIMARY COOLANT PUMP
PDT-P139-30B	DELTA P-INTACT LOOP SG
PE-BLH-001	ABS PRES LPIS BRK LN UPSTRM VENTURI
PE-BLH-002	ABS PRES LPIS BRK LN UPSTRM FILTER
PE-BLH-003	ABS PRES LPIS BRK LN UPSTRM VENTURI
PE-BL-001A	PRESSURE-BROKEN LOOP COLD LEG
PE-BL-002A	PRESSURE-BROKEN LOOP HOT LEG
PE-PC-002	PRESSURE-INTACT LOOP HOT LEG
PE-PC-005	PRESSURE-INTACT LOOP REF.
PE-PC-006	PRESSURE-INTACT LOOP REF.
PTP165-01-19	PRESS-PCS ON O1 SAMPLE LINE
PTP165-01-20	PRESS-N2 SUPPLY-O1 SAMPLE LINE
PTP165-01-2	O1 PURGE GAS PRESSURE

TABLE A-1 (continued)

Measurement Identification	Measurement Description
PTP165-F140	RECOMBINER PURGE GAS PRESSURE
PTP165-F1-5	ARGON SUPPLY PRESSURE
PTP165-F1-8A	PRESS-F1 CARRIER GAS LINE
PTP165-F1-8B	PRESS-F1 LINE-UPSTM FLOW ORIFICE
PTP165-F1-8C	PRESS-F1 CARRIER GAS LINE
PTP165-F2-43	PRESS-F2-LINE-UPSTM FLOW ORIFICE
PT-P004-010A	PRESSURE-SCS 10 INCH LINE FROM SG
PT-P004-022	CONDENSATE RECEIVER PRESSURE
PT-P004-034	PRESSURE-SCS FEEDWATER
PT-P004-085	PRESSURE-SCS 12 INCH CONDENSOR IN
PT-P120-029	PRESSURE-ECCS ACCUMULATOR B
PT-P120-043	PRESSURE-ECCS ACCUMULATOR A
PT-P138-056	PRESSURE-BST VAPOR SPACE CH B
PT-P138-057	PRESSURE-BST VAPOR SPACE CH C
PT-P139-004	PRESSURE-INTACT LOOP HOT LEG CHANNEL C
PT-P139-042	PRESSURE CONTAINMENT CHAN B
PT-P139-05-1	PRESSURE-PRESSURIZER
RE-T4-096	BST RAM
RE-T-77-1A1	NIS-POWER RANGE CHANNEL A PEAK
RE-T-77-1A2	NIS-POWER RANGE CHANNEL A LEVEL
RE-T-77-2A1	NIS-POWER RANGE CHANNEL B PEAK
RE-T-77-2A2	NIS-POWER RANGE CHANNEL B LEVEL
RE-T-77-3A1	NIS-POWER RANGE CHANNEL C PEAK
RE-T-77-3A2	NIS-POWER RANGE CHANNEL C LEVEL
RE-T-85-1	NIS-SOURCE RANGE CHANNEL 1
RE-T-85-2	NIS-SOURCE RANGE CHANNEL 2
RE-T-86-3	NIS-INTERMEDIATE RANGE CHANNEL 3
RE-T-86-4	NIS-INTERMEDIATE RANGE CHANNEL 4
RE-T-87-4A1	NIS-POWER RANGE CHANNEL D PEAK
RE-T-87-4A2	NIS-POWER RANGE CHANNEL D LEVEL
RPE-PC-001	PUMP SPEED-PRIMARY COOLANT PUMP 1
RPE-PC-002	PUMP SPEED-PRIMARY COOLANT PUMP 2
RP-CRDM2-PT	ROD POSITION ROD 2 CRD PULSE TOTALIZER
RP-CRDM2-TC	ROD POSITION ROD 2 TURNS COUNTER
RP-CRDM4-PT	ROD POSITION ROD 4 CRD PULSE TOTALIZER
RP-CRDM4-TC	ROD POSITION ROD 4 TURNS COUNTER

TABLE A-1 (continued)

Measurement Identification	Measurement Description
RP-CRDM6-PT	ROD POSITION ROD 6 CRD PULSE TOTALIZER
RP-CRDM6-TC	ROD POSITION ROD 6 TURNS COUNTER
RP-CRDM8-PT	ROD POSITION ROD 8 CRD PULSE TOTALIZER
RP-CRDM8-TC	ROD POSITION ROD 8 TURNS COUNTER
SP-BLH-001	SAT PRESS-LPIS BRK LN INLET
SP-BLH-002	SAT PRESS-LPIS BRK LN INLET
SP-BLH-003	S/T PRESS-LPIS BRK LN GAMMA SPECT
SP-BLH-004	SAT PRESS-LPIS BRK LN GAMMA SPECT
SP-BLH-005	SAT PRESS-LPIS BRK LN FILTER INLET
SP-BLH-006	SAT PRESS-LPIS BRK LN VENTURI INLE
SP-BLH-007A	SAT PRESS-LPIS BRK LN VENTURI INLE
SP-BLH-007B	SAT PRESS-LPIS BRK LN VENTURI INLE
SP-BLH-008	SAT PRESS-LPIS BRK LN VENTURI OUTL
SP-PC-002B	SATURATION PRESS-INTACT LOOP HL
SP-P139-019	SATURATION PRESS-PRESSURIZER
SP-P139-020	SATURATION PRESS-PRESSURIZER
SP-SG-003	SATURATION PRESSURE, STEAM GENERATOR
SP-SG-004	SATURATION PRESSURE, STEAM GEN, MIDDLE
SP-1ST-005	SATURATION PRESS-DOWNCOMER STALK 1
ST-BLH-001	SAT TEMP-LPIS BRK LN UPSTRM VENTURI
ST-BLH-002	SAT TEMP-LPIS BRK LN UPSTRM FILTER
ST-BLH-003	SAT TEMP-LPIS BRK LN UPSTRM VENTURI
ST-BL-001A	SAT TEMP-BROKEN LOOP, CL
ST-BL-002A	SAT TEMP-BROKEN LOOP, HL
ST-PC-002	SATURATION TEMP, INTACT LOOP, HL
ST-PC-005	SATURATION TEMP, INTACT LOOP, CL
ST-P139-05-1	SATURATION TEMP, SG INLET
TC-5IC8-27	TEMP FUEL CENTERLINE/FAS PIN I8 27
TC-5K08-27	TEMP FUEL CENTERLINE/FAS PIN K8 27
TC-5M04-27	TEMP FUEL CENTERLINE/FAS PIN M4 27
TC-5M08-27	TEMP FUEL CENTERLINE/FAS PIN M8 27
TEP165-0121B	NITROGEN PURGE GAS PIPE TEMPERATURE
TEP165-F130A	TEMP-F1 LINE-OUTLET RV
TEP165-F1-38	PIPE TEMP DS OF DILUTION FILTER F1
TEP165-F1-8A	TEMP-F1 CARRIER GAS LINE

TABLE A-1 (continued)

Measurement Identification	Measurement Description
TEP165-F1-8B	TEMP-F1 LINE UPSTM FLOW ORIFICE
TEP165-F1-8C	TEMP-F1 CARRIER GAS LINE
TEP165-F2-38	TEMP-F2 LINE-UPSTM DILUTION FILTER
TEP165-F2-45	TEMP-F2 LINE-UPSTM FLOW ORIFICE
TE-BLH-001	WALL TEMP LPIS BRK LN INLET
TE-BLH-002	STM TEMP LPIS BRK LN INLET
TE-BLH-003	STM TEMP LPIS BRK LN GAMMA SPECTROMETER
TE-BLH-004	WALL TEMP LPIS BRK LN GAMMA SPECTROMETER
TE-BLH-005	STM TEMP LPIS BRK LN FILTER INLET
TE-BLH-006	WALL TEMP LPIS BRK LN FILTER INLET
TE-BLH-007A	STM TEMP LPIS BRK LN VENTURI INLET
TE-BLH-007B	STM TEMP LPIS BRK LN VENTURI INLET
TE-BLH-008	WALL TEMP LPIS BRK LN VENTURI OUTLET
TE-PC-002A	TEMP-INTACT LOOP HL BOTTOM
TE-PC-002B	TEMP-INTACT LOOP HL MIDDLE
TE-PC-002C	TEMP-INTACT LOOP HL TOP
TE-P004-054	CONDENSATE RECEIVER TEMPERATURE
TE-P120-001	LIQUID TEMP-BWST
TE-P120-027	LIQUID TEMP-ECCS ACCUM B
TE-P120-041	LIQUID TEMP-ECCS ACCUM A
TE-P120-102	LIQUID TEMP-ECCS LP. HX B OUTLET
TE-P139-019	TEMPERATURE-PRESSURIZER VAPOR
TE-P139-020	TEMPERATURE-PRESSURIZER LIQUID
TE-P139-029	COOLANT TEMP-INTACT LOOP COLD LEG
TE-P139-28-2	TEMPERATURE-INTACT LOOP COLD LEG
TE-P139-32-1	PRIMARY COOLANT HOT LEG TEMP CHANNEL
TE-P141-094	PCCS HEAT EXCH INLET TEMP
TE-P141-095	PCCS HEAT EXCH OUTLET TEMP
TE-SG-001A	COOLANT TEMP-IL SG INLET PLENUM
TE-SG-002A	COOLANT TEMP-IL SG OUTLET PLENUM
TE-SG-003	LIQUID TEMP-SCS SG DOWNCOMER
TE-SG-004	LIQUID TEMP-SCS SG DOWNCOMER
TE-SG-005	LIQ - TEMP SCS SG DOWNCOMER
TE-SV-001	LIQUID TEMP-BST STALK 1-107.2
TE-SV-002	LIQUID TEMP-BST STALK 1-93.0

TABLE A-1 (continued)

Measurement Identification	Measurement Description
TE-SV-003	LIQUID TEMP-BST STALK 1-74.7
TE-SV-004	LIQUID TEMP-BST STALK 1-57.2
TE-SV-005	LIQUID TEMP-BST STALK 1-39.0
TE-SV-006	LIQUID TEMP-BST STALK 1-14.7
TE-SV-007	LIQUID TEMP-BST STALK 2-107.2
TE-SV-008	LIQUID TEMP-BST STALK 2-93.0
TE-SV-009	LIQUID TEMP-BST STALK 2-74.7
TE-SV-010	LIQUID TEMP-BST STALK 2-57.2
TE-SV-011	LIQUID TEMP-BST STALK 2-39.0
TE-SV-012	LIQUID TEMP-BST STALK 2-14.7
TE-T055-002	TEMPERATURE-CONTAINMENT AMBIENT
TE-1A11-020	TEMP-CLADDING/FA1 PIN A11 20 IN.
TE-1B10-037	TEMP-CLADDING/FA1 PIN B10 37 IN.
TE-1B11-028	TEMP-CLADDING/FA1 PIN B11 28 IN.
TE-1B11-032	TEMP-CLADDING/FA1 PIN B11 32 IN.
TE-1C11-021	TEMP-CLADDING/FA1 PIN C11 21 IN.
TE-1C11-039	TEMP-CLADDING/FA1 PIN C11 39 IN.
TE-1F07-019	TEMP-CLADDING/FA1 PIN F7 19 IN.
TE-1F07-026	TEMP-CLADDING/FA3 PIN F7 26 IN.
TE-1ST-001	COOLANT TEMP-RV INSTR STALK 1 DC
TE-1ST-002	COOLANT TEMP-RV INSTR STALK 1 DC
TE-1ST-003	COOLANT TEMP-RV INSTR STALK 1 DC
TE-1ST-004	COOLANT TEMP-RV INSTR STALK 1 DC
TE-1ST-005	COOLANT TEMP-RV INSTR STALK 1 DC
TE-1ST-006	COOLANT TEMP-RV INSTR STALK 1 DC
TE-1ST-008	COOLANT TEMP-RV INSTR STALK 1 LP
TE-1ST-009	COOLANT TEMP-RV INSTR STALK 1 LP
TE-1ST-010	COOLANT TEMP-RV INSTR STALK 1 LP
TE-1ST-011	COOLANT TEMP-RV INSTR STALK 1 LP
TE-1ST-012	COOLANT TEMP-RV INSTR STALK 1 LP
TE-1ST-013	COOLANT TEMP-RV INSTR STALK 1 LP
TE-1ST-015	COOLANT TEMP-RV INSTR STALK 1 DC
TE-1UP-001	COOLANT TEMP-UPPER END BOX
TE-1UP-002	COOLANT TEMP-UPPER END BOX
TE-1UP-005	COOLANT TEMP-ON OTT FE-1UP-1

TABLE A-1 (continued)

Measurement Identification	Measurement Description
TE-1UP-006	METAL TEMP-SUPPORT COLUMN FA1
TE-1UP-007	METAL TEMP-SUPPORT COLUMN FA1
TE-2E08-045	TEMP-CLADDING/FA2 PIN E8 45 IN.
TE-2F07-015	TEMP-CLADDING/FA2 PIN F7 15 IN.
TE-2F08-032	TEMP-CLADDING/FA2 PIN F8 32 IN.
TE-2F09-026	TEMP-CLADDING/FA2 PIN F9 26 IN.
TE-2G14-011	TEMP-CLADDING/FA2 PIN G14 11 IN.
TE-2G14-030	TEMP-CLADDING/FA2 PIN G14 30 IN.
TE-2G14-045	TEMP-CLADDING/FA2 PIN G14 45 IN.
TE-2H02-028	TEMP-CLADDING/FA2 PIN H2 28 IN.
TE-2H13-021	TEMP-CLADDING/FA2 PIN H13 21 IN.
TE-2H13-049	TEMP-CLADDING/FA2 PIN H13 49 IN.
TE-2H14-028	TEMP-CLADDING/FA2 PIN H14 28 IN.
TE-2H14-032	TEMP-CLADDING/FA2 PIN H14 32 IN.
TE-2H15-026	TEMP-CLADDING/FA2 PIN H15 26 IN.
TE-2H15-041	TEMP-CLADDING/FA2 PIN H15 41 IN.
TE-2I14-021	TEMP-CLADDING/FA2 PIN I14 21 IN.
TE-2I14-039	TEMP-CLADDING/FA2 PIN I14 39 IN.
TE-2LP-001	COOLANT TEMP-LOWER END BOX
TE-2LP-002	COOLANT TEMP-LOWER END BOX
TE-2LP-003	COOLANT TEMP-LOWER END BOX
TE-2UP-001	COOLANT TEMP-UPPER END BOX
TE-2UP-002	COOLANT TEMP-UPPER END BOX
TE-2UP-003	COOLANT TEMP-UPPER END BOX
TE-2UP-004	METAL TEMP-SUPPORT COLUMN FA2
TE-2UP-005	METAL TEMP-SUPPORT COLUMN FA2
TE-3A11-030	TEMP-CLADDING/FA3 PIN A11 30 IN.
TE-3B11-028	TEMP-CLADDING/FA3 PIN B11 28 IN.
TE-3B11-032	TEMP-CLADDING/FA3 PIN B11 32 IN.
TE-3C11-021	TEMP-CLADDING/FA3 PIN C11 21 IN.
TE-3C11-039	TEMP-CLADDING/FA3 PIN C11 39 IN.
TE-3F07-026	TEMP-CLADDING/FA3 PIN F7 26 IN.
TE-3UP-001	COOLANT TEMP-UPPER END BOX
TE-3UP-006	METAL TEMP-SUPPORT COLUMN FA3
TE-3UP-008	TEMP-COOLANT LLT ABOVE FA3

TABLE A-1 (continued)

Measurement Identification	Measurement Description
TE-3UP-010	TEMP-COOLANT LLT ABOVE FA3
TE-3UP-011	TEMP-COOLANT LLT ABOVE FA3
TE-3UP-012	TEMP-COOLANT LLT ABOVE FA3
TE-3UP-013	TEMP-COOLANT LLT ABOVE FA3
TE-3UP-014	TEMP-COOLANT LLT ABOVE FA3
TE-3UP-015	TEMP-COOLANT LLT ABOVE FA3
TE-3UP-016	TEMP-COOLANT LLT ABOVE FA3
TE-4E08-045	TEMP-CLADDING/FA4 PIN E8 45 IN.
TE-4F07-015	TEMP-CLADDING/FA4 PIN F7 15 IN.
TE-4F08-032	TEMP-CLADDING/FA4 PIN F8 32 IN.
TE-4G08-021	TEMP-CLADDING/FA4 PIN G8 21 IN.
TE-4G14-011	TEMP-CLADDING/FA4 PIN G14 11 IN.
TE-4G14-030	TEMP-CLADDING/FA4 PIN G14 30 IN.
TE-4G14-045	TEMP-CLADDING/FA4 PIN G14 45 IN.
TE-4H13-015	TEMP-CLADDING/FA4 PIN H13 15 IN.
TE-4H13-037	TEMP-CLADDING/FA4 PIN H13 37 IN.
TE-4H14-028	TEMP-CLADDING/FA4 PIN H14 28 IN.
TE-4H15-026	TEMP-CLADDING/FA4 PIN H15 26 IN.
TE-4H15-041	TEMP-CLADDING/FA4 PIN H15 41 IN.
TE-4I14-039	TEMP-CLADDING/FA4 PIN I14 39 IN.
TE-4LP-001	COOLANT TEMP-LOWER END BOX
TE-4LP-003	COOLANT TEMP-LOWER END BOX
TE-4UP-001	COOLANT TEMP-UPPER END BOX
TE-4UP-002	COOLANT TEMP-UPPER END BOX
TE-4UP-003	COOLANT TEMP-UPPER END BOX
TE-4UP-004	METAL TEMP-SUPPORT COLUMN FA4
TE-4UP-005	METAL TEMP-SUPPORT COLUMN FA4
TE-5C06-027	TEMP-GUIDE TUBE FA5 LOC C6 27"
TE-5C06-066	TEMP-GUIDE TUBE FA5 LOC C6 66 IN.
TE-5C07-042	TEMP-INTERNAL CLAD FA5 PIN C7 42"
TE-5C09-010	TEMP-INTERNAL CLAD FA5 PIN C9 10"
TE-5C09-027	TEMP-INTERNAL CLAD FA5 PIN C9 27"
TE-5C10-027	TEMP-GUIDE TUBE FA5 LOC C10 27"
TE-5C12-010	TEMP-INTERNAL CLAD FA5 PIN C12 10"
TE-5C12-027	TEMP-INTERNAL CLAD FA5 PIN C12 27"

TABLE A-1 (continued)

Measurement Identification	Measurement Description
TE-5D09-027	TEMP-INTERNAL CLAD FAS PIN D9 27"
TE-5D13-042	TEMP-INTERNAL CLAD FAS PIN D13 42"
TE-5E05-027	TEMP-GUIDE TUBE FAS LOC E5 27"
TE-5E11-027	TEMP-GUIDE TUBE FAS LOC E11 27"
TE-5E-010	SHROUD TEMP EAST SIDE 10 IN.
TE-5E-027	SHROUD TEMP EAST SIDE 27 IN.
TE-5E-032	SHROUD TEMP EAST SIDE 32 IN.
TE-5E-042	SHROUD TEMP EAST SIDE 42 IN.
TE-5F03-027	TEMP-GUIDE TUBE FAS LOC F3 27"
TE-5F09-010	TEMP-INTERNAL CLAD FAS PIN F9 10"
TE-5F09-027	TEMP-INTERNAL CLAD FAS PIN F9 27"
TE-5F13-066	TEMP-GUIDE TUBE FAS LOC F13 66"
TE-5G04-010	TEMP-INTERNAL CLAD FAS PIN G4 10"
TE-5G04-027	TEMP-INTERNAL CLAD FAS PIN G4 27"
TE-5G12-010	TEMP-INTERNAL CLAD FAS PIN G12 10"
TE-5G12-027	TEMP-INTERNAL CLAD FAS PIN G12 27"
TE-5G13-027	TEMP-INTERNAL CLAD FAS PIN G13 27"
TE-5H06-027	TEMP-INTERNAL CLAD FAS PIN H6 27"
TE-5H08-027	TEMP-GUIDE TUBE FAS LOC H8 27"
TE-5H10-027	TEMP-INTERNAL CLAD FAS PIN H10 27"
TE-5H12-027	TEMP-GUIDE TUBE FAS LOC H12 27"
TE-5I03-027	TEMP-INTERNAL CLAD FAS PIN I3 27"
TE-5I04-042	TEMP-INTERNAL CLAD FAS PIN I4 42"
TE-5I12-042	TEMP-INTERNAL CLAD FAS PIN I12 42"
TE-5J03-066	TEMP-GUIDE TUBE FAS LOC J3 66"
TE-5J07-010	TEMP-INTERNAL CLAD FAS PIN J7 10"
TE-5J07-027	TEMP-INTERNAL CLAD FAS PIN J7 27"
TE-5J09-042	TEMP-INTERNAL CLAD FAS PIN J9 42"
TE-5J13-027	TEMP-GUIDE TUBE FAS LOC J13 27"
TE-5K05-027	TEMP-GUIDE TUBE FAS LOC K5 27"
TE-5K11-027	TEMP-GUIDE TUBE FAS LOC K11 27"
TE-5L07-010	TEMP-INTERNAL CLAD FAS PIN L7 10"
TE-5L07-027	TEMP-INTERNAL CLAD FAS PIN L7 27"
TE-5L08-027	TEMP-GUIDE TUBE FAS LOC L8 27"
TE-5L09-042	TEMP-INTERNAL CLAD FAS PIN L9 42"

TABLE A-1 (continued)

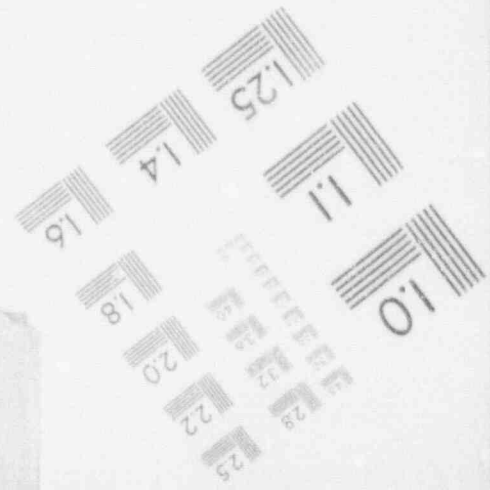
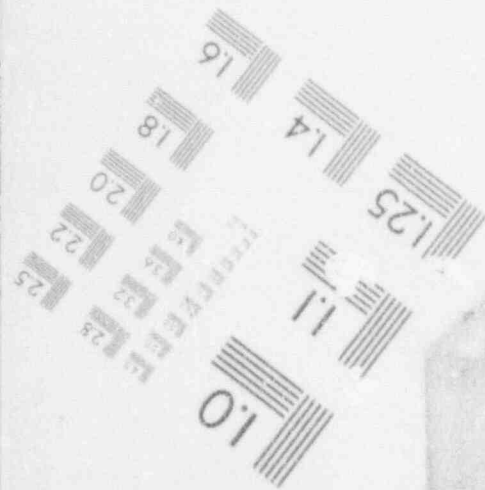
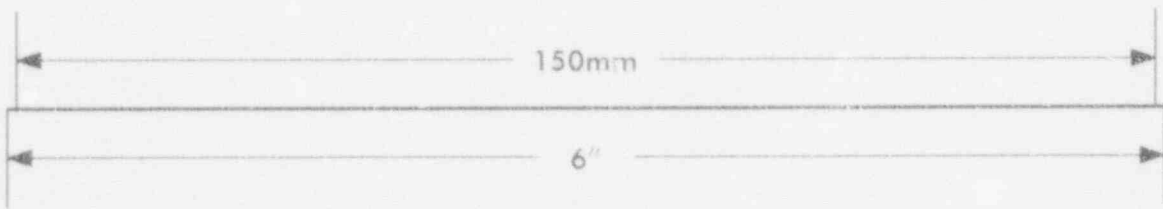
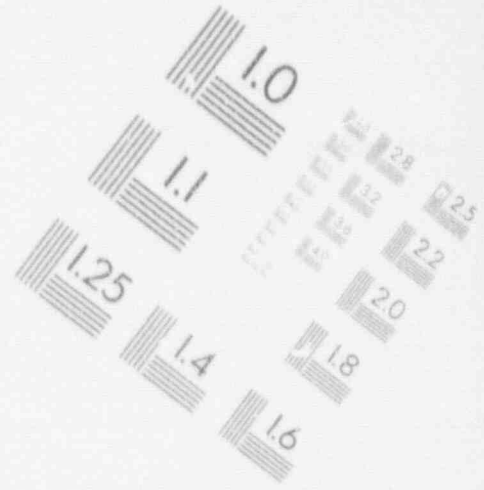
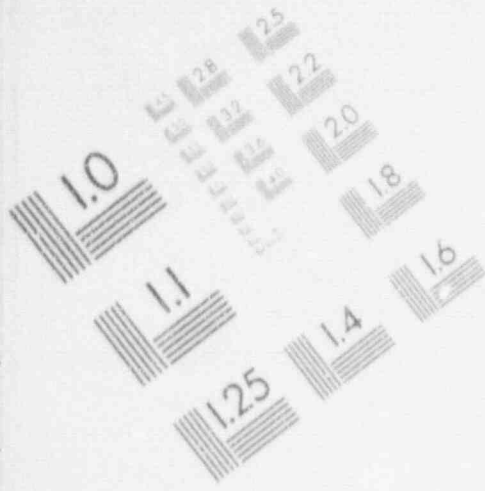
Measurement Identification	Measurement Description
TE-5M06-027	TEMP-GUIDE TUBE FA5 LOC M6 27"
TE-5M07-010	TEMP-INTERNAL CLAD FA5 PIN M7 10"
TE-5M07-027	TEMP-INTERNAL CLAD FA5 PIN M7 27"
TE-5M09-042	TEMP-INTERNAL CLAD FA5 PIN M9 42"
TE-5M10-066	TEMP-GUIDE TUBE FA5 LOC M10 66 IN
TE-5N-010	SHROUD TEMP NORTH SIDE 10 IN.
TE-5N-027	SHROUD TEMP NORTH SIDE 27 IN.
TE-5N-032	SHROUD TEMP NORTH SIDE 32 IN.
TE-5N-042	SHROUD TEMP NORTH SIDE 42 IN.
TE-5S-010	SHROUD TEMP SOUTH SIDE 10 IN.
TE-5S-027	SHROUD TEMP SOUTH SIDE 27 IN.
TE-5S-032	SHROUD TEMP SOUTH SIDE 32 IN.
TE-5S-042	SHROUD TEMP SOUTH SIDE 42 IN.
TE-5UP-004	COOLANT TEMP-UPPER END BOX
TE-5UP-017	COOLANT TEMP-UPPER END BOX
TE-5UP-019	COOLANT TEMP - UPPER END BOX
TE-5UP-023	COOLANT TEMP - UPPER END BOX
TE-5UP-024	COOLANT TEMP - UPPER END BOX
TE-5UP-025	COOLANT TEMP - UPPER END BOX
TE-5UP-025	COOLANT TEMP - UPPER END BOX
TE-5UP-027	COOLANT TEMP - UPPER END BOX
TE-5UP-028A	COOLANT TEMP - UPPER END BOX
TE-5UP-028B	COOLANT TEMP - UPPER END BOX
TE-5UP-029A	COOLANT TEMP - UPPER END BOX
TE-5UP-029B	COOLANT TEMP - UPPER END BOX
TE-5UP-030A	COOLANT TEMP - UPPER END BOX
TE-5UP-030B	COOLANT TEMP - UPPER END BOX
TE-5UP-031A	COOLANT TEMP - UPPER END BOX
TE-5UP-031B	COOLANT TEMP - UPPER END BOX
TE-5UP-032A	COOLANT TEMP - UPPER END BOX
TE-5UP-032B	COOLANT TEMP - UPPER END BOX
TE-5UP-033A	COOLANT TEMP - UPPER END BOX
TE-5UP-033B	COOLANT TEMP - UPPER END BOX
TE-5UP-188A	METAL SURFACE TEMP-UPPER END BOX
TE-5UP-188B	METAL SURFACE TEMP-UPPER END BOX

TABLE A-1 (continued)

Measurement Identification	Measurement Description
TE-5UP-188C	METAL SURFACE TEMP-UPPER END BOX
TE-5UP-188D	METAL SURFACE TEMP-UPPER END BOX
TE-5UP-194G1	METAL SURFACE TEMP-UPPER END BOX
TE-5UP-194G2	METAL SURFACE TEMP-UPPER END BOX
TE-5UP-197B1	METAL SURFACE TEMP-UPPER END BOX
TE-5UP-197B2	METAL SURFACE TEMP-UPPER END BOX
TE-5UP-212G1	METAL SURFACE TEMP-UPPER END BOX
TE-5UP-212G2	METAL SURFACE TEMP-UPPER END BOX
TE-5UP-215B1	METAL SURFACE TEMP-UPPER END BOX
TE-5UP-215B2	METAL SURFACE TEMP-UPPER END BOX
TE-5UP-250G1	METAL SURFACE TEMP-UPPER END BOX
TE-5UP-250G2	METAL SURFACE TEMP-UPPER END BOX
TE-5UP-251B1	METAL SURFACE TEMP-UPPER END BOX
TE-5UP-251B2	METAL SURFACE TEMP-UPPER END BOX
TE-5W-010	SHROUD TEMP WEST SIDE 10 IN.
TE-5W-027	SHROUD TEMP WEST SIDE 27 IN.
TE-5W-032	SHROUD TEMP WEST SIDE 32 IN.
TE-5W-042	SHROUD TEMP WEST SIDE 42 IN.
TE-6E08-045	TEMP-CLADDING/FA6 PIN E8 45 IN.
TE-6F07-037	TEMP-CLADDING/FA6 PIN F7 37 IN.
TE-6F09-041	TEMP-CLADDING/FA6 PIN F9 41 IN.
TE-6G08-039	TEMP-CLADDING/FA6 PIN G8 39 IN.
TE-6G14-011	TEMP-CLADDING/FA6 PIN G14 11 IN.
TE-6G14-030	TEMP-CLADDING/FA6 PIN G14 30 IN.
TE-6G14-045	TEMP-CLADDING/FA6 PIN G14 45 IN.
TE-6H13-015	TEMP-CLADDING/FA6 PIN H13 15 IN.
TE-6H13-037	TEMP-CLADDING/FA6 PIN H13 37 IN.
TE-6H14-028	TEMP-CLADDING/FA6 PIN H14 28 IN.
TE-6H14-032	TEMP-CLADDING/FA6 PIN H14 32 IN.
TE-6H15-026	TEMP-CLADDING/FA6 PIN H15 26 IN.
TE-6I14-021	TEMP-CLADDING/FA6 PIN I14 21 IN.
TE-6I14-039	TEMP-CLADDING/FA6 PIN I14 39 IN.
TE-6LP-001	COOLANT TEMP-LOWER END BOX
TE-6LP-002	COOLANT TEMP-LOWER END BOX
TE-6LP-003	COOLANT TEMP-LOWER END BOX

1

IMAGE EVALUATION TEST TARGET (MT-3)



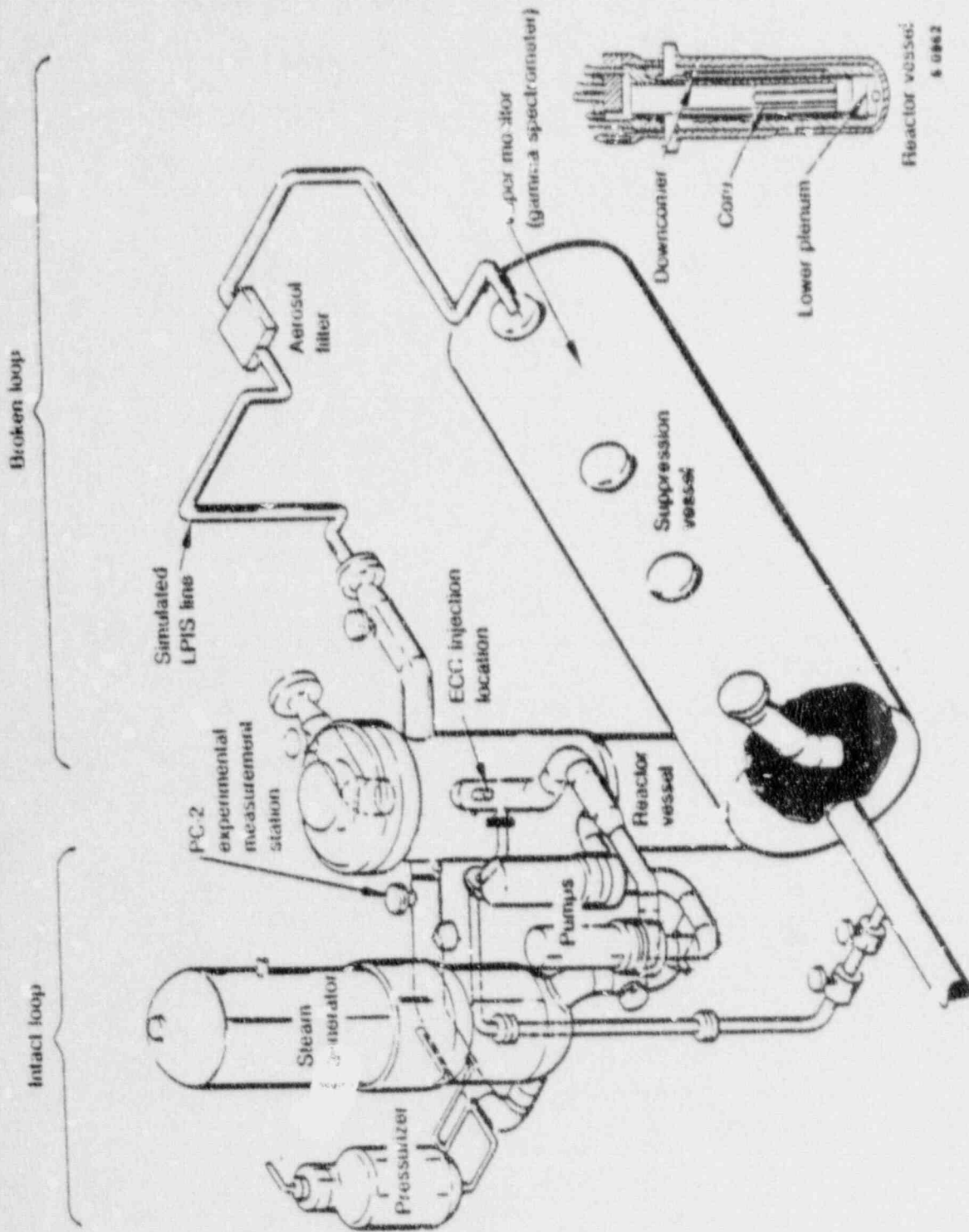


Figure A-1. Axonometric representation of the LOFT primary coolant system.

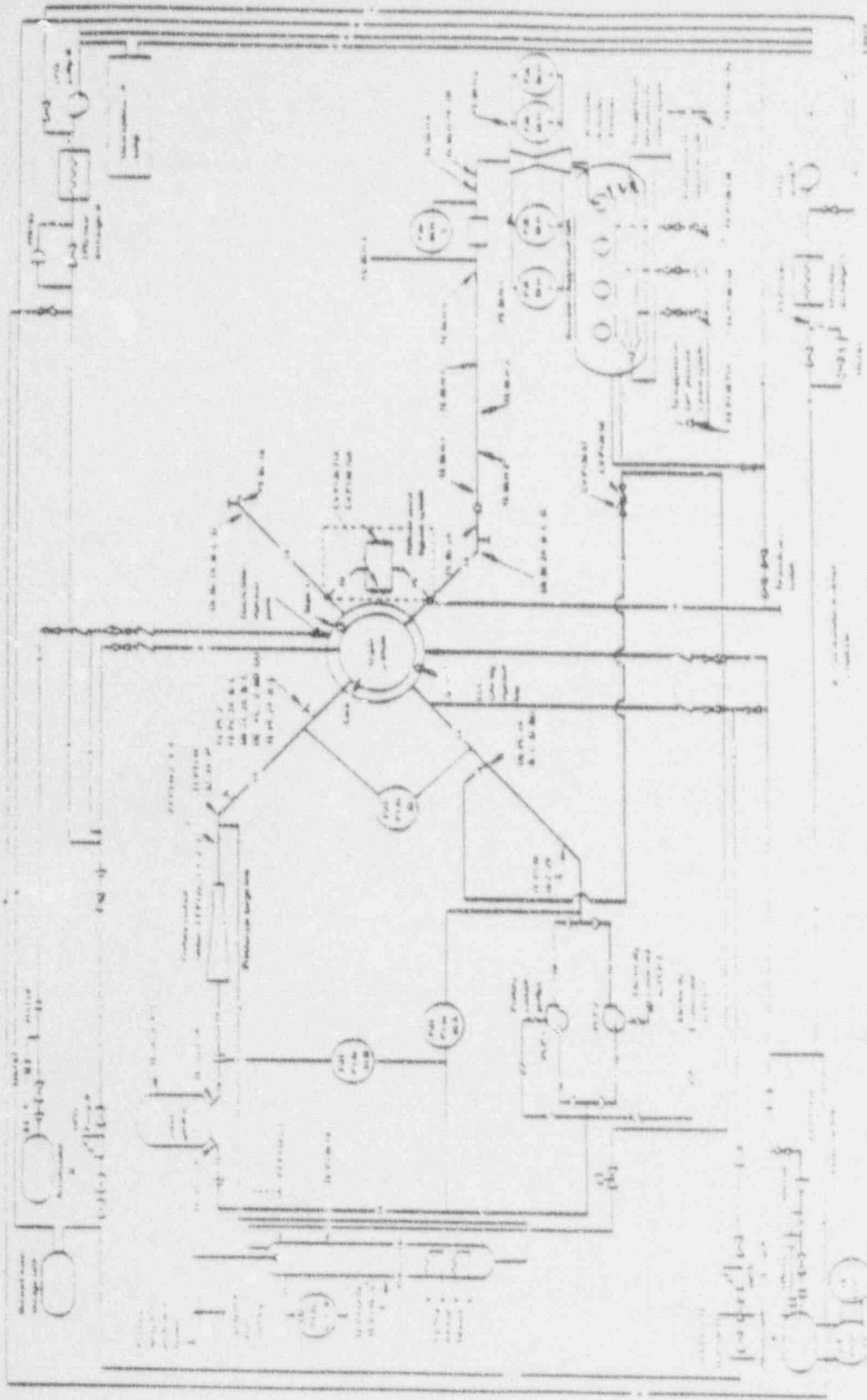
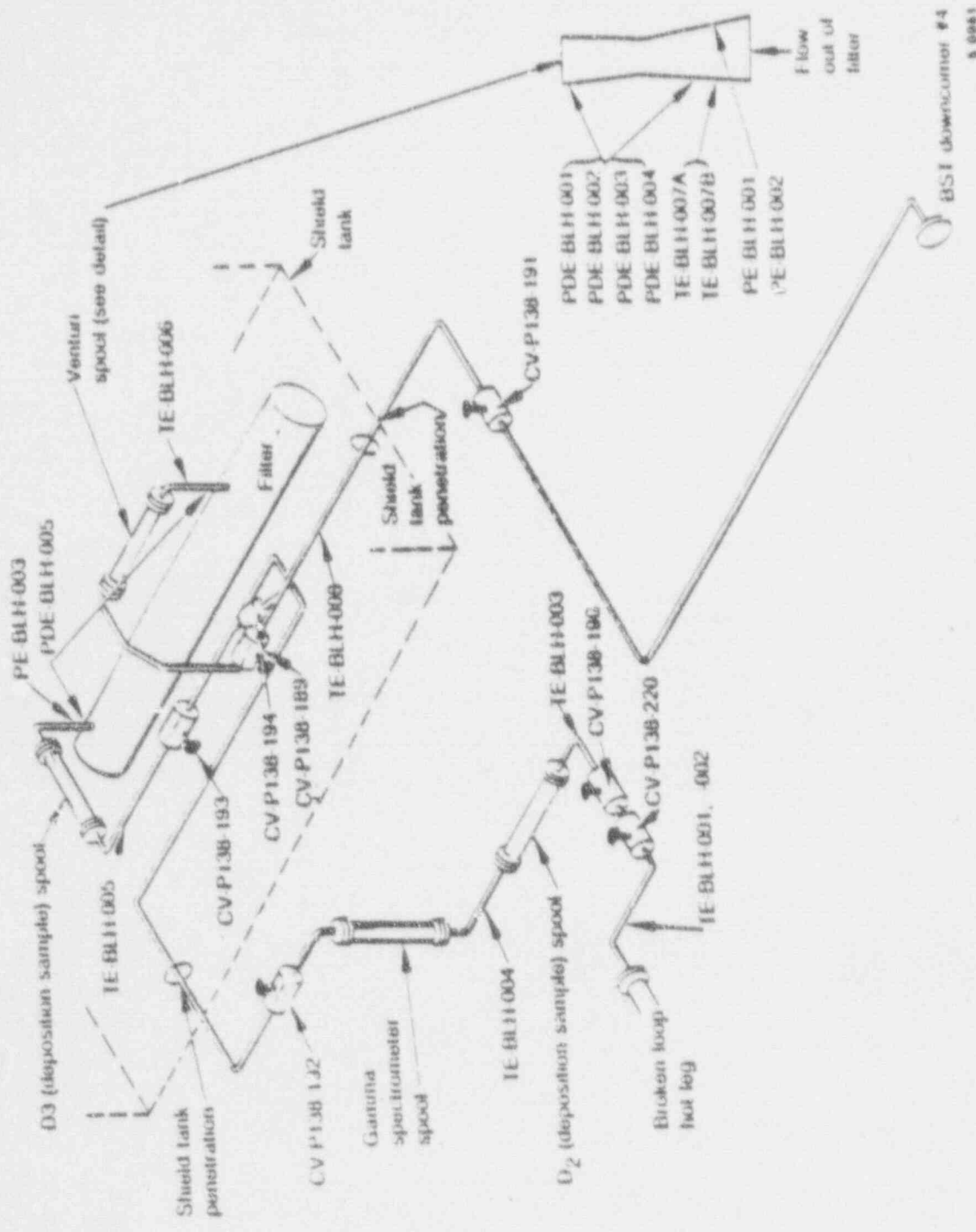


Figure A-2 10FT Piping Schematic with Instrumentation.



BST downcomer #4
5 0083

Figure A-3 Simulated IPT5 Breakline Instrumentation

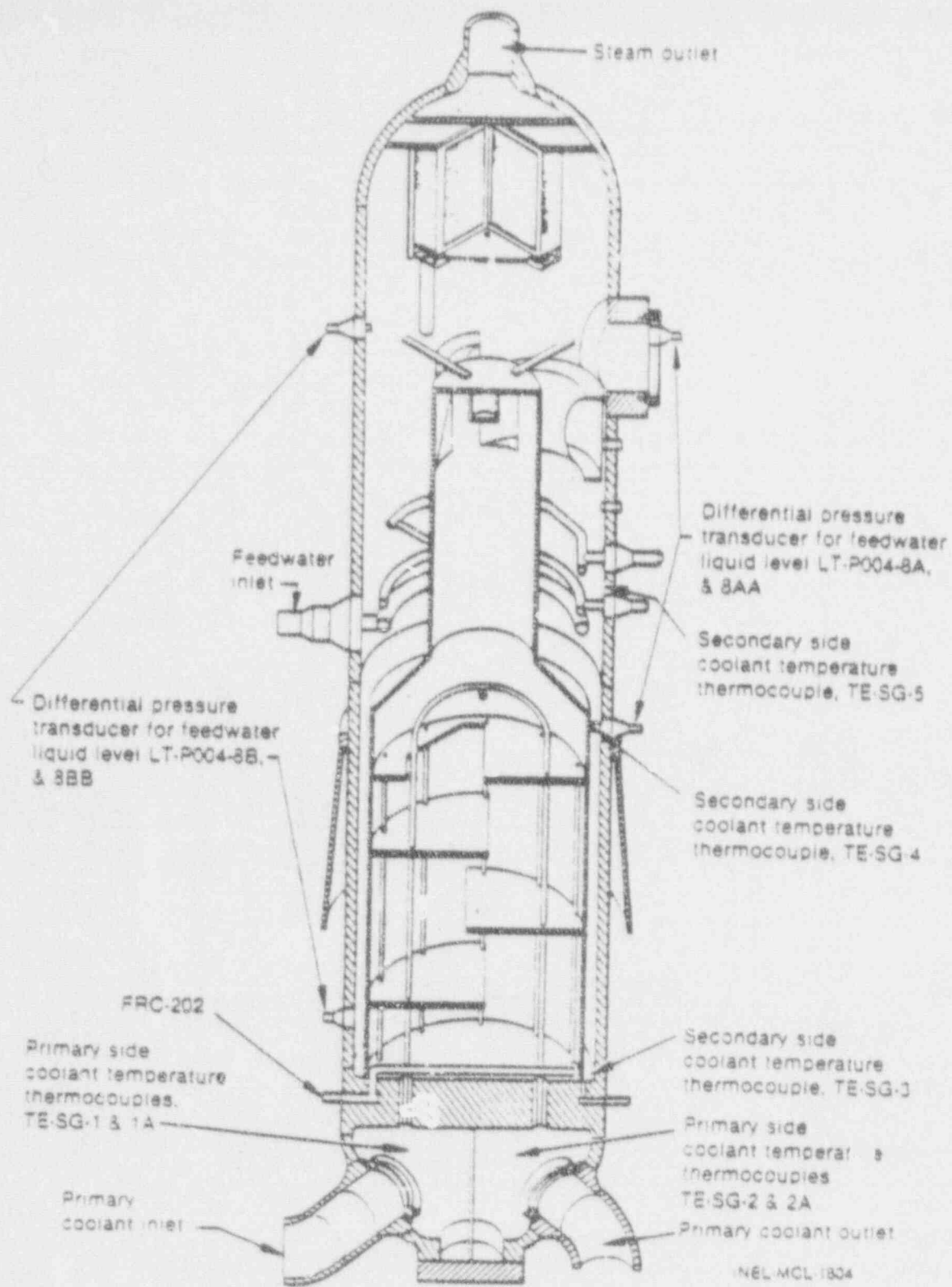


Figure 4-4 Instrument Locations - Steam Generators

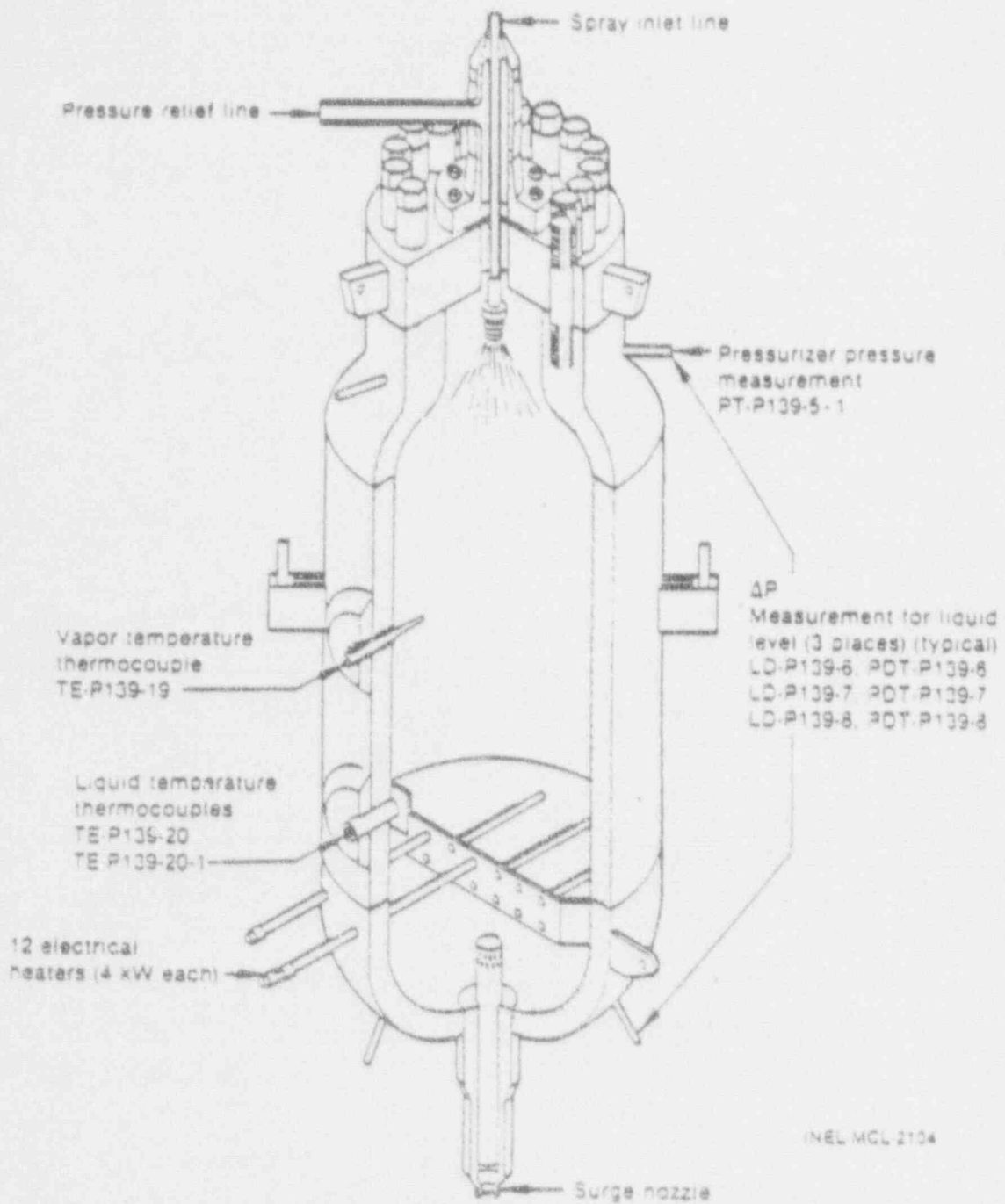
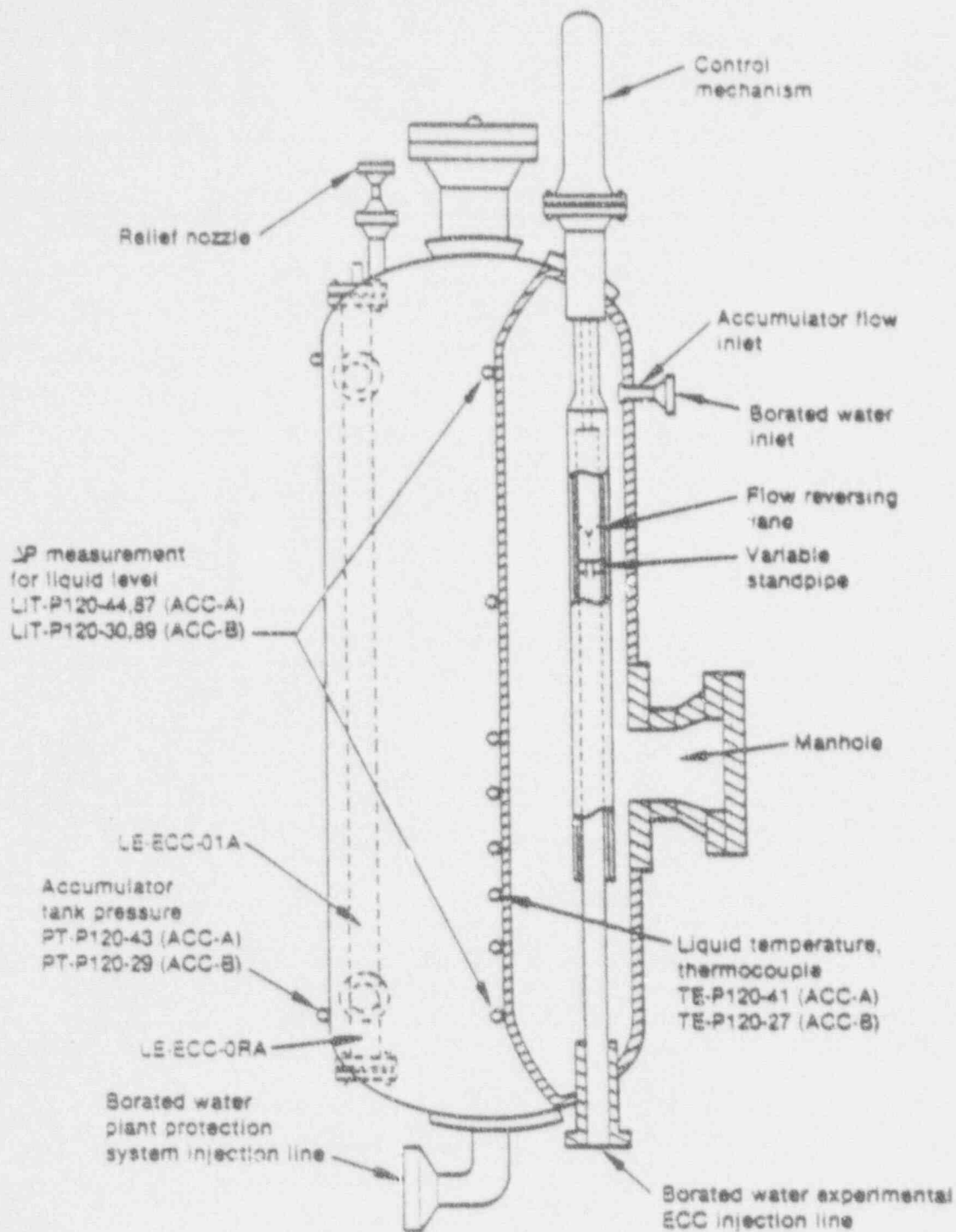
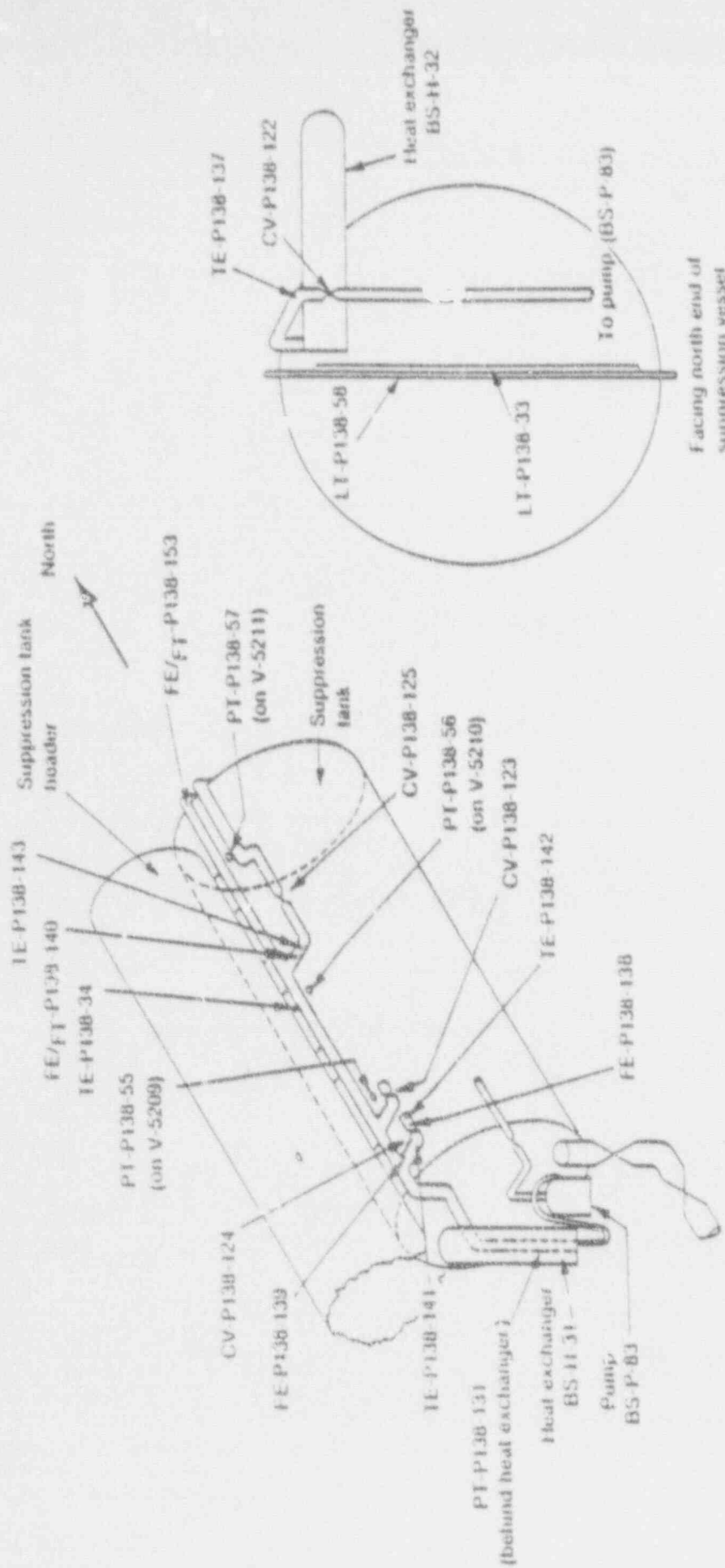


Figure A-5 Instrument Locations - Pressurizer



INEL-MCL-4902

Figure A-6 Instrument Locations - Accumulator Tank



CNELL MCA 4201

Figure A-7 Instrument Locations - Suppression Vessel (Extern)

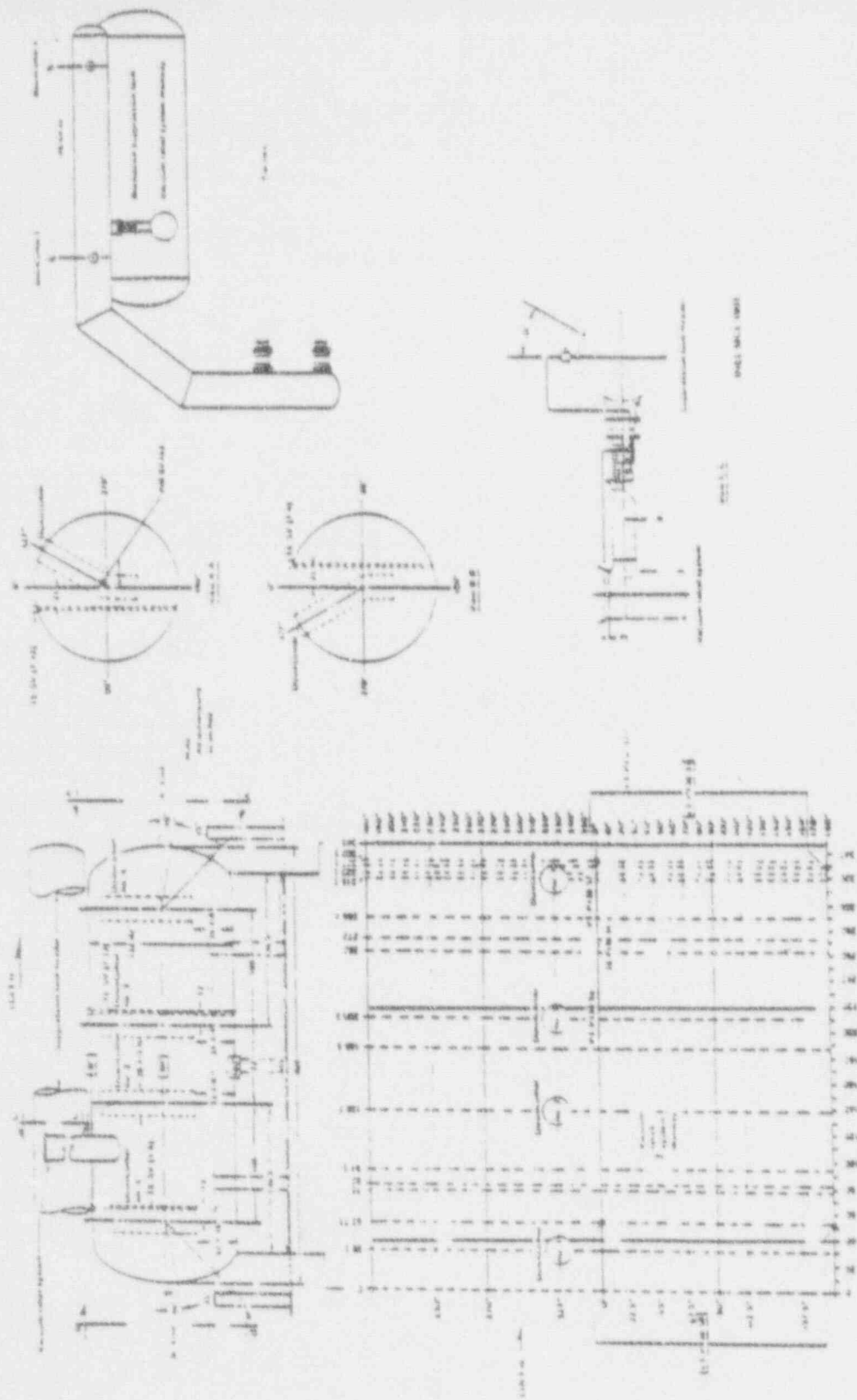


Figure A-B Instrument Locations - Suppression Vessel (Internal)

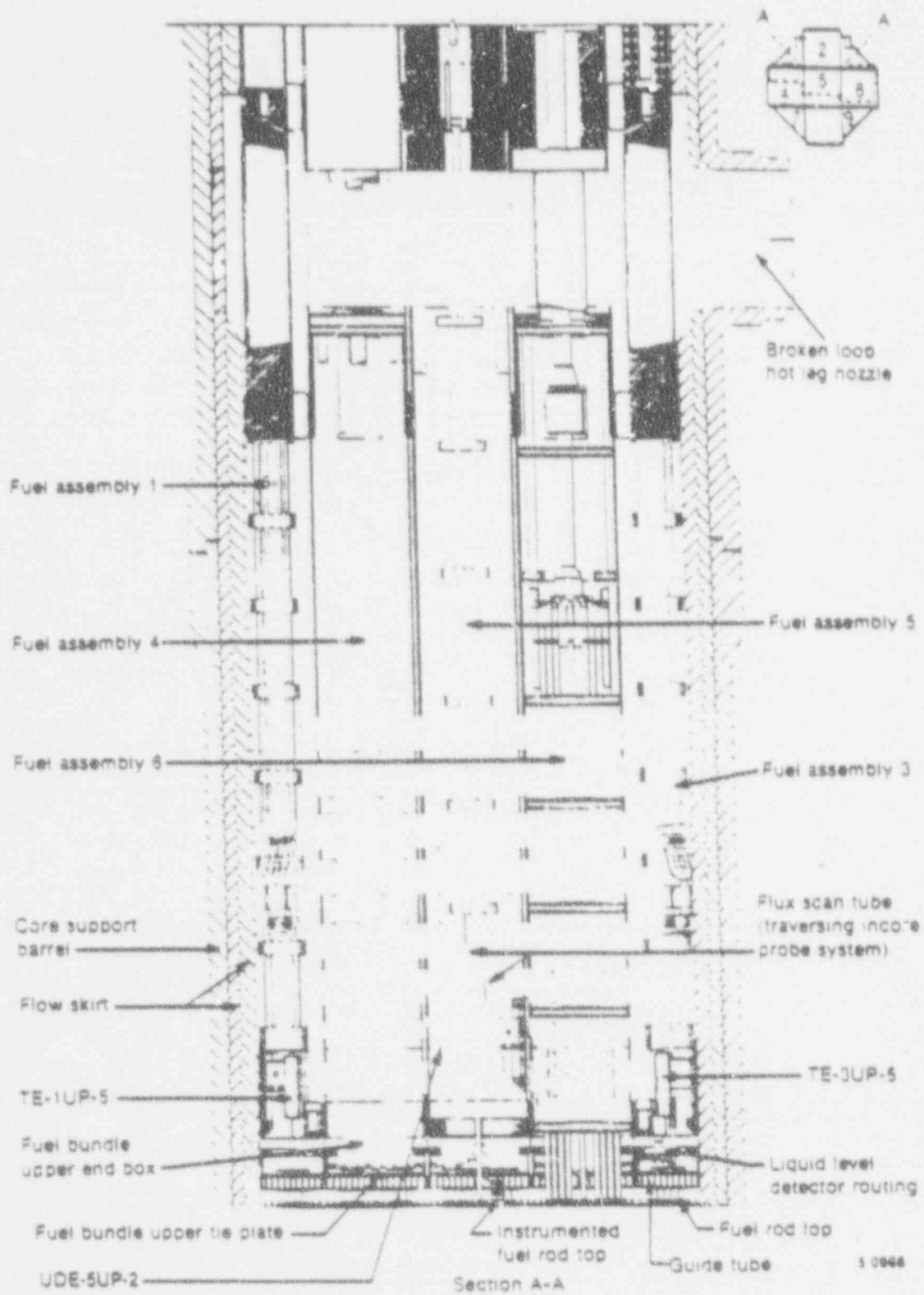
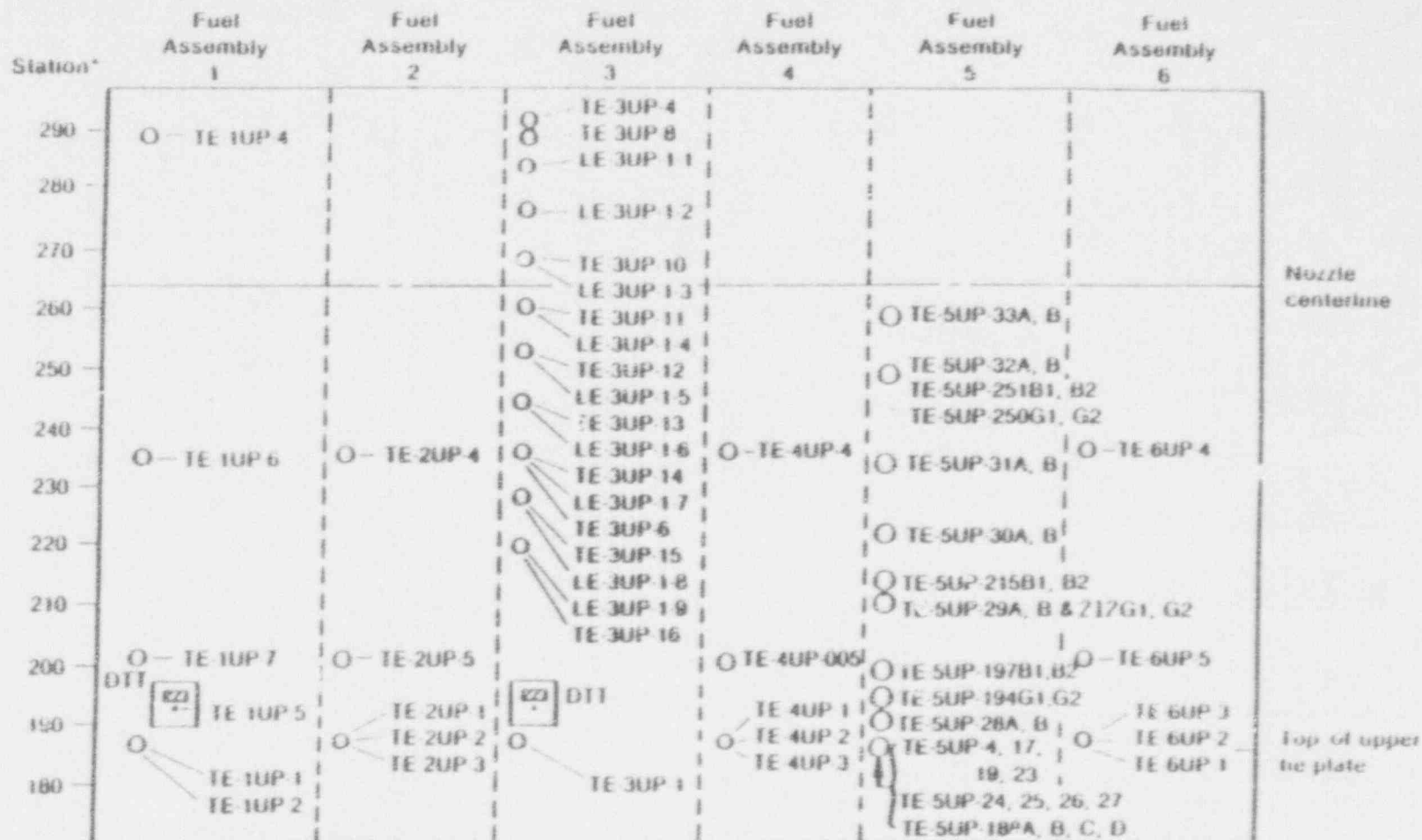


Figure A-9 LOFT Upper Plenum Instruments (Side View)



* Station numbers are a dimensionless measure of relative elevation within the reactor vessel. They are assigned in increments of 25.4 mm with station 300.00 defined at the core barrel support ledge inside the reactor vessel flange.

S 0971

Figure A-10 Instrument Elevations - Reactor Vessel Upper Plenum

ORNL-4419
June 1965
RCL

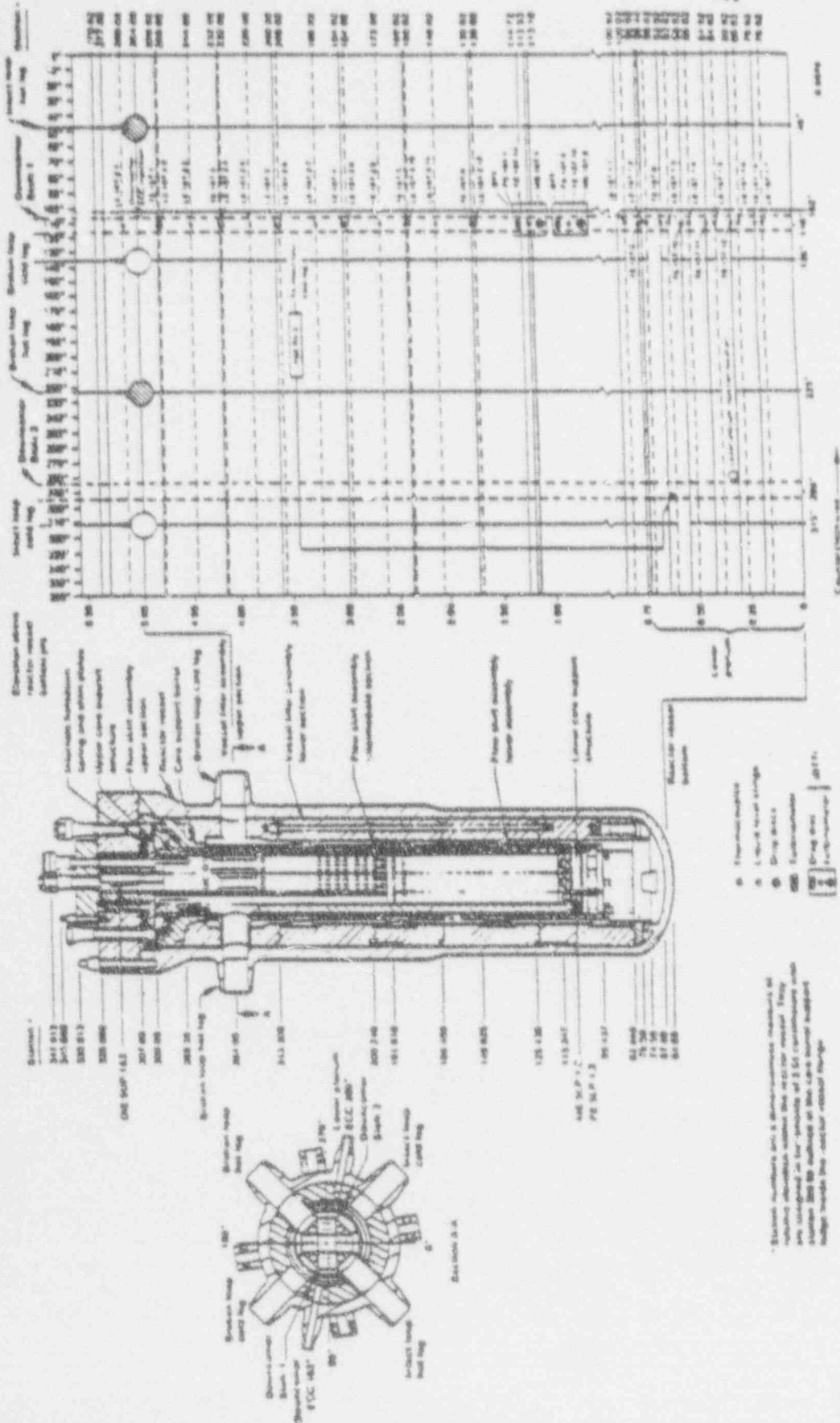
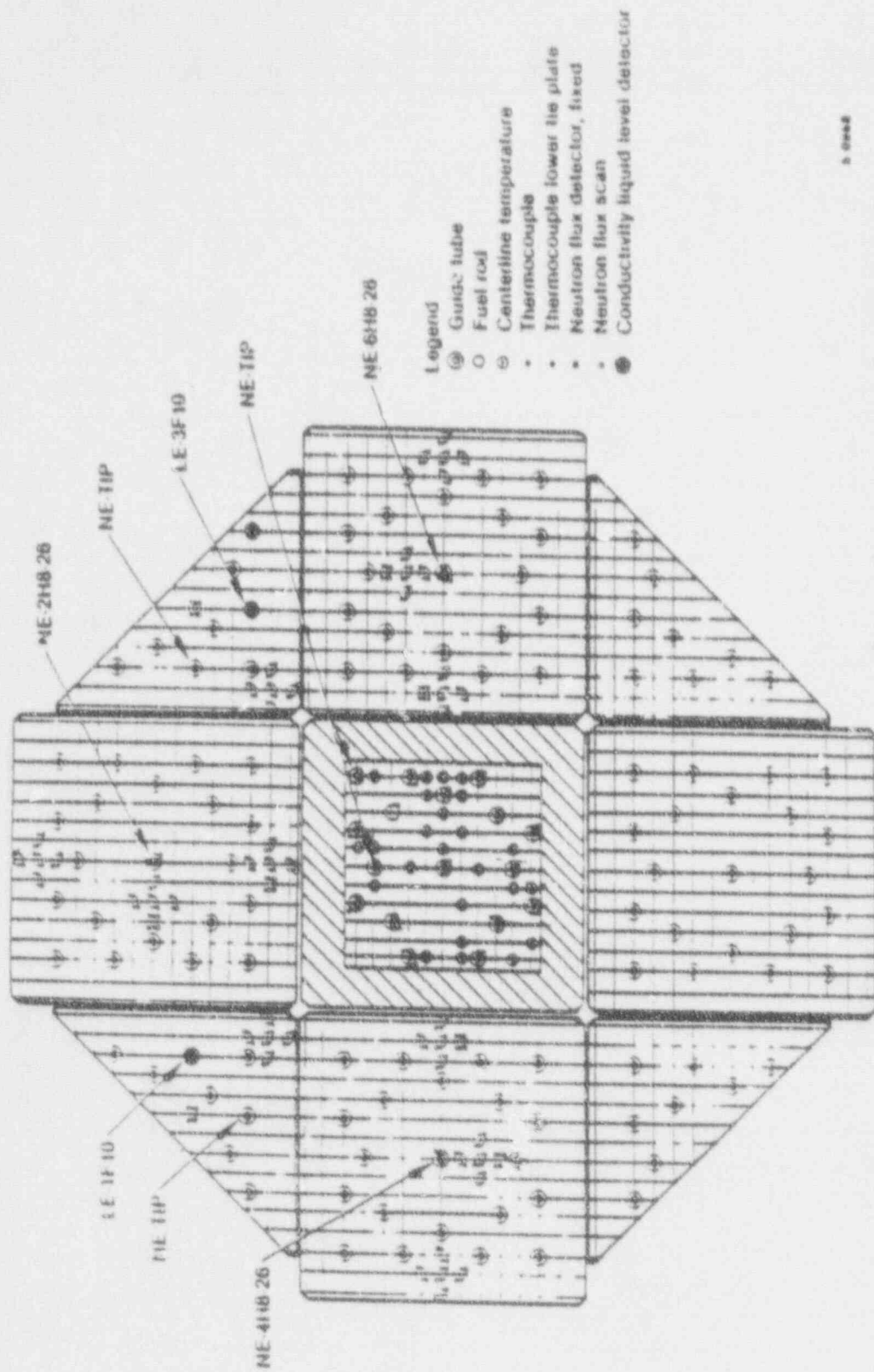


Figure A-11 LOFT reactor vessel station numbers.



5 0000

Figure A-12 Instrument Locations - Liquid Levels and Neutron Detectors In Reactor Vessel (Top View)

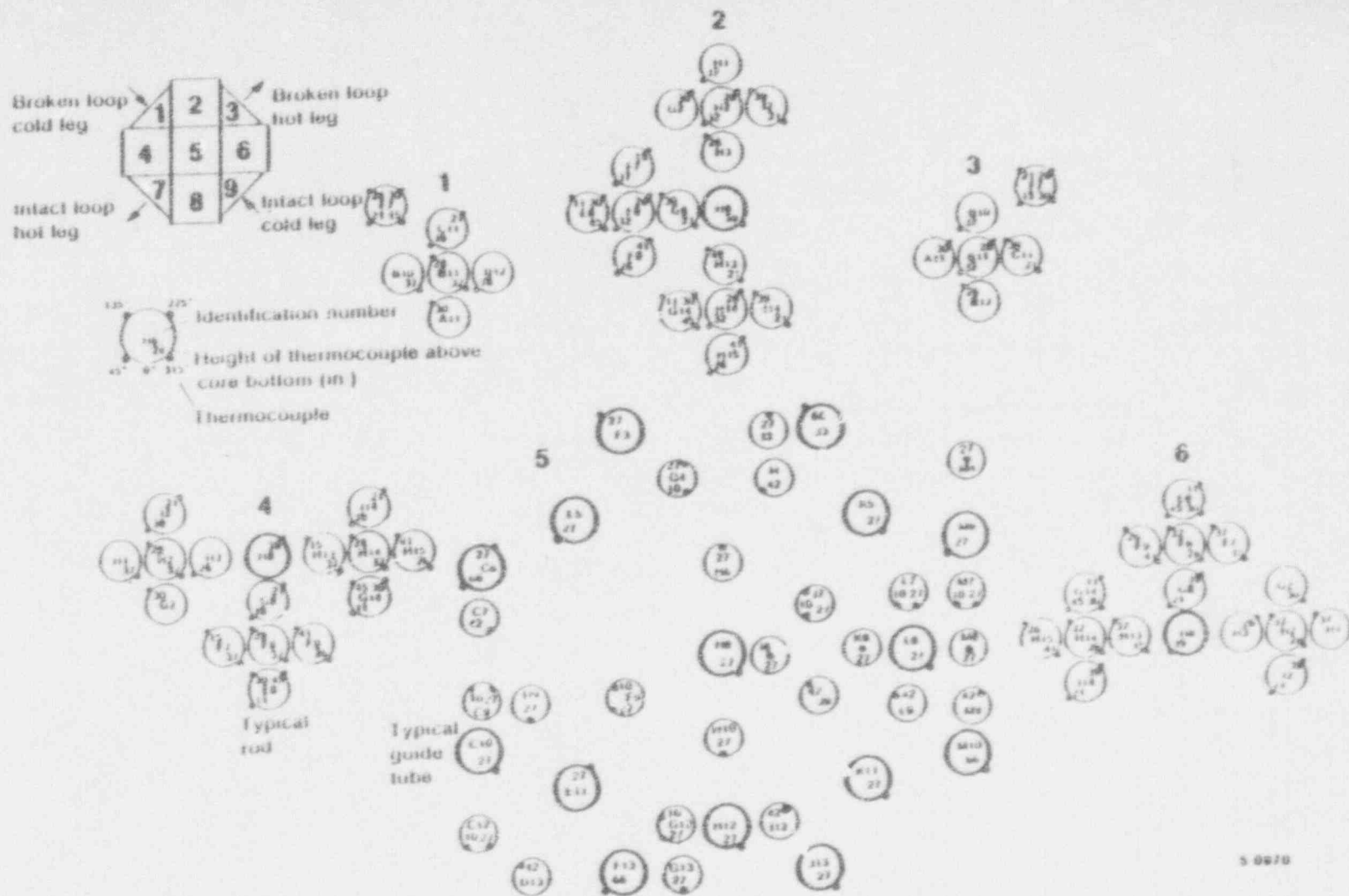
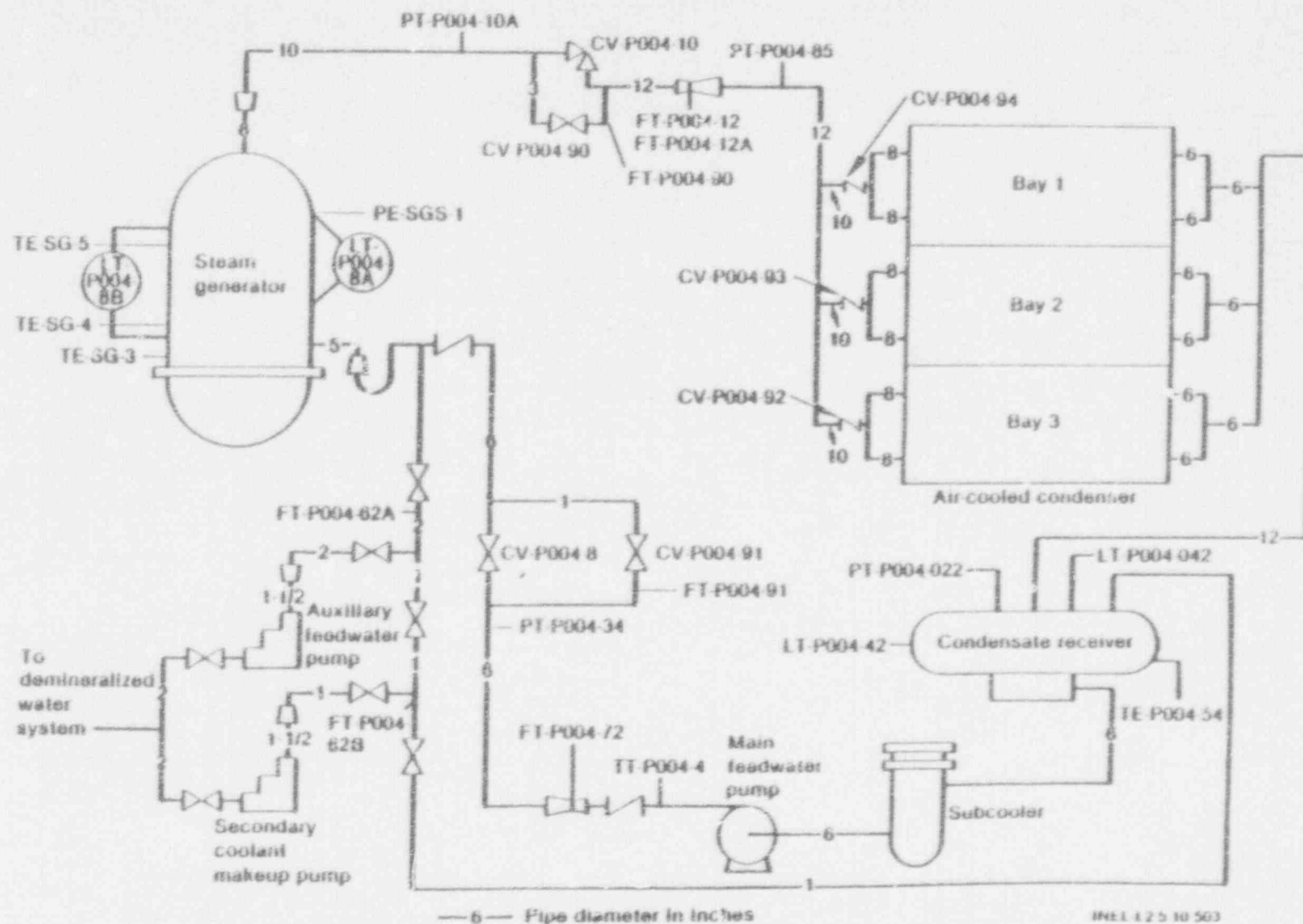


Figure A-13 Instrument Locations - Angular position of Thermocouples on Core Fuel Assemblies

A-20



INEL 125 10 503

Figure A-14 LOFT Secondary Coolant System Insulation

LP-PP-2 Center Fuel Bundle
Instrumentation

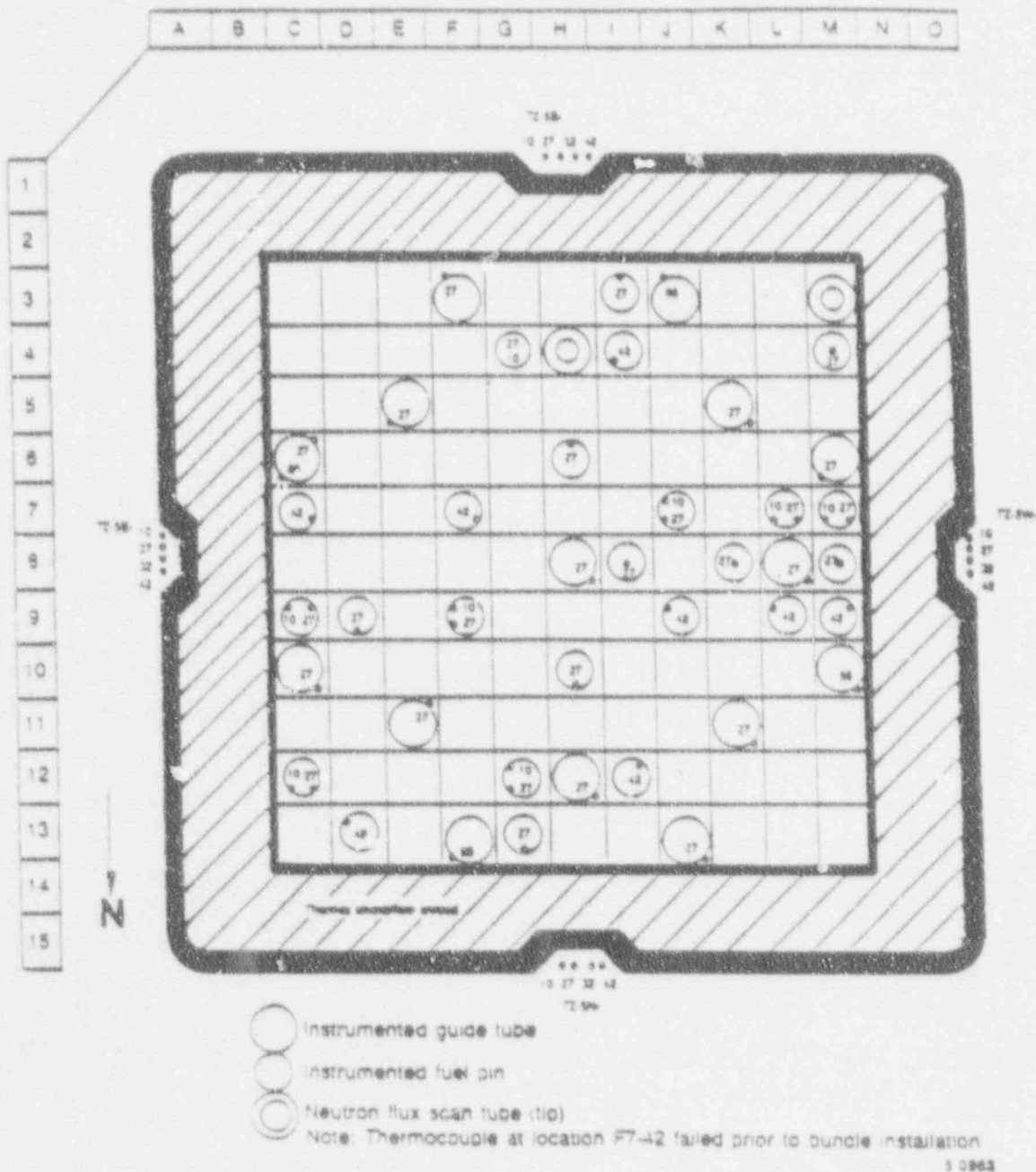


Figure A-15 Center Fuel Bundle
Instrumentation

REFERENCES

A.1 M. L. Carboneau et al. "OECD LOFT Fission Product Experiment LP-FP-2 Fission Product Data Report", OECD-LOFT-T-3805, May 1987.

A.2 OECD LOFT Experiment LP-FP-2: Tape Descriptions and Supplementary Information.

APPENDIX B

BRIEF DESCRIPTION OF THE COMPUTER CODES USED FOR THE ANALYSES

APPENDIX B

BRIEF DESCRIPTION OF THE COMPUTER CODES USED FOR THE ANALYSES

The RELAP5/MOD2 computer code ^(B-1) was used to calculate the transient thermal-hydraulic responses for the LOFT system during Experiment LP-FP-2. The SCDAP/MOD1 ^(B-2) computer code was used to calculate the core behavior in detail during the heatup phase. This appendix gives a summary of the more important features of these two codes.

B.1 RELAP5/MOD2 Computer Code

RELAP5/MOD2 is an advanced, best-estimate computer program developed at the Idaho National Engineering Laboratory (INEL) for the analysis of Loss-of-Coolant Accident (LOCA) and other PWR transients.

RELAP5/MOD2 is based on a one-dimensional, nonhomogeneous and nonequilibrium transient two-phase flow model for the flow of steam-water-noncondensable mixtures in LWR cooling systems. A generic modeling approach is used in which thermal-hydraulic system components are "built" by means of code input, from basic code components, such as fluid control volumes, junctions, pipes, heat structures, reactor kinetics and control components. A few specialized hydrodynamic models are provided for components such as separators, jet pumps, turbines, valves and accumulators, but specialization has been avoided as much as possible in order to produce a code having few inherent limitations.

The two-phase fluid model consists of two phasic mass, two momentum and two energy equations. In RELAP5/MOD1, only one energy equation (the mixture energy equation) is used along with the specification that one phase exists at the local saturation temperature. The use of a second energy equation provides more flexibility to model more general nonequilibrium states.

The basic RELAP5/MOD2 two-phase model is supported by constitutive models for interphase drag, interphase mass transfer, wall heat transfer, and wall friction. All of these constitutive models are closely related through the

geometry of the two-phase mixture or the flow regime. The interphase drag and wall friction models dominate the nonhomogeneous character of the mixture while the interphase mass transfer and wall heat transfer models dominate the nonequilibrium character of the flow.

Special process models are incorporated into the basic hydrodynamic model for phenomena that are either too complex for mechanistic modeling or involve large spatial gradients and would require fine nodalization to accurately resolve. Examples of these processes are form losses, abrupt area changes, choked flow, and reflood.

The hydrodynamic model is solved in a staggered mesh using, as the basic option, a semi-implicit finite difference scheme which is stable for time steps lesser than the material Courant limit. The implicitness is chosen such that a system of linear equations results which can be reduced to a single pressure equation. The system of pressure equations form a sparse matrix of order equal to the number of hydrodynamic volumes and is solved directly using a sparse matrix routine. The remaining dependent variables are calculated by back substitution. The user can also use a quasi-implicit numeric scheme as an option (for more details see Reference B-1).

Heat transfer processes are modeled by means of "heat structures" in which a transient heat conduction solution is used with a variety of boundary conditions including convective heat transfer to fluid control volumes. The heat structures can be used to model nuclear fuel pins, steam generator tube walls, and piping system boundaries with environmental heat losses. The convective boundary condition uses a boiling heat transfer to the steam-water system. In general the transient heat conduction solution is obtained using an one-dimensional implicit centered difference scheme which results in a tridiagonal matrix for each heat structure. However, when the reflood model is used, a two-dimensional conduction scheme is used for cylindrical or rectangular heat structures. The two-dimensional finite difference equations are solved using the Alternative-Direction Implicit (ADI) method, and a fine mesh-rezoning scheme is implemented to efficiently use this two-dimensional heat transfer model for reflood calculations.

The solutions of the heat transfer package are explicitly coupled to the hydrodynamics and are advanced at a time step equal or greater than the hydrodynamic time step. Again, the code gives the user the option to use a

quasi-implicit coupling between the hydrodynamic and the heat transfer models.

The reactor kinetics model is a point formulation and includes moderator, Doppler, and boron concentration feedback. The reactor kinetics model is advanced in time using a Runge-Kutta integration scheme with a truncation error time-step control. The integration interval may be smaller than the thermal-hydraulic time step; however, the feedback functions are updated only at each thermal-hydraulic time step.

The reactor controls are simulated by means of control components such as summers, function generators, integrators, differentiators, delay lines, lead/lags, and a rotating shaft for coupling of turbines, pumps, generators, and motors. The control system integration is performed by a serially implicit Euler scheme using the same time step as the thermal-hydraulic system.

B.2 SCDAP Computer Code

The SCDAP/MOD1 computer code (B.2), (B.3), (B.4) has been developed at the INEL under the sponsorship of the Office of Research of the United States Nuclear Regulatory Commission. SCDAP models the progression of light water reactor core damage following a LOCA, including core heatup, cladding ballooning and rupture, oxidation, hydrogen generation, fission product release, and control rod and fuel material liquefaction and relocation.

Version 21 of the SCDAP/MOD1 code uses thermal-hydraulic boundary conditions to calculate the behavior of fuel bundle components provided they have not significantly lost their original geometry. The structures treated by SCDAP/MOD1/V21 include fuel rods, control rods, and a shroud. This capability was extended to include empty control rod guide tubes or instrument tubes using the fuel rod component. The fuel rod component models calculate the thermal response, the mechanical response, and the response during the early stages of disruption of the fuel rod. The thermal models consider the important thermal effects, which include convective and radiation heat transfer, heat conduction, zircaloy oxidation, and transport of hydrogen. The thermal models also consider the radiation heat exchange between the component surfaces and the coolant fluid. The cladding oxidation model includes the hydrogen blanketing and steam limitation effects, and both side

oxidation (only available for the latest code version 21). The mechanical models predict the ballooning of cladding and several consequent effects. Cladding ballooning results in reduced flow area and an increased cladding surface, both of which affect rod cooling and hydrogen generation rates.

The models which describe the early stages of disruption predict the amount of liquefied fuel and cladding material and the relocation position. Additional models are provided to describe oxidation, liquefaction, and solidification of control rods and guide tubes. A thermal shroud component model is built in, which utilizes fine nodalization to calculate heat conduction through multiple material layers.

The material properties used in SCDAP are obtained from Reference B.5 with additional information for the control rod and shroud insulator material (ZrO_2) supplied by the fuel module design engineers (B.6)

B.3 REFERENCES

- B.1 V.H. Ransom, et al., "RELAP5/MOD2 Code Manual", NUREG/CR-4312, EGG-2396, August 1985.
- B.2 G.A. Berna et al., "SCDAP/MOD1/VO, A Computer Code for the Analysis of LWR Vessel Behavior During Severe Accident Transients", IS-SAAM-84-002, June 1984.
- B.3 C. M. Allison et al., "Draft Preliminary Report for Comment. SCDAP/MOD1 Theory and Models", FIN A6360, January 1985.
- B.4 L. J. Siefken, "Transmittal of Updates to Standalone SCDAP to correct error in fuel heat capacity", LWS-7-87, April 1987.
- B.5 D. L. Hagrman, et al., "MATPRO-Version 11 (Revision 2), A Handbook of Materials Properties for use in the Analysis of Light Water Reactor Fuel Rod Behavior", NUREG/CR-0497, TREE-1280, Rev. 2, August 1981.
- B.6 G.A. Dinneen et al., "LP-FP-2 Supplement to the LOFT Integral Test System Final Safety Analysis Report", OECD-LOFT-I-11-5113, December 1984.

APPENDIX C

RELAP5/MOD2 INPUT DATA FOR EXPERIMENT LP-FP-2

APPENDIX C

RELAP5/MOD2 INPUT DATA FOR EXPERIMENT LP-FP-2

The input data used for the RELAP5/MOD2 base case posttest calculation of Experiment LP-FP-2 presented in section 5 is on microfiche in a pouch on the inside of the report back cover.

Microfiche titled "F2PSTSS" contains the steady state input deck. Microfiche titled "F2PSTTT" contains the input deck for the initiation of the transient; and finally microfiche titled "FP2RCR" contains the input decks for the successive core renodalizations.

APPENDIX D

SCDAP/MOD1 INPUT DATA FOR EXPERIMENT LP-PP-2

APPENDIX D

SCDAP LOFT INPUT DATA FOR EXPERIMENT LP-FP-2

Listing of SCDAP input data prepared for the center bundle analysis presented in section 6.2 is provided on the attached microfiche; in the pouch on the inside of the report back cover. The title of the microfiche is "SCDAPCRb".

APPENDIX E

COMPUTER RUN STATISTICS

APPENDIX E

COMPUTER RUN STATISTICS

In order to assess the computational efficiency of one code the NRC recommends to use (see Table 4 in Reference E-1) the following parameters:

1. Plot of CPU Time vs. Transient time
2. Plot of Time Step vs. Transient time
3. Grind time (in ms), defined as

$$\frac{\text{CPU} \times 1000}{C \times \text{DT}}$$

where

CPU is the total execution time in s
DT is the total number of time steps
C is the total number of control volumes in the model

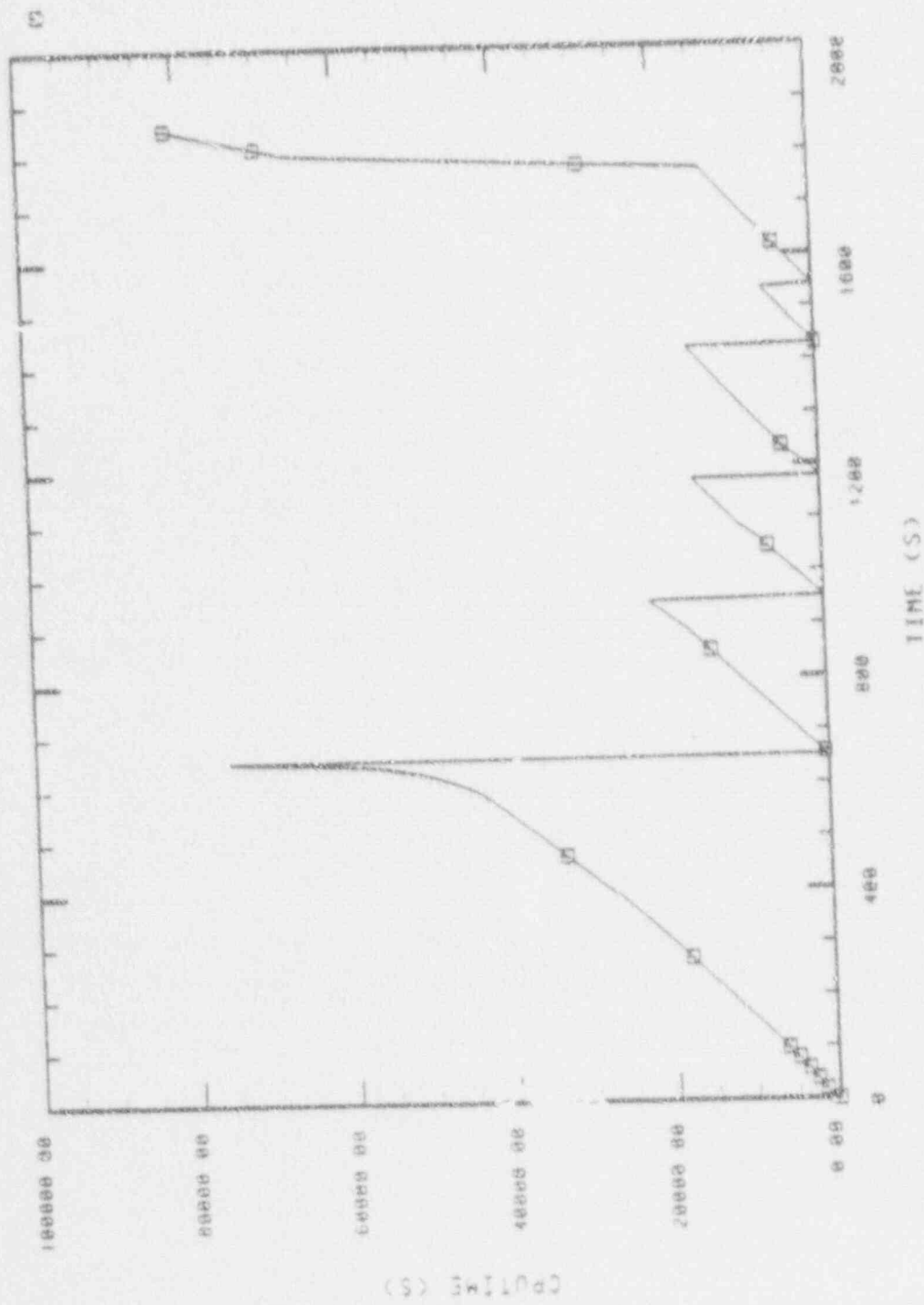
4. Type of machine used to perform the calculation.

In the following sections we present the run statistics we got in our calculations

E. 1 RELAP5/MOD2 Run Statistics

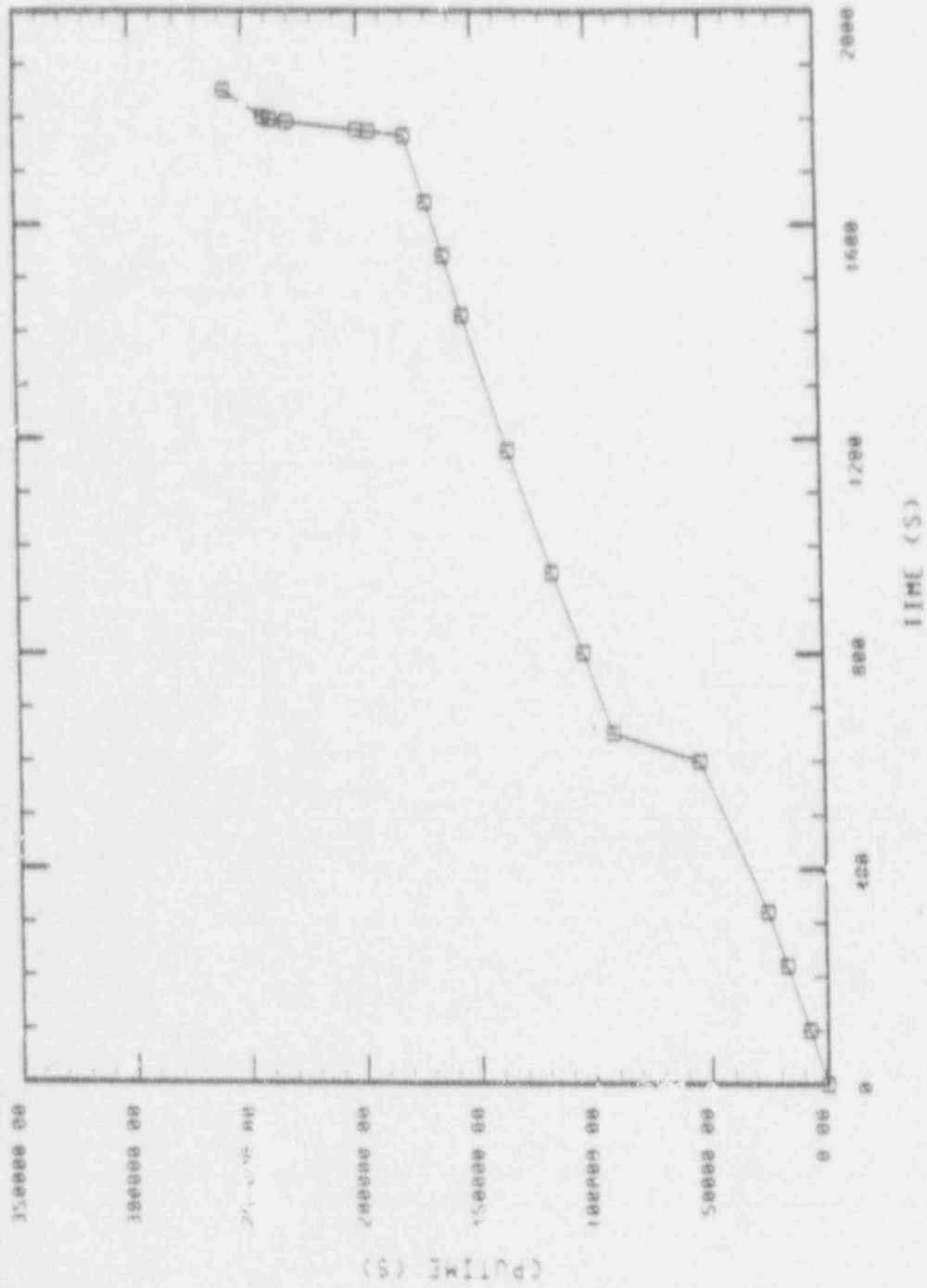
Figure E-1 shows the CPU time versus the transient time consumed in the RELAP5/MOD2 base calculation (section 5). Here we note that RELAP5/MOD2/36.04 set to zero the CPU time counter every time we made a renodalization. We think this is a code deficiency and it should be corrected in future code versions.

In any case, Figure E-2 presents the right curve, showing the total accumulated CPU time versus transient time. The total CPU time was 61.43 hr on a CDC CYBER 830 machine for a total of 1850 s of transient time. This makes an average ratio of 120 CPU/PROBLEM TIME for the LP-FP-2 transient. However



RELAPS/MOD2/36 04 CPU TIME (S) VERSUS
 TRANSIENT TIME (BASE CALCULATION)
 COMPUTER CDC CYBER 830 (NOS 2 4 3)

Figure E-3



RELAPS/MOD2 TOTAL CPU TIME (S)
 VERSUS TRANSIENT TIME (BASE CALCULATION)
 COMPUTER CDC CYBER 830 (NOS 2 4 3)

Figure E-2

the average ratio for almost all the transient is about 70 CPU/PROBLEM TIME, except for two particular time periods. First of all, at about 600s the code began to reduce the time step (increasing drastically the CPU time) due to water property errors in the LPIS line. Initially this LPIS line was simulated using 3 volumes. To avoid this code instability we reduce the line to only 2 volumes, recovering the average ratio of 70 for the CPU time. And finally, when the core reflood started, (1770s) we were forced to reduce the maximum time step down to 1ms to get convergence (Very hot core reflooded by cool water). This again increased dramatically the total CPU time.

The grind time for this case was calculated as follow

$$\frac{221,136.2}{134 \times 61.988} \times 1000 = 26.6 \text{ ms.}$$

too high compared to standard RELAP5/MOD2 calculations. However, the reader should be aware of the complexity of the LP-PP-2 transient and the two code problems above mentioned.

The run time of the sensitivity study was practically the same as the base case calculation.

E.2 SCDAP/MOD1 Run Statistics

The CPU time used for the analysis is not available in the SCDAP graphic file. Therefore we can only use the grind time to assess the SCDAP efficiency.

The total CPU time was 2.16 hr of a CDC CYBER 830 for a total of 1350 s of transient time. This makes an average of 5.8 CPU-to-problem time ratio. The grind time was calculated to be

$$\frac{7772.5 \text{ (CPU sec)}}{5 \text{ (components)} \times 2254 \text{ (time steps)}} \times 1000 = 689.7 \text{ ms}$$

Though the CPU time-to-Problem time ratio is better for SCDAP than for RELAP5, the SCDAP grind time (the best code efficiency parameter) is much

higher than the RELAPS one, because of the complex nature of the thermo-mechanical phenomena simulated with SCDAP.

E.3 References

E.1 P. Ting et al. "Guidelines and Procedures for the International Code Assessment and Applications Program", NUREG-1271, April 1987.

NRC FORM 335 12-80 NRCM 1102, 3201, 3202		U.S. NUCLEAR REGULATORY COMMISSION		REPORT NUMBER (Assigned by NRC. Add Vol., Supp., Rev., and Addendum Numbers, if any.)	
BIBLIOGRAPHIC DATA SHEET <i>(See instructions on the reverse.)</i>				NUREG/IA-0049 ICSP-LP-FP-2	
2. TITLE AND SUBTITLE Thermal-Hydraulic Post-Test Analysis of OECD LOFT LP-FP-2 Experiment				3. DATE REPORT PUBLISHED MONTH YEAR April 1992	
				4. FIN OR GRANT NUMBER A4682	
5. AUTHOR(S) J.J. Pena, S. Enciso, F. Reventos				6. TYPE OF REPORT	
				7. PERIOD COVERED (inclusive Dates)	
8. PERFORMING ORGANIZATION - NAME AND ADDRESS (If NRC, provide Division, Office or Region, U.S. Nuclear Regulatory Commission, and mailing address; if contractor, provide name and mailing address.) Consejo de Seguridad Nuclear Madrid, Spain					
9. SPONSORING ORGANIZATION - NAME AND ADDRESS (If NRC, type "Same as above". If contractor, provide NRC Division, Office or Region, U.S. Nuclear Regulatory Commission, and mailing address.) Office of Nuclear Regulatory Research U.S. Nuclear Regulatory Commission Washington, DC 20555					
10. SUPPLEMENTARY NOTES					
11. ABSTRACT (200 words or less) An assessment of RELAP5/MOD2 and SCDAP/MOD1 against the OECD LOFT experiment LP-FP-2 is presented. LP-FP-2 studies the hypothetical release of fission products and their transport following a large-break LOCA scenario. The report comprises a general description of the LP-FP-2 experiment, a summary of thermal-hydraulic data, a simulation of the LP-FP-2 experiment, results of the RELAP5/MOD2 base calculation, the RELAP5/MOD2 sensitivity analysis, the SCDAP/MOD1 nodalization for an LP-FP-2 experiment, the results of the SCDAP/MOD1 calculation, and the summary and conclusions.					
12. KEY WORDS/DESCRIPTORS (Use words or phrases that will assist researchers in locating the report.) ICAP Program RELAP5/MOD2 SCDAP/MOD1 LP-FP-2 Experiment				13. AVAILABILITY STATEMENT Unlimited	
				14. SECURITY CLASSIFICATION (This Page) Unclassified (This Report) Unclassified	
				15. NUMBER OF PAGES	
				16. PRICE	

THIS DOCUMENT WAS PRINTED USING RECYCLED PAPER

UNITED STATES
NUCLEAR REGULATORY COMMISSION
WASHINGTON, D.C. 20555

OFFICIAL BUSINESS
PENALTY FOR PRIVATE USE, \$300

SPECIAL DELIVERY PERMIT
POSTAGE AND FEE PAID
NO. 1234
WASHINGTON, DC

120555139531 1 1ANICI
US NRC-0ADM
DIV FOIA & PUBLICATIONS SVCS
TPS-PDR-NUREG
P-211
WASHINGTON DC 20555